CONCEPTUAL DESIGN OF A THERMALHYDRAULIC LOOP FOR MULTIPLE TEST GEOMETRIES AT SUPERCRITICAL CONDITIONS NAMED SUPERCRITICAL PHENOMENA EXPERIMENTAL TEST APPARATUS (SPETA)

by

Adepoju Adenariwo

A Thesis Submitted in Partial Fulfillment of the Requirements for the Degree of

Master of Applied Science

in

The Faculty of Energy Systems and Nuclear Science

University of Ontario Institute of Technology

April, 2012

THESIS DEFENCE FORM

ABSTRACT

The efficiency of nuclear reactors can be improved by increasing the operating pressure of current nuclear reactors. Current CANDU-type nuclear reactors use heavy water as coolant at an outlet pressure of up to 11.5 MPa. Conceptual SuperCritical Water Reactors (SCWRs) will operate at a higher coolant outlet pressure of 25 MPa. Supercritical water technology has been used in advanced coal plants and its application proves promising to be employed in nuclear reactors. To better understand how supercritical water technology can be applied in nuclear power plants, supercritical water loops are used to study the heat transfer phenomena as it applies to CANDU-type reactors.

A conceptual design of a loop known as the Supercritical Phenomena Experimental Apparatus (SPETA) has been done. This loop has been designed to fit in a 9 m by 2 m by 2.8 m enclosure that will be installed at the University of Ontario Institute of Technology Energy Research Laboratory. The loop include components to safely start up and shut down various test sections, produce a heat source to the test section, and to remove reject heat. It is expected that loop will be able to investigate the behaviour of supercritical water in various geometries including bare tubes, annulus tubes, and multi-element-type bundles. The experimental geometries are designed to match the fluid properties of Canadian SCWR fuel channel designs so that they are representative of a practical application of supercritical water technology in nuclear plants. This loop will investigate various test section orientations which are the horizontal, vertical, and inclined to investigate buoyancy effects. Frictional pressure drop effects and satisfactory methods of estimating hydraulic resistances in supercritical fluid shall also be estimated with the loop.

Operating limits for SPETA have been established to be able to capture the important heat transfer phenomena at supercritical conditions. Heat balance and flow calculations have been done to appropriately size components in the loop. Sensitivity analysis has been done to find the optimum design for the loop.

ACKNOWLEDGEMENTS

Financial support from the NSERC/NRCan/AECL Generation IV Energy Technologies Program and NSERC Discovery Grants is gratefully acknowledged. Financial support from the Ontario Graduate Scholarship (OGS) program is sincerely appreciated.

I am truly grateful to my supervisor, Dr Harvel, for his encouragement, support, and guidance during the duration of this work. I would also like to thank Dr. Pioro for providing his expert advice on my research.

I would like to thank my colleagues Adam Lipchitz, Jeffrey Samuel, Amjad Farah, Graham Richards, Craig Freeburn, and Maxim Kinakin, for their stimulating discussions on my thesis. I am especially thankful to Adam Lipchitz for not only engaging discussions but providing transportation which made my commute a whole lot easier. I wish to thank the entire group of the Nuclear Design Laboratory at UOIT for giving me the best working environment and providing me with tools used in my research.

I appreciate the support, good company, and comraderie from my friends Omololu Oyewole-Eletu, Okimi Peters, and Waheed Olagunju, and helping me get through the challenging times as a graduate student.

Lastly, I am thankful to my parents and siblings for providing emotional support for me and encouragement throughout the duration of my graduate studies.

TABLE OF CONTENT

LIST OF FIGURES

LIST OF TABLES

NOMENCLATURE

A	area, m^2
A_r	area ratio
Cp	specific heat capacity, J/kgK
C_μ	constant defined by k_e-ϵ model
D	diameter, m
f	friction factor
G	mass flux, kg/m^2s
g	acceleration due to gravity, m/s^2
h	heat transfer coefficient, W/m^2K
H	enthalpy, J/kg
hL	heat loss
k	thermal conductivity, W/m·K
K	local head loss coefficient
k_e	turbulent kinetic energy, m^2/s^2
L	length, m
$\dot{m}$	mass-flow rate, kg/s
NL	total length of heat exchanger tubes, m
P	pressure, Pa
q	heat flux, W/m^2
Q	heat transfer rate, W
r	radius, m
R	Surface Roughness, m
U	overall heat transfer coefficient, W/m^2K

t	thickness, m
T	temperature, ℃
u	fluid velocity in x-direction, m/s
v	kinematic viscosity, Pa.s
V	velocity, m/s
v	fluid velocity in y-direction, m/s
z	fluid velocity in z-direction, m/s
Z	elevation, m

Greek Letters

α	thermal diffusivity, m^2/s
ϵ	dissipation rate, m^2/s^3
ρ	density, kg/m^3
Δ	difference
η	efficiency
μ	dynamic viscosity, Pas

Dimensionless numbers

Nu	Nusselt number ($h \cdot D_{hy} / k$)
Pr	Prandtl number ($\mu \cdot c_p / k$)

$\overline{\mathbf{Pr}}$	average Prandtl number
Re	Reynolds number ($G \cdot D_{hy} / \mu$)

Subscripts and Superscripts

a	acceleration
ave	average
b	bulk
cr	critical
f	friction
g	gravity
h	head
hy	hydraulic
i	inner
in	inlet
l	form factor
min	minimum
o	outer
out	outlet
pc	pseudocritical
t	turbulent
th	thermal
w	wall

Abbreviations and Acronyms

AC	Alternating Current
AECL	Atomic Energy of Canada Limited
BWR	Boiling Water Reactor
CANDU	CANada Deuterium Uranium
CFD	Computational Fluid Dynamics
CHF	Critical Heat Flux
DC	Direct Current
ERC	Energy Research Centre
FAC	Flow Accelerated Corrosion
FT	Flow Tube
Gen IV	Generation IV
GFR	Gas-cooled Fast Reactor
GIF	Generation IV International Forum
HTC	Heat Transfer Coefficient
HTS	Heat Transfer System
IPPE	Institute of Physics and Power Engineering
KPI	Kiev Polytechnic Institute
LFR	Lead-cooled Fast Reactor
LMTD	Log-Mean Temperature Difference
LWR	Light Water Reactor
MATLAB	MATrix LABoratory
MSR	Molten Salt Reactor

Mtoe	Million tonnes of oil equivalent
NIST	National Institute of Standards and Technology
NSPH	Net Suction Pump Head
NTU	Number of Transfer Units
PT	Pressure Tube
PV	Pressure Vessel
RANS	Reynolds Averaging Navier Stokes
REFPROP	REFerence fluid thermodynamic and transport PROPerties
RTD	Resistance Temperature Detector
SCW	SuperCritical Water
SCWR	SuperCritical Water-cooled Reactor
SFR	Sodium-cooled Fast Reactor
SPETA	Supercritical Phenomena Experimental Test Apparatus
SS	Stainless Steel
URANS	Unsteady Reynolds Averaging Navier Stokes
VHTR	Very High Temperature Reactor
3D	Three-Dimensional

CHAPTER 1

INTRODUCTION

The demand for energy today is greater than it has ever been with economic expansion and an increasing standard of living across all nations. Moreover, a projected increase of population from 6 billion to 8 billion by 2025 will contribute to a further increase in energy demand. While energy demand for developed countries has slowed down in recent years, the economic expansion of developing countries creates an exponential increase in demand.

Energy produced is mainly used for agricultural, commercial, domestic, industrial, and transportation purposes. Current operational energy sources which include fossil fuels, geothermal, hydroelectric, natural gas, nuclear, biomass, solar, and wind are not sufficient to match the expected growth in energy demand. Energy demand is expected to increase by an average annual rate of 1.7% for the next 20 years and by 2030, the total energy usage is projected to reach 191,895 TWh (16,500 Mtoe) compared to the energy usage of 119,789 TWh (10,300 Mtoe) in 2002 [**1**]. The million tonnes of oil equivalent (Mtoe) represents the amount of energy released by burning one million tonnes of crude oil [**1**]. The yearly electricity demand is expected to reach 31,600 TWh/year in 2030 at an average growth rate of 2.5% per year mainly due to domestic and industrial uses. The anticipated growth rate of electricity exceeds the total energy growth rate which suggests that electricity production is the dominant aspect of energy growth [**1**].

Renewable energy sources including biomass, wind energy, hydroelectric power, and solar energy are viable options; however, geographical locations must be favourable to implement these technologies. In addition to this limitation, they cannot in all scenarios, be controlled to provide a continuous base-load power and some cannot provide power on demand. The majority of the natural gas reserves are located at socioeconomically unstable regions which makes it difficult to extract and transport. As the demand for oil is on the rise, available

resources are declining and newer sources are located in geographic regions that are difficult or expensive to drill. The projected decline in world oil production has made energy the single most important problem facing humanity in the next 50 years [**2**]. Concerns about global climate change due to greenhouse gas emissions have created a concern for traditional fossil fuel coal plants. Greenhouse gas producing methods of energy production, which include fossil fuel such as coal, oil, and natural gas, provide 85% of today's energy needs which makes the dependency on fossil fuel a major environmental concern [**3**]. The development of cleaner and more efficient power is becoming an important aspect of energy production. In order to cope with the surge in crude oil prices and meet the Kyoto protocol, substitute forms of energy with stable prices, as well as carbon free technologies should be used to replace fossil fuels. Nuclear power possesses a number of favourable advantages which make it a viable option for production of the majority of future energy demands. It produces no direct greenhouse gases and outperforms petroleum-based fuels with more energy produced per unit mass. It can be installed in most geographical locations, can be operated safely, and is economically viable. Currently, there are 438 nuclear reactors operating in 30 countries which constitutes of 16% of the global energy and represents the largest non-greenhouse producing share of energy sources [**4**]. Nuclear power produces 15% of the energy sources in Canada and alone provides 52% of the electricity sources for Ontario [**5**].

In 1950, the first generation of nuclear reactors were built for advancement of the CANDU and other reactor technologies. Second generation reactors which became operational in 1970s were built for power distribution for commercial purposes. Significant advancements in economics and safety of the design were incorporated in generation III reactors and a number of them were built mainly in East Asia. Generation III+ nuclear reactors (such as ACR-1000) are being developed as improvements to their predecessors and are near deployment in various countries. The next generation reactors, known as the Generation IV

(GEN IV) reactors, are under development and the deployment of the first Gen-IV nuclear reactor is scheduled for 2030. The designs of these reactors are expected to be highly economical, proliferation resistant, possess improved safety and produce minimal waste. The prospect of the new designs has gained global attention and stimulated R&D in development of various GEN IV concepts.

The Generation IV International Forum (GIF) forum was established in 2001 as an international cooperative effort to investigate the future-generation nuclear energy systems that will be adopted since most of the current operating reactors will be out of service by 2030. The countries in the forum include Argentina, Brazil, Canada, France, Japan, the Republic of Korea, Switzerland, the Republic of South Africa, the United Kingdom, and the United States of America. The six systems under consideration are the Gas-Cooled Fast Reactors (GFRs), Lead-Cooled Fast Reactors (LFRs), Molten Salt Reactors (MSRs), Sodium-Cooled Fast Reactors (SFRs), SuperCritical-Water-Cooled Reactors (SCWRs), and Very-High-Temperature Reactors (VHTRs) [**4**]. The SCWR system is highly economical due to its high efficiency and the R&D of this concept is of particular interest to Canada.

Although the background for the development of SCWRs has been established from knowledge of previous LWRs and supercritical fossil-fired power plant systems, no SCWRs have been built. In order to be able to take advantage of the higher efficiencies SCWRs promise, key problems with the application of the supercritical technology in nuclear plants have to be studied. The effect of design input variables such as flow properties, flow stability, efficiency, heat transfer, three-dimensional effects, transient phenomena, pressure drop, and other phenomena need to be extensively understood. The complexity of new systems can be best understood through experiment; however due to the high cost of operating a full-scale system, it is not economical to build one. Scaled down thermalhydraulic systems may be built as substitutes to such systems.

Scaling laws can be applied to develop similarities between the scaled-down system and the actual system under study. Consequently, SCWR systems can be studied to a great extent by reproducing similar conditions in a scaled-down experimental thermalhydraulic loop. Existing experimental loops are insufficient to capture all of the expected phenomena. Datasets can be obtained from experiments and heat transfer correlations can be developed for different boundary and initial conditions from experimental data.

1.1 Objective and Problem Statement

The objective of this thesis is to design an experimental test apparatus to investigate thermalhydraulic phenomena in multiple test geometries at supercritical conditions for different fluids. The test apparatus will be designed for installation at the University of Ontario Institute of Technology Energy Research Centre (ERC). The loop includes components to safely start up and shut down various test sections, produce a heat source to the test section, and to remove rejected heat. The test apparatus will be designed mainly for the following purposes:

- Satisfy test requirements for GEN IV nuclear reactor concepts
- Ensure loop can produce all of the required physical phenomena including 3D effects and deteriorated heat transfer regimes
- Ensure loop fits within the constraints (dimensions and power requirements) of the ERC
- Understand the supercritical fluid phenomenon including 3D effects and deteriorated heat transfer regimes that need to be addressed by the loop

The effect of the mass flux, heat flux, pressure, and test section diameter on thermodynamic properties will be investigated. Heat transfer at supercritical pressures is very different from that at subcritical pressures due to the substantial variations of the physical properties of fluids at around the pseudo-critical

temperature and it is important to investigate the issues that may come up as it applies to SCWRs.

Chapter 2 of this work will discuss the background of Gen IV nuclear reactor technology requirements and capabilities of existing heat transfer loops and will identify the gaps in the existing knowledge that need to be covered by the new facility. Chapter 3 will provide the theory and methodology used to identify the phenomena that the test apparatus must be able to produce and the method to design the test apparatus. Chapter 4 describes computational fluid dynamics and work that has been done to investigate into the phenomena. Chapter 5 will describe the design of the experimental facility. Chapter 6 will discuss how the apparatus meets the requirement of Gen IV design. Chapter 7 will give the concluding remarks and Chapter 8 will give recommendations for future work.

CHAPTER 2

BACKGROUND AND LITERATURE REVIEW

2.1 Nuclear Reactor Technology in Canada

In the 1950s, the early prototype reactors were under development in many countries for the production of electricity. By 1962, the first small-scale prototype CANDU reactor named the Nuclear Power Demonstration (NPD) commenced operation, producing 20 MW of electricity [**6**]. This achievement was followed by the commencement of the Douglas Point prototype in 1967, located at the development site on Lake Huron. The technology for these Generation I reactors formed the basis necessary for larger commercial CANDU units to follow [**6**]. The first two commercial units, of a capacity of 500 MW each, were built at Pickering. Two additional units were added to the Pickering station during the period between 1971 and 1973 and these four units became the Pickering-A station. Four additional units were added at Pickering-B, Bruce-A, and Bruce-B in a multi-unit station concept.

The success of these reactors led Atomic Energy of Canada Limited (AECL) to the development and subsequent sale of four CANDU-6 units. CANDU-6 reactors use heavy water (D_2O) as their coolant and moderator. They operate at a pressure of approximately 10 MPa and at inlet and outlet temperatures of 260 ^{o}C and 310 ^{o}C respectively.

2.2 Generation IV Initiatives

In order to advance the nuclear energy technology to meet future energy demands, the Generation IV International Forum (GIF) was formed. The Generation IV nuclear energy systems are to be licensed, constructed, and operated in a manner that will provide competitively priced and reliable energy.

The main goals set for the GEN IV systems are classified into four areas which include sustainability, economics, safety and reliability, and proliferation resistance. The goals are elaborated as follows:

Sustainability - Generation IV nuclear energy systems will provide sustainable energy that meets clean air objectives, promotes long-term, and effective fuel utilization systems. The system will minimize and manage the nuclear waste by reducing the long-term burden on the environment, thereby protecting public health and the environment.

Economics - Generation IV nuclear energy systems will have a significant life-cycle cost advantage over other energy sources and will possess a low level of financial risk with a possible gain compared to other energy projects.

Safety and Reliability - Generation IV nuclear energy systems will operate in a safe and reliable way and will have a very small probability for and degree of damage to the core with the elimination of offsite emergency response.

Proliferation Resistance and Physical Protection - Generation IV nuclear systems will discourage the development of any weapons-grade materials and provide physical protection against acts of terrorism.

Various nuclear energy systems have been developed based on the GIF goals. The selected Gen IV design concepts were evaluated with the above criteria and a list of viable options has been established.

2.2.1 Generation IV Concepts

Six Generation IV systems have been selected for development [**4**]. These six systems are the Gas-cooled Fast Reactor System (GFR), Lead-cooled Fast Reactor System (LFR), Molten Salt Reactor System (MSR), Sodium-Cooled Reactor System, (SFR), Very-High-Temperature Reactor System (VHTR), and

SuperCritical-Water-Cooled Reactor System (SCWR). A brief description of each follows here:

Gas-Cooled Fast Reactor (GFR): This is a fast neutron helium-cooled system operating at inlet and outlet temperatures of 490 ^{o}C and 850 ^{o}C respectively. It uses a direct Brayton cycle gas turbine for high thermal efficiency. The reference reactor has a thermal output of 600 MW and electrical output of 288 MW_e. Fuel configurations being considered include pin or plate-based fuel assemblies and prismatic blocks [**4**].

Lead-Cooled Fast Reactor System (LFR): This system uses a lead or lead/bismuth eutectic liquid metal as coolant. The reactor has a thermal output of 120-400 MW and a possible coolant outlet temperature of 550 ^{o}C depending on the technology advancement materials. The different power ratings envisioned for this type of reactor include a large monolithic plant option at 1200 MW_e, a modular system rated at 300-400 MW_e, and a battery of 50-150 MW_e that features a very long refuelling interval. This system is designed for distributed generation of electricity and other energy products including hydrogen and portable water [**4**].

Molten Salt Reactor System (MSR): In this system, the fuel is a circulating liquid mixture of sodium, uranium fluorides and uranium. The flow of the fuel through graphite core channels produces heat which is transmitted through heat exchangers to produce power. The reference plant power level is 1000 MW_e. It operates at low pressures below 0.5 MPa and has coolant outlet temperatures above 700 ^{o}C allowing an increase in thermal efficiency [**4**].

Sodium-Cooled Reactor System, (SFR): This reactor uses liquid sodium as coolant. The first is a 150-500 MW_e reactor with a uranium-plutonium-minor-actinide-zirconium metal alloy fuel and the second is a 500-1500 MW_e reactor with a mixed uranium-plutonium oxide as fuel. Both have outlet temperatures ranging from 500 ^{o}C to 530 ^{o}C. The recycle technology of this system is a major aspect of the R&D [**4**].

Very-High-Temperature Reactor System (VHTR): This is helium cooled, graphite moderated fast neutron reactor. The VHTR system has coolant inlet temperature of 600 ^{o}C and can have outlet temperatures above 1000 ^{o}C which makes it suitable for hydrogen production and any other high temperature processes and processes requiring intensive energy. It operates at moderated pressure of 9 MPa and a thermal output of 600 MW [**4**].

The Supercritical Phenomena Experimental Apparatus (SPETA) may be used to perform experiments for other Generation IV concepts other than SCWRs since their temperatures and pressures are within the design limits of the apparatus. However, design changes may be required for GFR experiments and SPETA may not be suitable for VHTR because of the very high outlet temperatures.

2.2.2 SuperCritical Water-Cooled Reactor (SCWR) Concepts

The facility designed in this thesis, will concentrate on the SCWR concept as that is made by Canada. SuperCritical-Water-cooled Reactors (SCWRs) use supercritical water as a coolant which improves thermal efficiency for the system. SCWRs operate at 25 MPa with an outlet temperature up to 650 ^{o}C. Both fast and thermal neutrons SWCRs are being considered. The two reactor design types include the Pressure tube (PT) and Pressure Vessel (PV).

The concept of SCWRs is a modification and combination of various current reactor designs. The concept of high pressure is obtained from Pressurised Water Reactors (PWR) which operate at 16 MPa and current supercritical coal plants that operate up to 30 MPa. Some experimental reactors use superheaters with outlet temperatures above the critical temperature of water, but below the pseudocritical point. A direct cycle where steam from the core is fed directly to the turbine is used in Boiling Water Reactors (BWRs). Lastly, modern supercritical water turbines that operate at pressures of 25-30 MPa and inlet temperatures of about 600 ^{o}C have successfully operated at thermal plants for many years. Light water is used as coolant in SCWRs just like Light Water

Reactors (LWRs). The base technology for the design of SCWRs is available due to its similarities with current LWRs.

Supercritical water technology has been applied to coal-fired plants and there have been improvements in the balance of plant technology (i.e., turbine). The breakthroughs in materials engineering technology have made the concept of SCWRs more attractive in recent years. Due to their similarities, SCWRs are expected to have success at adopting some of the materials and structures technology advancements in supercritical fossil-fired plants.

SCWRs have some advantages that make them feasible candidates for the Generation IV concept. Some of these advantages include:

- SCWRs can offer higher efficiency of 40-45% compared to the 30-35% efficiency that can be obtained in LWRs.
- Since the coolant exists as a single phase, the deteriorated heat transfer that occurs during dry out or nucleate boiling is eliminated.
- The use of steam dryers, steam separators, recirculation pumps and steam generators can be eliminated and SCWR design can use fewer components providing a simplified reactor design.
- There is a reduction in the operational cost of the plant in savings from a higher output per mass of uranium, reducing uranium cost.
- SCWR can support co-generation of hydrogen due to higher temperatures.

The two SCWR reactor types currently proposed are a large reactor PV with wall thickness of 0.5 m or greater to contain the reactor core or using set PT. The PV-type reactor as seen in Figure 2.1 is similar to the PWRs/BWRs and is being developed by the United States [**7**]. The PT-type reactor as seen in Figure 2.2 is similar to the conventional CANDU or RBMK reactors. It is being developed in

Canada and Russia by the Atomic Energy of Canada (AECL) and the Research and Development Institute of Power Engineering (RDIPE and NIKIET) respectively [**7**].

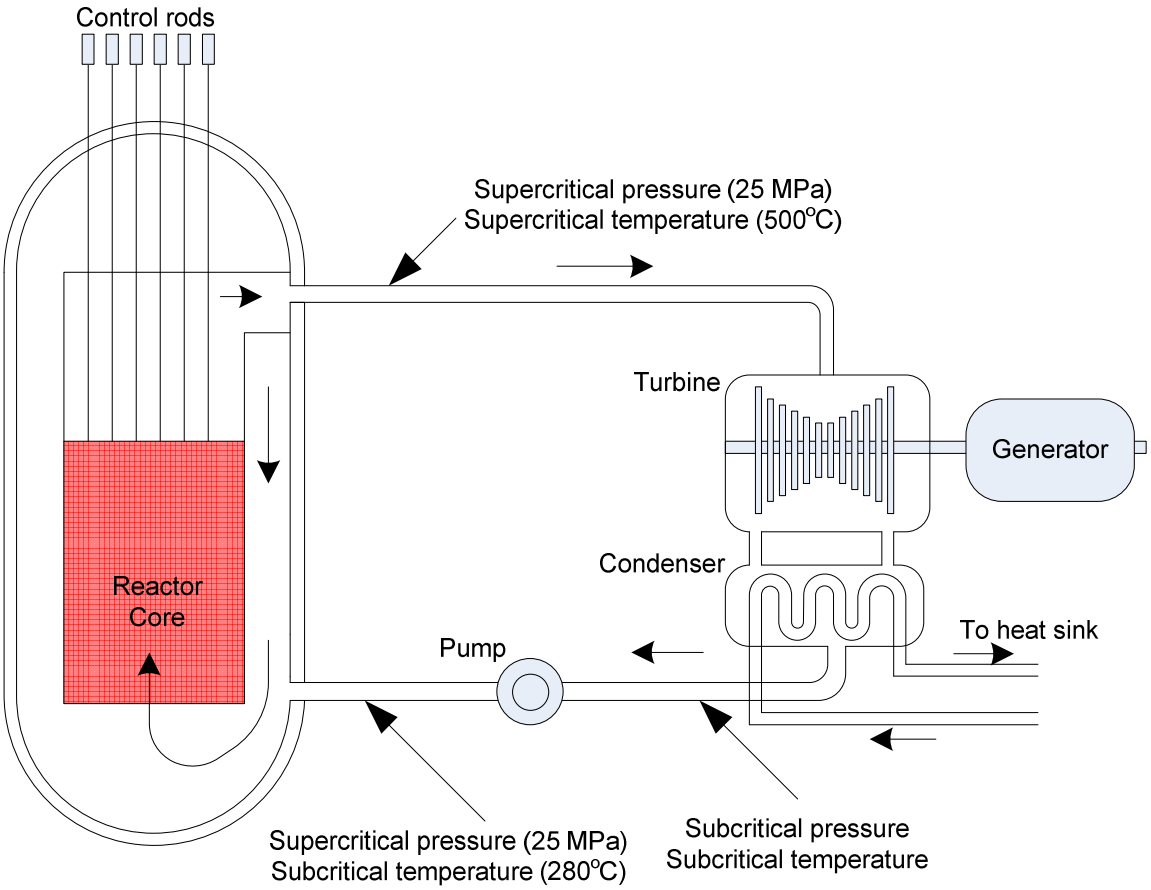

Figure 2.1: United States Pressure Vessel SCWR Concept

The pressure vessel option is a direct cycle design. The pressure is used to pressurise the feed water to the reactor core and superheated steam from the reactor is directed to the turbine to generate electricity. The steam is then condensed and pumped back to the reactor. The start up for SCWRs is an important aspect that needs to be studied. The pumps in the PV concept provide

pressurization for the SCWRs. An important aspect that needs to be studied is a method of keeping superheated steam contained in the PV and away from the high pressure pumps. Superheated steam is however needed in the reactor core and the turbine for improved heat transfer and higher efficiency. The method of control needs to be investigated.

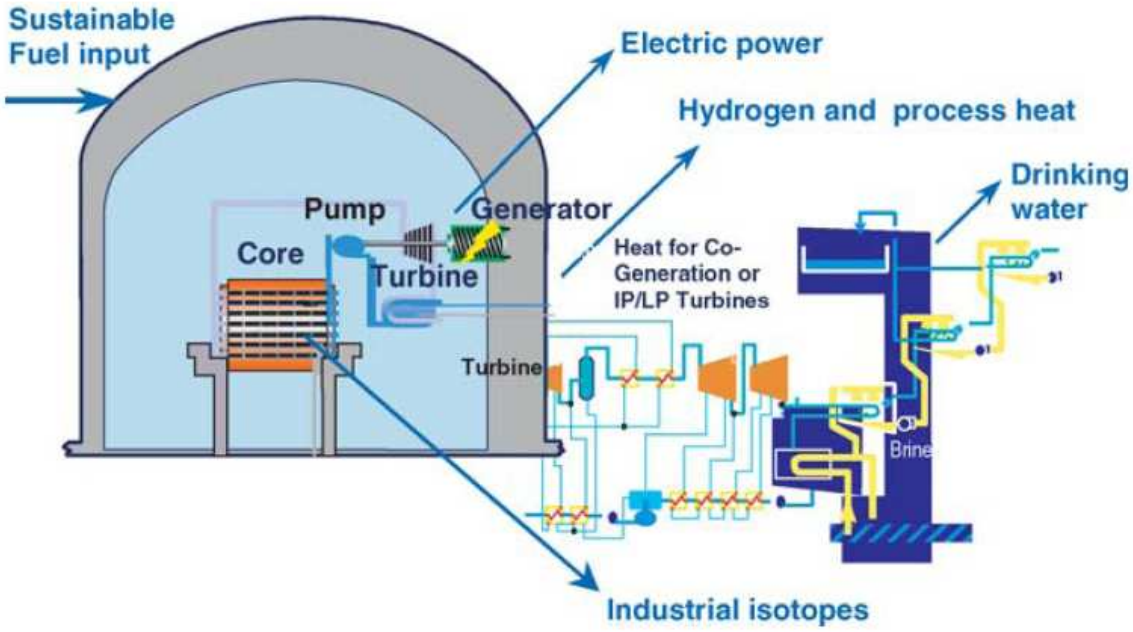

Figure 2.2: Pressure Tube SCWR for Multipurpose Application [7]

The PT design as shown in Figure 2.2 is similar to conventional Heavy Water Reactors with the added flexibility of changing the input parameters such as the heat flux and coolant flow rate which is not present in PV Reactors. The pressure channel design includes the fuel design, channel power, core lattice pitch, and flow circuit parameters. To reduce the severe axial flux variation due to the large drop in density as the coolant is heated, a re-entrant arrangement option has been proposed. The re-entrant option in the PT option contains the coolant flowing downwards unheated and heated in the upward flow. In the PV design, the coolant flows in opposite directions as the PT coolant flow. In both designs,

the pressure boundary temperatures can be reduced by partly insulating the pressure-retaining vessel of the channel wall using the first pass of the unheated flow.

Three thermodynamic cycle options being considered for SCWRs include the direct, indirect, and dual cycle. The direct cycle has the highest efficiency of the options since it eliminates the need for steam generation. The supercritical water from the reactor is fed directly to the turbine. In the indirect and dual cycles, heat exchangers are used to transfer the heat to the feed water to the turbine at steam temperature of 600 ^{o}C and pressure of 25 MPa. Supercritical water to supercritical water and supercritical water to superheated steam are the two concepts of heat exchangers being considered [**8**]. The coolant is limited to the primary side in the indirect and dual cycles making them desirable from a safety point of view.

SWCRs have a unique advantage of requiring very low coolant mass-flow rates because of the high thermal capacity. Mass-flow rates can be up to eight times less than modern PWRs, reducing pumping power and saving operating cost. The reduced mass-flow rate is as a result of improved transport properties around the pseudocritical point of water.

SCWRs are anticipated to have an improved efficiency of 45 - 50 % from current nuclear power plants which is around 30 - 35 %. The improved efficiency is best explained by the supercritical water properties (which are discussed shortly). A phase change beyond the pseudocritical point of water provides better transport properties which increases the heat removed from the reactor core by the coolant. The fluid phase above the pseudocritical point has steam-like density and liquid-like conductivity which improve its heat transport properties. Specific heat capacity peaks around the pseudocritical point and decreases beyond this point which suggests phenomena occurring in this range that needs to be further studied and understood.

2.2.3 SuperCritical Water (SCW) Properties

At a specific temperature and pressure, the liquid and gaseous phases of a fluid become indistinguishable. The critical point of a fluid, which is characterized by T_{cr} and P_{cr}, is defined as the point at which the fluid exists as a single phase. The fluid exhibits both liquid and gaseous properties. The critical pressure for water is 22.064 MPa and the critical temperature of water is 373.95 ^{o}C [**8**]. At higher pressures, this occurs at higher temperatures as shown by the pseudocritical line on a pressure-temperature diagram as shown in Figure 2.3.

There is a significant change of fluid properties around the pseudocritical point. SCWRs operate at a pressure of 25 MPa and the properties at this pressure are of particular interest. The pseudocritical temperature at this pressure is 384.9 ^{o}C. Figure 2.4 (a-f) show various fluid properties at a pressure of 25 MPa. The thermophysical properties including specific heat, density, thermal conductivity, dynamic viscosity, kinematic viscosity, and Prandtl number are obtained from NIST REFPROP (National Institute of Standards and Technology, REFerence PROPerties) [**9**] at 0.1 ^{o}C intervals.

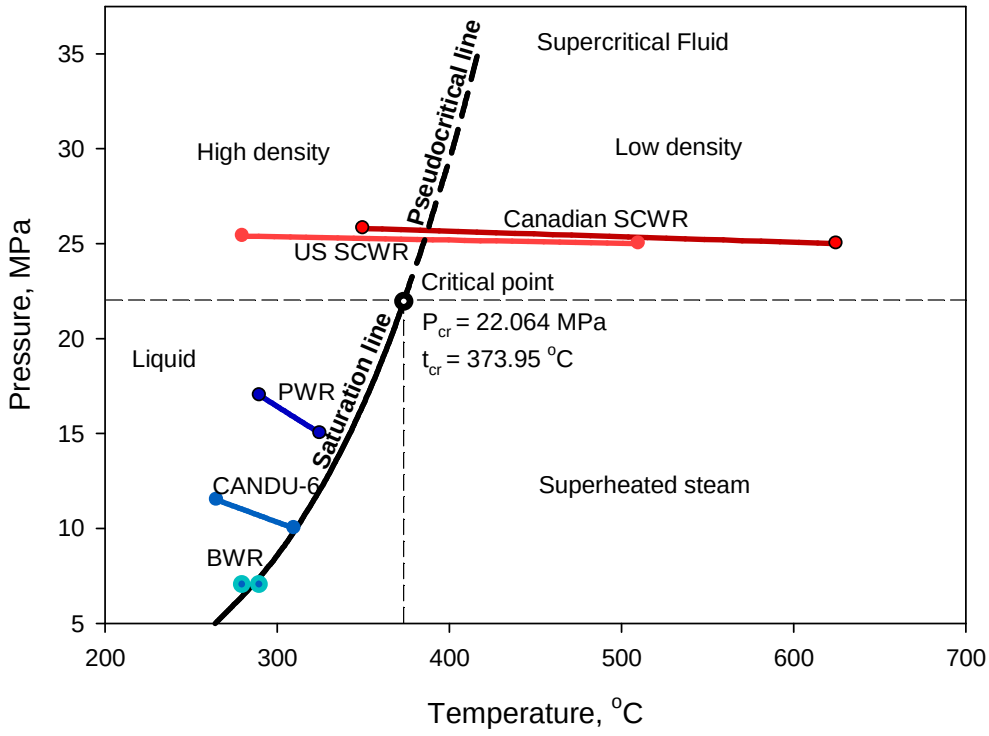

Figure 2.3: Typical operating conditions of SCWR, BWR, PWR, and CANDU-6

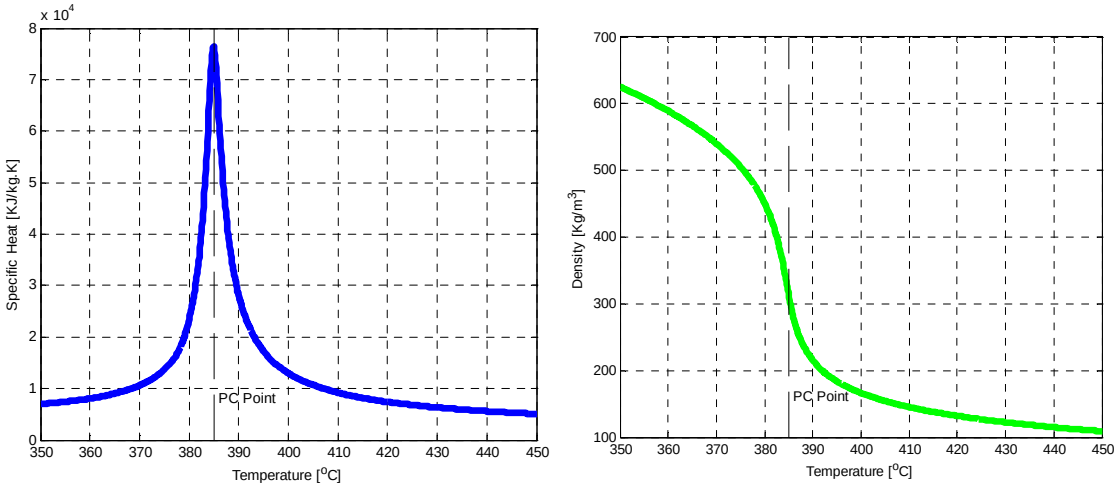

Figure 2.4 (a): Specific Heat vs. Temperature of water in the pseudocritical region at 25 MPa, **(b):** Density vs. Temperature of water in the pseudocritical region at 25 MPa

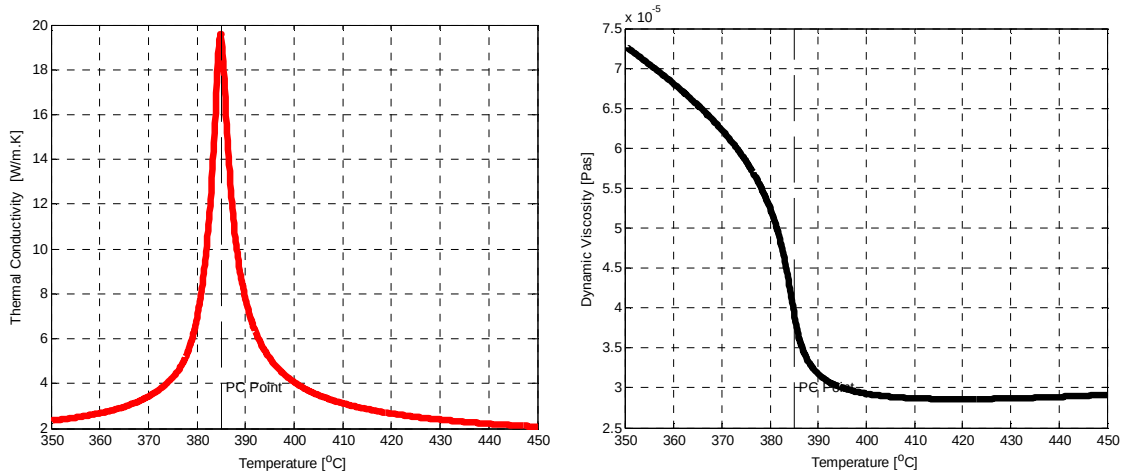

Figure 2.4 (c): Thermal Conductivity vs. Temperature of water in the pseudocritical region at 25 MPa, **(d):** Dynamic Viscosity vs. Temperature of water in the pseudocritical region at 25 MPa

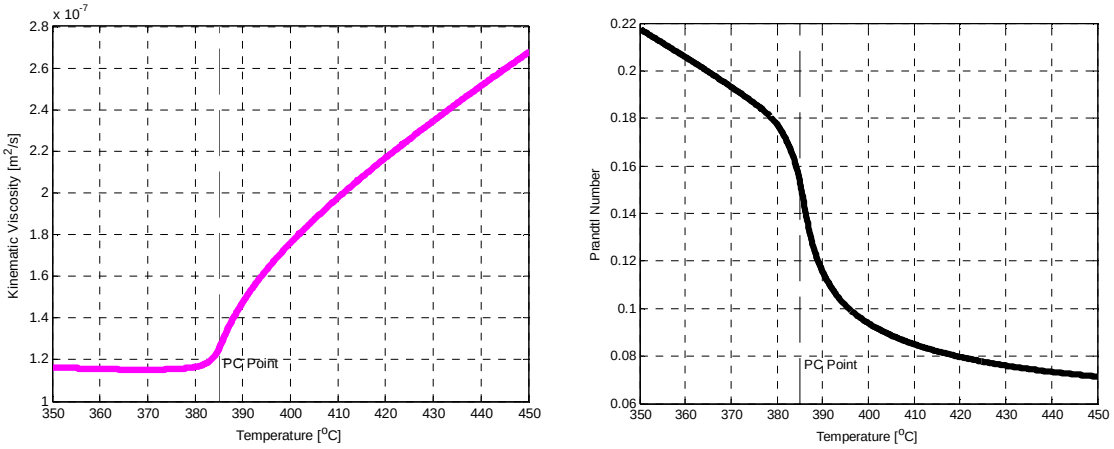

Figure 2.4 (e): Kinematic Viscosity vs. Temperature of water in the pseudocritical region at 25 MPa, **(f):** Prandtl Number vs. Temperature of water in the pseudocritical region at 25 MPa

The properties of water show the most significant changes within ±15 ^{o}C of the pseudocritical point. Specific heat and thermal conductivity peak at the pseudocritical point at and rises at exponential rates. Density, dynamic viscosity, and Prandtl number show a drastic reduction before and after the pseudocritical point. Density and dynamic viscosity have their point of inflection at the pseudocritical point while Prandtl number changes slope about 2-3 ^{o}C after the pseudocritical point. The kinematic viscosity remains relatively constant before the pseudocritical point, but increases with a decreasing exponential slope thereafter.

The nature of variation of the thermodynamic and transport properties around the pseudocritical point creates a complex relationship in the heat transport equations that have been simplified in numeric models and thus cannot be captured by numeric simulations. Experimental work has to be performed to gather data and study how the heat transfer equations are affected and how they can be modified to account for the varying fluid properties around the pseudocritical region.

2.3 Review of Existing Supercritical Water Loops

Supercritical water loops are designed to operate in the pseudocritical range. Experiments that have been performed have used different test sections including vertical flow in circular tubes which is the most investigated arrangement for the test section. SCW loops typically operate at pressures up to 25 MPa with inlet temperatures ranging from 300 ^{o}C to 380 ^{o}C and outlet temperatures up to 600 ^{o}C. A review of existing supercritical water loop test facilities follows.

2.3.1 Institute of Physics and Power Engineering (IPPE) SCW Test Facility, Obninsk, Russia

This loop (Figure 2.5) uses distilled and de-ionized water and operates at pressures up to 28 MPa with outlet water temperatures up to 500 ^{o}C [**7**]. Water flows from the pump through a flowmeter before it is preheated. The flow continues through the test section as the water gets heated. Cooling is achieved downstream of the test section by using a mixing cooler. Heat is removed from the water by heat exchangers in the main loop before it flows back to the pump. High pressure gas N_2 is used to pressurize the loop [**7**].

The test section is a vertical stainless steel circular tube (12Cr18Ni10Ti, thermal properties are similar to SS 304) with ID, 10 mm, wall thickness 2 mm, and average surface roughness of R_{ave} = 063 - 0.8 µm. Two heated circular rods 1 m and 4 m length have been used. The test section is heated by an AC supply of 600 kW (uniform heat flux) with electrical current passing from the inlet to the outlet power terminals (copper clamps). The test section is wrapped with thermal insulation to minimize heat loss. Table 2.1 shows the operating conditions of the IPPE supercritical water loop.

Table 2.3 shows a list of the operating conditions of the experiments that have been performed on supercritical water in bare tubes. Horizontal and vertical orientations have been investigated for bare tubes. Although bare tubes have been investigated extensively, there has not been a lot of study on other geometries.

The operating conditions for the IPPE loop are given in Table 2.1.

Table 2.1: Operating conditions of IPPE supercritical water loop [7]

P (MPa)	T_{in} (^oC)	T_{out} (^oC)	T_w (^oC)	q (kW/m^2)	G (kg/m^2s)
24.5 - 25	300 - 380	360 - 390	<700	90 - 1050	200; 500; 1000
24	320 - 350	380 - 406	<700	160 - 900	500; 1000; 1500

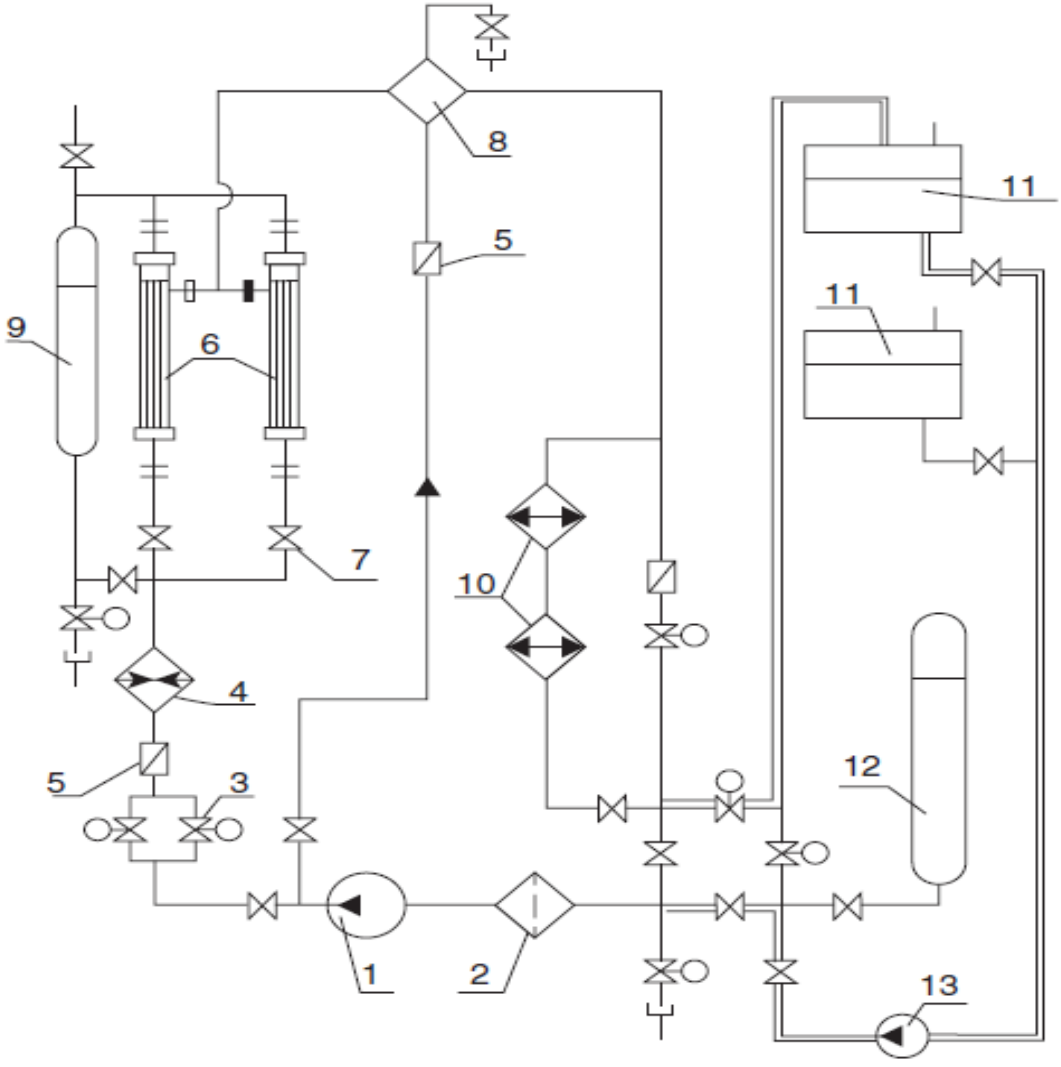

Figure 2.5: Schematic of the Institute of Physics and Power Engineering (IPPE) loop [7]; 1-circulating pump, 2-mechanical filter, 3-regulating valves, 4-electrical heater, 5-flowmeter, 6-test section, 7-throttling valve, 8-mixer-cooler, 9-discharge tank, 10-heat exchangers-main coolers, 11-feedwater tank, 12-volume compensator, and 13-feedwater pump

2.3.2 Kiev Polytechnic Institute (KPI) SCW Test Facility, Kiev, Ukraine

Figure 2.6 shows the schematic of the SCW loop design for the KPI test facility [**7**]. It operates at pressures up to 28 MPa and outlet temperatures up to 600 ^{o}C. Water with a pH of 7.2 is used in the loop. Water is pumped from a reservoir to the loop with boosting and two main plunger pumps connected in parallel. A set of pressure valves and a turbine-type flowmeter are located before the preheater. The preheater is a tube-in-tube type with a rating of 75 kW. The test section is then heated and the water is cooled by a tube-in-tube cooler and passes through a set of throttling valves before it returns to the reservoir.

The test section is a vertical stainless steel circular tube (1Cr18Ni9Ti) [**7**]. The heated test sections used had lengths of 0.36 m and 0.6 m for an inner diameter of 6.28 mm, and lengths of 0.4 m and 0.6 m for an inner diameter of 9.5 mm with average surface roughness of 0.25 - 0.5 μm. Upward and downward flows have been investigated. Thermocouples were used to measure bulk-fluid temperatures. The test sections were heated by an AC supply of 120 kW (60 V × 2000 A) or DC supplies of 90 kW (18/36 V × 5000/2500 A). Table 2.2 shows the operating conditions of KPI supercritical water loop. The operating conditions of the KPI loop are given below.

Table 2.3 shows a list of SCW experiments that have been performed in circular tubes. This table was created to show the operating pressures, temperatures, heat fluxes, mass fluxes, and orientations of experiments performed at supercritical conditions for water. The sets of range of experiments have been obtained from a reference publication [**7**] and may not be available in English.

Table 2.2: Operating conditions of KPI supercritical water loop [7]

P (MPa)	T_{in} (^{o}C)	H_{in} (kJ/kg)	q (kW/m^2)	G (kg/m^{2}s)
23.5	20 - 380	106 - 2222	≤515	250; 500

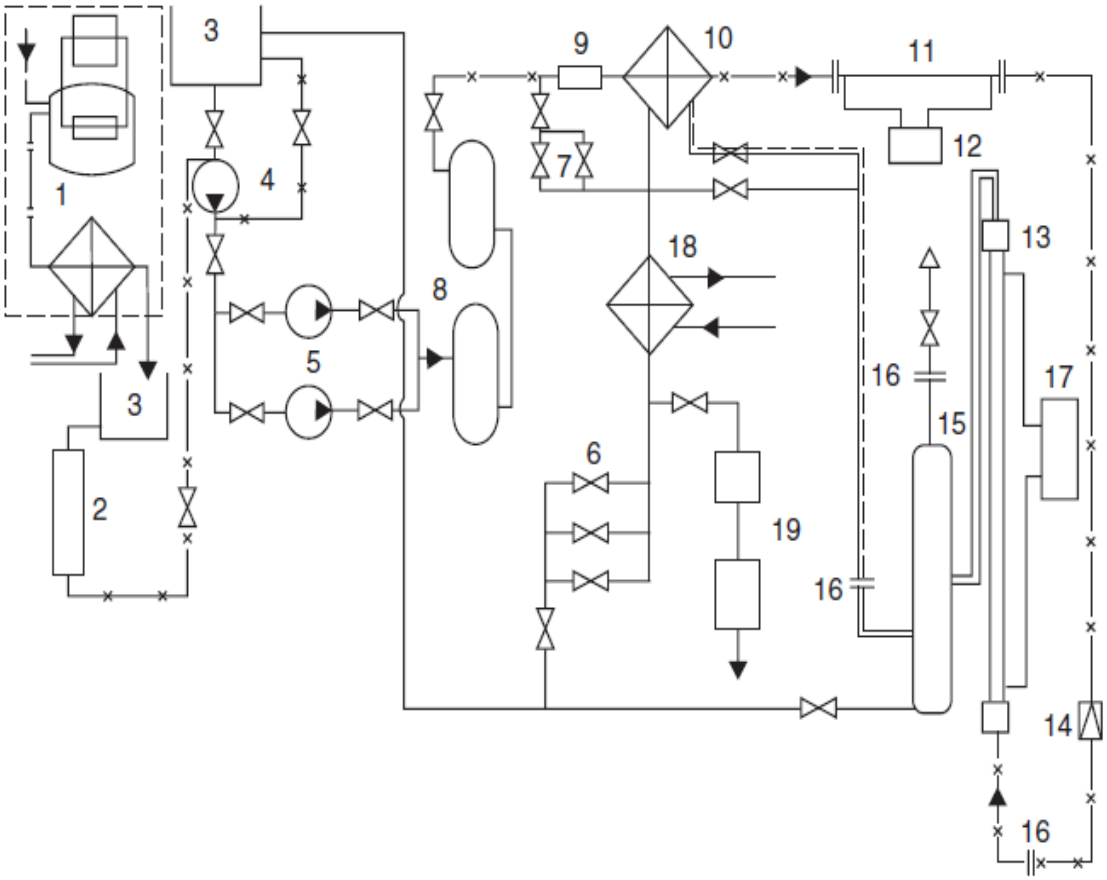

Figure 2.6: General schematic of SCW KPI experimental setup [7]; 1-electro-distillator, 2-ion-exchange filter, 3-accumulator reservoirs, 4-boosting pump, 5-plunger pumps, 6 and 7-regulating valves, 8-damping reservoir 9-turbine flowmeter 10-heat exchanger, 11-electrical preheater, 12-electrical generator(s), 13-test section, 14-throttling valve, 15-damping reservoir, 16-electro-isolating flanges 17-main power supply, 18-cooler, 19-throttling valve

Table 2.3: Range of investigated operating parameters for experiments with water flowing in circular tubes at supercritical pressures

Reference	P (MPa)	T (^{o}c)	q (kW/m^2)	G (kg/m^{2}s)	(Geometry) Flow Direction
Yamagata et al 1972 [10] in [7]	22.6-29.4	T_{in}=230 - 540	116 – 930	310 - 1830	(D/L=7.5/1.5; 10/2 mm/m) Horizontal and vertical SS tubes: Upward, downward and horizontal flow
Alekseev et al 1976 [11] in [7]	24.5	T_{in}=100-350	100-900	380-820	(D/L=10/4 mm/m) Vertical tube
Bazargan et al. 2005 [12] in [7]	23-27	T_{in} =405-670	≤310	330-1230	(D/L=6.3/1.5 mm/m) Horizontal Inconel tubes: Horizontal flow
Barulin et al. 1971 [13] in [7]	22.5-26.5	T=50-500 T_w=60-750	200-6600	480-5000	(D=3;8;20mm L/D<300) Upward downward and horizontal flow
Randall 1956 [14] in [7]	27.6-55.2	T=204-538 T_w=204-760	310-944	2034-5425	(D=1.27; 1.57; 1.9 mm L=0.203 m) Hastelloy C vertical tube
Doroshchuk et al 1959 [15] in [7]	24.3	T=100-250	3060-3900	3535-8760	(D=3 mm L= 0.246 m) Downward flow
Shitsman 1962 [16] in [7]	22.8-26.3	T_b=300-425 T_w=260-380	291-5820	100-2500	(D_{ext}=46 mm L= 0.17 m) Upward and horizontal flow
Shitsman 1963 [17] in [7]	22.6-24.5	T=280-580	280-1100	300-1500	(D=8 mm L= 1.5 m) SS tube
Swenson 1965 [18] in [7]	23-41	T=75-576 T_w=93-649	200-1800	542-2150	(D=9.42 mm L= 1.83 m)
Smolin and Polyakov 1965 [19] in [7]	25.4; 27.4; 30.4	T_b=250-440	700-1750	1500-3000	(D=10; 8 mm L= 2.6 m) Upward flow
Vikhrev et al 1967 [20] in [7]	24.5; 25.3	H=230-2750	230-1250	485-1900	(D=7.85; 20.4 mm L= 1.515; 6 m)
Shitsman 1967 [21] in [7]	24.3-25.4	T=300-320	730-520	600-690	(D= 8; 16; mm L= 1.5; 1.6 m) Upward and horizontal flow
Bourke and Denton 1967 [22] in [7]	23.0-25.4	T=310-380	1200-2200	1207; 2712	(D= 4.06 mm L= 1.2 m)
Styrikovich et al. 1967 [23] in [7]	24	H=1260-2500	350-870	700	(D= 22)
Krasyakova et al. 1967 [24] in [7]	23; 24.5	H=400-2721	100-1400	90-2000	(D= 20 mm L= 2.8 m) Upward, downward and horizontal flows
Krasyakova et al. 1977 [25] in [7]	24.5	H=400-1900	100-1400	90-2000	(D= 20 mm) Upward and downward flows
Alferov et al. 1969 [26] in [7]	14.7-29.4	T=160-365	170-600	250-1000	(D/L=14/1.4; 20/3.7 mm/m)

Reference	P (MPa)	t (^oC)	q (kW/m^2)	G (kg/m^2s)	(Geometry) Flow Direction
Ackerman 1970 [27] in [7]	22.8-41.3	T_{in}=77-482	126-1730	136-2170	Smooth (D=9.4; 11.9, 24.4 mm, L=1.83 m; D=18.5 mm L=2.74 m) and ribbed (D=18 mm, L=1.83 m, six helical ribs, pitch 21.8 mm) tubes
Ornatskiy et al. 1971 [28] in [7]	22.6; 25.5; 29.7	H=100-3000	400-1800	500-3000	(D=3 mm, L=0.75 m) Upward and downward flows
Belyakov et al. 1971 [29] in [7]	24.5	H=420-3140	230-1400	300-3000	(D=20 mm, L4-7.5 m) Vertical and horizontal SS tube: Upward and horizontal flows
Glushchenko et al. 1972 [30] in [7]	22.6; 25.5; 29.5	H=85-2400	1150-3000	500-3000	(D=3; 4; 6; 8 MM, l=0.75-1 m) Upward flow; D=3 mm downward flow
Chakygin et al 1974 [31] in [7]	26.5	T_{in}=220	-	445-1270	(D=10 mm, L=0.6 m) Upward and downward flows
Lee and Haller 1974 [32] in [7]	24.1	T=260-383	250-1570	542-2441	(D=38.1; 37.7 mm, L=4.57 m)
Alferov et al. 1975 [33] in [7]	26.5	T=80-250	480	447	(D=20 mm, L=3.7 m) Upward and downward flows
Kamenetskii 1975 [34] in [7]	23.5; 24.5	H_{in}=100-350	1200	50-1700	(D=21; 22 mm, L=3 m) Non-uniform circumferential heat flux
Harrison and Watson 1976 [35] in [7]	24.5	T=50-350	1300-2300	940; 1560	(D=1.64; 3.1 mm, L=0.4, 0.12 m) Vertical and horizontal flows
Watts and Chou 1982 [36] in [7]	25	T=150-310 T_w=260-520	175-440	106-1060	(D=25; 32.2 mm, L=2 m) Upward and downward flow
Kirillov et al. 1986 [37] in [7]	25	T_{in}=385	400;600	1000	(D=10 mm, D_{ext}=14 mm, L=1 m)
Razumovskiy et al. 2005 [38] in [7]	23.5	T_{in}=20-380	<515	250-500	(D=6.28-9.5 mm) Vertical flow
Chen 2004 [39] in [7]	24	H_{in}=1350; 1600	300	400	SS vertical and inclined tubes (smooth with uniform and non-uniform radial heating and ribbed)
Pis'mennyy et al. 2005 [40] in [7]	23.5	T_{in}=20-380	<515	250;500	(D=6.28 mm L=600; 360 mm; D=9.50 mm L=600; 400 mm) Vertical SS tubes
Kirillov et al. 2005 [8] in [7]	23-25	T_{in}=300-380	90--1050	200-2000	(D=10 mm, L=1.4 m) Vertical SS tubes
Seo et al. 2005 [41] in [7]	23-24.5	H_{in}=1500; 2500	210-933	430-1260	(D=7.5-8 mm) Vertical flow
Treshchev et al. 1977 [42] in [7]	23-25	T_{in}=300	815	750	-
Goldmann 1961 [43] in [7]	34.5	T=204-425	291-5820	100-2500	(D_{ext}=46 mm, L=0.17 m) Upward and horizontal flows
Malkina et al. 1972 [44] in [7]	24.5-31.4	T=20-80	470-2300	U=7-10 m/s	(D=2; 3 mm, L=0.15 m) Upward flow

2.3.3 Supercritical CO_2 and Freon Loops

Although water has been the most investigated fluid in the near-critical and supercritical regions, experimental studies using supercritical water require high pressure, high temperature, and high electrical power. The high power requirement of these experiments can be costly, unaffordable, and can sometimes introduce technical difficulties. In order to mitigate this challenge, heat transfer experiments can be performed in scaled model systems. Two scaling modelling techniques are available: geometric modelling and fluid modelling. The geometric modelling technique simplifies the flow channels to circular tubes or small rod bundles instead of full scale prototype rod bundles. Fluid scaling modelling technique involves using a substitute fluid for water. Typical fluids have critical pressures and temperatures significantly lower than that of water. The scaling procedure ensures that the physics determining the dynamics of the system are almost completely preserved. Fluid-to-fluid scaling of SCW loops can be done with minimal design modifications to the loop. By proper selection of surrogate fluids and operating pressure and temperature, the heat power required can be significantly reduced making it economical to run supercritical fluid experiments. A direct approach to validate the scaling method is done by comparing different versions of test data obtained from experiments using different fluids.

Carbon dioxide is often used as a working supercritical fluid in various thermodynamic cycles and can be used as substitute fluid. Carbon dioxide is often used as the working fluid in various thermodynamic cycles and heat transfer experiments because of its lower critical pressure and temperature. CO_2 which has a much milder critical condition (7.38 MPa, 31.0 ^{o}C) than that of water shows similar characteristics to water. In this respect, CO_2 can be used as a surrogate fluid to take advantage of the low experimental cost. It is the next most investigated fluid at near-critical and supercritical regions after water. Some other substitute fluids that have been used include Freon compounds [**45**,**46**]. Table 2.4 shows the properties at the critical point of various fluids. The critical point of

CO_2 is much lower than water and Freon compounds have even lower critical points making them preferred for supercritical fluid experiments at lower heat fluxes.

Figure 2.7 shows a typical CO_2 test loop. It is initially charged with CO_2 by an air-driven compressor. A gear pump drives the CO_2 through the test section and it heats up. An accumulator filled with nitrogen gas, is located at the discharge of the pumps and is used to reduce any fluctuations in flow. It is then cooled down by the heat exchanger to a pre-set temperature and then circulated through the loop before it returns back to the pump. Water is used as a coolant in the heat exchanger. The pre-heater and power supply control the bulk inlet and outlet temperatures of the fluid. Manual flow controls are used to control flow and a Coriolis-type flow meter is used to measure flow.

Table 2.4: Critical Parameters of water, CO_2, and Freon compounds [9]

Fluid	P_{cr} (MPa)	T_{cr} (^oC)	ρ_{cr} (kg/m^3)
Water	22.06	374.0	322.4
CO_2	7.38	31.0	467.6
Freon-12	4.14	112.0	565.0
Freon-134a	4.06	101.1	511.9

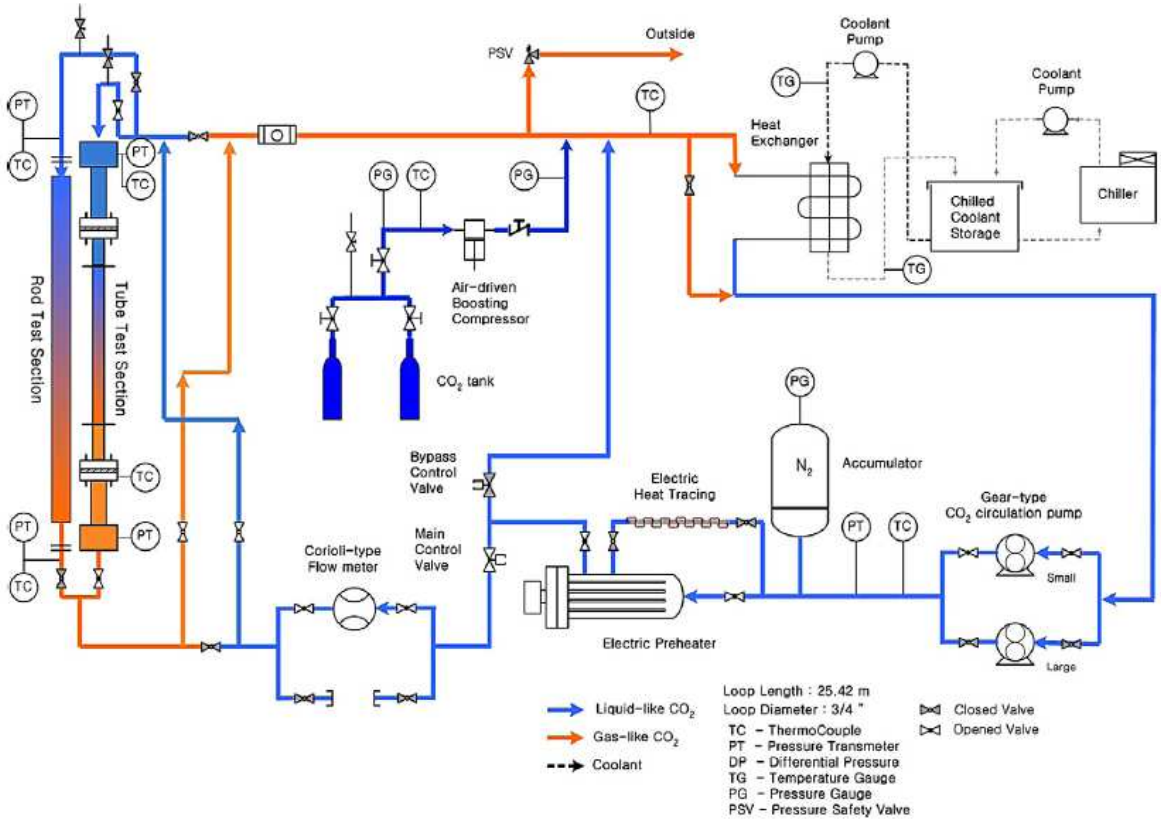

Figure 2.7: Schematic of SPHINX test facility [47]

Table 2.5: Operating conditions of SPHINX supercritical CO_2 loop [47]

P (MPa)	T_{in} (^oC)	T_{out} (^oC)	q (kW/m^2)	G (kg/m^2s)
8.14 - 8.93	5 - 37	80-100	30-170	285-1200

The test section is a vertical 3 m (heated length of 2.65 m) long tube made of Inconel 625. The inner diameter of the test loop is 6.32 mm and a tube of inner diameter of 20 mm was used for the main loop. Upward and downward flows are measured. Thermocouples are attached onto the tube at 50 mm intervals to measure wall temperatures. The main loop is insulated to minimize any heat loss to the atmosphere. The operating conditions of this loop are listed in Table 2.5.

Table 2.6 shows the experiments that have been performed with supercritical CO_2. This table was created to show the operating pressures, temperatures, heat fluxes, mass fluxes, and orientations of experiments performed at supercritical conditions for CO_2. Fluid flow through a vertical tube test section arrangement was used in majority of the experiments.

Table 2.7 shows the experiments performed on Freon compounds. This table shows the operating pressures, temperatures, heat fluxes, mass fluxes, and orientations of experiments performed at supercritical conditions for Freon-12. Only a few experiments have been performed using Freons at supercritical conditions and there is not a lot of data available. More experimental work is needed to study supercritical heat transfer in Freons.

Table 2.6: Range of investigated parameters for experiments with CO_2 flowing in circular tubes at supercritical pressures

Reference	P (MPa)	T (^oC)	q (kW/m^2)	G (kg/m^2s)	(Geometry) Flow Direction
Bringer and Smith 1957 [48**] in [**7**]**	8.3	T_{in}=21-49	31-310	100-1300	(D=4.57 mm L=0.61 mm) Inconel tube
Petukhov et al. 1961 [49**] in [**7**]**	8.8-10.8	T_{in}<21 T_{out}<49	-	Re=(50-300)>10^3	(D=6.7 mm, L=0.67 m) Copper tube
Wood and Smith 1964 [50**] in [**7**]**	7.4	T_{in}<27.5 T_{out}<31.4	30-120	U=3-5 m/s	(D=22.9 mm, L=1.435 m)
Krasnoshechekov and et al. 1966 [51**] in [**7**]**	7.9; 9.8	20-110	430-2520	1135-7520	(D=4.08 mm, L=0.208 m) SS tube
Tanaka et al. 1967 [52**] in [**7**]**	9.2	27-40	14-81	m=0.23-0.47 kg/s	(10 mm) Natural circulation
Shiralkar et al. 1969 [53**] in [**7**]**	7.6, 7.9	T_{in}=10-32	125-190	680-2710	(D=6.22; 3.175 mm, L=1.52 m)
Bourke et al. 1970 [54**] in [**7**]**	7.44-10.32	T_{in}=15-35	8-350	311-1702	(D=22.8 mm, L=4.56 m) SS tube upward and downward flows
Ikryannikov et al. 1972 [55**] in [**7**]**	7.8-9.8	T_{in}=15-50	5.8-9.3	Re=(30-500).10^3	(D=29 mm, L=2.3 m) SS tube
Petukhov et al. 1972 [56**] in [**7**]**	9.8	T_{in}=12-13	85-505	960	(D=4.3 mm, L=0.33 m) Upward flow
Silin 1973 [57**] in [**7**]**	7.9; 9.8	T_w<860	<1100	200-2600	(D=2.05; 4.28 mm) Vertical and horizontal tubes
Miropol'skiy and Baigulov 1974 [58**] in [**7**]**	7.9	T_{in}=22-30	67-224	670-770	(D=21 mm, L=1.7m) Copper tube
Baskov et al. 1974 [59**] in [**7**]**	8; 10	T_{in}<17 T_{out}<212	≤640	1560-4170	(D=4.12 mm, L=0.375m)
Protopopov and Sharma 1976 [60**] in [**7**]**	7.5; 8; 9; 10	T_{in}=14-54	3.5-110	-	(D=9.2; 19.6 mm)
Fewster 1976 [61**] in [**7**]**	7.6	T_{in}=10-25	10-300	180-2000	(D=8;19 mm, L=1 m) Vertical SS tube
Ankudinov and Kurganov 1981 [62**] in [**7**]**	7.7	T_{in}=20	<1540	2100-3200	(D=8 mm, L=1.84 m) Vertical and horizontal tubes with helical wire insert

Reference	P (MPa)	T (^oC)	q (kW/m^2)	G (kg/m^2s)	(Geometry) Flow Direction
Vlakhov et al. 1981 [63**] in [**7**]**	-	-	0.5-20	0.8-6.2	(D=7.85 mm, L=1.52 m) Vertical SS tube
Afonin and Smirnov 1985 [64**] in [**7**]**	0.98-9.8	H_{in}=730	180-1250	100-1100	(D=6 mm, L=2.5 m) Steel tube
Dashevskii et al. 1987 [65**] in [**7**]**	7.5-7.9	T_{in}=29.5-54.7	0.5-85	1.9-265	(D=7.85 mm, L=1.52 m) Downward flow
Kurganov and Kaptil'nyi 1993 [66**] in [**7**]**	9	T_{in}=25-35	40-260	800; 1200	(D=22.7 mm) Upward and downward flow
Walisch et al. 1997 [67**] in [**7**]**	8-40	50-120	Q=0.4-2 kW	m=0.8-50 g/s	(D=10 mm, L=1.5 m) Inconel 600 tube
Pettersen et al. 2000 [68**] in [**7**]**	8.1-10.1	15-70	10-20	600-1200	(D=0.79 mm, L=540 mm) 25 Parallel circular channels
Liao and Zhao 2002 [69**] in [**7**]**	7.4-12	T_{in}=20-110	$(1\text{-}20).10^4$	m=0.8-50 g/s	(D=0.70; 1.4; 2.16 mm, L=0.11 m)
Jackson et al. 2003 [70**] in [**7**]**	7.25-8.27	T_{in}=8-20	5-57	100-560	(D=19.05 mm, L=2.46 m) Upward and Downward flows
Fewster and Jackson 2004 [71**] in [**7**]**	7.6	T_{in}=10	50-460	300-3300	(D=5.08; 7.88 mm, L=1.2) Upward and downward flows
Jiang et al. 2004 [72**] in [**7**]**	9.5	T_{in}=33-51	31-108	m=1.5-4.2 kg/h	(D=0.95 mm, L=0.05 m) Copper tube (D=4 mm) Porous tube (D= 4 mm, particle OD 0.2-0.28 mm)
Kim et al. 2005 [73**] in [**7**]**	7.8; 8.1; 8.9	T_{in}=27	<150	400-1200	(D=4.4 mm, L=2 m) Vertical Inconel tube upward flow
Pioro and Khartabil 2005 [74**] in [**7**]**	7.4-8.8	T_{in}=20-40	15-615	900-3000	(D=8 mm, L=2.2 m) Vertical Inconel tube

Table 2.7: Range of investigated parameters for experiments with Freon-12 flowing in circular tubes at supercritical pressures

Reference	P (MPa)	T (^oC)	q (kW/m^2)	G (kg/m^2s)	(Geometry) Flow Direction
Holman and Boggs 1960 [75**] in [**7**]**	3.45-6.55	T_{in}<65.6 T_{out}<204.4	-	-	(D=10.92 mm) Closed natural circulation loop
Gorban' et al. 1990 [76**] in [**7**]**	1.08-4.46	T_{in} =20-140	6-290	500-2000	(D=10 mm, L=1 m)

2.3.4 Common Approach Used in Supercritical Water Loop Design

Most supercritical water loops have similar components, some of which include a preheater (to heat the required test section to the inlet temperature), pressurizer (often filled with nitrogen), test sections (vary in design and orientation), coolers, a bypass to the preheater (to recirculate the fluid from the test section), feed pumps, feed/reservoir tanks (to store and feed working fluid to the loop), power supply (to heat up the test section), and filters/purification system.

Supercritical Freon and CO_2 loops have similar designs and with a few modifications, the supercritical Freon and CO_2 loops can be used to perform experiments on supercritical water at lower power.

2.3.5 Operating Experience with Supercritical Loops

There have been a few lessons learnt from previous supercritical fluid experiments. Some of the observations include measurement procedures and pressure control of the loop. These operating experiences are listed below.

- For direct-heating applications, a DC power supply is preferred to an AC power supply. The Critical Heat Flux (CHF) values at boiling obtained with a direct heating DC supply may differ from those obtained in a direct heating AC supply.

- The measurement of surface temperature with a DC power supply requires a well tip insulated thermocouple from the electrically heated surface since there is an average offset across the probe junction in a DC supply.

- A simple circular geometry does not model the thermalhydraulic behaviour of any actual subchannel geometry; however, it is good practice to use simple tubes of internal diameters close to the equivalent hydraulic

diameter of a typical subchannel. The length of the tube also should be equivalent to the average bundle length.

- A material with a high value of specific electrical resistivity should be chosen so that the resistivity is independent of the temperature and the heat flux is uniform throughout the test section. This allows a wider range of test section thickness and heated length. Inconel 600 or Inconel 718 are the best choices for these conditions.

- RTDs are preferable to use compared to thermocouples since they are usually more accurate, but at low wall temperature measurements (typically below 260 ^{o}C), fast response thermocouples provide the best method of measurement.

- In order to eliminate any concerns with gas solubility, pressurization achieved with electrically heated element installed in a PV is preferred to pressurization with inert gas through a membrane or direct contact between the gas and the loop working fluid. The volume of the PV should be at least several times larger than the internal total volume of the loop to facilitate stable pressure control during operation.

2.4 Need for a Supercritical Fluid Loop

Supercritical fluid technology is a relatively new area and there are few experimental loops available to provide data to study this phenomenon. In order to develop this technology further, more experimental data is needed to investigate different supercritical conditions. Although various experimental loops have been built, there remain some areas that have not been investigated:

- The majority of the experimental studies on supercritical fluids investigate heat transfer of water in vertical and horizontal circular tubes. There have been few experiments on annuli and bundle arrangements. More work is needed to investigate bundle arrangements so that experimental data can be directly scaled to Canadian SCWRs.

- Despite growing activities in heat transfer modelling at supercritical conditions using fluid models, reliable fluid-to-fluid scaling methods have not been established to be able to transfer test data in substitute fluids directly to the conditions of a prototype fluid as it applies to SCW.

- The majority of the empirical correlations used for supercritical conditions do not predict well, the Heat Transfer Coefficient (HTC) around the pseudocritical region. There is a need to develop more advanced correlations to do so.

2.4.1 Identify Gap with Existing Database

There have been a lot of experiments done on SCW was discussed in previous sections. Table 2.8 shows the conditions at which the majority of the loops operated. A wide range of heat fluxes have been investigated which includes the heat flux of the conceptual Canadian SCWR channel of 1330 kW/m^2. The range of mass fluxes also includes the mass fluxes in a Canadian SCWR channel. Higher mass fluxes are of interest in order to investigate the effect of high mass fluxes on supercritical heat transfer phenomena. With Canadian SCWR channels having outlet bulk temperatures of 625 ^{o}C, it is important to ensure that SPETA can provide such boundary conditions. Experiments that have been performed in the supercritical water experiments have generally been below 580 ^{o}C which have been limited by material properties but higher bulk temperatures can be investigated now due to advancements in material technology over the decades.

Table 2.8: Range of experiments previously performed for SCW

P (MPa)	T_b (^oC)	q (kW/m^2)	G (kg/m^2s)
22-29	100-580	90≤6600	100≤3000

The majority of the experiments that have been performed started in the 1950's; however, experimental datasets from these experiments have not been published and are not available for analysis. Most of the earlier supercritical experiments were performed on loops that are currently not in operation or are out of commission. From the literature review as listed in Table 2.3, there have been only a few SCW experimental results that have been published in the last decade which suggest that the loops that were used to perform these experiments are still in operation. These experiments are work done by Seo [**41**], Pis'mennyy [**40**], Chen [**39**], Razumovskiy [**38**], and Bazargan [**12**]. However, not all the data from these experiments are readily available for use which necessitates the development of SPETA.

2.4.2 Analyses Requirement

Heat transfer at supercritical pressures deviates from the normal mode at subcritical regions. A change in density of the fluid around the pseudocritical point introduces different modes of heat transfer. The three heat transfer modes that occur include:

- Normal subcritical heat transfer
- Improved heat transfer with higher values of HTC compared to those of subcritical heat transfer.
- Deteriorated heat transfer with lower values of HTC compared to those of subcritical heat transfer regimes. This occurs before the pseudocritical point at higher heat fluxes and lower mass fluxes

These phenomena result in regions of low density and high density fluids which make the heat transfer regime more complex than a single phase heat transfer. Experiments are needed to understand the various phenomena. In order to understand the physics governing these changes, a number of areas are worthy of investigation. These aspects include the following:

- As a result of large changes of density around the pseudocritical region, instability is introduced into the thermalhydraulic system. Flow oscillations may also cause unstable behaviour of the system. Experimental data to study instability of the system are very limited, therefore more numerical and experimental investigations are essential to study this occurrence.

- Analytical and numerical estimations of hydraulic resistances at near-critical and supercritical pressures have been developed. However, satisfactory methods of estimating hydraulic resistance have not yet been established. A more accurate method of predicting thermalhydraulic resistances is of particular interest.
- In a previous study [**77**], it was discovered that the pseudocritical point in a heated section will first occur close to the wall. The temperature profile shows that the pseudocritical point will occur close to the wall first before it occurs in the bulk fluid. The density is lowest at the wall and increases towards the bulk fluid. The variation of the density from the wall to the bulk fluid coupled with the change of the fluid density close to the pseudocritical point as show in Figure 2.4 (b) induces a complex density change in the fluid. Before the pseudocritical point, the near wall density is lower than the bulk and is significantly reduced further compared to the bulk as it approaches the pseudocritical point. The density gradient is much steeper close to the wall as a result of the pseudocritical point occurring first close to the wall and the temperature being higher at the wall. This occurrence may give an insight to understanding the deteriorated heat transfer regime that is observed before the

pseudocritical point in supercritical heat transfer. This complex relation needs to be investigated and studied through experiments.

2.4.3 Industrial Need

Supercritical fluid loops can not only be applied to SCWR technology but can also be applied in coal-fired electricity plants and other higher efficiency power cycles. Due to the significant density change of water near the critical point, it can be used as a separation agent for solvent applications. The development of this technology can improve processes in certain areas including chemical extraction, cryogenic refrigeration, deposition and preparation of materials, and heat pump systems [**78**].

CHAPTER 3

METHODLOGY AND REQUIREMENTS

3.1 Methodology for Loop Development and Design

The design of SPETA was developed based upon industry requirements and from a review of existing designs of supercritical fluid loops. Literature review of existing loops was done and a list of experimental conditions from previous loops was studied to determine the existing gaps in the range of experimental conditions previously researched. This exercise provides the type of information that remains to be researched using experimental facilities and represents an important input requirement into the design. In addition, the status of the previous loops is assessed to determine to what extent they could meet the remaining research requirements.

In order to understand how to develop SPETA, the common approach used to design supercritical water loops and experiences obtained from operating those loops needed to be studied. Supercritical loop components are studied and their importance to the system is also determined. Figure 3.1 shows the methodology used to establish the design requirements for the loop.

After the study of existing loops, the design of the loop was carried out through an iterative process until a conceptual design was obtained. Figure 3.2 shows the process for designing the loop

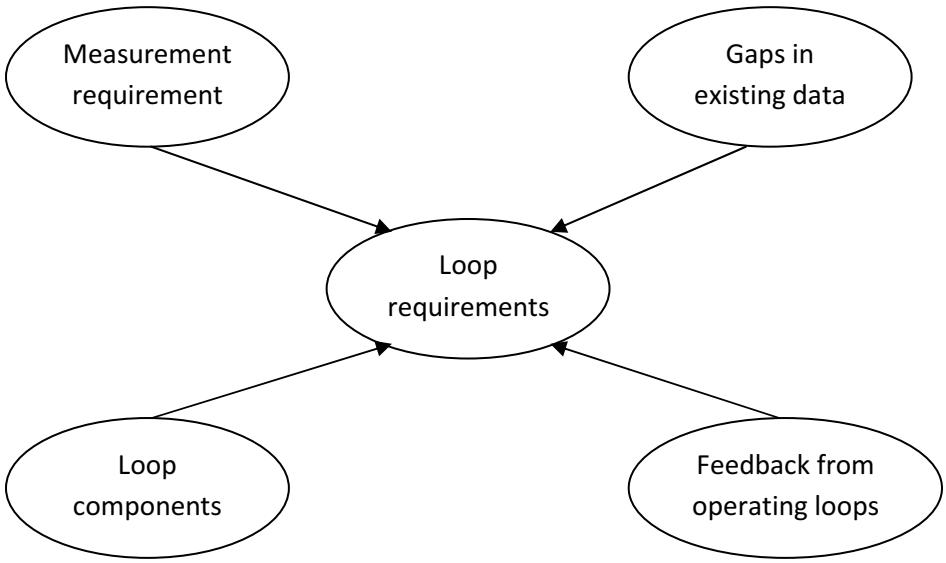

Figure 3.1: Methodology for creating loop requirement

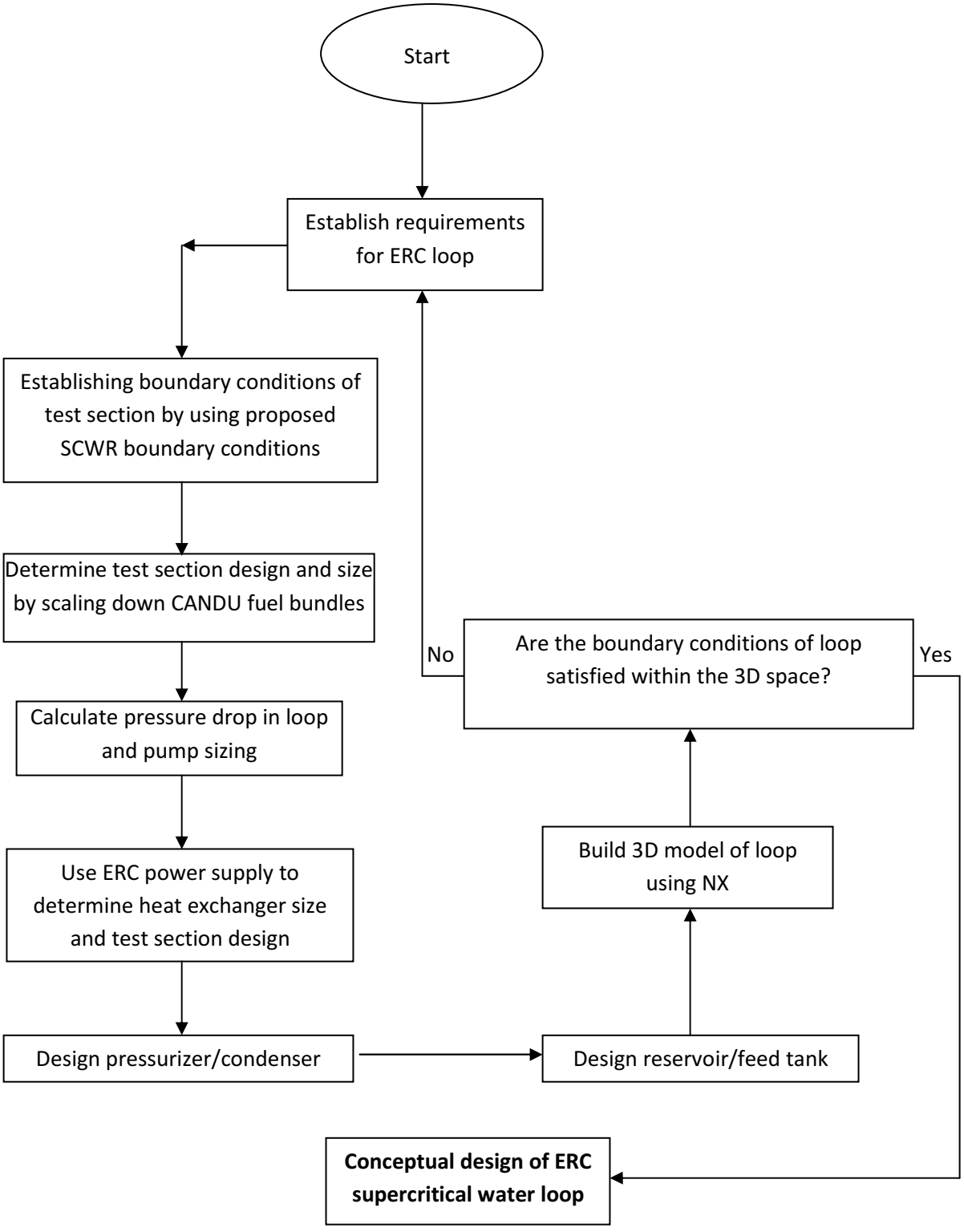

Figure 3.2: Methodology for SPETA design

3.2 Developing Test Section

The SCW loop design was developed from the design of the test section boundary conditions which were determined from scaling down SCWR boundary conditions.

3.2.1 Reference Model

The test model for SPETA used for analyses is a 4 m long tube with an inside diameter of 10 mm is shown in Figure 3.3. It is heated from 300 ^{o}C to 625 ^{o}C at 25 MPa. This model represents the maximum test section length (constrained by the laboratory enclosure) and the maximum mass flow rate (determined by the power available to heat up test section) required to allow enough time to heat up water such that the boundary conditions of a Canadian SCWR channel is satisfied. However, a variation of this reference case was used in analyses to obtain a set of conditions upon which alternative concepts could be evaluated. Variations in hydraulic diameter, channel configuration, channel length, and power were examined as part of the design process to ensure a flexible design and to ensure the support components in the loop are appropriately sized. It is important to state that this is only a reference model and does not represent the loop test section design.

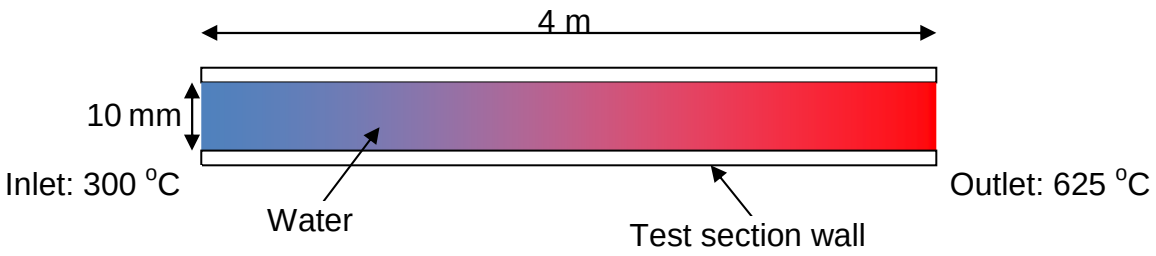

Figure 3.3: Reference model for test section

3.2.2 Establishment of Boundary Conditions

The boundary conditions for the heat transfer facility are developed to include the proposed operating condition of Canadian SCWR with a design pressure of 25 MPa and coolant temperature up to 625 ^{o}C [**79**]. The outlet coolant temperature is chosen to take full advantage of the turbine inlet temperature as seen in fossil fired power plant technology. Table 3.1 shows the parameters of the pressure tube-type Canadian SCWR reactor concept. The operating parameters of SPETA shall be capable of operating at comparable conditions as Canadian SCWR concepts for a more representative modelling and to allow validation of experimental and numerical results on SCWRs.

Table 3.1: Operating specifications of Canadian SCWR [**79**]

Parameters	**Pressure Tube Canadian SCWR**
Thermal Power, MW	2540
Electric Power, MW	1220
Pressure, MPa	25
Inlet temperature, ^{o}C	350
Outlet temperature, ^{o}C	625
Number of Channels	300
Flowrate/Channel, kg/s	4.4
Average Channel Power, MW_{th}	8.47
Mass flux, kg/m^{2}s	1320

The average channel power of 8.47 MW_{th} is chosen for a 12-bundle channel of full length of 5.772 m for analyses [**79**]. The conceptual design of SPETA has a maximum test section length of 4 m with available power supply 1.22 MW_{th} to heat the fluid. At this power, a reduction in the flow area of the test section can

be used to obtain equivalent mass fluxes and heat fluxes as Canadian SCWR concepts.

The use of the facility shall be extensively applicable use in heat transfer experiments which include the use of various working fluids other than water. The majority of supercritical water experiments have been performed between 22-30 MPa (Table 2.3). Numerical analyses done on SCWRs have utilized pressures range from 24-25 MPa. Supercritical CO_2 experiments typically range from 7-10 MPa (Table 2.6) and supercritical Freon experiments are run at lower pressures. The operating conditions of these various experiments are a subset of the operating conditions the loop is designed for.

Although SPETA is designed to run supercritical water experiments at extreme operating conditions, it shall be able to run milder experiments using substitute fluids. The facility shall also be designed with a modular test section to accommodate different bundle geometries.

3.2.3 Limitation of Facility

The heat transfer facility shall be designed for installation in the ERC at the University of Ontario Institute of Technology. Rooms available for various components are:

- ERC B052 – Nuclear Design Laboratory
- ERC 1052 – Thermalhydraulics Laboratory
- ERC B02X – Electrical Support Room
- ERC B032 – Equipment Support Room

ERC B052 and ERC 1052 can house major loop components with respective heights of 5 m and 4 m. The loop area is a 2 m by 4.8 m rectangular area in both rooms with removable slabs on the floor of ERC 1052. ERC B02X is available for the electrical power supplies and ERC B032 is available for low pressure support

systems such as storage tanks and purification equipment. Combined, the labs are provided with electrical power of 110 V, 220 V, and 600 V supply, air supply at 0.276 MPa (40 psi), natural gas supply, chilled water at 20 ^{o}C, and the usual lighting and fire protection.

These design inputs will be used for sizing the test sections, pumps, heat exchangers, pressurizers, and other support equipment.

3.2.4 Geometry of Test Section

To meet the needs of the Canadian SCWR, an estimation of the type of fuel channel design is necessary. The actual design has not been finalized due to a lack of reactor physics and materials research combined with incomplete understanding of the thermalhydraulics. Fuel development usually begins as a derivative of the previous designs based upon separate effects studies. As such, the reference bundle designs for the current Canadian SCWR assessment are the existing CANDU fuel bundles [**80**].

Four types of Canadian SCWR bundle design concepts were considered namely the current 37-element type used for production, and the original 43-element CANFLEX, Variant-18 CANFLEX, and Variant-20 CANFLEX bundles. The 37-element bundle contains 37 elements while the CANFLEX, Variant-18 and the Variant-20 bundles each have 43 elements. Each bundle type has four rings of elements namely the centre ring, inner ring, intermediate ring, and outer ring with the number of elements in each ring different from each other. The centre element is heated in the 37-Element bundle and the CANFLEX bundle, but unheated and filled with Dysprosium (a burnable neutron absorber which can reduce void reactivity) in the Variant-18 and Variant-20 bundles. The elements in each ring have different external diameters as shown in Table 3.2.

Table 3.2: Canadian SCWR Fuel Bundle Parameters used as Design Inputs

Parameter	37-element	43-element	Variant-18	Variant-20
Total Number of Elements	37	43	43	43
Number of element in the centre ring	1	1	1	1
Number of elements in the inner ring	6	7	7	7
Number of elements in the intermediate ring	12	14	14	14
Number of elements in the outer ring	18	21	21	21
Diameter of centre ring element (mm)	13.08	13.5	18.0	20.0
Diameter of inner ring element (mm)	13.08	13.5	11.5	11.5
Diameter of intermediate ring element (mm)	13.08	11.5	11.5	11.5
Diameter of outer ring element (mm)	13.08	11.5	11.5	11.5
Heated Bundle Length (mm)	481	481	481	481

Experiments for SPETA will be carried out on test sections with thermalhydraulic characteristics similar to the Canadian SCWR fuel. The facility will allow variations in design within a reasonable range of the reference design. The chosen geometries for the initial test sections include a bare tube, an annulus tube, and a 7-element fuel bundle. The different bundle types will model various

Canadian SCWR bundles. Figure 3.4 shows the geometries that will be used in the test section of SPETA.

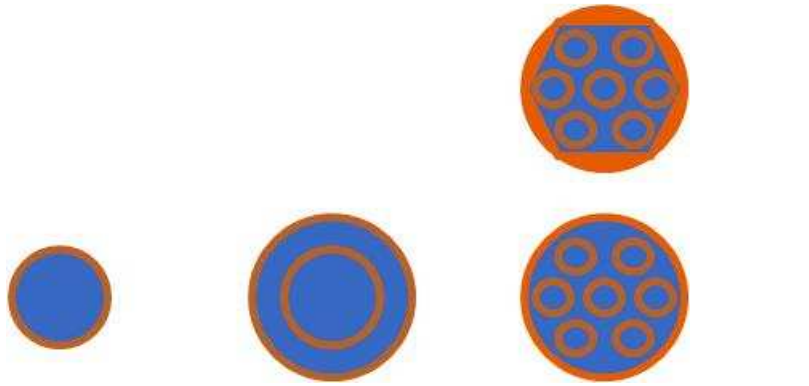

Figure 3.4: Schematic of SPETA test section geometries

The circular bare tube has been chosen as the simplest case for studying supercritical fluids. It is the most investigated geometry for fluids flowing through a pipe at near critical and pseudocritical regions [**10**,**12**,**13**,**26**,**47**,**74**,**78**]. There is abundant data on supercritical fluid flow through circular tubes. Hence, this geometry would ensure that the facility could reproduce some of the existing experimental data to allow comparative studies to be performed.

The annulus tube geometry is the next most investigated flow geometry. In general, forced convective heat transfer in an annulus tube is different from that in a circular tube, even at subcrtical pressures. Three heating modes can exist: (i) outer surface heated, (ii) inner surface heated, and (iii) both surfaces heated. Internally-heated annulus geometry for supercritical water has been investigated by McAdams [**81**], Kondrat'ev [**82**], and Hong [**83**] and externally-heated annulus geometry was investigated by Ornatskiy [**84**]. The annulus geometry is of interest since it has a two-dimensional heat transfer scenario since heat can be applied to both the internal and external surface of the annulus.

Bundle arrangements will be investigated with SPETA. This basic bundle arrangement is the simplest model that can be investigated to capture the thermalhydraulic phenomena as a result of subchannel interaction in a Canadian SCWR fuel channel. The 7 element bundle arrangement is of particular interest. Other array configurations may be considered at a later time.

3.2.5 Scaling of Test Section

Experiments are carried out to predict behaviour of practical problems. Given that many practical fluid mechanics engineering problems can be solved by using equations and analytical procedures, a large number of problems rely on experimentally measured data for verification of physics models.

An important purpose of experiments is being able to use results obtained elsewhere. The concept of similitude can be used to achieve this such that measurements made in the laboratory can be applied to similar systems outside of the laboratory. Laboratory apparatus are often used to study phenomenon of interest under carefully controlled circumstances. In order to facilitate this, it is important to establish and understand the relationship between the laboratory work and the practical system under investigation since running separate experiments for each practical problem poses a few challenges. These problems can be solved by the use of dimensional analysis. Of the two modelling techniques available (geometric and fluid modelling), the geometric modelling techniques can be used to compare the dimensions of experimental test sections and fluid modelling is used to compare different fluid properties [**45**].

SPETA test section geometries should possess similar dimensionless flow parameters as the Canadian SCWR fuel bundle concepts under study. Dimensionless flow parameters are flow properties that are used to characterize a flow to predict flow behaviour of a similar flow. There are a few dimensionless

properties of fluid flow that can be used to relate experimental and practical problems as shown in Table 3.3. A dimensionless property that applies to all fluid mechanics problem is the Reynolds number. This parameter is of particular interest since the geometric properties of the experimental bundles differ from the Canadian SCWR bundles they are intended to simulate. For geometric scaling, the Reynolds number is the dimensionless quantity of interest. The Euler number is not of particular interest in the scaling of the experimental bundle type since it is relevant along the length of the test-section. Euler number is not significant to the geometric scaling of the Canadian SCWR bundles. The Euler number becomes important in a fluid-to-fluid scaling for instance, water-to-CO_2 or water-to-Freon modelling where there are significant differences in pressures between the experiment and the practical problem [**45**].

Table 3.3: Some common variables and dimensionless groups in fluid mechanics

Variables: Acceleration of gravity, g; Bulk modulus, E_v; Characteristic length, l; Density, ρ; Frequency of oscillating flow, ω; Pressure, p; Speed of sound, c; Surface tension, σ; Velocity, V; Viscosity, μ			
Dimensionless Groups	**Name**	**Interpretation (Index of Force Ratio Indicated)**	**Types of Applications**
$\frac{\rho V l}{\mu}$	Reynolds number, Re	$\frac{\text{inertia force}}{\text{viscous force}}$	Generally of importance in all types of fluid dynamics problems
$\frac{V}{\sqrt{gl}}$	Froude number, Fr	$\frac{\text{inertia force}}{\text{gravitational force}}$	Flow with a free surface; multiphase flow
$\frac{p}{\rho V^2}$	Euler number, Eu	$\frac{\text{pressure force}}{\text{inertia force}}$	Problems in which pressure, or pressure differences are of interest
$\frac{\rho V^2}{E_v}$	Cauchy Number, Ca	$\frac{\text{inertia force}}{\text{compressibility force}}$	Flows in which the compressibility of the fluid is important
$\frac{V}{c}$	Mach Number, Ma	$\frac{\text{inertia force}}{\text{comperssibility force}}$	Flows in which the compressibility of the fluid is important
$\frac{\omega l}{V}$	Strouhal number, St	$\frac{\text{inertia (local) force}}{\text{viscous (convective) force}}$	Flows with a characteristic frequency of oscillation
$\frac{\rho V^2 l}{\sigma}$	Weber number, We	$\frac{\text{inertia force}}{\text{surface tension force}}$	Problems in which surface tension is important

The Reynolds, Re, number was used as a dimensionless property to scale the Canadian SCWR bundles to experimental models. Reynolds number is defined by Equation 3.5.

The Reynolds number of the Canadian SCWR fuel bundle is scaled with the proposed experimental fuel geometries. The scaling law makes it possible to equate both Reynolds numbers for similarity in fluid behaviour.

$$(\mathrm{Re})_{\mathrm{SCWR}} = (\mathrm{Re})_{\mathrm{experimental}} \tag{3.1}$$

The Canadian SCWR geometric and fluid properties were scaled down using dimensionless Reynolds numbers so that similar experimental results can be expected from the same dimensionless quantities. The inlet point was picked as the reference position for scaling. Choosing this point of reference ensures that the boundary and initial conditions at the inlet can be paired. This means that if the boundary condition at the inlet for the experimental bundle is set to the boundary condition at the inlet for the Canadian SCWR concept, the initial conditions will be consequently matched. Similar results along the bundles will be expected for the experimental models and the Canadian SCWR bundles if all boundary conditions in both models are set to be equal.

A circular bare tube is chosen as the simplest experimental fuel type. The inside diameter of the bare tube is the dimension of concern since it represents the hydraulic diameter of the tube. The parameters of the CANFLEX bundle are shown in Table 3.4.

The flow area $\mathrm{A_{flow}}$, is calculated with Equation 3.2. The total cross-sectional area of the pins $\sum \mathrm{A_{pins}}$, is subtracted from the inner cross-sectional area of the pressure tube $\mathrm{A_{pressure\,tube}}$. The number of pins and dimensions are obtained from Table 3.2.

$$\mathrm{A_{flow}} = \mathrm{A_{pressure\,tube}} - \sum \mathrm{A_{pins}} \tag{3.2}$$

The hydraulic diameter D_{hy}, is calculated with Equation 3.3. The wetted perimeter P_{wetted} is the sum of the pin external flow perimeters and the inner pressure tube inner flow perimeter.

$$D_{hy} = \frac{4A_{flow}}{P_{wetted}} \tag{3.3}$$

Table 3.4: CANFLEX-type Fuel Channel Parameters for a 37-element and 43-element fuel bundle

Fuel Channel Properties		
Parameter	**37-element**	**43-element**
Pressure tube inner diameter (m)	0.10345	
Mass flow rate (kg/s)*	4.37	
Inlet temperature (^oC)	350	
Inlet pressure (MPa)	25	
Inlet bulk density (kg/m^3)	625.9	
Inlet kinematic viscosity $(m^2/s)\ 10^6$	0.1163	
Inlet dynamic viscosity $kg/(ms)\ 10^6$	72.76	
Flow area (m^2)*	0.003449	0.003625
Wetted Perimeter (m)	1.845	1.929
Hydraulic diameter (m)	0.00748	0.00752
Mass flux $(kg/(m^2s))$	1267	1206
Inlet Reynolds number	130700	124500
Inlet bulk velocity (m/s)	2.033	1.926
VD_{hy} (m^2s) at inlet	0.0152	0.01448

*Note: Pressure tube mass flow is a reference Canadian SCWR mass flow rate. Pin outer diameter and number of pins and are from Table 3.2

The mass flux G, is calculated with Equation 3.4 and is defined by the mass flow rate $\dot{m}$, divided by the flow area $\mathrm{A_{flow}}$.

$$\mathrm{G} = \frac{\dot{m}}{\mathrm{A_{flow}}} \tag{3.4}$$

The Reynolds number and bulk fluid velocity at the inlet are calculated with Equations 3.5 and 3.6 respectively where G is the mass flux; $\mathrm{D_{hy}}$ is the hydraulic diameter of the bundle and μ is the dynamic viscosity of the fluid passing through the fuel channel. $\mathrm{V_{inlet}}$ represents the inlet velocity and $\mathrm{v_{inlet}}$ represents the kinematic viscosity.

$$Re_{inlet} = \frac{G D_{hy}}{\mu_{\mathrm{inlet}}} \tag{3.5}$$

$$\mathrm{V}_{inlet} = \frac{Re_{inlet} v_{\mathrm{inlet}}}{D_{hy}} \tag{3.6}$$

The dimension of the bare tube is suitable for comparison; however, due to the practicality of controlling velocity or mass flux, it is important to characterize the bare tube for different flow rates. Using the same flow criterion (i.e. equal Reynolds number), the dimension of the bare tube was varied and the equivalent velocities and mass fluxes were calculated.

3.3 Theory

The fundamental theory of the thermalhydraulic models and how they are developed for different components of the loop are discussed here.

3.3.1 Heat Transferred by Test Section to Fluid

The boundary conditions of the test section are used to calculate the heat added to the fluid as it flows from the inlet to the outlet of the test section. The heat transferred to the fluid from the test section is obtained from Equation 3.7. The enthalpy H, is a function of the heat specific capacity C_p, and bulk temperature T, of the fluid in the test section. The subscripts o, and i, represent the outlet and inlet conditions respectively.

$$q = \dot{m}(H_o - H_i) = \dot{m}\left(C_{p,o}T_o - C_{p,i}T_i\right) \tag{3.7}$$

3.3.2 Heat Removed by Heat Exchangers from Fluid

A shell and tube heat exchanger design is used to perform the heat balance calculations. It is provided with chilled water to remove the heat added by the test section. The heat extracted from the heat exchanger will be channeled to the roof top of the facility building and cooled by an appropriate cooling tower which will be designed at a later time.

Figure 3.5 shows a typical shell and tube heat exchanger in a counter-flow arrangement. Hot water from the test section flows from left to right through the tubes in the heat exchanger and chilled water flows from the right to left in the shell of the heat exchanger. The enthalpy, h, and mass flow rate, $\dot{m}$, of water is used to calculate the heat removed by the heat exchanger. The total heat removed by the heat exchangers in the loop should be equivalent to the heat added to the fluid at the test section for proper heat balance.

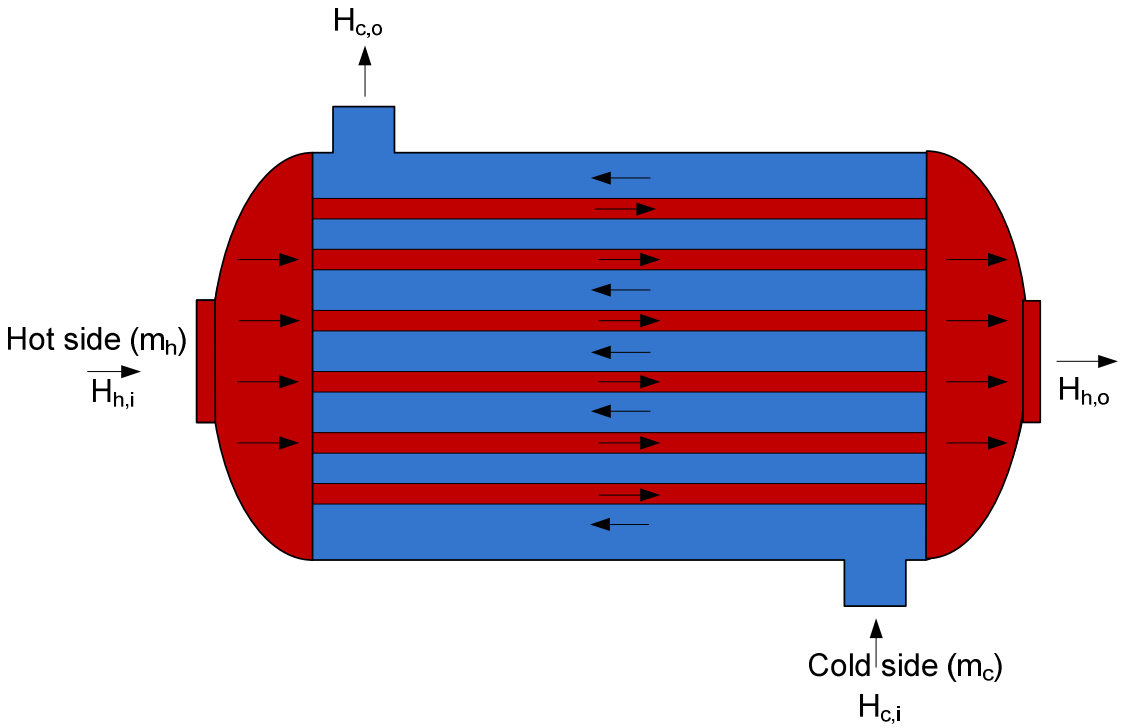

Figure 3.5: Schematic of heat exchanger

The outlet boundary condition of the heat exchanger can be controlled. Equation 3.8 shows how. A change of mass flow of the cold side can be used to obtain the desired outlet temperature from the hot side of the fluid. The outlet boundary condition of the heat exchanger also depends on the size of the heat exchanger which is investigated in this work.

$$q_{\text{test section}} = q_{\text{heat exchangers}} = \dot{m}_h\left(H_{h,i} - H_{h,o}\right) = \dot{m}_c(H_{c,o} - H_{c,i}) \quad (3.8)$$

3.3.3 Heat Transfer Coefficient Calculation

There are a number of correlations that have been developed for supercritical conditions, all of which use bulk fluid properties. The correlations have been obtained from experimental data from various supercritical water experiments. More improved correlations have been developed over the last decade [**18, 76, 85-89**]. Appendix E shows various heat transfer correlations developed for supercritical fluids.

The correlation of Gupta [**90**] is the most accurate for bundles but needs to be validated with experiments [**86**]. However, the correlation of Mokry (et al.) [**91**] provides the most accurate correlation for circular tubes and is used in the calculation of the convection heat transfer coefficient in this work. The heat transfer coefficients of the fluid, at the inner and outer surfaces (h_i and h_o respectively) are calculated using the correlation of Mokry (et al.) [**91**].

The Nusselt number is calculated with Equation 3.9, where Re, represents the Reynolds number of the bulk fluid, Pr, represents Pradtl number, and ρ, represents the density of the fluid. The subscripts b, and w, represent the bulk fluid properties and fluid properties at the wall respectively.

$$Nu_b = 0.0061 {Re_b}^{0.904} \overline{Pr}^{0.684} \left(\frac{\rho_w}{\rho_b}\right)^{0.564} \quad (3.9)$$

The total coefficient of convection heat transfer U, is calculated using Equation 3.10, where k, represents the conductivity of the fluid, Nu, represents the Nusselt number, and D, represents the hydraulic diameter of the flow.

$$U = Nu \frac{k}{D} \quad (3.10)$$

The total heat transfer is coefficient U, is estimated using the Equation 3.11, where h, represents the heat transfer coefficient, r, represents the radius, k, represents the fluid conductivity, L, represents the length, and A, represents the area. The subscripts o, and i, represent the outer and inner properties respectively.

$$\frac{1}{UA_o} = \frac{1}{h_o A_o} + \frac{\ln\left(\frac{r_o}{r_i}\right)}{2\pi kL} + \frac{1}{h_i A_i} \tag{3.11}$$

This equation can be simplified to Equation 3.12.

$$\frac{1}{U} = \frac{1}{h_o} + \frac{r_o \ln\left(\frac{r_o}{r_i}\right)}{k} + \frac{r_o}{r_i h_i} \tag{3.12}$$

3.3.4 Tube length calculation

The total minimum tube length required in the heat exchanger can be calculated using the Number of Transfer Units (NTU) method. The following equation is used to calculate the minimum length of the tube required to satisfy the boundary conditions of the heat exchanger tube inlet and outlet. The values of NTU can be obtained from the heat exchanger effectiveness where NL, represents the total length of the tubes in the heat exchanger, and C_p, represents the specific heat capacity of the fluid in the heat exchanger.

$$NL = \frac{NTUC_{min}}{U(2\pi D_o)} \tag{3.13}$$

$$C_{min} = (\dot{m}C_p)_{min} \tag{3.14}$$

The value of C_{min} depends on the mass flow rate $\dot{m}$, and specific heat capacity C_p, of either the hot or cold side of the shell and tube heat exchanger. C_{min}, is the lower value of the product of the specific heat capacity and the mass flow rate between the hot and cold side which is the hot (tube interior) side in this case.

Using the Log Mean Temperature Difference (LMTD) method, the required total length of the heat exchanger is calculated using Equations 3.15 and 3.16.

$$NL = \frac{q}{\Delta T_{log\,mean} U(2\pi D_o)} \tag{3.15}$$

$$\Delta T_{log\,mean} = \frac{(T_{in\,hot} - T_{out\,cold}) - (T_{out\,hot} - T_{in\,cold})}{\ln\left(\frac{T_{in\,hot} - T_{out\,cold}}{T_{out\,hot} - T_{in\,cold}}\right)} \tag{3.16}$$

The LMTD method is a more conservative approach and will be investigated in the design of the heat exchanger.

3.3.5 Wall Thickness of Pipes and Pressurizer

The pressurizer and the pipe in the loop are subjected to very high pressures so it is essential to design its walls to withstand high pressures. The minimum thickness, t, of a cylindrical shell pressure vessel can be determined by ASME codes with Equation 3.17. The wall thickness for a given outer radius, R_o, can be determined for a internal design pressure, P. The maximum allowable stress, S, can also be determined given all other variables. The weld joint efficiency factor, E, used in this work was assumed to be unity.

$$t = \frac{PR_o}{SE - 0.6P} \quad (3.17)$$

3.3.6 Pressure Drop Calculation

Although pressure drop of supercritical fluid is not fully understood, similar subcritical fluid flow methods of pressure drop estimation have been used. These methods consist of four components:

- Frictional loss
- Acceleration loss
- Gravitational loss
- Form/local loss

The total pressure drop at supercritical pressures can be estimated based on general correlations for pressure drop at subcritical pressures with correction factors for the effect of significant thermophysical property variations and high heat flux.

Mathematically, the overall pressure drop, ΔP, across a length can be calculated by adding the friction Δp_f, acceleration Δp_a, gravitational Δp_g, and local/form loss Δp_l, as shown in Equation 3.18.

$$\Delta p = \Delta p_f + \Delta p_a + \Delta p_g + \Delta p_l \quad (3.18)$$

Friction losses result from friction between the fluid and the flow channel as a result of the surface roughness of the channel. It is the irreversible component of pressure drop caused by shear stress at the wall. It is primarily affected by a change in tube diameter, velocity gradient, and viscosity.

Acceleration loss is the result of a change of the speed of the fluid. This is significant in a channel with varying flow area and fluid density. This is expected in the loop since the thermophysical properties of fluid changes especially around the pseudocritical point with acceleration effects as will be seen from the CFD work discussed in chapter 4.

Gravitational losses result from a change in the hydrostatic head of water. It only occurs in vertical channels. The change in hydrostatic pressure in the loop is not significant at high pressures and will not be a major concern for the loop but still needs to be incorporated.

Form losses result from the change of the shape of the path flow. These changes can be as a result of change in flow direction in elbows and bends, flow blockages in valves, junctions, and change in flow area resulting from large expansions or contractions. Flow obstructions are expected to occur in valves and flowmeters along the loop. Bends or elbows are expected to be encountered throughout the loop and are included in the pressure drop calculations.

Friction pressure drop can be calculated with Equation 3.19. This equation can be applied to both single-phase and homogeneous two-phase flow which makes it suitable for fluid applications. The friction pressure drop is the most important pressure drop component since it accounts for the kinetic pressure drop which is calculated throughout the loop.

$$\Delta p_f = f \frac{L}{D_{hy}} \frac{G^2}{2\rho A^2} \tag{3.19}$$

The friction pressure drop depends on the surface roughness which is contained in the friction factor, f, the flow properties contained in the mass flux, G, the fluid properties which is contained in ρ, and the geometry of the component which includes the length, L, hydraulic diameter, D_{hy}, and cross sectional area, A. The

density and velocity of the fluid are inversely proportional for a constant area. The density in the equation accounts for the velocity component of the pressure drop.

The pressure drop calculation as a result of the expansion or contraction of the fluid can be expressed as shown in Equation 3.20.

$$\Delta p_a = \frac{(1-A_r^2)G^2}{2\rho A_o^2} \quad (3.20)$$

The area ratio, A_r, is the ratio of the smaller are to the larger area where there is a change in flow area and is equal to 1 when there is no change in area. The pressure drop is dependent on the smaller flow area, A_o, regardless of the direction of flow. It is important to note that the acceleration pressure drop is only a component of contraction and expansion and does not apply to the acceleration of the fluid as a result of heating since this has already been accounted for in the friction pressure drop which represents the kinetic component of the pressure drop.

The gravitational pressure drop or elevation pressure drop is a static component of the total pressure drop and depends on elevation. Equation 3.21 shows the formula that is used to calculate the gravitational pressure drop.

$$\Delta p_g = \rho g \, \Delta Z \quad (3.21)$$

The elevation pressure drop depends on the vertical change, ΔZ, of the elevation of the fluid. For any loop, this value is equal to zero since the total change of the height from any point to the same point around the loop is zero. This component was not taken into account for the loop pressure drop calculation.

Local pressure drop depends on each case. It can be calculated by using Equation 3.22. The local loss coefficient, K, differs for different geometries and devices and is uniquely applied to each case. The values have to be carefully chosen to reflect the most representative case for each control volume. This pressure drop is applicable in valves, junctions, flowmeters, elbows, bends, and changes in area.

$$\Delta p_l = K\frac{G^2}{2\rho A^2} \tag{3.22}$$

The boundary condition of the test section was used as the basis for estimating the pressure drop in the loop. The outlet pressure of the test section which corresponds to the global system pressure was used as a point of reference to estimate the pressure at different locations along the loop. The design boundary conditions of the test section are an inlet temperature of 350 ^{o}C and an outlet pressure of 25 MPa. A maximum outlet temperature of 625 ^{o}C was used to calculate a maximum heat supplied to the test section at the specified inlet temperature. The temperature boundary conditions for the next control volume was used to calculate the consequent pressure drop. Elbows and other pressure drop sources are accounted for in the pressure drop calculations. Consequently, given the temperature boundary conditions for all the control volumes, the pressure drop for each control volume can be calculated.

3.3.7 Pump Power calculation

The head losses in the loop can be used to determine the pump power needed to maintain the system pressure. The total head loss is a sum of the static head and dynamic head which are split into major and minor head loss. The major loss is the friction loss and the minor loss is the form loss which can be calculated with Equations 3.23. The total dynamic head and static head are calculated with Equations 3.24 and 3.25 respectively where V_{ave} represents the average velocity.

$$\text{total head system} = \text{dynamic head} + \text{total static head} \quad (3.23)$$

$$\mathrm{hL_{major}} = f\ \frac{\mathrm{L}}{\mathrm{D}}\frac{\mathrm{V_{ave}^2}}{2\mathrm{g}} \quad (3.24)$$

$$\mathrm{hL_{minor}} = \mathrm{K}\frac{\mathrm{V_{ave}^2}}{2\mathrm{g}} \quad (3.25)$$

The pump power is directly proportional to the flow capacity, q, density, ρ, gravity, g, and the differential head, $\Delta \mathrm{Z}$, of the fluid as shown in Equation 3.26.

$$\text{Pump Power} = \frac{q\rho g\,\Delta \mathrm{Z}}{3.6\times10^{6}} \quad (3.26)$$

The shaft power can be calculated with the pump efficiency as shown in Equation 3.27 by dividing the hydraulic power by the efficiency, η ,of the shaft.

$$\text{Shaft Power} = \frac{\mathrm{P_h}}{\eta} \quad (3.27)$$

3.4 Design Requirements of SPETA

Based on the literature review, an initial set of design requirements were established for SPETA. These requirements are the high level governing requirements. More detailed requirements are established as the design proceeds and usually are for specific components and scenarios.

SPETA shall meet the following requirements:

- The main components of the supercritical fluid loop shall fit in a 9 m by 2 m by 4.8 m laboratory enclosure inside ERC B051 and ERC 1052 with supporting equipment in neighbouring rooms.
    - This requirement ensures that the available space constraints are met.
- The supercritical fluid loop shall be able to pressurize water up to 25 MPa.
    - This requirement shall ensure that any of the supercritical fluids that may be studied in the future can be used as all of the other fluids have pseudocritical points below this pressure.
- Power supply of 1.22 MW shall be used to heat the water in the loop.
    - This requirement obtained from the power supply available for heating in the loop.
- Loop shall test different geometric test sections.
    - This requirement ensures that geometric effects can be investigated.
- The test section shall be 0.5 m to 4 m long.
    - This allows the pseudocritical point to be investigated at different locations and ensures that pressure drop and hence friction correlations can be investigated.
- The test section shall be able to heat water up to 625 ^{o}C.
    - This requirement ensures that test section outlet conditions will be similar to the conditions in the conceptual Canadian SCWR.
- Shall be able to provide a mass flux of up to 15000 kg/(m^{2}s) to the test section.
    - This design requirement that was obtained from the flow characteristics of the loop. This ensures high mass fluxes can be investigated in SPETA.
- The loop shall be able to provide water to the test section at a mass flow rate of 4.37 kg/s.

    - This ensures that the loop can simulate mass flow rates similar to the conceptual Canadian SCWR flow channel, for scaling purposes.
- The loop shall be equipped with instrumentation.
    - This requirement is to ensure that the loop thermalhydraulic properties can be monitored and controlled.
- There shall be a purification system for the loop.
    - This is to ensure that impurities do not interfere with supercritical properties of the fluid in the loop.

3.5 Design Modifications for Freons and CO_2

Although SPETA has been designed mainly for water, the materials for construction have been chosen, so that they are compatible with Freons and CO_2. So far, other alternate fluids have not been considered. The design modifications required for the storage and supply of Freons and CO_2, have not been performed.

The thermophysical properties of alternate fluids may affect the experimental setup of the loop. The pseudocritical pressures of Freons and CO_2 are significantly lower than that of water and as a result, modifications to the loop may need to be made. In order to use SPETA for these fluids, there are a few design changes that should be considered. These changes are:

- Separate storage tanks have to be designed for Freons and CO_2, to ensure that they are safely transported and attached to the loop.

- The feed pump may need to be changed to ensure that it is suitable for application to the alternate fluids.

- A pressurizer with a lower operating pressure may need to be used because the operating pressures of supercritical fluid experiments done with Freons and $CO_{2,}$ are much lower than the operating pressures of SCW experiments. This modification may be necessary if the pressurizer for SCW experiments is not suitable.

- A heat exchanger with a lower power rating may need to be used to ensure there is proper heat balance in the loop. The loop is designed with three different heat exchangers, so that only the heat exchanger with the lowest rating may be used.

CHAPTER 4

SUPERCRITICAL FLUID PHENOMENA AND COMPUTATIONAL FLUID DYNAMICS (CFD) WORK

This chapter identifies various supercritical fluid related phenomena that were identified by work that was done using computational fluid dynamics software (FLUENT). The following studies were examined:

- 3-dimesional effects of heat transfer in comparison to 1-dimensional methods using correlations
- The onset of the pseudocritical point in the 3-dimensional space
- The effect of friction at the wall on the various properties of water at supercritical conditions
- The deteriorated, normal, and enhanced heat transfer in supercritical water conditions
- Capability of FLUENT in modelling thermalhydraulic problems at supercritical conditions

This study uses numerical modelling to better understand SCW heat transfer and discover the best modelling methods to ensure that the test rig developed will be able to capture the phenomena. Numerical methods have advantages that make them suitable to study various physical phenomena. These advantages are discussed below.

4.1 CFD Modelling of Thermalhydraulic Problems

Laboratory experiments are generally performed to obtain results that can be used to study a phenomenon. These experiments can be repeated under different conditions to obtain more data; however, it may not be cost effective or time effective to study a phenomenon by repeating experimental work. Numerical

models are used to simulate experiments so that they can be repeated under different laboratory conditions without a major adjustment to the experimental work. CFD models provide a high level of scalar and vector detail which can be used to solve three-dimensional problems.

Although computational fluid dynamics provides locally more detailed data than a one dimensional correlation, it is only as realistic as the developed model and the physical representations included in the calculation. Numerical modelling cannot replace experimental results, but can be used as a tool to understand the behaviour of a model [**87**]. Validation of numerical calculation can then be done by performing the experiment using similar CFD conditions which can be done without clearly understanding the physical causes of the different heat transfer modes. Then the relationship between the thermalhydraulic characteristics and the global boundary conditions (heat and mass fluxes) can be identified. The change in the local variables which include the near wall velocity, temperature, and density can be studied in correlation with the boundary conditions.

The majority of the heat transfer correlations are not able to predict the normal and enhanced heat transfer regimes for high heat and mass fluxes, making numerical codes a more suitable method to simulate SCW conditions since they predict normal and enhanced heat transfer regime adequately. FLUENT can be used to model SCW problems with carefully defined boundary conditions. An understanding of the range of operating parameters as they affect the results must be understood in order to obtain reliable results.

4.2 Important Phenomena to Investigate at Supercritical Conditions

At pressures above the critical point, fluid properties vary sharply within a narrow temperature band. As a consequence of dependence on fluid properties, the

equations of state governing fluid flow and heat transfer are linked and non-linear under such conditions. Thus, some of the simplified concepts and widely employed assumptions such as negligible buoyancy and thermal expansion, no longer apply. Non-uniformity of fluid properties has an effect on bulk fluid property distribution and turbulence fields which affect the effectiveness of heat transfer.

The shear stress phenomenon across the wall to the bulk fluid at supercritical conditions is not well understood. The relationship between the shear stress, wall layer thickness, heat flux, and velocity needs to be established. This can help predict the relationship between the heat transfer coefficient and the shear stress, hence the frictional pressure drop. Although the friction pressure drop is not well known for smooth pipes in general, a decrease in friction factor around the pseudocritical region is reported [**88**]. Further studies need to be developed starting from classical definitions of the shear stress relations and friction factor; therefore, experimental testing must be able to accurately measure fundamental pressure drops. By extension, minor losses are also unknown.

The effect of buoyancy on heat transfer at pressures just above the critical point under conditions above the supercritical temperature needs to be investigated. There is a need for developing a method to distinguish between buoyancy-influenced heat transfer and heat transfer as a result of thermal expansion. Thus, precise and detailed measurements of temperature, velocity, and turbulence in heat transfer experiments with supercritical fluids are needed, especially for conditions where heat transfer is affected by thermal expansion or buoyancy effects.

The particular assumption that needs to be validated experimentally is whether the acceleration of flow due to strong heating affects the turbulence field encountered in fluids at supercritical pressure and, thereby thus causing a deterioration of the heat transfer. The validity of the assumption that the increase of bulk temperature is the dominant factor in reducing fluid density needs to be confirmed. The investigations of thermal boundary conditions other than the heat flux would help understand some fundamental aspects of heat transfer at supercritical conditions. Therefore, SPETA shall have a means to measure and control the temperature boundary condition to allow the application of heat flux and temperature boundary conditions.

The problem of comparing experimental data on heat transfer from different fluids and geometries needs to be addressed by establishing a more general basis for similarity and scaling in a more detailed and rigorous manner. Investigating other non-circular geometries would be useful in providing additional information in the development of similarity and scaling laws appropriate for supercritical fluids and the transition through the pseudocritical point.

In recent years, many researchers have performed heat transfer modelling under supercritical conditions using CFD [**89, 92-99**]. Some of these models have been compared to experimental data for heat transfer cases in horizontal and vertical pipe conditions. Results of the numerical modelling have shown good qualitative and quantitative agreement within a certain acceptable range of errors. Most numerical models have been performed with circular geometries and leaving other geometries underdeveloped. There is a need for the investigation of more complex geometries (subchannel geometry for instance) performed with experiments, in order to further develop more general methods for the similarity of behaviour of different models at supercritical conditions.

4.3 Model Setup and Boundary Conditions

A numerical study of heat transfer in a subchannel, using FLUENT-12 was done (full paper in Appendix A) to investigate the variation of thermalhydraulic properties (local velocity, temperature, and density) around the pseudocritical point of water. The purpose of the work was to investigate the capability of FLUENT in solving supercritical water models. Work has been done by Farah et al [**100**], to study a vertical bare tube with a diameter of 10 mm and 4 m long using a two dimensional axisymmetric model which suggest that FLUENT can identify the general SCW heat transfer phenomena. Work has also been done on complex geometries around the supercritical point. Kinakin [**77**], modelled two separate subchannels without turbulence inducers and Saunders [**101**], modelled a quarter of bundle geometry with turbulent inducers. Their works suggest that there is a balance between simplicity and accuracy of results. A trade-off is the accuracy of results when modelling more complex models.

In this study, two subchannels in the horizontal orientation were modelled with FLUENT numerical code, setting boundary conditions to constant pressure of 25 MPa and inlet coolant temperature of 357 ^{o}C. This work concentrates on modelling SCW flow in two subchannels located just before the bulk average pseudocritical point to determine what phenomena are captured by FLUENT.

The subchannel geometry is taken from 43-element CANFLEX bundle (shown in Figure 4.1) with inner and outer ring element diameters of 11.5 mm and 13.5 mm respectively. Each element is heated with a base heat flux of 250 kW/m^2, which is applied uniformly along the length of the subchannel model. This ensures that the pseudocritical points for each subchannel are close to each other so that there are no influences from neighbouring subchannels. An inlet boundary condition of coolant mass flux of 1330 kg/(m^{2}s) was applied to the model. The

flow properties are distributed as a function of the relative areas of the subchannels and, therefore, smaller subchannels have lower mass fluxes. The subchannel selected for analysis is modelled with symmetry. The heat flux for each pin is uniform around the pin; hence, the heat fluxes received by the subchannels of similar geometry are identical. The effect of the circumferential wall conduction is negligible and not taken into account since the subchannel is modelled in steady state.

The three-dimensional model was developed in GAMBIT 2.4.6 finite element modelling software. The mesh was applied to every single side of the face of the geometry in order to adequately resolve the radial components of the mesh. After the edge meshes were created, a hexahedral face mesh was generated using the Cooper meshing scheme [**102**]. After the face mesh was created, a volume mesh was created by extruding the face mesh to a length of 0.481 m. The volume mesh consists of 852,480 cells split into 48 divisions axially along its length as shown in Figure 4.2. This final mesh size was obtained by striking a balance between the resolution of the mesh and the maximum available RAM memory of the computer being used. A trial and error approach method was used to obtain an adequate mesh definition since it was very difficult and time consuming to run enough models to test for convergence for every possible mesh division on each of the 12 edge meshes. The no-slip boundary conditions at the walls of the elements were resolved within the boundary layers with the first layer located at 5 μm from the wall and a multiplying factor of 1.2 for the 3 subsequent layers. The total boundary layer thickness is about 268 μm.

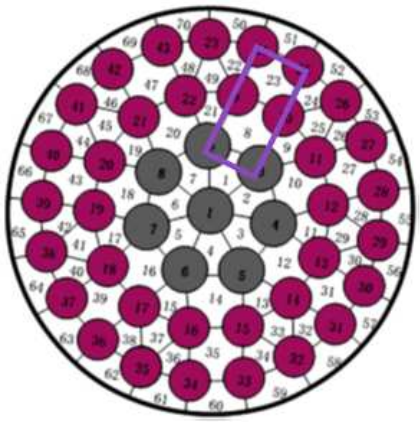

Figure 4.1: Schematic of CANFLEX-type bundle showing subchannels

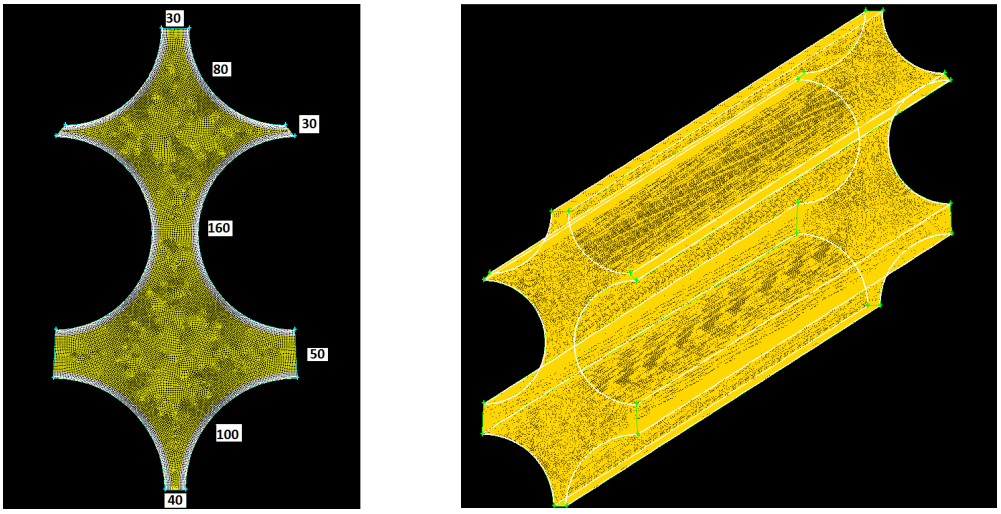

(a) Cross-sectional mesh view **(b) Isometric mesh view**

Figure 4.2: Mesh geometry of subchannel in Gambit

The mesh was then imported to FLUENT for analysis. The water properties were extracted from a National Institute of Standards and Technology Reference Properties (NIST REFPROP 8.0) database reference using a command line in FLUENT. The use of NIST REFPROP is essential since the fluid properties are near the region of the pseudocritical point of water. The fluid properties change significantly within a narrow range which causes the solver to become unstable.

The next step in FLUENT was to define the boundary conditions so that the solver fully understands the entirety of the mesh. The four boundary conditions that were applied are the mass-flow inlet, pressure-outlet, the no slip boundary conditions at the wall, and symmetry of the model. The boundary conditions at the walls of the fuel elements were set up so that heat flux could be applied and also ensure the no-slip boundary condition was satisfied. The inlet boundary condition allows the user to define the mass-flow, initial pressure, and direction of flow. The pressure-outlet condition serves to complement the inlet mass-flow condition. The symmetry boundary conditions were applied to the faces that were not bounded by the wall to ensure FLUENT treats the edge mesh as a symmetric across the edge.

The uniform 250 kW/m^2 heat flux boundary condition set for the wall is not representative of the heat flux distribution in a CANFLEX fuel bundle but was used in the model since larger heat fluxes produced fluid temperature values that were too large for the solver to handle as the NIST REFPROP database was limited to a maximum fluid temperature value of 1950 K. An effort to use the power factors which are typically around 0.6 to 1.13 for the elements in the rings in the CANFLEX bundle was attempted, but the FLUENT solver crashes because the fluid properties were out of the database range. Therefore, uniform heat flux was used for each element in the subchannel model. The absence of a turbulence inducer such as buttons, spacers, and endplates is the most probable

cause for the very high temperatures. It is expected that heat transfer will be enhanced with more turbulence and relatively high temperatures would not be encountered. However, due to the complexity of the model, turbulence generators were omitted in this work.

The k_e-ϵ turbulence model was adopted since it is a well known two-equation energy transport turbulence model developed by Jones and Launder [**103**]. The model works by conserving the energy contained within a turbulent region by means of transport equations that carry total energy (and its dissipation) along a geometrical flow path. The variables k_e and ϵ represent the total turbulent kinetic energy and the dissipation rate of energy respectively. The two quantities are described as follows:

$$k_e = \frac{u^2+v^2+z^2}{2} \qquad \left(\frac{m^2}{s^2}\right) \tag{4.1}$$

Where u, v, and z represent the one-dimensional velocities of fluid contained within the three dimensional domain. The dissipative energy term ϵ, is described as follows:

$$\epsilon = \rho C_\mu \frac{k_e^2}{\mu_t} \qquad \left(\frac{m^2}{s^3}\right) \tag{4.2}$$

Where ρ is the density of the fluid, C_μ is a constant taken to be 0.09 as defined by the standard k_e-ϵ model. The definition of ϵ can be expressed in a compact term:

$$\epsilon = \frac{k_e^{3/2}}{l} \quad \text{where} \quad l = \frac{\rho C_\mu}{\mu_t \sqrt{k_e}} \tag{4.3}$$

The characteristic length scale l, represents the maximum diameter of an energy containing eddy. The k_e-ϵ model is the most basic and documented turbulence model able to solve many complex flows.

In order to save computation time, the solution was obtained with an absolute convergence criterion of 10^{-5} for the each of the variables contained in the transport equation including continuity, x-, y- and z-velocity, energy, and epsilon. A higher convergence can be achieved with mesh refinement.

The simulation was performed using a coupled pressure-velocity second order algorithm. The RANS (Reynolds Averaging Navier Stokes) method was used as a steady case solution in order for the solution to converge. The instabilities in the code could not predict the unsteady state solution suggesting the need for refinement in the detail of the model.

4.4 Results Summary

Results obtained (Figures 4.3, 4.4, and 4.5) show a high gradient of properties (coolant velocity, density, and temperature) at the near wall region. The low velocity regions are located close to the wall as expected from the no-slip boundary condition. Low density fluid is found close to the wall of the subchannel which results from the coupling effect of higher heat transfer coefficient with low fluid velocity at the wall. Consequently, the temperature is significantly higher at near wall, regions but shows a more evenly distributed

profile at far wall regions. The non-uniformity of the fluid properties in the bulk fluid necessitates the division of the bulk fluid into two regions.

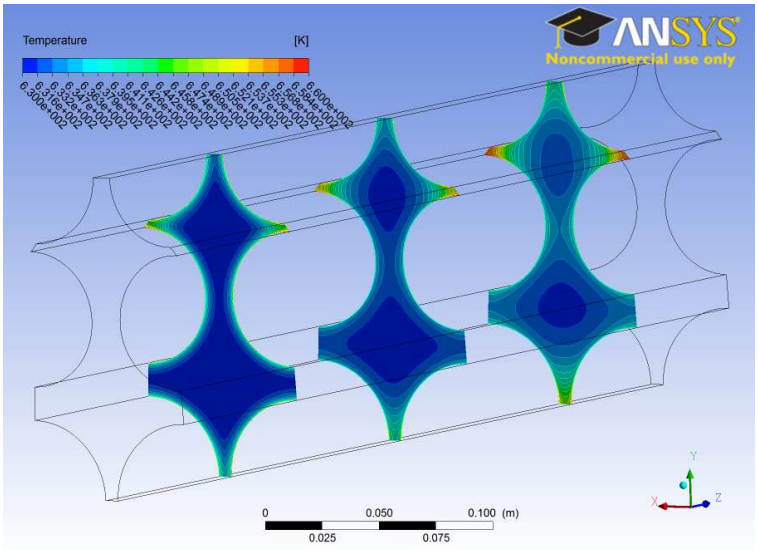

Figure 4.3: Axial cross-sectional temperature variation at a distance (z, from left to right) from subchannel inlet; (a) z = 0.1 m, (b) z = 0.25 m and (c) z = 0.4 m

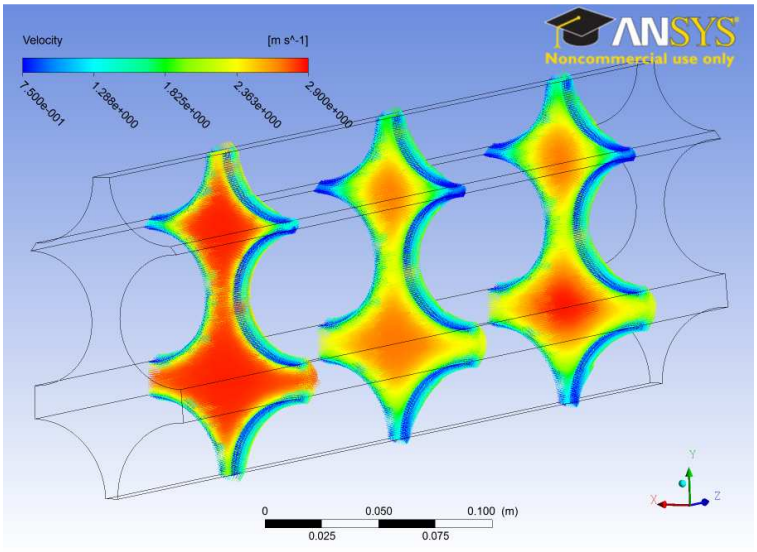

Figure 4.4: Axial cross-sectional velocity variation at a distance (z, from left to right) from subchannel inlet; (a) z = 0.1m, (b) z = 0.25 m and (c) z = 0.4 m

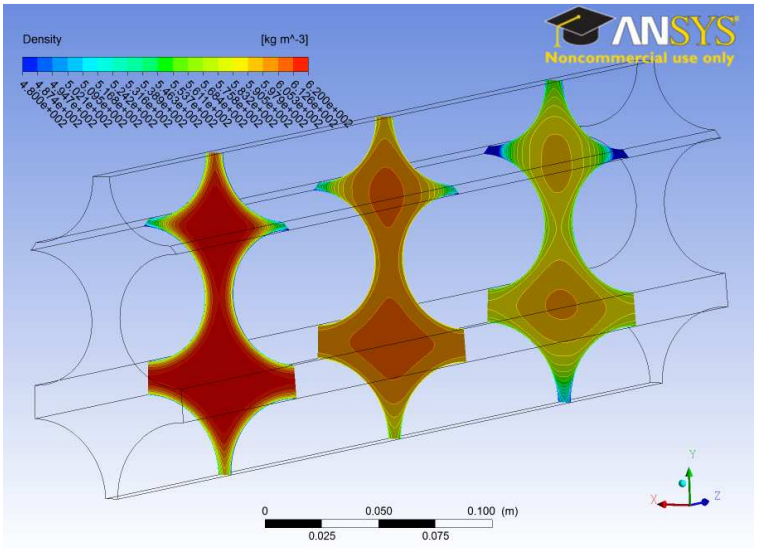

Figure 4.5: Axial cross-sectional density variation at a distance (z, from left to right) from subchannel inlet; (a) z = 0.1m, (b) z = 0.25m and (c) z = 0.4m

The heat transfer in SCW before the pseudocritical point can thus be divided into two regions: the first is the near wall region which consists of the fluid near the heated solid wall where the main mode of heat transfer is by heat conduction and the second region is the bulk region where the main mode of heat transfer is by convection. Figure 4.6 shows a typical (not from simulation) fluid property variation located upstream just before the pseudocritical point. This figure was drawn to show the steep change in the fluid properties in the near-wall and far-wall regions. The velocity, density, and temperature profiles change steeply in the near-wall region where the density gradient is the steepest. In the bulk region, thermalhydraulic properties change gradually. The friction forces are not significant in this region and this region can be treated as a bulk fluid.

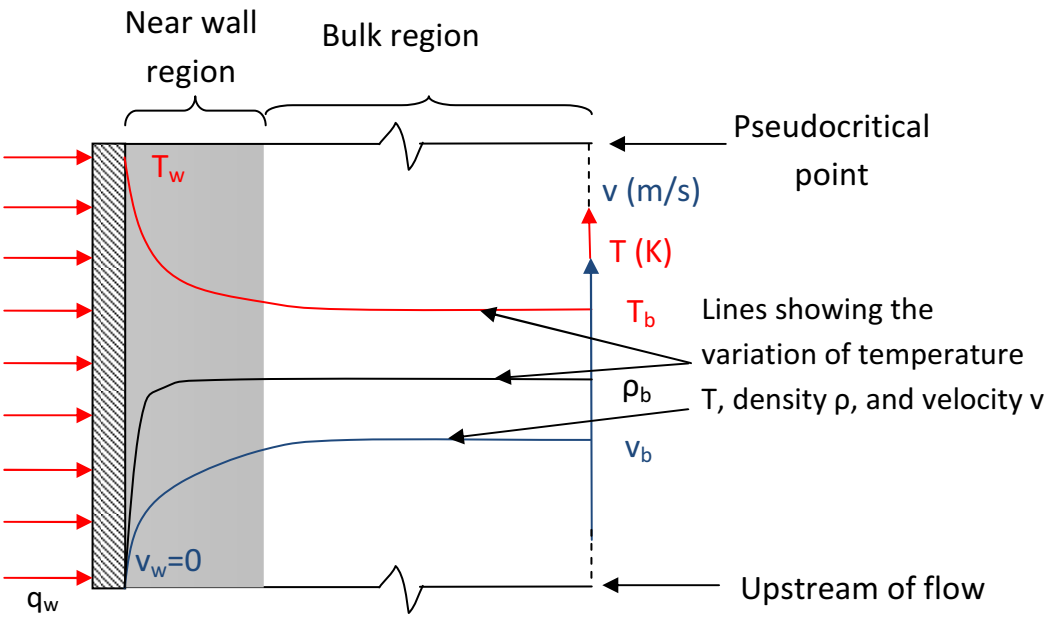

Figure 4.6: Near wall and bulk regions of heat transfer in SCW

In the CFD subchannel model, the farther the fluid region is from the wall, the larger the variation with the near wall properties. The subchannel under study consists of two subchannels of slightly different sizes due to the arrangement of the pins in the bundle. The lower subchannel has a larger cross-sectional area than the higher subchannel. The results show that the coolant in the upper subchannel has a higher bulk density compared to the lower subchannel due to the better heat transport properties. This shows that the viscous boundary layers have been resolved adequately in the model.

Consequently, the fluid within the narrow spacing between the subchannel walls has higher temperature values. The upper subchannel of the model under study has two pairs of walls with the smallest spacing between them (Appendix A). The

boundary layers of each wall pair are very close to each other with a spacing of about 10 μm between them. The viscous effect is significant in this region without adequate distance to develop a bulk region between them. As the coolant heats up along the subchannel, the temperature increases with maximum values located at the narrow spacing in the upper subchannel which mainly contains low density fluid, as shown in Figure 4.3. The no-slip boundary condition at the wall ensures a low coolant velocity at the near wall region. Low coolant velocity means low heat transport properties which in turn causes heat to build up close to the wall of the element in the narrow spacing. This region contains the fluid with the highest temperature which subsequently means pseudocritical phenomena will occur first at this region

The heat transfer mode along the subchannel varies along the subchannel. As the coolant is heated from the inlet, a localized low density region develops in low velocity regions as shown in Figures 4.4 and 4.5. Deteriorated heat transfer usually occurs at high heat fluxes and mass fluxes. It is usually located before the pseudocritical point of water is reached along the length of the channel. The regime of heat transfer can change from normal to deteriorated to enhanced modes in SCW heat transfer. The heat transfer regime in SCW depends on localized fluid conditions such as thermal profile, inlet temperature, pressure, mass flux, and heat flux; thus, the deteriorated heat transfer is affected by the local conditions. Physically, the change of the mode of heat transfer from normal to deteriorated heat transfer is not fully understood, but the development of localized low density fluid regions is believed to be the reason for this phenomena.

4.5 FLUENT's Capability to Simulate Supercritical Water Models

From the results, it is seen that the RANS method used in FLUENT code like other low Reynolds number turbulence models, over-responds to the strong non-uniformity of fluid properties which is encountered around the pseudocritical point. This can be seen in the results where the turbulence field is well resolved far from the wall, but unstable close to the near wall region due to an inadequate level of detail in the meshing. Consequently, the FLUENT code is unable to predict deteriorated heat transfer since this corresponds to the onset of the non-uniformity of fluid properties. However, it predicts accurately the region far from the onset of the pseudocritical point where thermophysical properties of the fluid show gradual variations. It is thus able to predict normal and enhanced heat transfer accurately, but deteriorated heat transfer to a lesser degree.

FLUENT resolves the far wall turbulence better than the near wall no-slip boundary conditions. This is due to the non-uniformity in the properties at the transition to pseudocritical conditions which are more drastic at narrow passages, as seen from the results on the subchannel modelling of fluid at supercritical conditions. This can be solved by improving the level of detail in the boundary layer development. For better results, the boundary layer should be non-uniform along the channel.

As observed from the results, FLUENT performs well around the pseudocritical region at low heat and mass fluxes, but seems to be unstable at high heat and mass fluxes. The stability may be a result of bulk fluid acceleration due to strong heating and may further increase the non-uniformity in the fluid properties, consequently affecting heat transfer. This hypothesis needs to be confirmed by experiments.

CHAPTER 5

THERMALHYDRAULIC EXPERIMENTAL LOOP DESIGN

This chapter discusses the conceptual design of SPETA. Section 5.1 describes an overview of the overall design.

5.1 Description of Test Facility Layout and Enclosure

Figure 5.1 shows a schematic of the conceptual design of SPETA. Water is pumped from a reservoir tank through the feed pump to the main pump which shall operate at a pressure head of up to 25 MPa. A set of control valves and flowmeters are located before the preheater. A tube-in-tube electric preheater powered by both AC and DC power supplies of 360 kW (120 V × 3000 A) each shall be used to heat the fluid to the inlet temperature of the test section. The test section inlet flow rate is measured with a flowmeter. The test section shall be made of Inconel 600 which shall be connected to the loop by flanges to allow for multiple geometries. A DC supply of 500 kW (120 V × 4167 A) shall be used to heat the test section. The locations of the pressure taps and thermocouples used to measure pressure drop and wall temperatures will be based on the requirements of the particular test. A cooler is located after the test section to extract some heat which may be recycled back to before the inlet of the preheater. Three heat exchangers are connected in series (only two are shown in Figure 5.1) with the flexibility to operate only one, two or all three simultaneously. A flow meter and control valve are used to measure the flow and control the flow respectively as the fluid recirculates back to the pump.

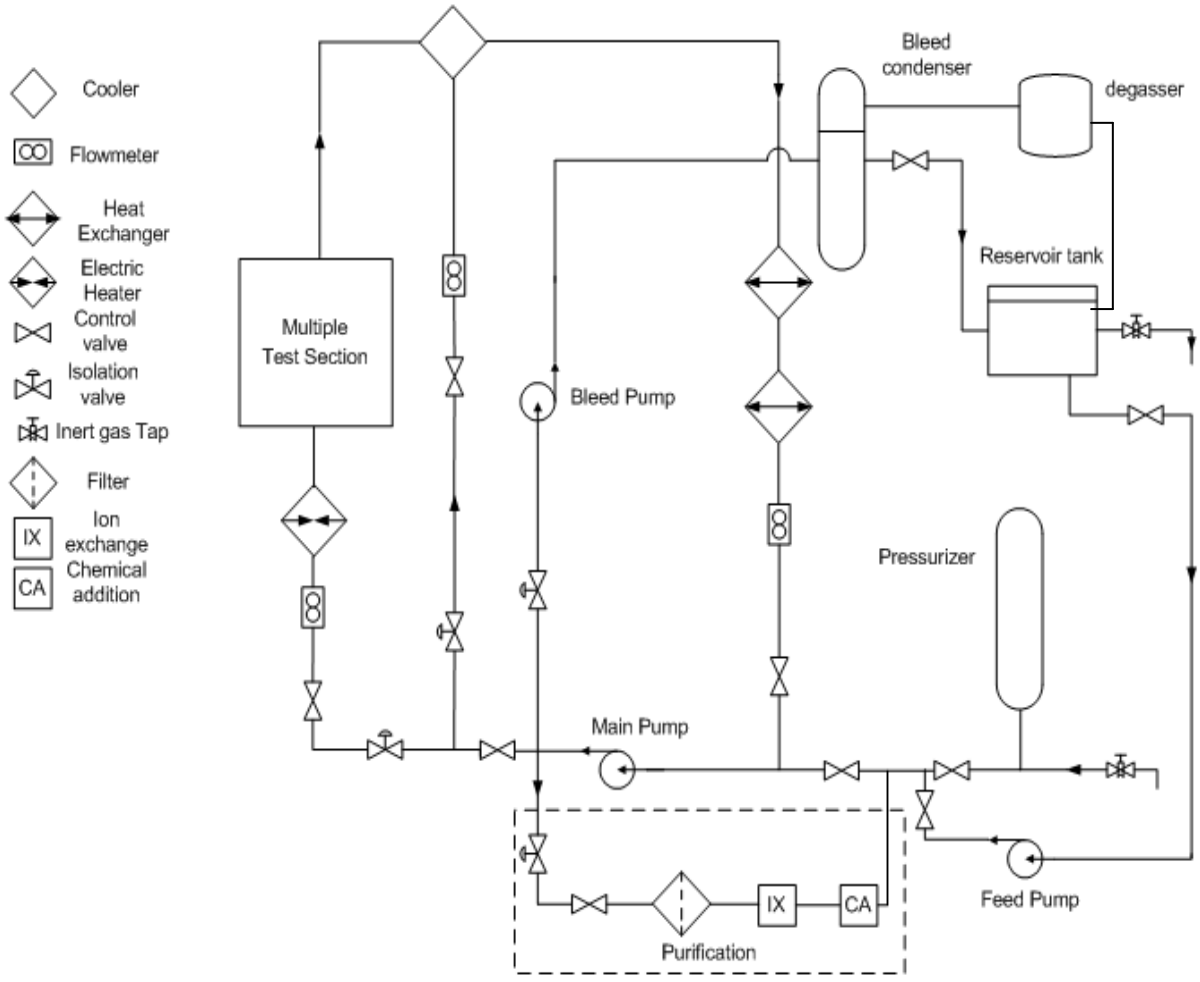

Figure 5.1: Schematic of SPETA; 1-main pump, 2-control valves 3-isolation valves, 4-flowmeter, 5-electrical preheater, 6-multiple test section, 7-cooler, 8-heat exchanger, 9-purification system, 10-bleed condenser, 11-reservoir tank, 12-feedwater pump, 13-reservoir, 14-control valve

The bypass line serves to conveniently redirect the working fluid if need arises. A centrifugal pump will be used to bleed the fluid to a bleed condenser which cools the fluid. The vapour is extracted by a degasser leaving the liquid behind which is pumped to the reservoir. The reservoir tank is used to store the working fluid. The tank is equipped with a tap at the bottom which can be used to vary the level of fluid in the tank. A feed pump circulates the fluid through the loop and the flow rate is controlled by control valves. The system pressure of the loop is controlled by a pressurizer located before the feed pump. The pressurizer is equipped with an over-pressure relief system to relieve any pressure built up in the system. Any leakages in the loop can be detected by a lower liquid level in the pressurizer. The loop is equipped with a tap located before the feed pump to inject inert gas in the loop for maintenance.

A purification system is used to clean the fluid used in the loop. Only 5% of the flow will be filtered when the loop is in operation. The recycled fluid is pumped back into the loop.

The proposed operating conditions for SPETA are shown in Table 5.1.

Table 5.1: Proposed operating limits of SPETA

P (MPa)	T_b (^oC)	q (kW/m^2)	G ($kg/m^2.s$)	Q(kW)
≤30	≤625	≤5000	≤15000	1220

The facility can be enclosed in a 9 m by 2 m by 4.8 m laboratory with adequate room for modifications. Table 5.2 shows the preliminary design concept of some key components of the facility. The components have been selected so that they can be used to run experiments that are similar and comparable to the proposed SCWR concepts.

Table 5.2: Design inputs of loop and components

Proposed design input	**Selection(s)**
Test Section Orientation	Vertical, Horizontal
Test section geometries	Bare tube, annulus tube, 7 element bundle
Temperature measurement	K-type thermocouple
Working Fluid	Distilled Water, CO_2, R-134a
Test section heating type	Direct electrical heating
Test section material	Inconel 600
Power Source	Alternating Current, Direct Current
Control valve type	Globe Valves
Isolation valve type	Gate Valves (Wedge type)
Flowmeter type	Coriolis, orifice or turbine flowmeters
Absolute Pressure Measurement	Piezoelectric pressure transducer
Differential Pressure Measurement	Strain gauge pressure transducer
Main heat exchanger type	Shell and tube
Cooler type	Shell and tube
Heat exchanger coolant fluid	Water
Pump type	Centrifugal
Joint Fixtures	Flanges
Preheater type	Tube-in-tube

5.2 Test Section Design

This section describes the scaling laws that were applied to the development of the test section geometry. The dimensions and geometries of the test section are scaled such that it is representative of SCWR fuel channel dimensions as discussed in chapter 3.

To provide optimum flexibility for research, SPETA will be able to use both a vertical test section with a maximum length of 4 m and a horizontal test section with a maximum length of 2 m. Angled test sections between the vertical and horizontal concepts will be possible. The use of different orientations shall be facilitated by modification of the piping system between the fixed pump and the heat exchangers and the test section. The area that will be occupied by the test section shall be sufficient to accommodate these modifications.

5.2.1 Test Section Material

The test section will be directly electrically heated as stated in Table 5.2. The material of choice should have a relatively high value of specific electrical resistivity that does not significantly vary with temperature to ensure constant heating throughout the power manoeuvre. This allows for variation of the test section geometry, heated area, wall thickness, and heated length to obtain different flux profiles. With a relatively constant resistivity as temperature changes, the local heat flux is uniform along the test section length for a uniform cross-sectional area and geometry regardless of the local wall temperature. Inconel 600 and Inconel 718 are the most suitable material with this property. Inconel 600 has a higher conductivity than Inconel 718 making it a more suitable choice. Recommended material choices for the rest of the loop are SS-304, SS-316, Hastelloy C276, Hastelloy B2, and Monel 400 due to their corrosion-

resistance properties and high strength (Refer to Appendix F). It allows fluids like Freon and other chemicals to be used in the loop. Hastelloy C276, Hastelloy B2, and Monel 400 are suitable for even more corrosive environments and are excellent choices for material of construction.

5.2.2 Diameter and Inlet Conditions

A nominal hydraulic diameter needs to be chosen for sizing of the entire loop and other components. The nominal hydraulic diameter needs to be equivalent to expected industrial conditions with a reasonable allowance to accommodate future changes in designs. A sizing study was done to determine the nominal diameters and appropriate allowance for the loop design. The methodology used to establish the limits for the conceptual hydraulic diameter for the test section in the loop has been developed, based on Figure 5.2 which shows the percentage of the pressure drop in the test section as a fraction of the pressure drop in the loop at various hydraulic diameters of the test section. The figure was obtained by calculating the pressure drop using MATtrix LABoratory (MATLAB) program in Appendix C.

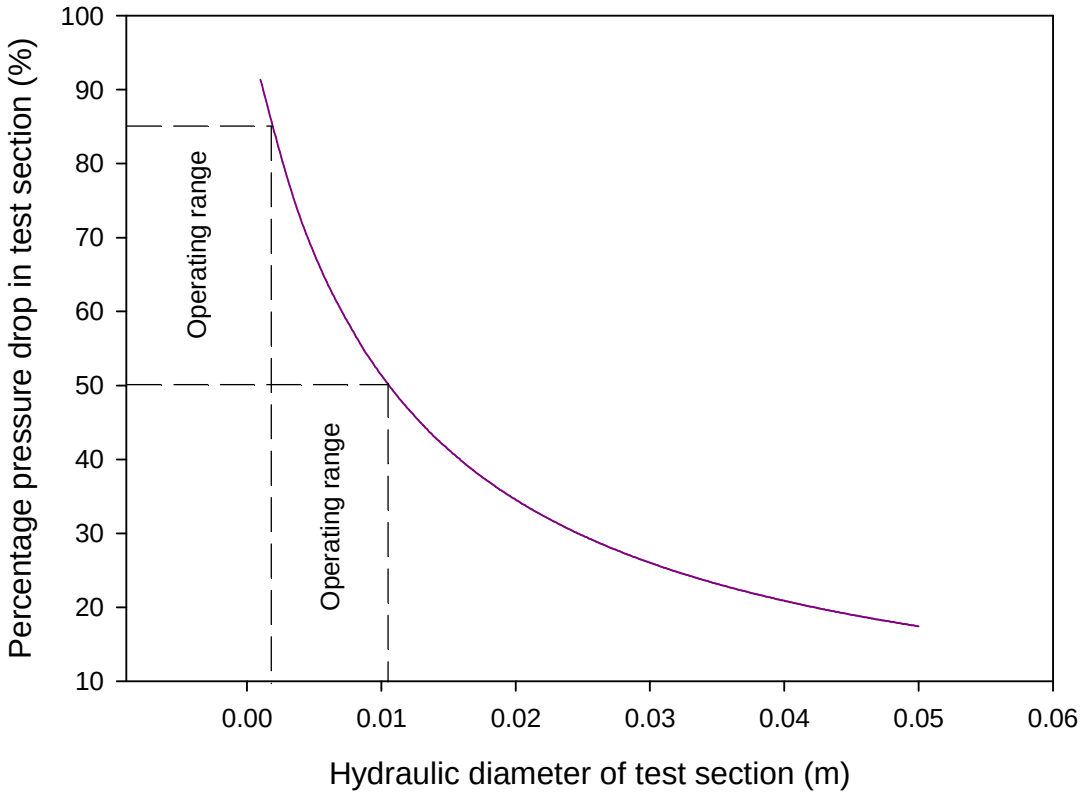

Figure 5.2: Percentage pressure drop in the test section at different test section hydraulic diameters

An important phenomenon that needs to be studied is the pressure drop in the test section. In order to study the pressure drop at supercritical pressures, a significant percentage pressure drop (50%-85%) should be present in the test section of the loop. The corresponding hydraulic diameter of the test section required in order to achieve a high pressure drop in the loop ranges from 0.001-0.011 m. The hydraulic diameter of the test section should be sized at a maximum of 20% of the loop piping which is designed at a diameter of 0.05 m which can be read from Figure 5.2.

The methodology for the development of the average velocity range of the water in the loop is based on the accelerated corrosion rates as a result of high velocity of water in the loop. Studies have shown that above water velocities of 5.2-6.1 m/s, Flow Accelerated Corrosion (FAC) becomes significant [**104**] which varies linearly with the velocity. Based on operation experience at the Point Lepreau Generation Station, the FAC corrosion rate of the feeders which are fabricated from 106 Grade B carbon steel pipe, after 17 years of operation is a maximum of about 106 μm/year [**105**]. Steel alloys with a higher chromium content of at least 0.33%, have 50% reduction in the FAC corrosion rate under the same condition. By deduction, pipes fabricated from stainless steel which have at least 18% of chromium content will have corrosion rates expected to be reduced by more than 50% of the carbon steel. Studies have shown that the corrosion rate is linear with time and has a squared dependence with coolant average linear velocity [**105**]. This suggest that the corrosion rate of feeders made of stainless steel after 20 years of operation at an average coolant velocity of 25 m/s, the FAC corrosion rate will be less than 100 μm/year. The average coolant velocity will remain less than 25 m/s over the period of operation to be able to achieve 20 years of operation without replacement of piping.

Graphs of velocities and mass fluxes are plotted against the hydraulic diameter for the experimental bundle design. The reference fluid for the graphs is light water. Figure 5.3 shows the mass flux required for each bundle type relative to a corresponding hydraulic diameter to obtain the same Reynolds number. Curves of different Reynolds numbers show the effect of hydraulic diameter on the mass flux. It is assumed that the Reynolds number is a sufficient scaling factor for test section sizes which thus means that inertia and viscous forces will be the dominant components that need to be maintained.

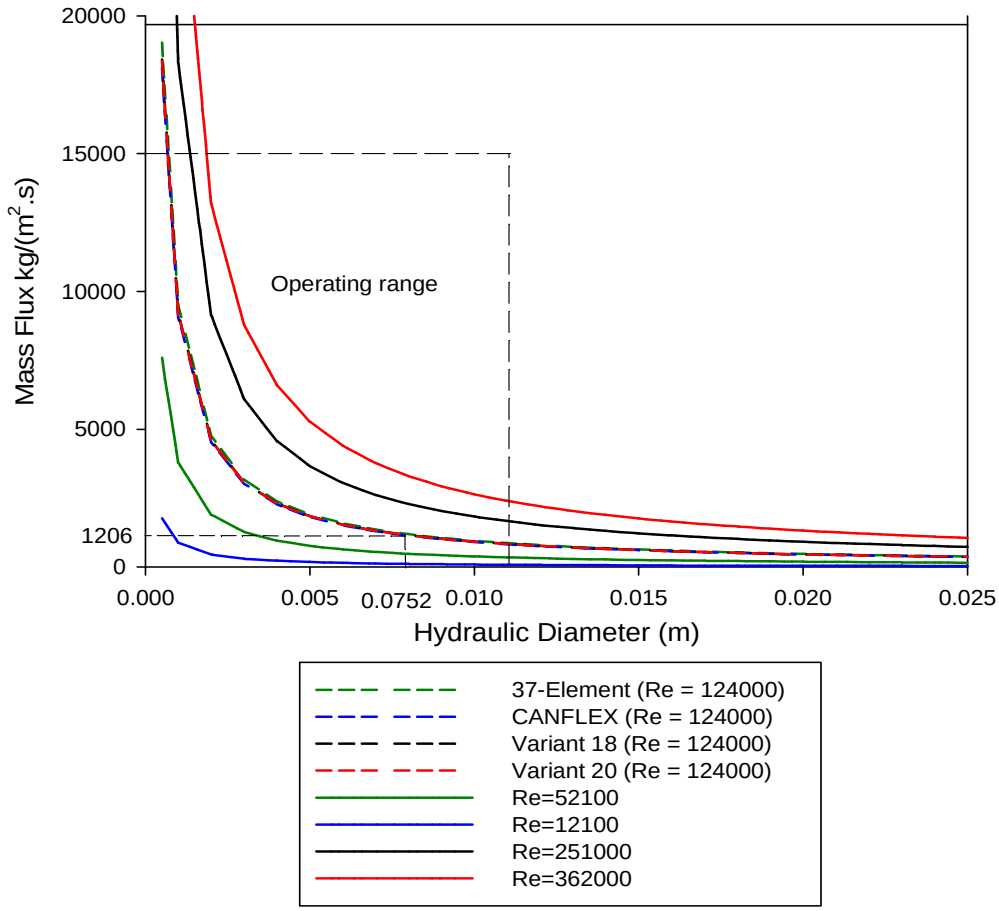

Figure 5.3: Mass flux to hydraulic diameter variation for different bundle types

Each curve on Figure 5.2 has constant Reynolds number which implies that all of the bundle types have similar geometric properties; consequently, inertia and viscous forces are similar for the various bundle types. This is expected since the hydraulic diameter is fixed for each bundle type. The mass flux for a CANFLEX type SWCR bundle is identified in Figure 5.3 at 1206 kg/(m^{2}s) with a corresponding hydraulic diameter of 0.00752 m. For a particular hydraulic diameter, a higher mass flux can be achieved by increasing the velocity or the density, or a combination of both flow properties. For a typical inlet bulk density of 625 kg/m^3, the maximum mass flux that can be achieved with an average inlet

velocity of 25 m/s is 15000 kg/(m^{2}s) which is the product of the bulk density and velocity. SPETA shall be able to provide the test section with a mass flow rate of 15000 kg/(m^{2}s).

Figure 5.4 shows how the bare tube and annulus tube (inside and outside) diameters vary with the inlet velocity of the fluid. The annulus tube shows a similar trend as the bare tube. With the annulus and bare tube having equal hydraulic diameters, both the internal and external diameters of the annulus have larger values than the bare tube.

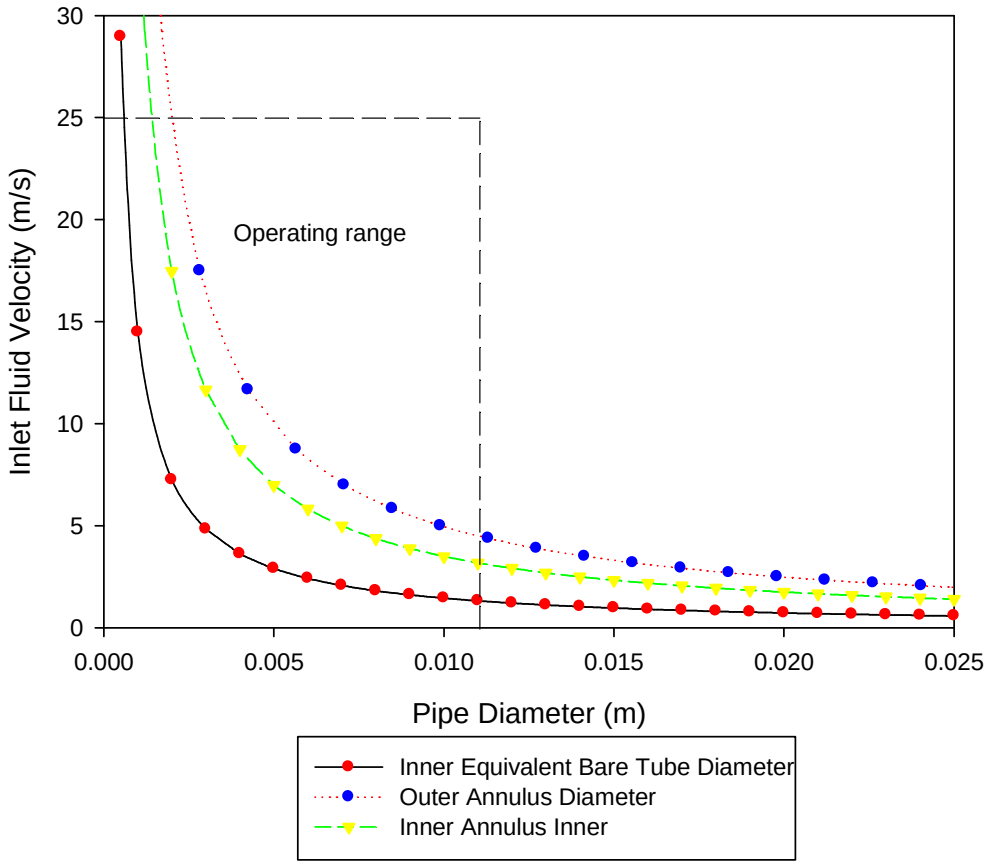

Figure 5.4: Scaled bare tube and annulus diameters for CANFLEX type bundle

In order to keep the element-to-bundle size ratio of the 7-element bundle (Figure 5.5), the element diameter is plotted against the inside diameter as shown in Figure 5.6. The element diameter shows a linear correlation to the hydraulic diameter of the bundle.

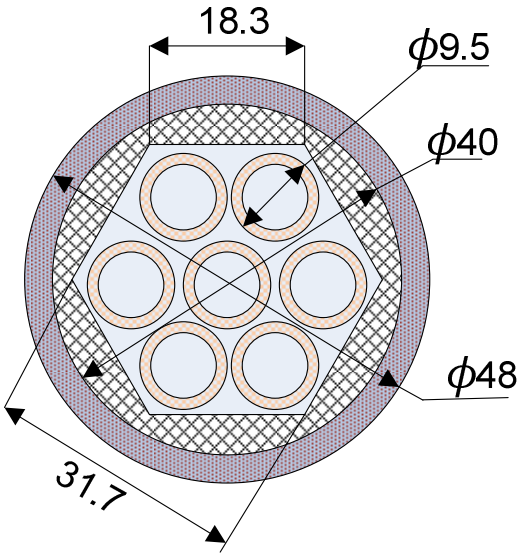

Figure 5.5: Kirillov's 7-Element bundle (Dimensions in mm)

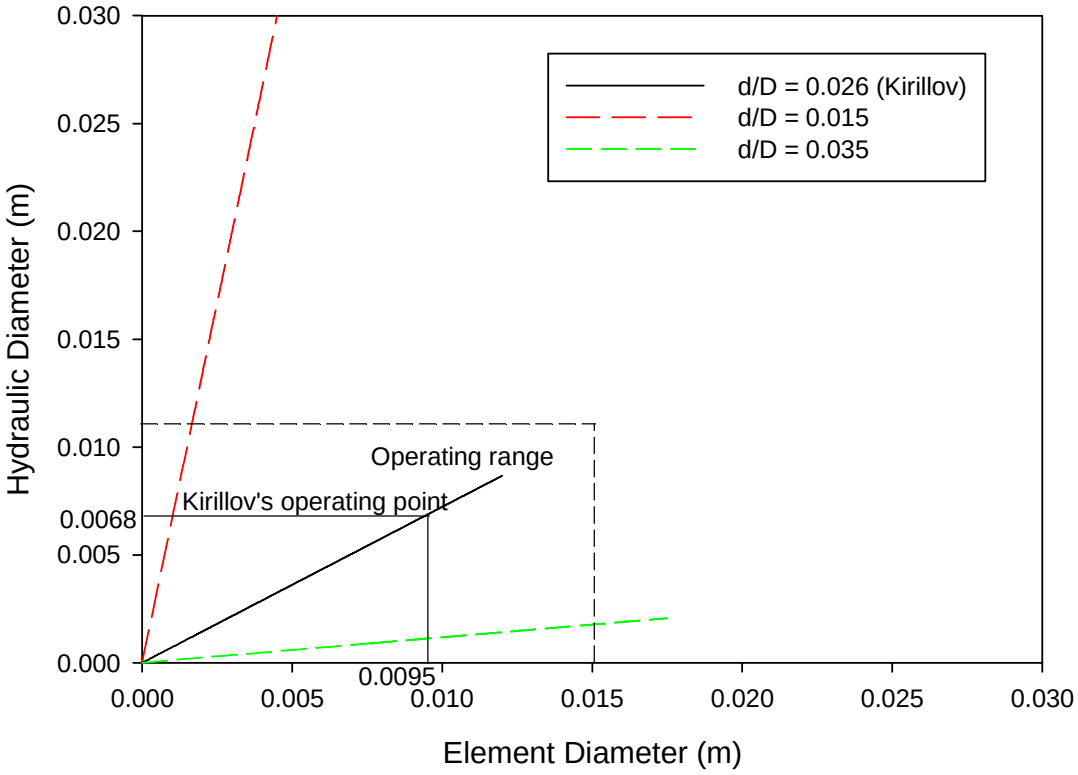

Figure 5.6: Hydraulic diameter against element diameter for 7-element bundle

Figure 5.7 shows the variation of the element diameter with the inlet velocity of the bundle. The Reynolds number for any point along this line is equal to the Reynolds number of the reference CANFLEX bundle. An increase in the size or diameter of the element would mean and a decrease in velocity to achieve the same dimensionless Reynolds number as the CANFLEX bundle.

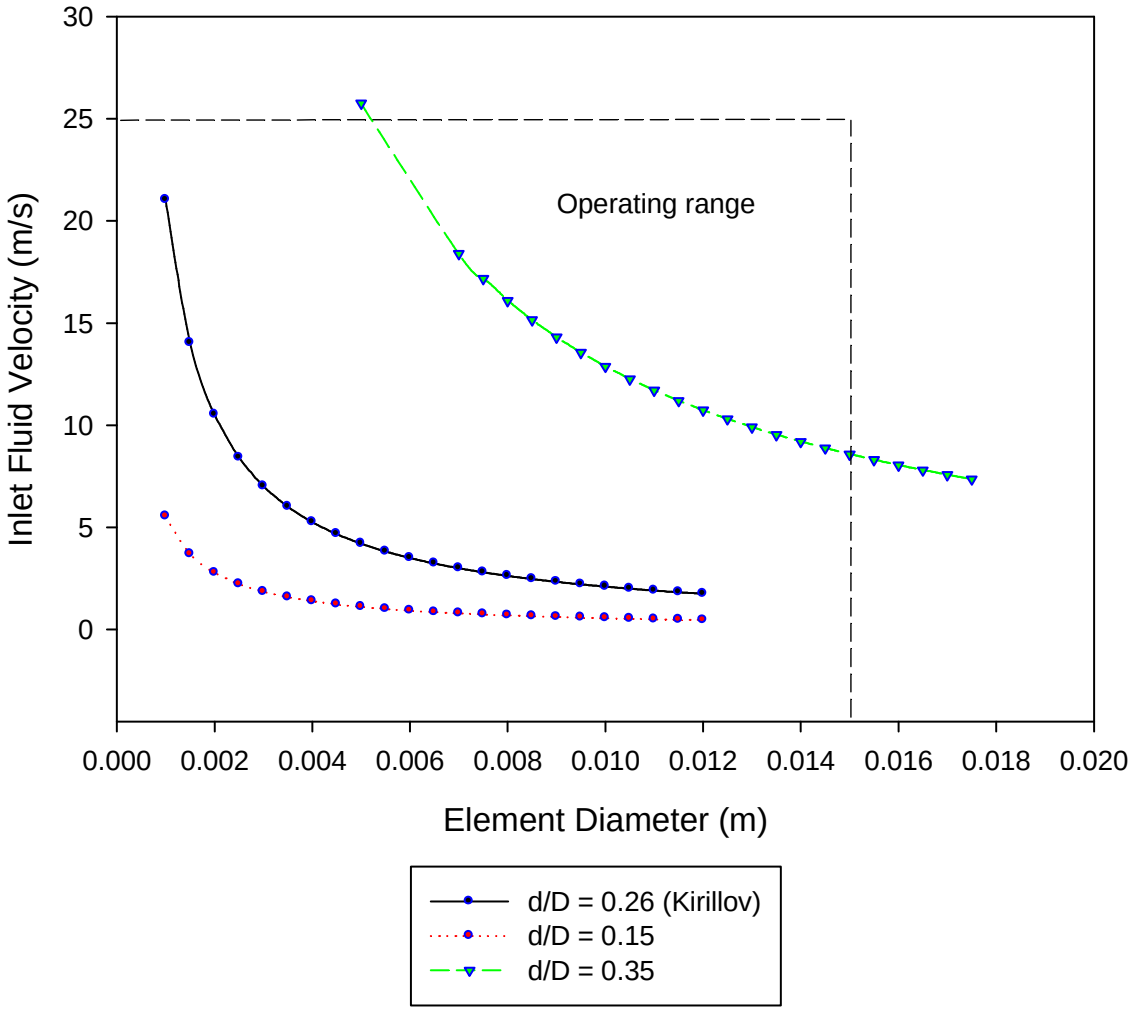

Figure 5.7: Element diameter against velocity for 7-element bundle

Figure 5.8 shows the variation of the experimental bundle inner diameter with the inlet velocity of the fluid. As expected, the trend in the change of the internal diameter of the bundle is similar to the change of the diameter of the element

since the ratio of the dimensions of the element diameter to the diameter of the 7-element bundle is kept constant.

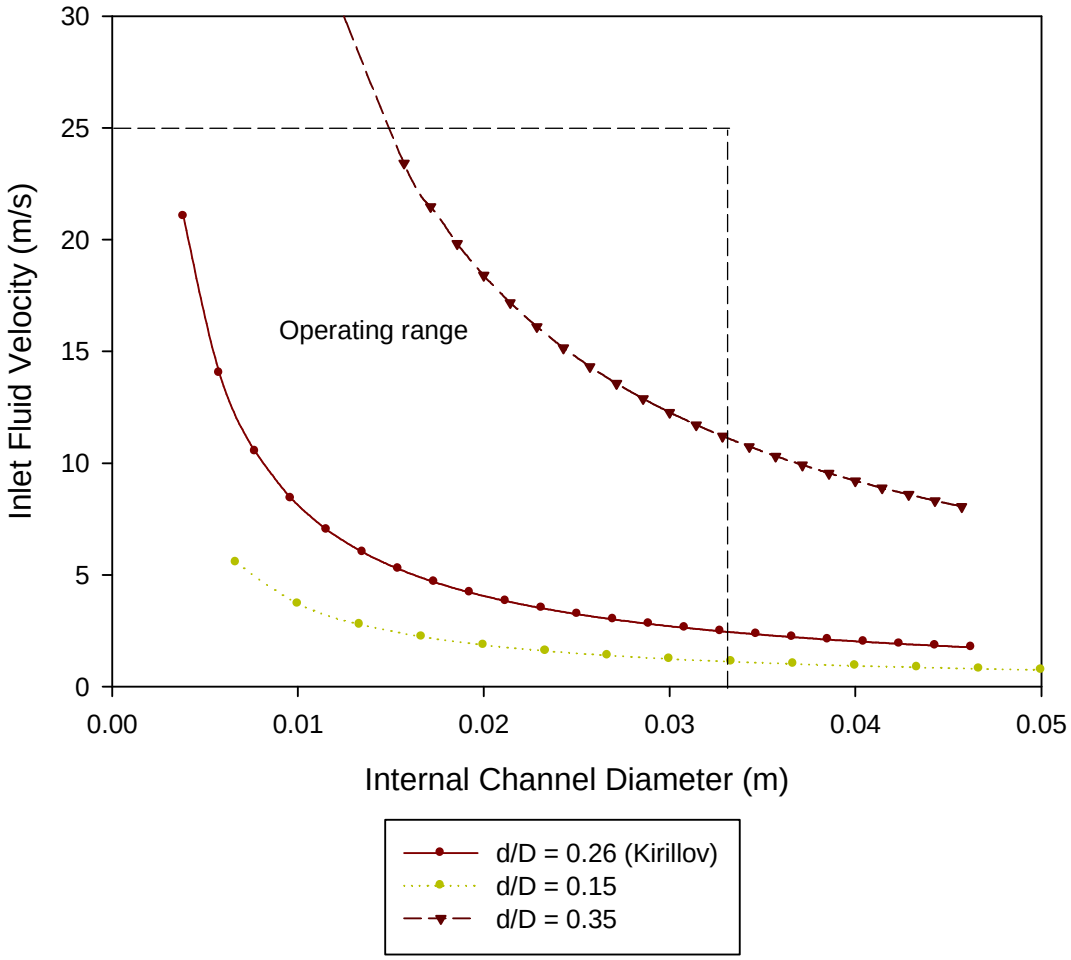

Figure 5.8: Internal diameter against fluid inlet velocity for 7-element bundle

5.3 Heat Exchanger

This section presents the description of the cooler required to remove heat from the fluid.

A simple case of a single-tube heat exchanger with a tube inlet temperature of 625 ^{o}C and an outlet temperature of 500 ^{o}C was considered at first. In the initial calculation, a mass flow rate of 4.37 kg/s was used as reference for comparable analysis with a feeder flow rate for the Canadian SCWR design. Under these input conditions, a total of 15 MW of energy is needed used to raise the temperature at the inlet from 350 ^{o}C to 625 ^{o}C at the outlet. However, the power requirement in the loop limited to 1.22 MW. This implies that a lower flow rate is required to operate the loop in order to achieve the temperature boundary conditions in the test section. The mass flow needed to satisfy the temperature boundary condition was 0.35 kg/s. The Canadian SCWR channel inlet and outlet temperature conditions may not be satisfied if the mass flow rate water is greater than this value, but comparisons from results can be done with different boundary conditions.

The value of the heat transfer, Q, was estimated to be 1.4 MW

5.3.1 Heat Exchanger Type

A shell and tube design was chosen for the cooler and heat exchangers. A series arrangement of heat exchangers was chosen so that if less heat is to be removed, the fluid can bypass as many heat exchangers as required.

The design temperatures for the inlet and outlet temperatures of the heat exchangers are known. The maximum tube length of all the heat exchangers combined was calculated for the set boundary conditions in Tables 5.3 and 5.4. The first approximation of the pressure at the outlet was estimated based on an

initial estimate of the tube length in the heat exchanger. The low pressure drop in the test section will not significantly affect the thermophysical properties of the fluid so the first approximation of the outlet pressure is adequate for the calculation.

Table 5.3: Boundary conditions for the tube side of heat exchanger

Tube Side of Cooler		
Water Property	**Inlet**	**Outlet**
Temperature (^{o}C)	625	500
Pressure (MPa)	24.60	24.56
Density (kg/m^{3})	64.67	87.69

Table 5.4: Boundary conditions for the shell side of heat exchanger

Shell Side of Cooler		
Water Property	**Inlet**	**Outlet**
Temperature (^{o}C)	25	50
Pressure (MPa)	1	1
Density (kg/m^{3})	997.05	988.43

The minimum average tube length required to satisfy the boundary conditions of the single-tube shell and tube heat exchanger using the NTU method is 1.8 m.

The minimum average tube length required to satisfy the boundary conditions of the single-tube shell and tube heat exchanger using the LMTD method is 3.08 m.

The value of the calculated average heat transfer coefficient at the inner surface (hot side) of the tube is 1080 W/m^{2}K

The value of the calculated average heat transfer coefficient at the outer surface (cold side) of the tube is 290 W/m^{2}K

The values of the heat transfer coefficient at the inner surface and outer surface can be calculated with Equation 3.12. The value of the calculated total heat transfer coefficient is 229 W/m^2K

5.3.2 Tube Configuration

A single-pass type heat exchanger was chosen for analysis. Figure 5.9 shows a typical design for the heat exchanger. The baffle is used to improve mixing of the fluid in the shell side of the heat exchanger.

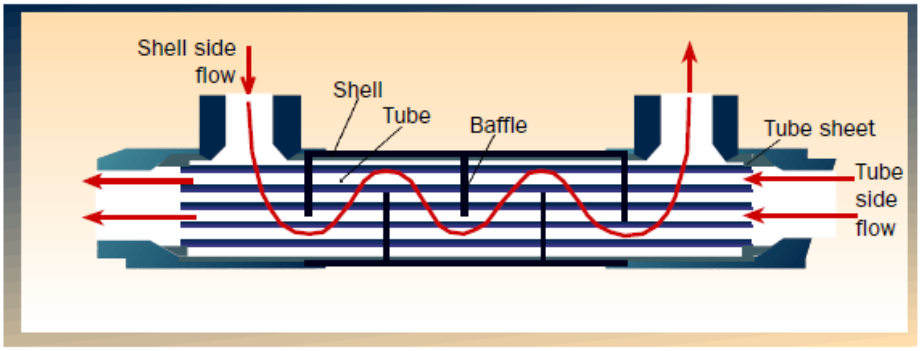

Figure 5.9: Single pass shell and tube heat exchanger [**106**]

5.3.3 Assumptions for calculation

A few assumptions were made to calculate the maximum length of the tube needed in the shell of the cooler. The following assumptions were made to simplify the estimation.

- The outlet and inlet temperatures of the tube are 625 ^oC and 500 ^oC respectively.

- The inlet and outlet temperature of the fluid in the shell are 25 ^{o}C and 50 ^{o}C respectively. The constant temperature assumption is used based on the NTU method.
- The fluid in both the tube and shell is water.
- The inlet mass flow rate of the shell and tube are 5 and 0.35 kg/s respectively. The same mass flux in the tube is used for calculations throughout the loop and that of the shell was selected based on heat exchanger for analysis.
- The wall temperature of the inner surface of the tube is 50 ^{o}C less than that of the bulk fluid at every point in the tube. This assumption is based on previous experimental [**80**] results on bare tubes in supercritical water experiments.
- The outer surface of the tube is the same temperature as the inner surface of the tube at every point in the tube. This is equivalent to a high thermal conductivity of the tube making the resistivity negligible.
- There is no fouling in the tube.
- Mokry's correlation [**91**] was used to calculate Reynolds numbers both in the tube and on the shell side of the tube.
- Both NTU and LMTD methods were used to estimate the tube length.
- The counter flow arrangement is used.

5.3.4 Sizing of Heat Exchanger

Typically, heat exchangers have length to diameter ratios of 6:1 to 8:1. Typical tube lengths are 2.4, 3.0, 3.7, 4.9 or 6.0 m with the most common tube length ranging from 4.9 to 6.0 m. Tube outer diameter sizes are typically from $\frac{1}{4}$ of an inch (6.35 mm) to $1\frac{1}{2}$ inches (38.1 mm) with the most common diameters values of $\frac{3}{4}$ (19.1 mm) and 1 inch (25.4 mm). Shell diameters usually range from 100 - 500 mm.

The number of tubes and the length of each tube can be determined for the heat exchanger. The number of tubes in the heat exchanger is designed so that its length can be kept to a minimum. The design length for the maximum tube length for the heat exchanger is 1 m. The value of the length required is calculated for 10 tubes with the mass flow split evenly across all tubes. Inner tube diameters are 0.0085 m each with outer diameters of 0.095 m which corresponds to a 3/8 inch outer diameter pipe.

A Basco type-500 (See Appendix I) straight-tube type heat exchanger has a shell inner diameter of $3\frac{1}{4}$ inches (82.6 mm) and can accommodate 60, $\frac{1}{4}$ inch (6.35 mm) tubes or 24, $\frac{3}{8}$ inch (9.53 mm) tubes [**107**].

Table 5.5 shows the calculated number of tubes required to satisfy the inlet and outlet boundary conditions of a Basco 500 straight-tube type heat exchanger. The different power ratings estimate using the number of tubes in the heat exchanger was calculated with the MATLAB code in Appendix D.

Table 5.5: Number of 1 m long tubes required for different power ratings the Basco 500 straight-tube type heat exchanger containing 3/8 inch (9.53 mm) tubes

Power rating (MW)	Inlet Temperature (^oC)	Outlet Temperature (^oC)	Number of tubes
100	625	530.5	3
200	625	458.0	6
400	625	389.0	8
600	625	374.5	9
800	625	291.0	13
1000	625	160.0	20

Table 5.6: Length of tubes required for different power ratings of the Basco 500 straight-tube type heat exchanger containing 24, 3/8 inch (9.53 mm) tubes

Power rating (MW)	Inlet Temperature (^oC)	Outlet Temperature (^oC)	Length of each tube (m)
100	625	530.5	0.12
200	625	458.0	0.23
400	625	389.0	0.30
600	625	374.5	0.36
800	625	291.0	0.54
1000	625	160.0	0.84

Table 5.6 shows that the longest tube required for the three heat exchangers (200 MW, 400 MW and 600 MW) required for the loop is less than 0.5 m which satisfies the design requirement for the heat exchangers.

Based on these calculations, it was estimated that three single pass heat exchangers of 200 MW 400 MW and 600 MW will be adequate to remove the heat from the loop. Three different heat exchangers of different ratings are used in order to allow various heat transfer experiments to be performed. Each heat exchanger will have about 10 cm outside diameter and will be less than 50 cm in length.

An independent design was done by Brampton Plate and Structural Steel Rolling Inc (See Appendix J) to estimate the heat exchanger size suitable for SPETA. With the same boundary conditions as in Tables 5.3 and 5.4, the heat exchanger designed was found to be 1.2 m long with a shell diameter of 16.3 cm. This verifies the analysis done in this work on the Basco type-500 heat exchanger.

5.4 Valves

A research into valves was done and the most appropriate ones for SPETA were selected with basic specifications needed to purchase the appropriate valves.

5.4.1 Control valves

The loop as shown in Figure 5.10 shows the control valves circled in the layout of the conceptual design of SPETA. In order to make sure the valve is suitable for the loop, a look into various valves was done and the most appropriate type of valve was chosen.

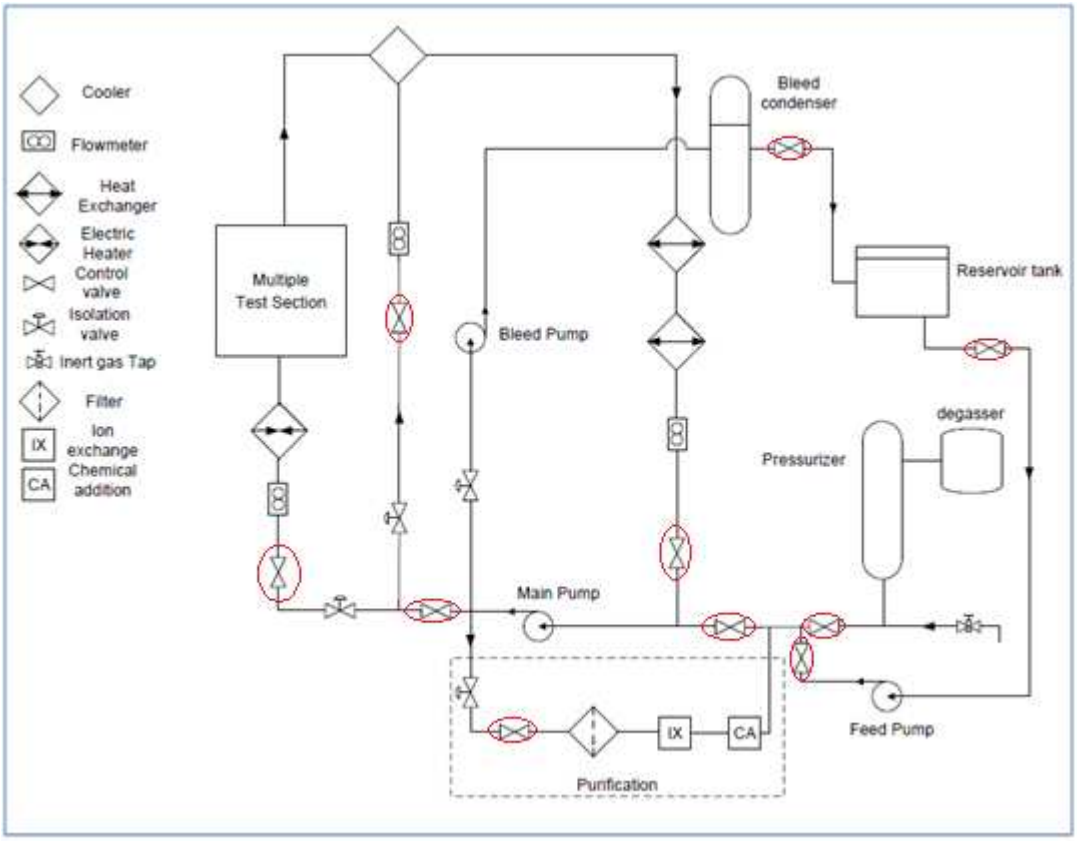

Figure 5.10: Layout of loop showing control valves

Control valves are used for modulating/throttling flow with the valve closure element (globe or gate) varying between the fully closed and fully open positions. Modulating valves are used where an automatic, repeatable, and accurate control of the fluid parameter is required. A remote control is required to control valves, so that the effect of flow rate on thermalhydraulic properties during experiments can be studied. The valve closure element is positioned at a fixed percentage of valve opening before each experiment, to satisfy a specific flow requirement. When the system flow requirement changes, the valve is manually repositioned while loop is offline, to provide the necessary hydraulic resistance and pressure drop.

The following valves can be used for throttling/modulating applications:

- Globe valves
- Butterfly valves
- Diaphragm valves

Globe valves are the proposed choice of flow control due to their adaptability. Globe valves compared to ball and butterfly valves, have a higher flow resistance. The resistance to cavitation and noise is higher in globe valves compared to low-resistance valves (ball and butterfly valves), due to a lower flow capacity in globe valves. The flow capacity of a globe valve is about one-third of low-resistance valves. Butterfly valves, like conventional ball valves, cannot provide fine control at lower flow rates.

5.4.2 Isolation Valves

The loop as shown in Figure 5.11 shows the isolation valves which are circled in the layout of the conceptual design of SPETA. Isolation valves shown in the loop are not going to be operating at high temperatures, but are subjected to high pressures, so it is necessary that they can withstand high pressures.

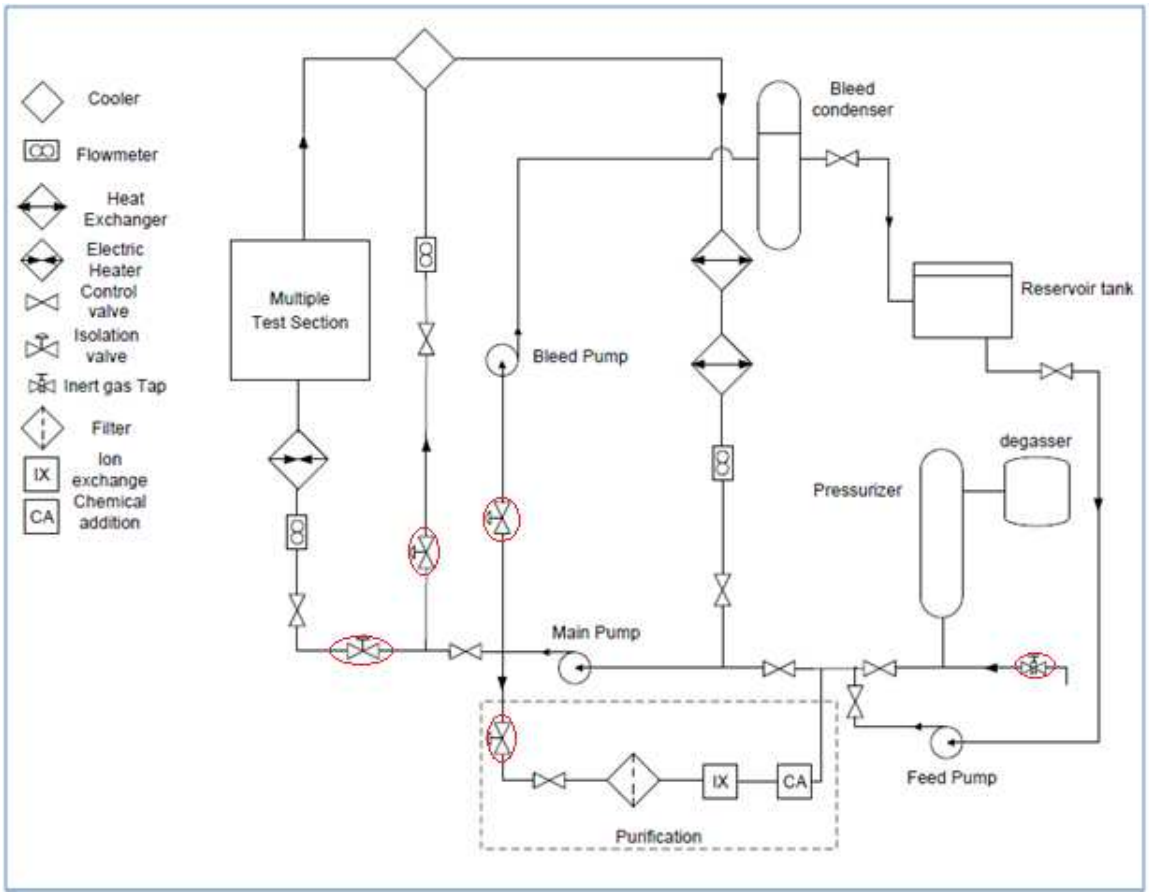

Figure 5.11: Layout of loop showing isolation valves

Isolation valves are used for on-off service with local or remote actuation. They function either close or open with a low leak rate when they are fully closed. They are typically used to isolate a component or a section of a system for maintenance and testing, or diversion of flow from one system component or piping section to another. Leakage can be described as the quantity of fluid passing through an assembled valve in a closed position with pressure differential across it.

Some types of valves that are capable of performing modulating functions as well as on-off functions include globe valves, ball valves, and butterfly valves. Other valves that are solely used for isolation include:

- Ball valves
- Gate valves
- Plug valves

Gate valves are the most suitable for SPETA since they can withstand high pressure and high temperature systems. Most gate valves are designed with a metal-to-metal seating which allows them to operate at much higher temperatures than polymeric-type seat materials. Gate valves offer the lowest possible pressure drop during fluid flow conditions since they provide minimum flow restriction. The wedge-type gate valve is the most common type of valve used in industrial piping [**108**]. It is used in straight-line fluid flow. When fully open, the gate is drawn up leaving an opening which is the same size as the pipe which results in minimal pressure drop. Gate valves are not suitable for throttling since they are hard to modulate; however, they function well as isolation valves.

The choices of materials that can be used to manufacture the valves include carbon steel, SS302, SS304, cast iron, and Hastelloys “B” and “C” because, of their high temperature and pressure resistances. They are also resistant to Freon compounds. Other materials that may be suitable for the manufacture of the valve designed for the loop are shown in Appendix F.

Some basic specifications that can be used to select the valves for SPETA are listed in Table 5.7.

Table 5.7: Basic specifications for valves

Proposed design input	Selection
Fluid type	Water
Temperature of fluid	25-300 ^{o}C
Viscosity	3-7.5 Pas
Specific gravity	1
Flow capacity	0.05 m^3/s
Inlet pressure of valve	0.1-30 MPa
Pressure drop across valve	0-3 kPa
Inlet and outlet pipe size	50 mm

5.5 Pumps

In order to design the main pump for the loop, the loop in its entirety had to be understood and the pressure drop across the main components had to be calculated to determine the size of the pump needed for the loop. Pressure drop design calculation was done for the loop with the design boundary conditions based on the heat balance in the loop.

5.5.1 Loop Boundary Conditions

Loops are designed so that they can perform a desired range of experiments. It is important to ensure that the thermalhydraulic devices in the loop are designed to perform their functions. The main objective of the scaling method is to transfer experimental data from a scaled model to the prototype model. It is essential to ensure the boundary and global conditions applied to the scaled model are similar to the system under study with a proper scaling method. The inlet temperature and outlet pressure boundary conditions of the components in the

system can be used as a yardstick to compare the prototype and actual models. Important global conditions particular to SPETA include the mass flux of the working fluid and heat flux applied to walls of the test section.

Figure 5.12 shows the layout of SPETA including the temperature boundary conditions of the main components in the loop. The boundary conditions in the loop are designed based on boundary conditions of the test section to enable the loop to perform the entire subset of experimental design conditions. The loop is divided into different modules of control volumes with each essential component having its own control volume. This allows the flexibility of changing the boundary conditions of each component in the loop. The effect of changing each component specification in the loop can then be studied.

The main control volumes chosen for SPETA include the volume around the heat sources or heat sinks which are the test section, cooler, heat exchanger, and preheater. These components are chosen since the fluid properties change significantly across their control volumes. The components between the heat sources and heat sinks are treated as infinitely insulated parts so that there is no heat loss to the external environment. A temperature variation occurs across heat sinks and sources, but no temperature variation occurs across the infinitely insulated sections.

The temperature boundary conditions of the loop are selected from the SCWR boundary conditions. Fluid at an inlet temperature of 350 ^{o}C is expected in the test section with an outlet temperature of up to 625 ^{o}C to take advantage of the fossil fired plant turbine technology. The temperatures throughout the loop are designed so that the loop can be safely operated. For instance, the working fluid must be cooled down to a suitable operating temperature range of the pump and

valves to avoid frequent maintenance or replacement. The cooler is used to recirculate some of the fluid back to the preheater in order to reuse it to heat the fluid. After this point, the majority of heat is removed by the heat exchanger and the fluid temperature is reduced to a suitable operating temperature (200 ^{o}C) for the pump.

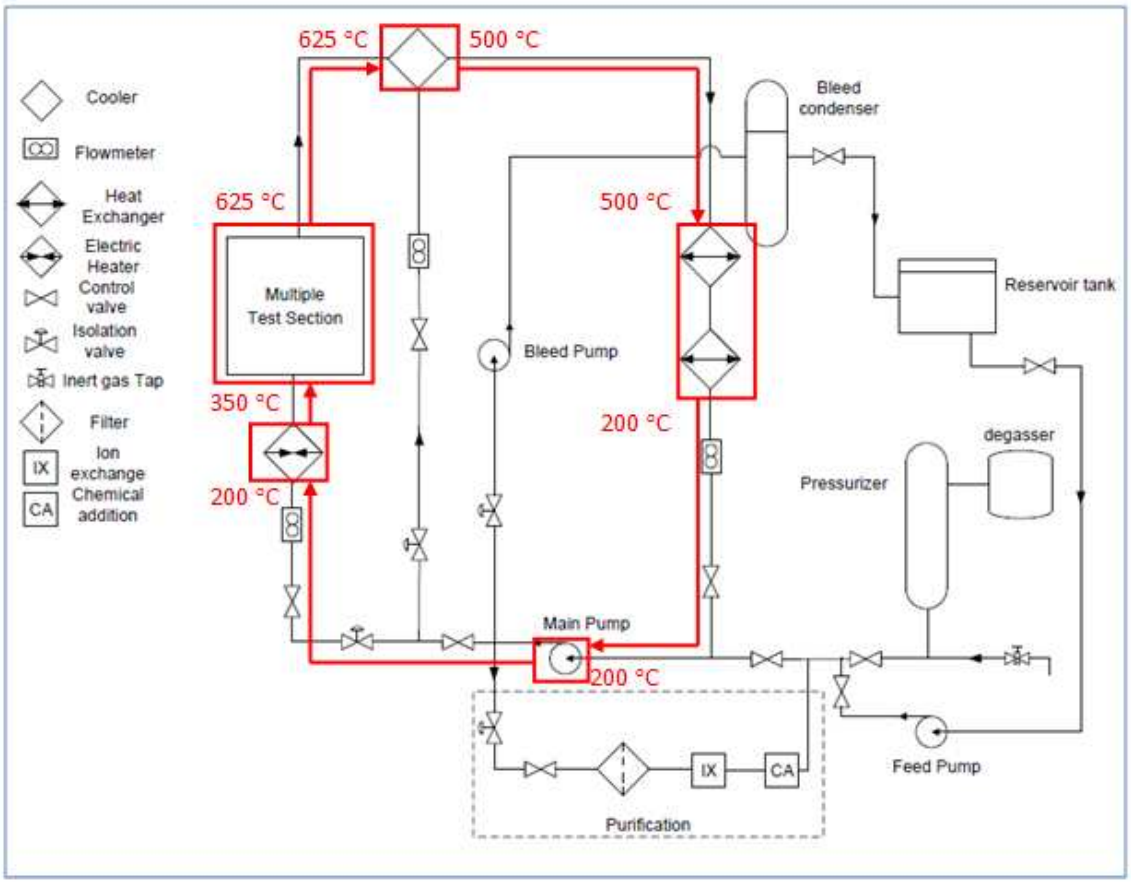

Figure 5.12 Schematic of SPETA showing the design temperatures

5.5.2 Pressure Drop Variation in Loop

The pressure drop was calculated for a full flow case (mass flux of 1206 kg/(m^2s)) in a bare tube with a hydraulic diameter of 7.52 mm throughout the loop. Constant hydraulic diameter was used in this analysis to solely see the effect of the fluid properties and loop characteristics on the pressure drop. The length of each control volume in SPETA was taken from the 3D drawing of the loop.

The pressure drop calculation in SPETA was done to characterise the feedwater pump. In order to verify the numerical code, hand calculations were performed independently to estimate the pressure drop along the loop as shown in Figure 5.13. The reference starting point of the pressure is at the outlet of the test section. The effect of the pump is shown on the graph as a gain in the pressure provided by the pump. This system loss is used to calculate the pump power required, which is shown later in this chapter.

A MATLAB code and a manually calculated method (Appendix B) were used to estimate the pressure drop. Figure 5.13 shows a comparison between the pressure drop in the loop obtained by using a MATLAB code and an independently manually calculated solution using the same formulae. The MATLAB result agrees with the manually calculated method within an error of 14 kPa which is 0.06% of the system pressure. The slight difference in the pressure drop may be explained by rounding errors introduced in the manually calculated method.

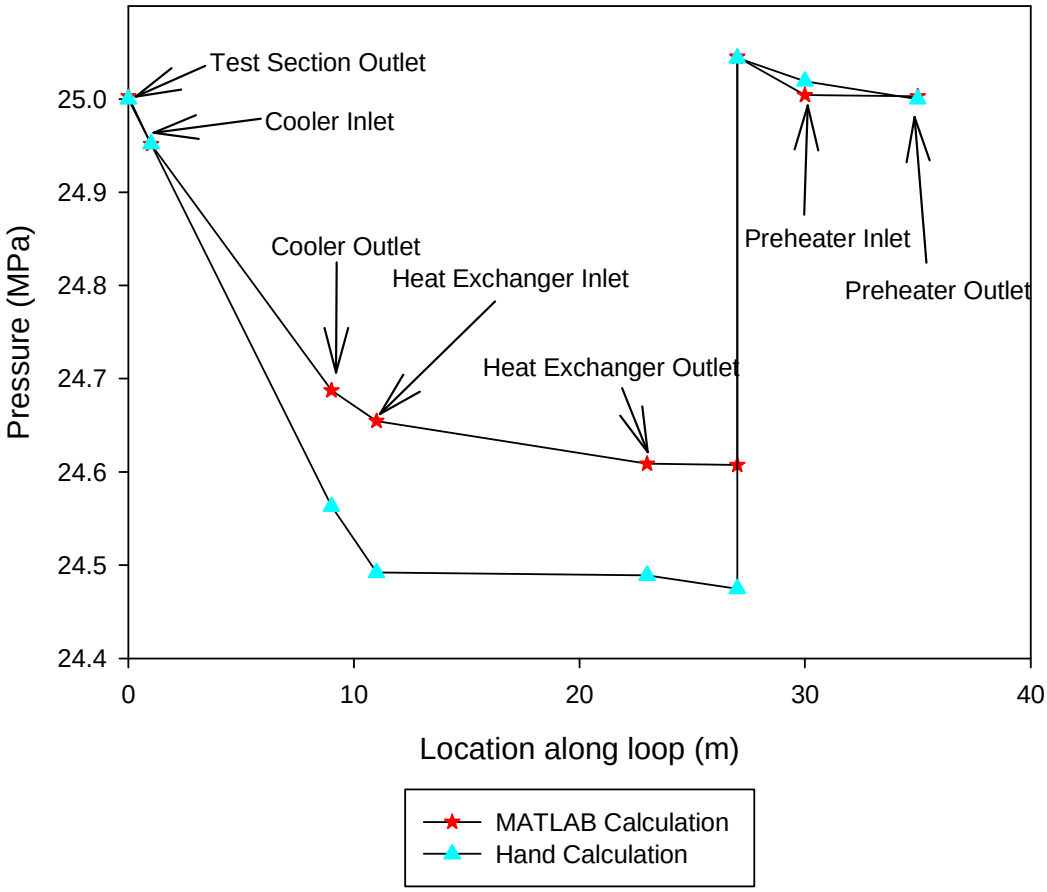

Figure 5.13 Comparison of calculated and numerically coded pressure drop

The cooler shows the largest pressure drop which is evident from the steep slope on the graph between the cooler inlet and cooler outlet. This result shows that the pressure drop in SCW is higher than at subcritical conditions. The cooler thus serves as a device to minimize the pressure drop in the system. The outlet temperature of the cooler can be modified to reduce this pressure drop. The lowest pressure drop occurs between the heat exchanger and the preheater which can be explained by the low temperature fluid. The temperature within this section is 200 ^{o}C which is below the pseudocritical point of water. A lower pressure drop is expected since pressure drop in the liquid phase is lower, compared to the pressure drop in the same fluid in the gaseous phase due to the

incompressible nature of liquids. The pressure drop in the loop can be reduced by keeping more of the working fluid below its pseudocritical point.

5.5.3 Pressure Drop Sensitivity

A sensitivity analysis was performed to study the effect of the mass flux and hydraulic diameter on the pressure drop. Flow cases of 25%, 50%, 75%, and 100% of full flow were considered. Figure 5.14 shows an exponential increase of pressure drop as the flow rate is increased. Maximum pressure drop is observed at full flow and the pressure drop decreases as the flow (mass flux) is reduced for the same diameter. Since the temperature was kept constant for different flow rates, the density of water at points marked throughout the loop remains the same for different flow rates. In practice however, a higher flow rate will result in better heat transfer and the temperatures at the points marked on the loop are expected to vary slightly for different flow rates. The trend however, shows that an increase in the mass flux will increase the pressure drop.

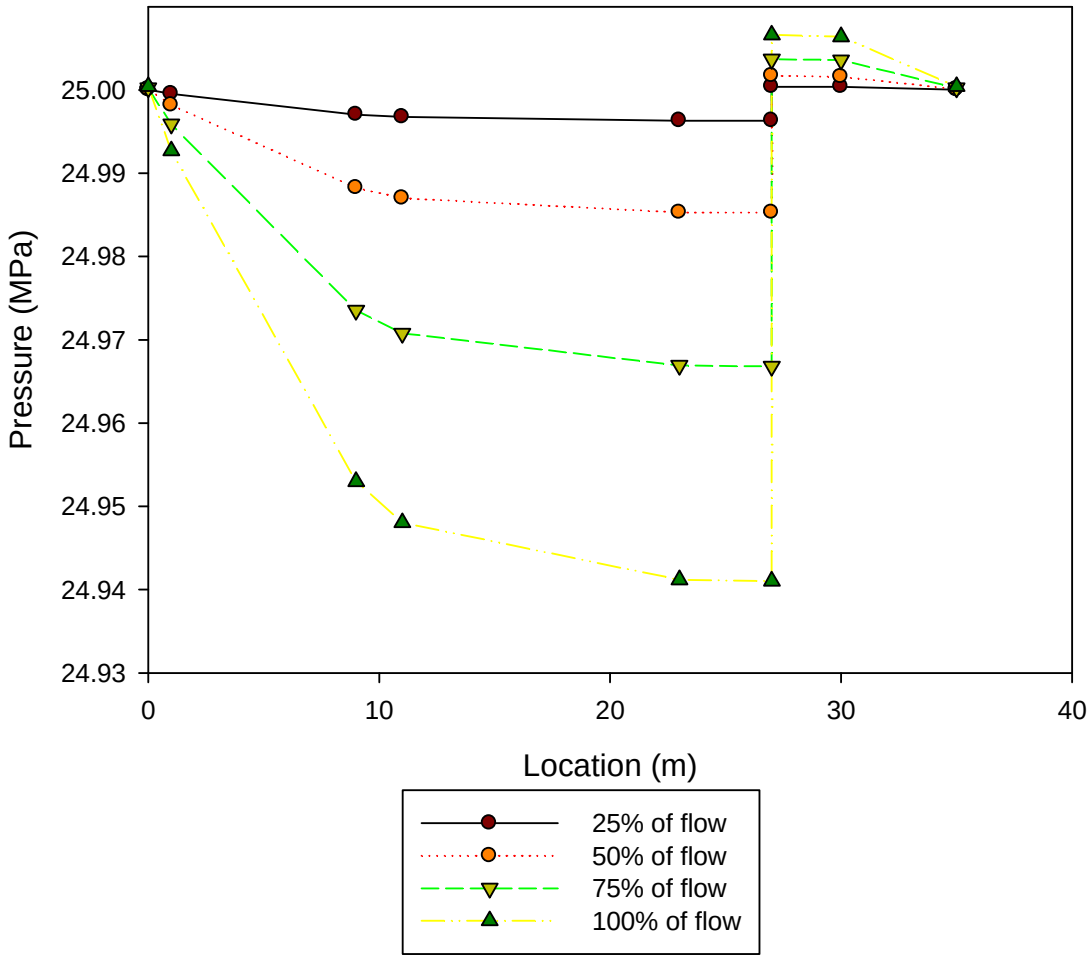

Figure 5.14 Effect of fluid flow change on pressure drop in loop

In Figure 5.15, the pressure drop decreases as the diameter is increased for the same full flow rate. The pressure drop decrease observed as the diameter is increased is not as large as the pressure drop reduction when decreasing the velocity of flow. This means the flow has more effect on the pressure drop than the diameter. From the flow and diameter sensitivity analysis, a minimum pressure drop will occur with a larger diameter pipe and a lower flow rate. The pressure drop can be minimized by increasing the pipe diameter in the loop and decreasing the mass flux.

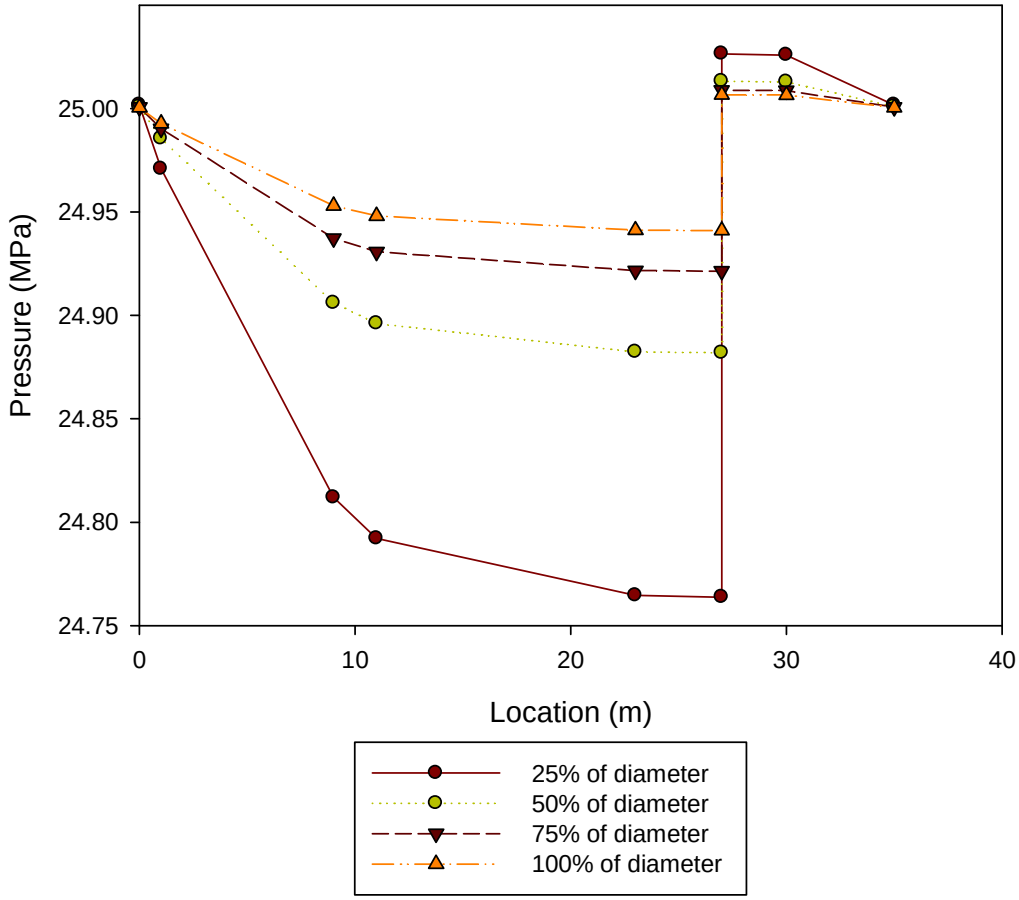

Figure 5.15 Effect of loop diameter change on pressure drop

5.5.4 Pump power

Figure 5.16 shows the pressure drop in the system including the pressure drop in the test section. Compared to Figure 5.13 with a loop diameter of 0.00752 m, the pressure drop was calculated with a larger design loop piping size of 0.05 m. The pressure drop in Figure 5.16 is lower than in Figure 5.13 which is as a result of the larger piping, which is confirmed by the diameter sensitivity analysis. The Figure 5.16 shows that there is a significant pressure drop in the test section

which enables the effect of pressure drop on heat transfer phenomena to be investigated. The total pressure drop calculated is 0.133 MPa which the pump must be able to provide.

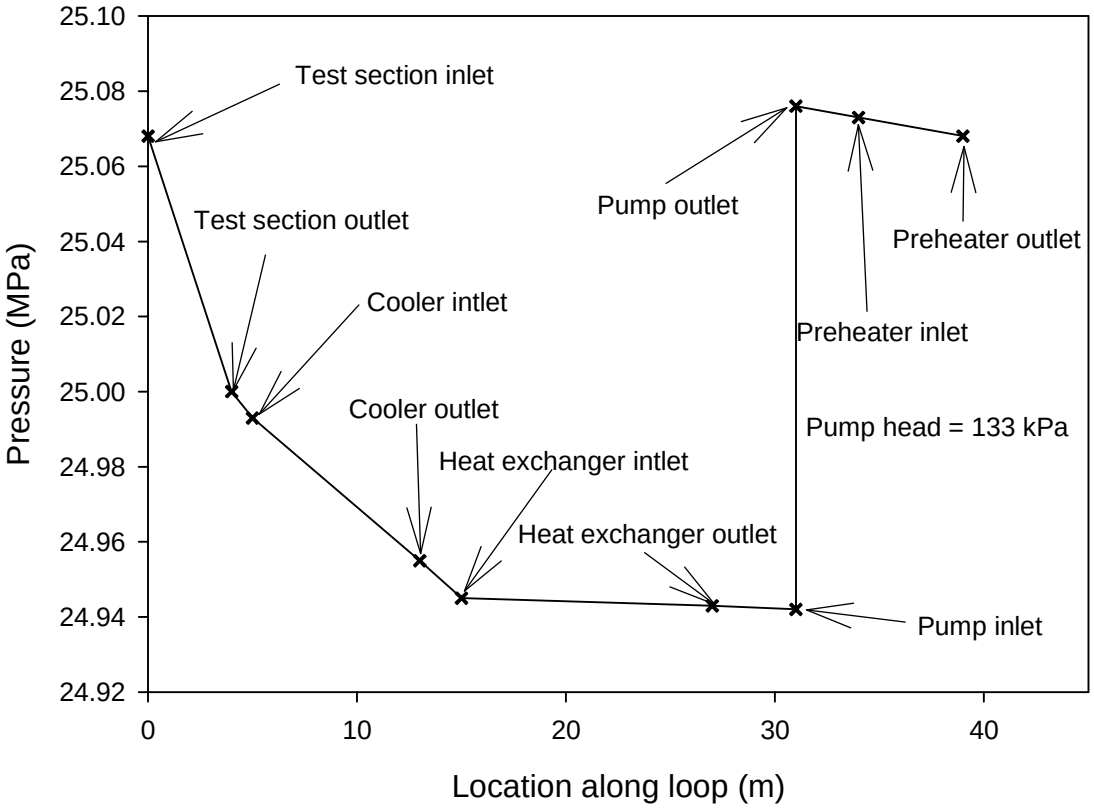

Figure 5.16 System pressure drop

Table 5.8 shows the number of elbows and valves in each control volume in the loop. Examples of calculations can be found in Appendix B. The head losses in each control volume were estimated so that the total head loss in the system was estimated. Any additional minor losses as a result of future design modifications will be accounted for in future designs.

Table 5.8: Head losses in SPETA

Section	Length (m)	Number of elbows/ Valves	Inlet Temperature (^oC)	Major (Friction) Head Loss (m)	Minor Head Loss (m)	
					Elbow loss	Valve loss
Test section	4	-/-	350	1.15	-	-
Test section to cooler	1	3/-	625	10.4	73.0	-
Cooler	8	2/-	625	61.3	35.9	-
Cooler to heat exchanger	2	2/-	500	11.8	27.7	-
Heat Exchanger	12	3/-	500	2.4	1.4	-
Heat Exchanger to Pump	4	2/1	200	0.2	0.3	0
Pump to preheater	3	1/1	200	0.2	0.2	0
Preheater	5	-/-	200	0.4	-	-

The density of the water which was taken at 25 MPa and 200 ^{o}C was 881 kg/m^{3}. The volumetric water flow rate of water used in the loop is 20.43 m^{3}/hr (mass flow rate of 5 kg/s divided by a density of 881 kg/m^{3}). The appropriate pump head required to maintain the fluid system at 25 MPa is 990 m (obtained from the MATLAB code in Appendix C, not accounting for compressibility). The approximate hydraulic pump power required to operate the loop with a shaft efficiency of 50% at these conditions is 105 kW, which is calculated from Equations 3.26. This pump power is an over estimated pump power rating; however, if proper sizing needs to be done, the pump manufacturer has to be contacted with the various flow specifications to obtain a more accurate pump power rating.

Figure 5.17 shows the system curve and appropriate pump curves for SPETA. The system curve is a characteristic of the loop design which is determined by the friction losses and minor losses which are dependent on the flow rate of water in the loop. The pump head curve and the Net Suction Pump Head (NSPH) are pump curves that are determined by the manufacturer. Figure 5.17 shows typical pump curves that are suitable for SPETA. In order to select a pump, a variety of pump curves can be drawn on the system curve to make the best pump selection based on the operating conditions.

Under the operating design conditions, the available NSPH in the loop is about 2700 m which is much greater than the typical amount required by pumps since the system design pressure for the loop is very high. The amount of available NSPH decreases with system pressure which means that less NSPH is available in the loop at lower pressures. In order to prevent cavitation of the pump, the amount of NSPH required by the pump must be smaller than the available NSPH in the loop. At high bulk fluid temperatures, the amount of NSPH available in the loop is lower in comparison to that at low bulk fluid temperatures. Therefore, In

order to prevent cavitation of the feedwater pump, it is important to turn off all heat sources before reducing the system pressure. Consequently, is also important to pressurize the system before turning on heat sources.

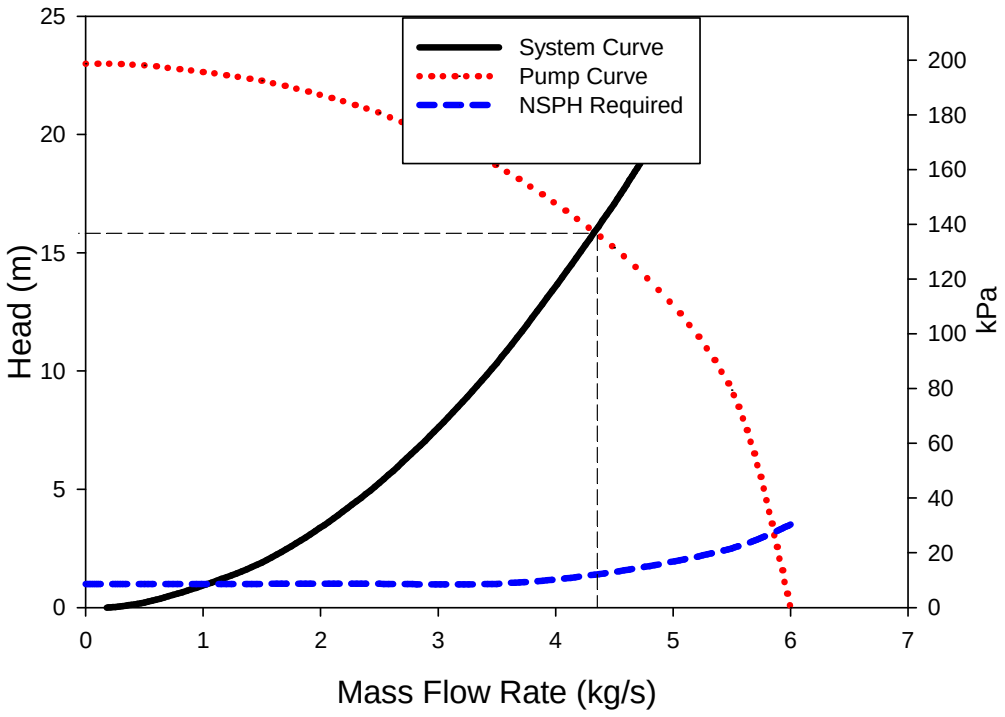

Figure 5.17 Pump curve

5.6 Pressure and Inventory Control

The pressure and inventory control of SPETA is adapted from the drum-type supercritical coal plant arrangement since it eliminates the need for a high power feedwater pump. This design has been chosen so that the feedwater pump for the loop does a minimal amount of work to operate the loop. This design also makes the inventory control easier since the drum provides a sink for excess

inventory in the loop and allows a slow response time to regain equilibrium during power manoeuvres.

5.6.1 Starting up SPETA

Dating back to the 1950s, the first generations of supercritical coal units were unreliable and difficult to control because earlier designs were unable to easily move back and forth between supercritical and subcritical operational modes. The feedwater pumps had to keep producing a pressure of 27.6 MPa even at low loads which required a large amount of energy consumption. However, in the 1960-1970's, the design has been modified to include drum boilers [**109**,**110**]. In this design, water changes to steam in the drum as it circulates through the loop and the steam is used to control the loop pressure. Although this eliminated the need for a high pump load, it translated to lower start-up time and lower responsiveness to load changes.

New generation supercritical coal-fired plants use the Benson once-through boiler. The once-through boiler does not have a large drum to store energy unlike the drum-type boiler. The Benson design provides the advantage of operating in sliding pressure mode which simplifies the start-up process. The sliding mode is the operation of the plant at different pressures to match the turbine load. This increases efficiency since there is no energy reserve for power manoeuvres, which means that the control system must exactly match the feedwater flow and turbine load. The flexibility this control system provides leads to a stable steady-state operation without oscillations [**110**].

A minimum mass flow rate is required within the evaporator tubes to prevent the tubes from overheating. This flow is provided by the recirculation pump that returns the heated water back to the boiler in a closed loop for maximum heat

recovery. This start-up phase is similar to the start-up phase of the drum which is used in steam-water separators. The Benson load represents the set point at which the drum-type control is switched to a once-through mode [**111**]. The drum-type arrangement is similar to the current CANDU design which uses a pressurizer to control the pressure during warm-up, and is equipped with a degasser or steam condenser.

PWRs, CANDUs, and supercritical coal plants use indirect cycles and allow a loop with a pressurizer in the primary side. In PWRs, two-phase flow is not allowed in the pressure vessel since a phase change affects reactivity; however, operating pressure is achieved with a pressurizer which is also used on the primary side of CANDUs and supercritical coal plants. In BWRs, the operating pressure is achieved with the feedwater pump during start-up. Although the pump requires a lot of energy, the increased efficiency from the direct cycle arrangement compensates for the feedwater pump power consumption.

SPETA will be designed similar to the drum-type supercritical coal plant arrangement since it eliminates the need for a high power feedwater pump. The loop will be provided with only 1.22 MW which will not allow a design with a big pump. The loop start-up will use a pressurizer and condenser to achieve the operating pressure. The advantage of this arrangement is that it allows easier pressure control as seen in the drum-type coal fired plants and current CANDU reactors. It also eliminates the need for a big pump as used in BWRs. It should be noted that the feedwater pump can be used to start-up the loop which eliminates the use of a pressurizer; however, pressure control is easier with the pressurizer-condenser arrangement, than when with a feedwater pump.

5.6.2 Level Control in a Pressurizer

The level of water in the pressurizer changes during pressure control. If the main circuit pressure is low, inventory will flow from the pressurizer to the circuit via the connection nozzle. The reverse will occur if the main circuit pressure is higher than the pressurizer pressure. With this action, the pressurizer serves as a giant dashpot to accept or provide inventory in order to keep the main circuit quite stable.

Two setpoints are required to operate the pressurizer. Level control in the pressurizer is important for the following reasons:

- It prevents the electric heaters from being exposed on low levels, therefore reducing the risk of burning out the heating elements. The heaters are automatically switched off on low level causing a loss of pressure control (i.e., pressure cannot be increased with the heaters).
- It prevents the system from going “solid” as a result of a high level. Loss of vapour space results in loss of pressure control.

As reactor power is increased, the level controller increases the pressurizer level to accommodate the swell of the water with minimal action of the feed and bleed action. The level is lowest at low power which allows room for the excess coolant that enters the pressurizer during a power increase. The liquid level in the pressurizer is actuated by the use of feed and bleed valves. During a power increase, the pressurizer level will accommodate the expansion of the coolant and vice versa during a power decrease.

It is not practical to design a pressurizer to accommodate the swell from 0% power (cold) to 100% (hot); however, swell that occurs from 0% (hot) power to 100% (hot) can be accommodated by the feed and bleed system and the storage tank. An advantage of using a pressurizer is that it results in the addition/removal

of inventory directly from the HTS to/from the pressurizer during transients. This minimises the heat loss and thermal stresses when compared to the solid state where the inventory is cooled as it leaves through the feed and bleed path.

5.6.3 SPETA Pressurizer Design

The pressurizer will be designed to operate with the heat transport system. Although it is not part of the main cycle, it is connected to the loop and needs to work with the loop. Saturation conditions are maintained in the pressurizer during operation.

Figure 5.18 shows the density variation of saturated water and steam with the density of the mixture as it changes to superheated steam. The graph shows an increase in average density as water transforms into superheated steam at 374 ^{o}C and 22.1 MPa. The increase in average density causes a swell in the pressurizer.

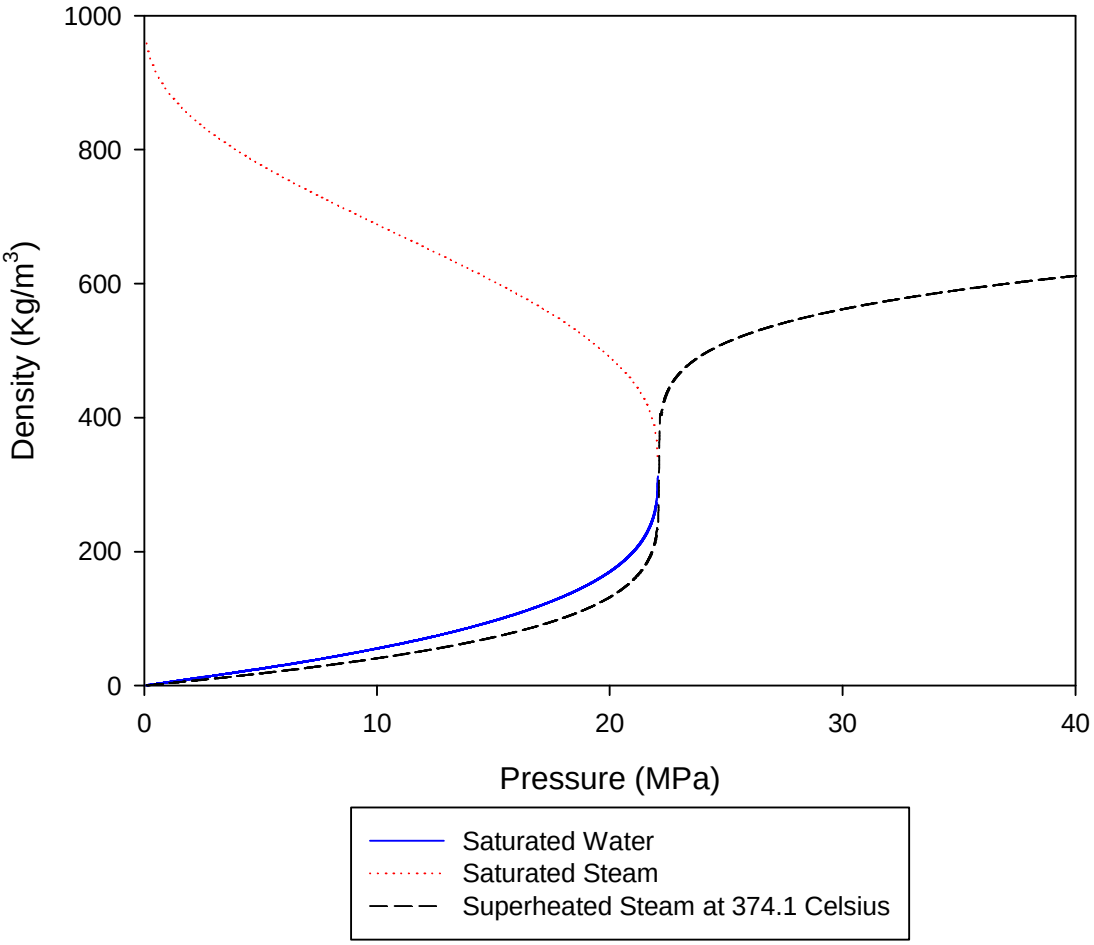

Figure 5.18 Density of superheated steam compared to saturated water

Figure 5.19 shows the volume swell for pressurised water with an increase in temperature. Each line represents the excess volume of the pressurizer by fraction needed to accommodate the inventory change as density increases. Different initial water levels of the pressurizer were investigated. The graph shows that as the initial volume of water in the pressurizer is increased, the inventory change is increased. The pseudocritical point is at 374 ^{o}C which can be seen on the graph as the point where the volume increase starts to rise exponentially. This region of operation should be avoided since the inventory increase is large. Thus, it is important to keep the pressurizer condition at subcritical saturated conditions.

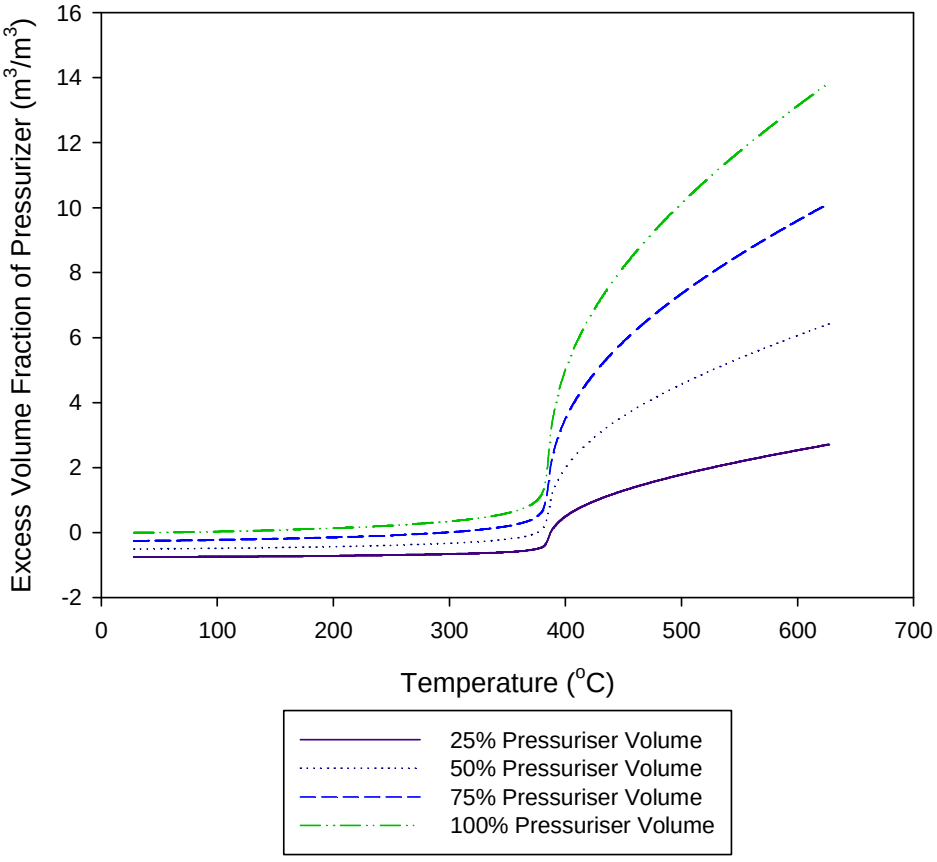

Figure 5.19 Volume swell with temperature variation at 25 MPa

Figure 5.20 shows the saturated temperature and pressure of water. The saturation pressure increases gradually from room temperature. At about 200 ^{o}C, the pressure variation starts to increase exponentially. This shows the operating conditions curve which the pressurizer operates.

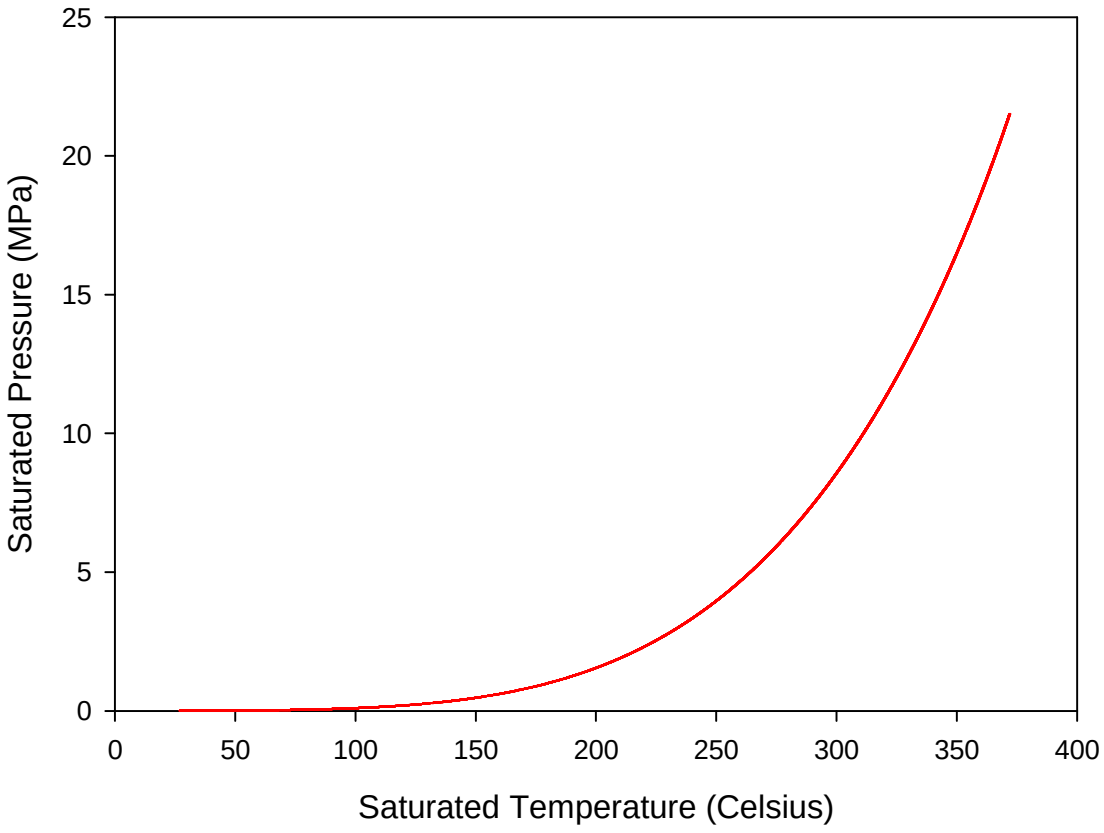

Figure 5.20 Saturated temperatures and pressures for water

To increase the system pressure, the steam pressure must be increased by switching on the electric heaters, thus increasing the temperature of water in the pressurizer. This causes the saturation temperature, and hence, pressure to increase. In order to decrease the system pressure, a liquid spray is used to cool the steam and the heater is turned off to decrease the pressure of the liquid water.

5.6.4 Pressurizer Steam Control

The swell in the pressurizer must be accomodated by the loop. Figure 5.21 shows the swell in the pressurizer after system warmup.

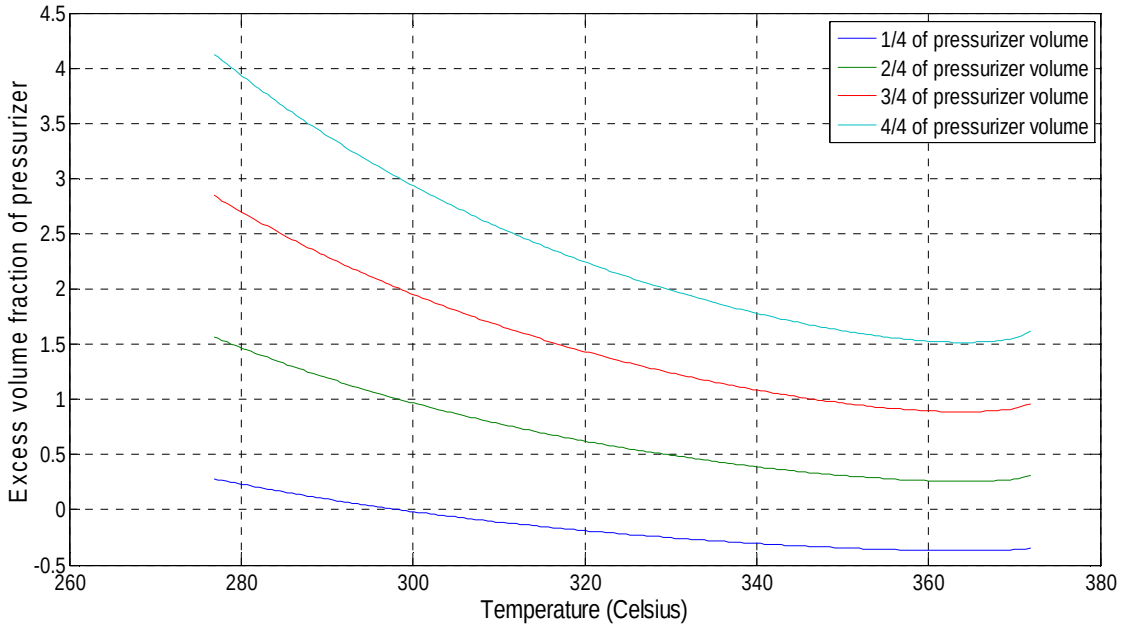

Figure 5.21 Swell in pressurizer during operation

The density difference between steam and water at saturated conditions is much higher at lower pressures. At higher pressures, the density difference between steam and water is reduced and they have similar densities as seen in Figure 5.18. The volume expansion of the fluid is reduced at higher pressure. Keeping

the pressurizer isolated during warm-up, ensures that the water in the pressurizer does not boil. Saturation pressure is established in the pressurizer at around 9 MPa for CANDU systems. When isolated, pressurizer is easier to control since the quality of steam can be controlled by the feed and bleed system to minimize the inventory volume change. Before the pressurizer is opened to the circuit, the fluid is heated to the start-up saturated conditions before it is connnected to the circuit. At higher pressures, the inventory expansion is not as large as shown in Figure 5.19.

5.6.5 Pressurizer Sizing

The pressurizer should be large enough to facilitate the pressure control. A cylindrical vessel of inner diameter of 0.49 m and a height of 1.5 m was designed.

The minimum thickness required from the pressurizer can be calculated using the ASME B31.1 code. Equation 3.17 shows the required equation for calculating the minimum required thickness. The required thickness for a pressurizer that is made of SS-304 is 0.06 m, which corresponds to a schedule 140 pipe.

Figure 5.21 shows the inventory change as a fraction of the pressurizer volume. The excess volume fraction represents the extra volume the fluid in the pressurizer expands during operation. The analysis has been normalised so that the result is independent of the pressurizer dimensions.

The steam quality represents the amount of steam (by mass), contained in the pressurizer compared to that of water, which is a function of density and volume. At higher pressures close to the pseudocritical point, the density of steam and water approach each other; thus, the steam quality is heavily dependent on the

steam volume at higher pressures. The results show that at higher steam qualities, the inventory increase is higher. Therefore, a lower steam quality is desired in the pressurizer. The steam quality can be reduced by bleeding some steam out of the pressurizer and raising the water level. This ensures the pressure is controlled within a setpoint.

5.6.6 Storage Tank Dimensions

The storage tank will store enough water to accommodate the volume expansion as a result of density change during the loop operation. The volume of fluid in the loop when in operation consists of the fluid in the pressurizer and through the loop.

Volume of fluid in loop: The volume of inventory has been calculated based on the diameter and length of the piping and test section. A total length of 39 m has been calculated through the loop which includes a test section length of 4 m. Given the test section inner diameter of 10 mm and the loop inner diameter of 50 mm, the volume of the loop is calculated to be 6.1×10^{-2} m^3.

Volume of pressurizer: The loop pressurizer has an internal diameter of 0.49 m and a height of 1.5 m. The volume is calculated to be 2.8×10^{-1} m^3. The volume of the pressurizer makes up most of the water in the storage tank.

Volume of expansion: The volume of expansion of the fluid in the pressurizer is controlled by the feed and bleed system. However, the storage needs to be able to accommodate the expansion. A bleed condenser primarily controls the inventory during operation, but the storage tank serves as a reservoir to accommodate the excess fluid expansion in the loop.

The storage tank required to allow 5 times the pressurizer volume expansion in the loop is 1.46 m^3.

5.7 Instrumentation

The measurement of the thermalhydraulic properties in the loop is done with various instruments suitable for supercritical water applications. Such measurements include temperature at various locations on the test section, flow measurements, and pressure measurements.

5.7.1 Temperature Measurement

The outside wall temperatures will be measured at different axial locations along the test section. The two types of sensors that can be used include Resistance Temperature Detectors (RTDs) and thermocouples. Thermocouples are the most common sensors used in experiments since they are easily available and affordable to use. RTDs are more expensive to use, but are more accurate than thermocouples. In general, RTDs are preferred for experiments because of their higher accuracy and repeatability; however, they cannot be used at temperatures above 500 ^{o}C.

The different thermocouple types include E, J, K, N, R, S, and T with each type having a pair of terminals made of different alloys. The K-type thermocouple (chromel-alumel) operates up to a maximum temperature of 1260 ^{o}C and is suitable for high the temperatures expected in supercritical water experiments [**112**]. The two types of RTDs include wire wound and thin film. The thin film RTD can operate up to 200 ^{o}C and will not be suitable for high temperatures while the wire wound RTD can operate at temperatures up to 500 ^{o}C. Thermocouples can be calibrated against RTDs so that there are no discrepancies in the measurements from both instruments.

The repeatability of experiments using thermocouples is highly dependent on application but is generally not as consistent RTDs. Thermocouples are, however more sensitive to temperature changes and respond faster than RTDs, but this is not important for supercritical fluid experiments since measurements are taken at steady state conditions. Table 5.9 shows the comparison between a K-Type thermocouple and a wire wound RTD.

Table 5.9: Comparison between the wire wound RTD and K-type thermocouple [**113**]

	Wire Wound RTD	K-Type Thermocouple
Temperature Range (^{o}C)	-200 to 500	0 to 1260
Accuracy (0 ^{o}C/200 ^{o}C)	±0.13/0.5	±2.2
Repeatability (^{o}C)	0.1	-
Time Response (s)	4-6	2-3

K-type thermocouples are best suited for supercritical water experiments which operate at temperatures up to 650 ^{o}C. Wire wound RTDs are more accurate and may be used in supercritical CO_2 and Freon experiments where temperatures are not as high.

K-type thermocouples (embedded in the test section at different locations), will be used to measure wall and bulk temperatures. The inlet temperature measurements will be performed with an RTD while the outlet temperature will be measured by a thermocouple. Thermowells which are essentially tubes will be used to protect the thermocouple sensor. Thermowells are to be bolted to onto the wall of the test section and the thermocouple can be inserted into them. This attachment enables easy accessibility and replaceability of thermocouples and RTDs for various experiments. A typical thermowell has a tip with a diameter of 6 mm [**114**], which enables it to be used as attachment for bulk flow temperature measurements for the test section.

5.7.2 Flow Measurement

Five flowmeter types that can be used to measure flow include differential pressure, positive displacement, velocity, mass, and open channel flowmeters [**108**]. Of this list, the mass and velocity flowmeters have the most potential for use for measurement since they can be used to measure both gas and liquid flows.

The choice of flow meters depends on the properties of the fluid of interest. Mass flux is the most important measureable flow property in supercritical fluid experiments since the properties of the fluid change, but mass is always conserved. Coriolis mass flowmeters measure mass flow rate directly. The mass flux can be calculated directly from the mass flow rate. It is particularly important for measurement at sections in the loop at higher temperatures since the viscosity and flow velocity change. At lower temperatures (typically 25 ^{o}C lower than the critical temperature), the viscosity of the liquid is constant and the volumetric flow rate can be measured with an orifice or a turbine flowmeter. The flowmeter must be properly designed to match the flow pipe, flow conditions and the liquid's properties.

5.7.3 Pressure measurement

The absolute pressure will be measured with a pressure transducer. An absolute pressure transducer measures pressure of a point relative to vacuum. The operating pressure of the loop will be measured with an absolute pressure transducer. Pressure drops will be measured by differential-pressure transducers. A differential-pressure transducer is used to measure the pressure between two different points on a system or between two systems. The differential-pressure transmitters will be place along the test section to measure the pressure drop.

There are three major types of pressure transducers namely strain gage, variable capacitance, and piezoelectric pressure sensors. Strain gauge transducers are usually used to measure differential pressures, but the Wheatstone bridge transducer is a strain gage sensor that can be used to measure absolute, gage, or differential pressure and can be used for low and high pressure applications. A capacitance pressure transducer contains a metal diaphragm and a fixed metal plate. It measures the change in capacitance between the two components as a function of their distances. It is usually used at low pressures and is generally very stable, but becomes unstable at high temperatures.

Since the loop operates at a high temperature, the capacitance transducer is not suitable for the pressure measurement. A strain gage pressure transducers will be used to measure the differential pressure. The operating pressure will be measured by either a piezoelectric pressure transducer or a Wheatstone bridge strain gauge transducer.

5.8 Three-Dimensional Layout of Thermalhydraulic Loop

SPETA has been modelled in NX Nastran 7.5. Figure 5.22 shows the pump, preheater, test section, heat exchangers, pressurizer, and condenser. Figure 5.23 shows the back room where the storage tanks that supply the fluid to the loop will be located. SPETA will occupy three lab spaces in the ERC building which are B052, ERC 1052 and ERC B033 (not shown in Figure 5.22 and 5.23). Figure 5.24 shows a close-up view of the test section, preheater, and feedwater pump in ERC B052. Figure 5.25 shows a close up view of the three heat exchangers, pressurizer, and condenser in ERC 1052. The vertical test section shall pass through an opening between the nuclear design laboratory (ERC B052) in the basement and the thermalhydraulic laboratory (ERC 1052) as shown in Figure 5.22. Support equipment will be located in ERC B033.

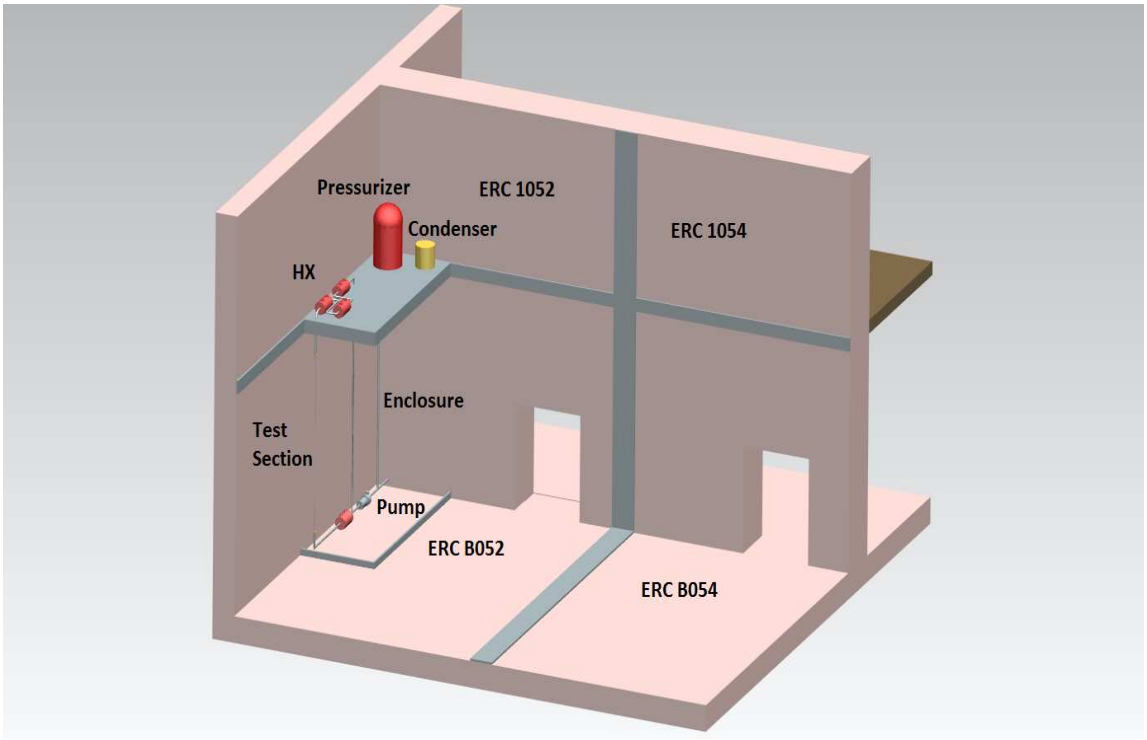

Figure 5.22 Three-dimensional layout of loop

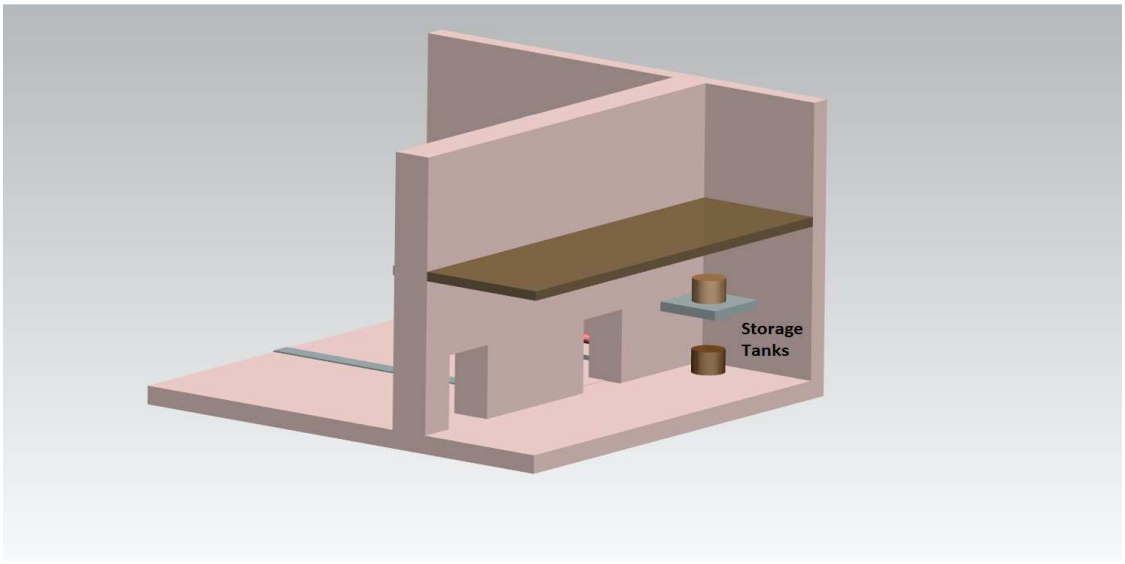

Figure 5.23 Backspace

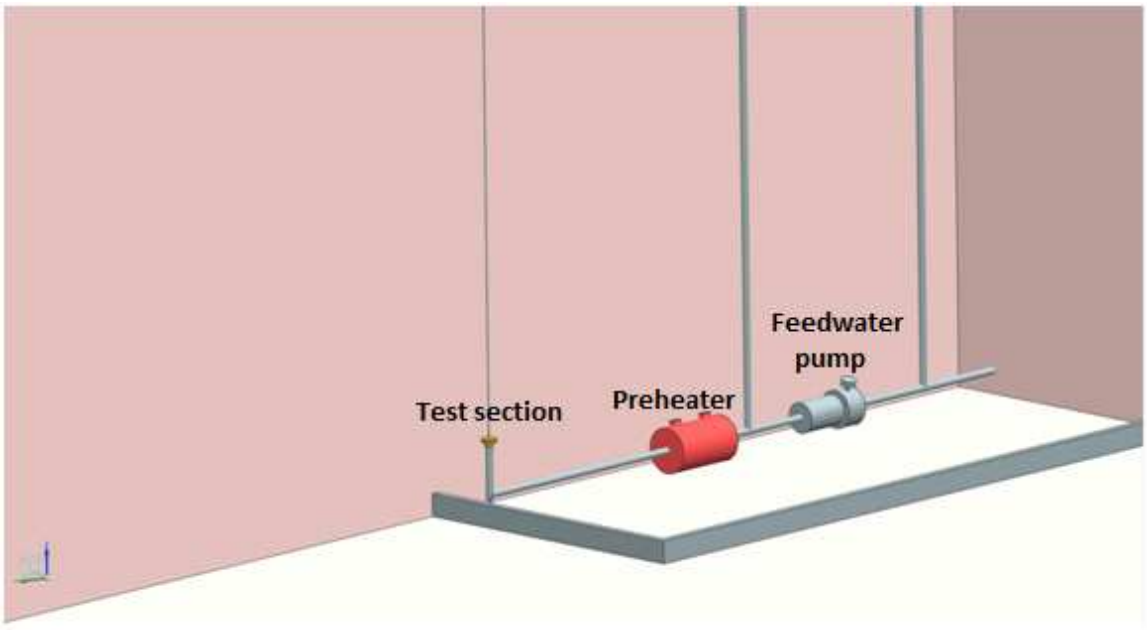

Figure 5.24 Three-dimensional view of loop showing the feedwater pump, preheater, and test section

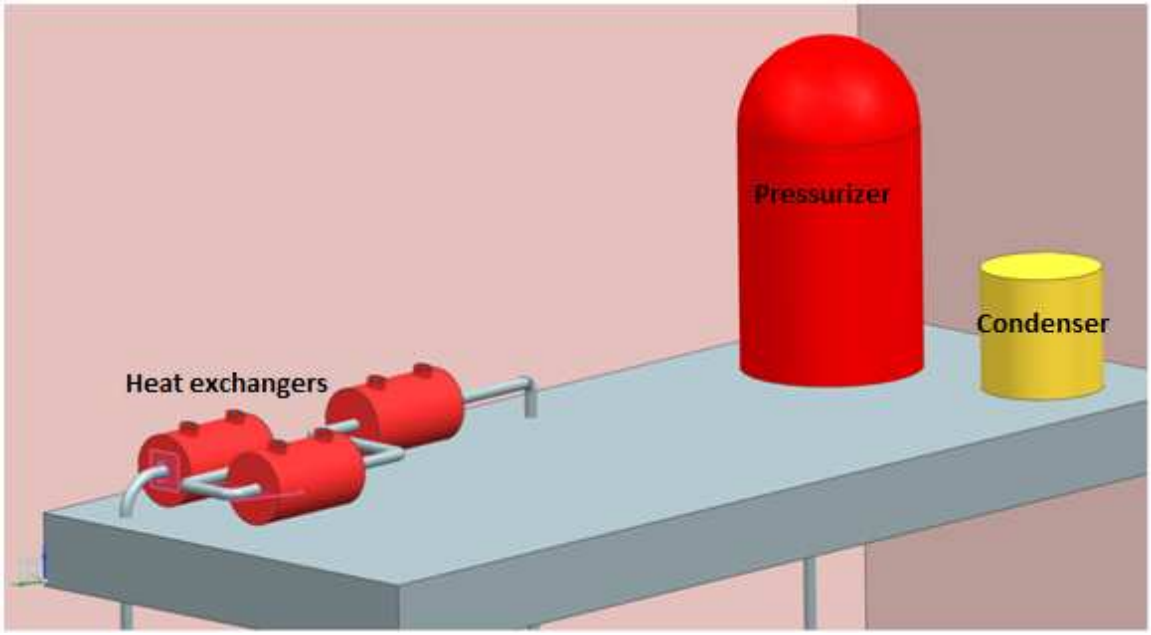

Figure 5.25 Three-dimensional view of loop showing pressurizer, condenser, and heat exchangers

The main components will be contained in ERC 1052 and B052. The control instruments (not shown in any of Figures 5.22-5.25) will be located in room B033. The enclosure for ERC 1052 and B052 have not been designed as of yet, but when designed, impact analysis on the enclosure should be performed to ensure that its integrity is maintained in the event of a pipe burst during the operation of SPETA. The design and installation of the control devices for the components and measuring instruments will be performed as future work.

CHAPTER 6

DESIGN REQUIREMENTS VERIFICATION

The following requirements have been met in the conceptual design of the Supercritical Phenomena Experimental Test Apparatus (SPETA).

- The main component of SPETA will fit in the 9 m by 2 m by 4.8 m enclosure inside ERC B052 and ERC 1052.
- SPETA has been designed to operate at pressures up to 25 MPa and the pressurizer can provide adequate pressure to the loop.
- The 1.22 MW power supply shall be able to provide adequate heat to provide outlet fluid temperatures of 650 ^{o}C and the heat exchangers are adequate to remove heat from the loop for proper heat balance.
- The conceptual loop design will allow different bundle geometries and orientations to be performed to investigate friction and buoyancy effects.
- Pressurizer design will provide adequate pressure to the system.
- High mass fluxes can be investigated in the loop with small test section diameters. However, a more powerful pump may be required to provide higher mass flow rates as is in the conceptual Canadian SCWR design.

CHAPTER 7

CONCLUDING REMARKS

A conceptual design of a supercritical water loop was established with similar boundary conditions as the conceptual supercritical water-cooled reactor design. This loop is constrained by a 9 m by 4.8 m by 2 m enclosure. Previous loops were investigated to adopt common supercritical water loop designs. Instrumentation methods are recommended based on operational experiences of previous loops. Computational fluid dynamics was used to study the supercritical heat transfer phenomena that occur at supercritical conditions. Heat balance calculations were done to ensure the energy flow in and out of the loop can be achieved. Pressure drop calculations were done to predict the losses that occur and account for them in the design of the loop. Start-up will be achieved with a pressurizer-condenser arrangement. After a thorough design process, it has been established that:

- The conceptual design of SPETA is practical.
- The loop is designed so that it can be adopted for other supercritical fluid experiments.
- When built, the loop can be used to carry out experiments with different bundle geometries.
- When built, the supercritical loop will produce experimental data that can be used to validate numerical models and verify previous experimental data.
- It will serve various applications involving high pressure or temperature for instance; the test section can be replaced with an autoclave.

Although a conceptual design has been done, a detail design of each component is required before the loop is built. Detail material selection process had not been done, however appropriate alloys have been recommended for construction. Appropriate methods to manufacture components and means to mount the equipment in the loop should be investigated. The purification system should be investigated after the detail design of SPETA is done.

The purification system and control design should be investigated in the detail design of SPETA.

CHAPTER 8

RECOMMENDATIONS AND FUTURE WORK

It is recommended that SPETA be built, based on the conceptual design described here.

When SPETA is built, initial experiments should be based on the reference model of a 4 m long 10 mm inner diameter tube for loop verification against existing data such as the Kirillov datasets. The data can be compared and experimental discrepancies can be established to benchmark the facility. The loop should be tested with other fluids such as Freon 12 and Freon 134a and used to perform experiments at various conditions.

Heat rejected by the heat exchangers can be used as a more useful form of heat such as district heating. The coolant can be valved out to the geothermal pipeline installed on the campus. This idea would require design modifications of the heat rejection system.

REFERENCES

[1] World Energy Outlook, "Organisation for Economic Co-Operation and Development/International Energy Agency," Paris, 2004.

[2] R.E. Smalley, "Future global energy prosperity: the terawatt challenge," *MRS Bull*, vol. 30, pp. 412-7, 2005.

[3] C.-C. Lee and Y.-B. Chiu, "Nuclear energy consumption, oil prices, and economic growth: Evidence from the industrialized countries," *Energy Economics*, vol. 33, no. 2011, pp. 236-248, 2010.

[4] U.S. DOE Nuclear Energy Research Advisory Committee and Generation IV International Forum, "A Technology Roadmap for Generation IV Nuclear Energy Systems," 2002.

[5] Ontario Power Generation. (2007, May) Energy Today Magazine. [Online]. http://www.energytodaymagazine.com/index.php?option=com_content&task=view&id=5750

[6] G.L. Brooks, "A Short History of the CANDU Nuclear Power System," 2002.

[7] I.L. Pioro and R.B. Duffey, *Heat Transfer and Hydraulic Resistance at Supercritical Pressures in Power Engineering Applications*. New York: ASME Press, 2007.

[8] P.L. Kirillov, R.S. Pomet'ko, A.M. Smirnov, and et al., "Experimental study on heat transfer to suprcritical water flowing in vertical tubes," in *International Conference on Nuclear Energy Systems for Future Generation and Global Sustainability*, Tsukuba, Japan, October 9-13, 2005.

[9] National Institute of Standards and Technology, "NIST Reference Fluid Thermodynamic Transport Properties - REFPROP," US Department of Commerce, NIST Standard Reference Database 23, 2007.

[10] K. Yamagata, K. Nishikawa, S. Haseqawa, and et al., "Forced convective heat transfer to supercritical water flowing in tubes," *International Journal of Heat and Mass Transfer*, vol. 15, no. 12, pp. 2575-2593, 1972.

[11] G.V. Alekseev, V.A. Silin, A.M. Smirnov, and V.I. Subbotin, "Study of the thermal conditions on the wall of a pipe during the removal of heat by water at a supercritical pressure," *High Temperature*, vol. 14, no. 4, 1976.

[12] M. Bazargan, D. Bazargan, and V. Chatoorgoon, "Effect of buoyancy on heat transfer in supercritical water flow in a horizontal round tube," *Journal of Heat Transfer*, vol. 127, p. 897, 2005.

[13] Yu.D. Barulin, Yu.V. Vikhrev, B.V. Dyadyakin, and et al., "Heat transfer during turbulent flow in vertical and horizontal tubes containing water with supercritical state parameter," *Journal of Engineering Physics*, vol. 20, no. 5, p. 665, 1971.

[14] D.G. Randall, "Some heat transfer and fluid friction experiments with supercritical water," NDA , 2051, 1956.

[15] V.E. Doroshchuk, V.L. Lel'chuk, and V.V. Modnikova,. Moscow-Leningrad, Russia: Gosenergoizdat Publishing House, 1959, pp. 33-40.

[16] M.E. Shitsman, "Investigation of heat transfer at water cooling in supercritical region," *Thermal Engineering*, vol. 9, no. 1, pp. 83-86, 1962.

[17] M.E. Shitsman, "Impairment of the heat transmission at supercritical pressures," *High Temperature*, vol. 1, no. 2, pp. 237-244, 1963.

[18] H.S. Swenson, J.R. Carver, and C.R. Kakarala, "Heat Transfer to Supercritical Water in Smooth-Bore Tubes," *Journal of Heat Transfer*, vol. 87, no. 4, pp. 477-484, 1965.

[19] V.N. Smolin and V.K. Polyakov, "Experimental investigation of heat transfer to water in tubes at supercritical pressure," *Transactions of TsKTI Boiler-Turbine Engineering*, no. 57, pp. 130-137, 1965.

[20] Yu.V. Vikhrev, Yu.D. Barulin, and A.S. Kon'kov, "A study of heat transfer in vertical tubes at supercritical pressures," *Thermal Engineering* , vol. 14, no. 9, pp. 116-119, 1967.

[21] M.E. Shitsman, "Temperature conditions of evaporative surfaces at supercritical pressure," *Electrical Stations*, vol. 38, no. 2, pp. 27-30, 1967.

[22] P.J. Bourke and W.H. Denton, "An unusual phenomenon of heat transfer near the critical point," U.K.A.E.A Research Group, Atomic Energy

Research Establishment, Harwell, Berkshire, Memorandum AERE-M 1946 August, 1967.

[23] M.A. Styrikovich, T.Kh. Margulova, and Z.L. Miropol'skii, "Problems in the development of designs of supercritical boilers," *Thermal Engineering*, vol. 14, no. 6, pp. 5-9, 1967.

[24] L.Yu. Krasyakova, Ya. M. Raykin, I.I. Belyakov, and et al., "Investigation of temperature regime of heated tubes at supercritical pressure," *Soviet Energy Technology*, vol. 1, pp. 1-4, 1967.

[25] L.Yu. Krasyakova, I.I. Belyakov, and N.D. Fefelova, "Heat transfer with a downward flow of water at supercritical pressure," *Thermal Engineering* , vol. 24, no. 1, pp. 1-9, 1977.

[26] N.S. Alferov, R.A. Rybin, and B.F. Balunov, "Heat transfer with turbulent water flow in a vertical tube under conditions of appreciable influence of free convection," *Thermal Engineering*, vol. 16, no. 12, pp. 90-95, 1969.

[27] J.W. Ackerman, "Pseudoboiling heat transfer to supercritical pressure water in smooth and ribbed tubes," *Journal of Heat Transfer*, vol. 92, no. 3, pp. 490-498.

[28] A.P. Ornatskiy, L.F. Glushchenko, and S.I. Kalachev, "Heat transfer with rising and falling flows of water in tubes of small diameter at supercritical pressures," *Thermal Engineering*, vol. 18, no. 5, pp. 137-141, 1971.

[29] I.I. Belyakov, L.Yu. Krasyakova, A.V. Zhukovskii, and N.D. Fefelova, "Heat transfer in vertical risers and horizontal tubes at supercritical pressure," *Thermal Engineering*, vol. 18, no. 11, pp. 55-59, 1971.

[30] L.F. Glushchenko and O.F. Gandzyuk, "Temperature conditions at the wall of an annular channel with internal heating at supercritical pressures," *High Temperatures*, vol. 110, no. 4, pp. 734-738, 1972.

[31] V.G. Chakrygin, M.B. Agafonov, and I.P. Letyagin, "Experimental determination of the limits of aperiodic instability at very high and supercritical pressures," *Thermal Engineering* , vol. 21, no. 1, pp. 17-22, 1974.

[32] R.A. Lee and K.H. Haller, "Supercritical water heat transfer development and applications," in *Proceeding of the 5th International Heat Transfer*

Conference, vol. IV, Tokyo, Japan, September 3-7, 1974, pp. 335-339.

[33] N.S. Alferov, B.F. Balunov, and R.A. Rybin, "Calculating heat transfer with mixed convection," *Thermal Engineering*, vol. 22, no. 6, pp. 96-100, 1975.

[34] B.Ya. Kamenetskii, "Heat-transfer characteristics of a nonuniformly cirumferentially heated pipe," *High Temperatures*, vol. 13, no. 3, pp. 613-616, 1975.

[35] G.S. Harrison and A. Watson, "An experimental investigation of forced convection to supercritical pressure water in heated small bore tubes," in *Proceedings of the institute of Mechanical Engineers*, vol. 190, 1976, pp. 429-435.

[36] M.J. Watts and C.T. Chou, "Mixed convection heat transfer to supercritical pressure water," in *Proceedings of the 7th International Heat Transfer Conference*, vol. 3, Munchen, Germany, 1982, pp. 495-500.

[37] P.L. Kirillov, A.A. Kolosov, and E.N. Petrova, "Temperature distribution in turbulent flow of water at supercritical pressures (circular tube)," *Institute of Physics and Power Engineering*, pp. 1-10, 1986.

[38] V.G. Razumovskiy, "Experimental study on heat transfer to supercritical water flowing in small diameter vertical tubes and low mass fluxes," Unpublished report 2005.

[39] T. Chen, "Two-Phase Flow and Heat Transfer Study," Xi'an Jiaotong University, China, 7-5605-1892-3, 2004.

[40] E.N. Pis'mennyy, V.G. Razmovskiy, E.M. Maevskiy, and et al., "Experimental study on temperature regimes to supercritical water flowing in vertical tubes at low mass fluxes," in *Proceedings of the International Conference on Nuclear Energy Systems for Future Generation and Global Sustainability*, Tsukuba, Japan, October 9-13, 2005, pp. 1-9.

[41] K.W. Seo, M.H. Anderson, M.L. Corradini, B.D. Oh, and M.H Kim, "Studies of supercritical heat transfer and flow phenomena," in *Proceeding of the 11TH International Topical Meeting on Nuclear Reactor Thermal Hydraulics (NURETH-11)*, Avignon, France, 2005.

[42] G.G. Treshchev and V.A. Sukhov, "Stability of flow in heated channesl in the supercritical region of parameters of state," *Thermal Engineering*, vol.

24, no. 5, p. 68, 1977.

[43] K. Goldmann, "Heat transfer to supercritical water at 5000 psi flowing at high mass-flow rates through round tables," in *International Heat Transfer Conference*, Colorado, USA, January 8-12, 1961, pp. 561-568.

[44] L.I. Malkina, G.P. Maksimova, N.L. Kafenqauz, and M.I. Fedorov, "Heat transfer to water with pseudoboiling," *Heat Transfer-Soviet Research*, vol. 4, no. 5, pp. 23-26, 1972.

[45] X. Cheng, X.J. Liu, and H.Y. Gu, "Fluid-to-fluid scaling of heat transfer in circular tubes cooled with supercritical fluids," *Nuclear Engineering Design*, vol. 241, pp. 498-508, 2011.

[46] Young D.F., and Okiishi T.H. Munson B.R., *Fundamentals of Fluid Mechanics*. Ames, Iowa, USA: John Wiley & Sons, Inc., 2006.

[47] Y.-Y. Bae, H.-Y. Kim, and D.-J. Kang, "Forced and mixed convection heat transfer to supercritical CO2 vertically flowing in a uniformly-heated circular tube," *Experimental Thermal and Fluid Science*, vol. 34, pp. 1295-1308, 2010.

[48] R.P. Bringer and J.M. Smith, "Heat transfer in the critical region," *AIChE Journal*, vol. 3, no. 1, pp. 49-55.

[49] B.S. Petukhov, E.A. Krasnoschekov, and V.S. Protopopov, "An investigation of heat transferto fluids in pipes under supercritical conditions," pp. 569-578, January 8-12, 1961.

[50] R.D. Wood and J.M. Smith, "Heat transfer in the critical region temperature and velocity profiles in turbulent flow," *AIChE Journal*, vol. 10, no. 2, pp. 180-186, 1964.

[51] E.A. Krasnoshchekov and V.S. Protopopov, "Experimental study of heat exchange in carbon dioxide in the supercritical range at high temperature drops," *High temperatures*, vol. 4, no. 3, pp. 375-382, 1966.

[52] H. Tanaka, N. Nishiwaki, and M. Hirata, "Turbulent heat transfer to supercritical carbon dioxide," in *Proceedings of the JSME Semi-International Symposium*, Tokyo, Japan, September 4-8, 1967, pp. 127-134.

[53] B. Shiralkar, D.J. Pulling, L.E. Gill, and W.H. Denton, "Forced convective heat transfer to turbulent CO2 in the supercritical region," *International Journal of Heat & Mass Transfer*, vol. 13, no. 8, pp. 1339-1348, 1970.

[54] P.J. Bourke, D.J. Pulling, L.E. Gill, and W.H. Denton, "Forced convective heat transfer to turbulent CO2 in the supercritical region," *International Journal of Heat and Mass Transfer*, vol. 13, no. 8, pp. 1339-1348, 1970.

[55] N.P. Ikryannikov, B.S. Petukhov, and V.S. Protopov, "An experimental investigation of heat transfer in the single-phase near-critical region with combined forced and free convection," *High Temperatures*, vol. 10, no. 1, pp. 80-83, 1972.

[56] B.S. Petukhov, V.S. Protopopov, and V.A. Silin, "Experimental investigation of worsened heat-transfer conditions with the turbulent flow of carbon dioxide at supercritical pressure," *High Temperatures*, vol. 10, no. 2, pp. 304-310, 1972.

[57] V.A. Silin, "Experimental investigation of deteriorated heat transfer regimes in turbulent flow of carbon dioxide of supercritical pressure," Moscow Power Institute, Moscow, PhD Thesis 1973.

[58] Z.L. Miropol'skiy and V.I. Baigulov, "Investigation in heat transfer, velocity and temperature profiles with carbon dioxide flow in a tube over the nearly critical region of parameters," in *Prioceedings of the 5th International Heat Transfer Conference*, vol. II, Tokyo, Japan, September 3-7, 1974, pp. 177-181.

[59] V.L. Baskov, I.V. Kuraeva, and V.S. Protopopov, "Heat transfer in the turbulent flow of carbon dioxide of supercritical pressre in a vertical tube cooling conditions," *MEI (Moscow Power Engineering Instituted)*, no. 179, pp. 140-149.

[60] V.S. Protopopov and G.K. Sharma, "Experimental investigation of heat transfer from a vertical surface to carbon dioxide with natural convection in the supercritical region of the parameter of state," *High Temperatures*, vol. 14, no. 4, pp. 693-698, 1973.

[61] J. Fewster, "Mixed, Forced and Free Convective Heat Transfer to Supercritical Pressure Fluids Flowing in Vertical Pipes," Unversity of Manchester, UK, PhD Thesis 1976.

[62] V.B. Ankudinov and V.A. Kurganov, "Intensification of deteriorated heat transfer in heated tubes at supercritical pressures," *High Temperatures*, vol. 19, no. 6, pp. 870-874, 1981.

[63] E.S. Vlakhov, Z.L. Miropol'skii, and L.R. Khasanov-Agaev, "Heat transfer to supercritical medium with mixed convection and rising flow in heated tubes," *Thermal Engineering*, vol. 28, no. 11, pp. 680-682, 1981.

[64] V.K. Afonin and O.K. Smirnov, "The effect of thermal unsteadiness on heat transfer in the supercritical region," *Thermal Engineering*, vol. 32, no. 3, pp. 163-166, 1985.

[65] Yu. M. Dashevskii, Z.L. Miropol'skii, and L.R. Khasanov-Agaev, "Heat transfer with flow of medium at supercritical parameters of state in channels with different spatial orientation," *Thermal Engineering*, vol. 34, no. 8, pp. 454-457.

[66] V.A. Kurganov and A.G. Kaptil'nyi, "Flow structure and turbulent transport of a supercritical pressure fluid in a vertical heated tube under the conidtions of mixed convection," *International Journal of Heat and Mass Transfer*, vol. 36, no. 13, pp. 3383-3392, 1993.

[67] T. Walisch, W. Dorfler, and Ch. Trepp, "Heat transfer to supercritical carbon dioxide in tubes with mixed convection," in *ASME proceedings of the 32nd National Heat Transfer Conference*, vol. 12, Baltimore, Mayrland, USA, 1997, pp. 79-98.

[68] J. Petterson, R. Rieberer, and A. Leister, "Heat transfer and pressure drop characteristics of super-critical carbon dioxide in microchannel tubes under cooling," in *Proceedings of the 4th IIR-Gustav Lorentzen conference on Natural Working Fluids* , Purdue, USA, 2000, pp. 315-323.

[69] S.M. Liao and T.S. Zhao, "Heat transfer of supercritical carbon dioxide flowing in heated horizontal and vertical miniature tubes," in *Proceedings of the 12th International Heat Transfer Conference* , 2002, pp. 501-506.

[70] J.D. Jackson, E. Lutterodt, and R. Weinberg, "Experimental studies of buoyancy-influenced convective heat transfer in heated vertical tubes at pressures just above and just below the thermodynamic critical value," in *Proceedings of the Joint International Conference on Global Environment and Nuclear Energy System/Advanced Power Plants*, Kyoto, Japan,

September 15-19, 2003, pp. 1-14.

[71] J. Fewster and J.D. Jackson, "Experiments on supercritical pressure convective heat transfer having relevance to SCWR," in *Proceedings of the International Congress on Advances in Nuclear Power Plants (ICAPP'04)*, Pittsburgh, PA, USA, June 13-17, 2004, pp. 537-551.

[72] S. He, W.S. Kim, P.-X Jiang, and J.D. Jackson, "Simulation of mixed convection heat transfer to carbon dioxlide at supercritical pressure," *Journal of Mechanical Engieering Science*, vol. 218, pp. 1281-1296, 2004.

[73] H.Ye. Kim, H. Kim, and J.J. Song et al., "Heat transfer test in a tube using CO2 at supercritical pressures," in *International Conference on Nuclear Energy Systems for Future Generation and Global Sustainability*, Tsukuba, Japan, October 9-13, 2005.

[74] I.L. Pioro and H.F. Khartabil, "Experimental study on heat transfer to supercritical carbon dioxide flowing upward in a vertical tube," in *13th International Conference on Nuclear Engineering (ICONE-13)*, Beijing, China, May 16-20, 2005.

[75] J.P. Holman and J.H. Boggs, "Heat transfer to Freon 12 near the critical state in natural-circulation loop," *Journal of Heat Transfer*, vol. 82, no. 3, pp. 221-226, 1960.

[76] L.M. Gorban, R.S. Pomet'ko, and O.A. Khryaschev, "Modeling of water heat transfer with Freon of supercritical pressure," *Institute of Physics and Power Engineering*, pp. 1-19, 1990.

[77] M. Kinakin, "Dual and Single Subchannel Flow in a 43 Element CANDU Type Fuel Bundle," University of Ontario Institute of Technology, Undergraduate Thesis 2011.

[78] X.-R. Zhang, L. Chen, and H. Yamaguchi, "Natural convective flow and heat transfer of supercritical CO2 loop in a rectangular circulation loop," *International Journal of Heat and Mass Transfer*, vol. 53, pp. 4112-4122, 2010.

[79] C.K. Chow and H.F. Khartabil, "Conceptual Fuel Channel Designs for CANDU-SCWR," *Nuclear Engineering and Technology*, vol. 40 (1), 2008.

[80] J. Samuel, G.D. Harvel, and I.L. Pioro, "Design concept and heat transfer analysis for a double pipe channel for SCWR type reactors," in *18th International Conference on Nuclear Engineering (ICONE-18)*, Xi'an China, May 17-21, 2010.

[81] McAdams W.H., Kennel W.E., and Addoms J.N., "Heat transfer to superheated steam at high pressures," *ASME*, vol. 72, no. 4, pp. 421-428, 1950.

[82] N.S. Kondrat'ev, "Heat transfer and hydraulic resistance with supercritical water flowing in tubes," *Thermal Engineering*, vol. 16, no. 8, pp. 73-77, 1969.

[83] Hong S.D., Chun S.Y., and Baek W.P., "Heat transfer characteristics of an internally-heated annulus cooled with R-134a near critical pressure," *Journal of the Korean Nuclear Society*, vol. 36, no. 5, pp. 403-414, 2004.

[84] Ornatskiy A.P., Glushchenko L.F., and Gandzyuk O.F., "An experimental study of heat transfer in externally-heated annuli at supercritical pressures," *Heat Transfer-Soviet Research*, vol. 4, no. 6, pp. 25-29, 1972.

[85] B.V. Dyadyakin and A.S. Popov, "Heat transfer and thermal resistance of tight seven-rod bundle, cooled with water flow at supercritical pressures," *Transactions of VTI*, vol. 11, pp. 244-253, 1977.

[86] G. Richards, A.S. Shelegov, P.I. Kirillov, I.L. Pioro, and G. Harvel, "Temperature profiles of a vertical bare 7-element bundle cooled with supercritical Freon-12," in *19th International Conference on Nulcear Engineering (ICONE-19)*, Chiba, Japan, May 16-19, 2011.

[87] A. Kiss and A. Aszodi, "Summary of Three Different Validation Cases of Coolant Flow in Supercritical Water Test Sections with the CFD Code ANSYS CFX 11.0," *Nuclear Technology*, vol. 170, no. 1, pp. 40-53.

[88] M. Angelucci, W. Ambrosini, and N. Forgione, "Prediction of wall friction for fluids at supercritical pressure with CFD models," in *14th International Topical Meeting on Nuclear Reactor Thermal Hydrualics (NURETH-14)*, Toronto, Canada, September 25-30, 2011.

[89] D. Palko and A. Henryk, "Investigation of the onset of heat transfer deterioration to supercritical water," in *4th International Symposium on Supercritical Water Reactors (ISSCWR-4)*, Heidelberg, Germany, March 8-

11, 2009.

[90] S. Gupta, S. Mokry, A. Farah, K. King, and I.L. Pioro, "Developing a new heat-transfer correlation for supercritical-water flowing in vertical bare tubes," in *Proceedings of the International Conference on Nuclear Engineering (ICONE-18)*, Xi'an China, May 17-21, 2010.

[91] S. Mokry, Y. Gospodinov, and I.L. Pioro, "Supercritical Water Heat-Transfer Correlation for Vertical Bare Tubes," in *International Conference on Nuclear Engineering (ICONE-17)*, Brussels, Belgium, July 12-16, 2009.

[92] A. Kiss and A. Aszodi, "Numerical experiment on different validation cases of water coolant flow in supercritical pressure test sections assisted by discriminated dimensional analysis part I: The dimensional analysis," in *14TH Internaional Topical Meeting on Nuclear Reactor Thermal Hydraulics (NURETH-14)*, Toronto, Canada, September 25-30, 2011.

[93] F. Roelofs, J.A. Lycklama a Nijeholt, E.M.J. Komen, M. Lowenberg, and J. Starflinger, "CFD Validation of a Supercritical Water Flow for SCWR Design Heat and Flux," in *International Congress on Advances in Nuclear Power Plants (ICAPP)*, Nice, France, May 13-18, 2007.

[94] T. Kaida, H. Mori, K. Kariya, M. Ohno, and Y. Hamamoto, "Heat transfer to supercritical pressure fluids flowing in tubes in superheated vapor region," in *5th International Symposium on Supercritical Water Reactors (ISSCWR-5)*, Vancouver Canada, March 13-16, 2011.

[95] H. Herbell, J. Starflinger, and T. Schulenberg, "Numerical Investigation of cooling heat transfer of supercritical water," in *5TH International Symposium on Supercritical Water Reactors (ISSCWR-5)*, Vancouver, Canada, March 13-16, 2011.

[96] M. De Rosa et al., "Lessons learned from the application of CFD models in the prediction of heat transfer to fluids at supercritical pressure," in *5TH International Symposium on Supercritical Water Reactors (ISSCWR-5)*, Vancouver, Canada, March 13-16, 2011.

[97] Eu. Saltanov, W. Peiman, Sh. Draper, and I. Pioro, "Heat-transfer analysis of supercritical-water and superheated-steam-cooled channels of SCWR," in *5TH International Symposium on Supercritical Water Reactors (ISSCWR-5)*, Vancouver, Canada, March 13-16, 2011.

[98] M. Jaromin and H. Anglart, "Sensitivity analysis of heated wall temperature and velocity distribution in CFD simulations of the upward flow of supercritical water," in *14TH International Topical Meeting on Nulcear Reactor Thermal Hydrualics (NURETH-14)*, Toronto, Canada, September 25-30, 2011.

[99] A.M. Vaidya, N.K. Maheshwari, P.K. Vijayan, and D. Saha, "Computational study of flow and heat transfer for water under supercritical conditions in a vertical pipe using NAFA CFD code," in *Proceedings of the 14TH International Topical Meeting on Nulcear Reactor Thermal Hydrualics (NURETH-14)*, Toronto, Canada, September 25-30, 2011, pp. 1-14.

[100] A. Farah, "Undergraduate Thesis Project," University of Ontario Institute of Technology, Oshawa, 2011.

[101] J.M. Saunders, "CFD Examination of Flow Effects Around a Canflex Fuel Bundle in Adiabatic Supercritical Conditions," University of Ontario Institute of Technology, Undergraduate Thesis Project 2011.

[102] T. Blacker, "The Cooper Tool," Sandia National Laboratories, Evanston, IL, 5th International Meshing Roundtable 1996.

[103] B.E. Launder and W.P. Jones, "The Calculation of Low Reynolds Number Phenomena with a Two-Equation Model of Turbulence," *Heat and Mass Transfer* , vol. 16, pp. 1119-1130, 1973.

[104] J. Robinson and T. Drews, "Resolving Flow-Accelerated Corrosion Problems in the Industrial Steam Plant," BetzDearborn, Trevose, PA, Technical Paper 468 9911 1999.

[105] Atomic Energy of Canada Ltd and New Brunswick Power Nuclear, "Flow Accelerated Corrosion and Cracking of Carbon Steel Piping in Primary Water - Operating Experience at the Point Lepreau Generating Station," in *Proceedings of the 12th International Conference on Environmental Degradation of Materials in Nuclear Power System – Water Reactors*, 2005, pp. 1-12.

[106] D.A. Barlett, "The fundamentals of Heat Exchangers," American Institute of Physics, 1996.

[107] "Basco type 500 heat exchangers manual," API Heat Transfer, Buffalo,

New York, USA, 2000.

[108] V. Varma, "Valve Application, Maintenance, and Repair Guide, EPRI report TR-105852v1," EPRI Distribution Center, Palo Alto, Carlifonia, 1999.

[109] C. Menten, "Supercritical Control: Technologies for supercritical boilers bring new efficiencies to coal-fired power plants but require specialized control strategies," *Control Engineering*, vol. 54, August, 2007.

[110] T. Schulenberg and D. Visser, "Thermal-hydraulics and safety concepts reactors," *14TH International Topical Meeting on Nuclear Reactor Thermal Hydrualics (NURETH-14)*, September, 2011.

[111] S.J. Goidich, S. Wu, Z. Fan, and A.C. Bose, "Design Aspects of the Ultra-Supercritical CFB Boiler," Foster Wheeler North America Corp,.

[112] Scanivalve Corp, "Pressure and Temperature Handbook," Liberty Lake, WA, 2006.

[113] B. Bergquist, "RTD or thermocouple, What is the right choice?," Burns Engineering, Minnetonka, MN, US, 2009.

[114] Pyromation Inc. (2010) Thermowells. [Online]. http://www.pyromation.com/lit/thermowellcatalog.pdf

[115] M. Naidin, S. Mokry, and I.L. Pioro, "SCW NPPs: Layouts and Thermodynamic Cycles," in *Nuclear Energy for New Europe*, Bled, Slovenia, September 14-17, 2009.

[116] G. Hazi and I.Farkas, "On the Pressure Dependency of Physical Parameters in Case of Heat Transfer Problems of SCW," in *International Conference on Nuclear Engineering (ICONE-16)*, Orlando, Florida, May 11-15, 2008.

[117] K.e.a. Kuehlert, "Fluid-Structure Interaction of a Steam Generator Tube in a Cross-Flow Using Large-Eddy Simulation," in *International Conference on Nuclear Engineering (ICONE-14)*, Miami, USA, July 17-20, 2006.

[118] A. Muhana and D.R. Novog, "Validation of FLUENT for Prediction of Flow Distribution and Pressure Gradients in a Multi-Branch Header under Low Flow Condition," in *International Conference on Nuclear Engineering (ICONE-16)*, Orlando, Florida, May 11-15, 2008.

[119] D. Wilcox, "Simulation of Transition with a Two-Equation Turbulence Model," *AIAA Jornal*, vol. 32, no. 2, pp. 247-255, 1994.

[120] J.D. Jackson, "Consideration of the Heat Transfer Properties of Supercritical Pressure Water in Connection with the Cooling of Advanced Nuclear Reactors," in *13th Pacific Basin Nuclear Conference*, Shenzhen City, China, October 15-21, 2002.

[121] A.A. Bishop, R.O. Sandberg, and L.S. Tong, "High Temperature Supercritical Pressure Water Loop: Part IV, Forced Convection Heat Transfer to Water at Near-Critical Temperatures and Super-Critical Pressures," Westinghouse Electric Corporation, Pittsburgh, Pennsylvania, 1964.

[122] Emerson Process Management, "Control Valve Handbook, Fourth Edition," Fisher, Marshalltown, Iowa, USA, 2005.

[123] "Heat exchanger design," Bramton Plate & Structural Steel Rolling Inc., Brampton, Ontario, Canada, 2012.

APPENDIX A: DETAILS OF COMPUTATIONAL FLUID DYNAMICS ANALYSIS FOR SUBCHANNELS

Title: Modelling of heat transfer between two fuel subchannels in supercritical water conditions using computational fluid dynamics

Authors: M. Kinakin, A. Adenariwo, G.D. Harvel, and I. Pioro

Abstract

This paper investigates the application of FLUENT in simulating a SuperCritical Water Reactor (SCWR) pressure tube type design. Computational Fluid Dynamics (CFD) can be used to study the unstable behaviour around pseudo-critical conditions along the fuel channel. In SCWRs, the coolant reaches its pseudo-critical temperature early in the reactor core and thermophysical properties undergo dramatic changes. The heat-transfer mechanism along the fuel channel also changes beyond the pseudo-critical point due to the fluid acting more like a gas-like.

The subchannels between different rings in the fuel string receive different heat fluxes and as a result, different heat transfer rates. The pseudo-critical point for different subchannels may occur at different axial locations. While experiments will be required to properly understand this effect, it is important to determine the current prediction capability of CFD type codes for this phenomenon as it will assist in defining the type of validation exercises necessary for design activities.

Introduction

There are a number of new concepts for nuclear reactors being developed worldwide as part of the Generation IV collaboration project. One such concept is a SuperCritical Water-cooled Reactor (SCWR), which is expected to have a thermal efficiency up to 50% [**115**]. SCWRs will use Super Critical Water (SCW) as a coolant, thus requiring operation at higher temperatures and pressures compared to those of current reactors. While current CANDUs and PWRs operate at a coolant pressure within 10 – 16 MPa, SCWRs will operate in the range of 25 MPa. The coolant would thus pass through the pseudocritical region somewhere along the channel [**7**].

Two types of SuperCritical Water-cooled Reactor (SCWR) concepts include a large Pressure Vessel (PV) Type as well as standard CANDU Pressure Tube (PT) Type Reactors. The current fuel-channel reference design for a PT Type Reactor consists of a bundle covered with a ceramic layer, enclosed by a pressure tube [**79**]. The outer surface of the pressure tube is in contact with the moderator, while a perforated liner protects the ceramic layer from the bundles, through which flows the primary coolant.

A typical fuel channel considered for a SCW type reactor contains a cylindrical bundle with rod type elements [**80**]. In such a design, the fuel bundle forms flow paths referred to as subchannels, each receiving heat from a set of 3 or 4 different cylindrical fuel elements. Optimum fuel bundle performance is affected by the design of the fuel bundle. This includes in particular heat transfer into gaps and subchannels, and the associated momentum and energy exchange between subchannels.

The subchannels between different rings of the fuel bundle have different heat fluxes, resulting in different heat-transfer rates. This configuration results in

some subchannels heating faster than others. For a supercritical fluid, the pseudocritical point may occur at different axial locations along each subchannel. Changes in the fluid behaviour due to fluid-property transitions may or may not occur due to the influence of the neighbouring subchannels. Even for low pressure fluids, the physics of fluid momentum and energy exchange between subchannels is not fully understood. While experiments will be required to fully understand this effect in supercritical conditions, it is important to determine the current prediction capability of CFD-type codes for this phenomenon as this will assist in defining the type of validation exercises necessary for design activities.

In this work, two subchannels in the horizontal orientation are modelled with the FLUENT code with boundary conditions consistent with SCWR fluid conditions near the pseudocritical point at 25 MPa and 384 ℃. The fluid flows parallel to the walls of the pin and heat fluxes for each fuel pin are varied around a base heat flux such that transitions through the channel would normally occur several centimetres away from each other if no influences of the neighbouring channels are considered. Computational fluid dynamics (CFD) modelling of a CANDU fuel subchannel is of particular interest at supercritical conditions to understand the heat transfer phenomena for the Gen-IV SCW CANDU design. While some work has been done in this field [**116**,**117**,**118**,**119**], additional work is necessary. This work concentrates on modelling SCW flow in two subchannels before the pseudocritical point to determine what phenomena is predicted by the FLUENT code.

Model Development

The FLUENT-12 CFD code is used for this work to perform the simulations. The geometry configuration was developed with GAMBIT finite element modelling software. While the fuel bundle design for the SCWR type reactor is not yet

chosen, a representative design is needed. For this work, the CANFLEX (43-element) CANDU fuel bundle design was chosen for this analysis.

Table 1 shows the properties of the CANFLEX bundle used in the analysis. The reference case is a Channel Thermal Power of 8.5 MW_{th} with uniformly distributed heat flux across the channel [**80**].

Table 1: CANFLEX-type Fuel Bundle Parameters near pseudocritical conditions [80**]**

Item	**Value**	**Unit**
Bundle Power	708.3	kW_{th}
Heated Length	0.481	m
Inlet Pressure	25	MPa
Coolant Inlet temperature	357	^{o}C
Coolant Mass Flux	1330	$kg(m^2/s)$
Centre Element Diameter	13.5	mm
Inner Element Diameter	13.5	mm
Intermediate Element Diameter	11.5	mm
Outer Element Diameter	11.5	mm
Centre Element Heat Flux	250	kW/m^2
Inner Element Heat Flux	250	kW/m^2
Intermediate Element Heat Flux	250	kW/m^2
Outer Element Heat Flux	250	kW/m^2

The channel contains 12 bundles arranged in series with enough spacing between each bundle to accommodate the bundle end plates. A heated bundle length of 0.481 m and a coolant mass-flow of 4.37 kg/s through the channel are chosen for this analysis. The pressure drop is not expected to change significantly along the bundle, thus a constant pressure of 25 MPa is assumed.

The inlet coolant temperature of 357 ^{o}C is chosen to match the inlet coolant bundle temperature of a previously modelled one-dimensional fuel channel design [**80**]. The analysed bundle is located prior to where the pseudocritical point is expected to occur in the channel. The coolant mass flux was calculated from an area ratio of the subchannel flow area and the channel flow area. A uniform base heat flux of 250 kW/m^2 is applied to each element surrounding the subchannels analysed in this model. This heat flux corresponds to a reduced power representative of the entrance region and is modelled uniform along the length.

The outer diameter of the fuel elements were measured from a CANFLEX fuel bundle prototype. The centre element and the elements located in the inner ring have an outside diameter of 13.5 mm while the intermediate and outer elements have an outer diameter of 11.5 mm.

Subchannel Selection

The geometry and layout for the 43 elements in a CANFLEX bundle are defined relative to the rings in the CANFLEX bundle. The radii of the inner, intermediate, and outer rings are located at distances of 16.5 mm, 34.6 mm, and 45.9 mm, respectively from the centre of the bundle. The centres of each element in each ring are located on the circumferences of their corresponding rings. The elements are equally spaced around the ring circumferences.

Figure 1 shows a CANFLEX-type fuel bundle schematic with the centre element (element-1) and inner elements (numbered from 2-8), intermediate elements (numbered from 9-22) and outer elements (numbered from 23-43). The subchannels, (numbered 1-70) represent the flow area of the bundle.

Subchannels 8 and 23 (similar to subchannels 20 and 47 or any pair of subchannels with similar geometry) are the subchannels under study, and as such are used as reference in this paper.

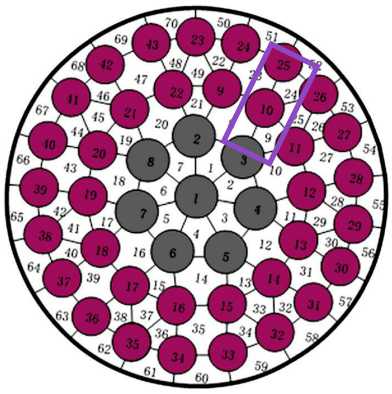

Figure 1: Schematic of CANFLEX-type bundle showing subchannels

Subchannels 8 and 23 receive different heat fluxes in accordance with the surrounding elements. Subchannel 8 receives heat from elements 2, 3, 9, and 10 with surrounding effects from subchannels 1, 9, 21, and 23. Subchannel 23 receives heat from elements 8, 10, 24, and 25 with surrounding effects from subchannels 8, 22, 24 and 51. The control volume selected for analysis is the union of the subchannels 8 and 23.

The subchannel selected for analysis is modelled with symmetry. The heat flux for each pin is uniform around the pin hence; the heat fluxes received by the subchannels of similar geometry are identical. The effect of the circumferential wall conduction is negligible and not taken into account since the subchannel is modelled in steady state. The flow properties are distributed as a function of the relative areas of the subchannels and therefore smaller subchannels have lower mass fluxes. This approach allows for the discretization of the model.

Mesh definition

The subchannel geometry and finite element model was generated in GAMBIT 2.4.6 software. The mesh consists of 852,480 cells axially split into 48 divisions along the length. Face meshing was first conducted before extruding the face. Boundary layers were applied to each element surface, consisting of an inflation of 1.2 with the first layer located at a distance of 5×10^{-6} m from the wall, representing the fuel element in this case. Each edge of the subchannel face was meshed with a mesh count per edge as shown in Figure 2. The numbers shown in the Figure represent the number of edge meshes for each edge. For instance element 10, of which half of the circumference is relevant in the subchannel geometry (refer to Figure 1), is divided into 160 equal spaces. Correspondingly, element 25 of which a quarter is relevant in the subchannel is divided into 80 equal spaces. The edge joining elements 10 and 25 is divided into 30 spaces which are in line with the boundary layers previously defined for both elements 10 and 25. The mesh division on this edge beyond the boundary layer of the neighbouring elements (10 and 25) is equally spaced. A mesh was then applied over the subchannel face.

The face was extruded without the mesh to 0.481m corresponding to the full heated length of 1 full bundle. An edge mesh was then applied to each axial edge of the subchannel volume before a volume mesh was generated using the hex/wedge cooper scheme option available in GAMBIT.

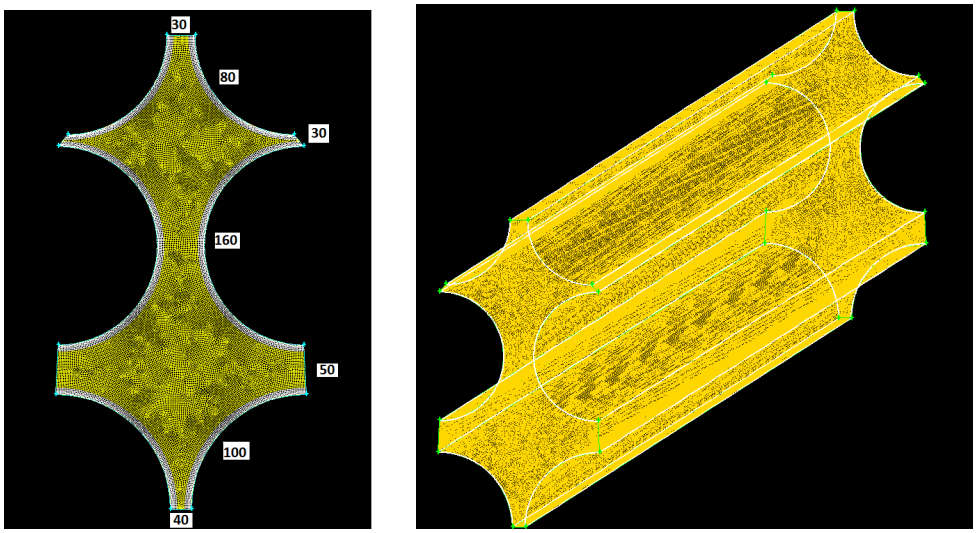

(a) Cross-sectional mesh view **(b) Isometric mesh view**

Figure 2: Subchannel mesh view; (a) Cross-sectional view (b) Isometric view

Viscous Model Selection

The k-ϵ turbulence model was adopted since it is the well known two-equation energy transport turbulence model developed by Jones and Launder [**103**]. The model works by conserving the energy contained within a turbulent region by means of transport equations that carry that total energy (and its dissipation) along a geometrical flow path. The variables k and ϵ represent the total turbulent kinetic energy and the dissipation rate of energy respectively. The two quantities are described as follows:

$$k = \frac{u^2+v^2+z^2}{2} \qquad \left(\frac{m^2}{s^2}\right) \qquad (1)$$

Where u, v, and z represent the one-dimensional velocities of fluid contained within the three dimensional domain. The dissipative energy term ϵ, is described as follows:

$$\epsilon = \rho C_\mu \frac{k^2}{\mu_t} \qquad \left(\frac{m^2}{s^3}\right) \qquad (2)$$

Where ρ is the density of the fluid, C_μ is a constant taken to be 0.09 as defined by the standard k-ϵ model. The definition of ϵ can be expressed in a compact term:

$$\epsilon = \frac{k^{3/2}}{l} \quad where \quad l = \frac{\rho C_\mu}{\mu_t \sqrt{k}} \qquad (3)$$

The characteristic length scale l, represents the maximum diameter of an energy containing eddy. The k- ϵ model is the most basic and documented turbulence model being able to solve many complex flows.

FLUENT Methodology

The mesh was exported from the GAMBIT 2.4.6 software and read into FLUENT for computational flow simulation. The Realizable k-ϵ (RKE) turbulence model with an enhanced wall treatment was used to solve the mesh, including use of the thermal effects option. The RANS (Reynolds Averaging Navier Stokes) approach was used to investigate for a steady solution.

Simulation was performed using a coupled pressure-velocity solver and solutions to the transport equations were conducted using second order algorithms. Momentum and pressure relaxation factors were each set to 0.5 and energy to 0.999 to mitigate initial oscillations in the solver. Under-relaxation provides a brake on the solution, allowing for smaller initial oscillations but requiring more iterations for convergence. Neglecting to apply a relaxation may cause the iteration to oscillate beyond the temperature range defined in the REFPROP database which consequently causes FLUENT to abort the solution.

The solution was solved with an absolute convergence criterion of 10^{-5} for the each of the variables contained in the transport equation including continuity, x-, y- and z-velocity, energy, and epsilon.

The adopted boundary condition includes no-slip at the solid walls (fuel element which are the curved surfaces as shown in Figure 2). The inlet fluid temperature was set to 357 ^{o}C with a turbulent intensity of 8%. The heat fluxes (refer to table 2) imposed on each element were applied as boundary conditions. Water properties at a pressure of 25MPa in the temperature range of interest were obtained from National Institute of Standards and Technology, reference Properties of database (NIST REFPROP) using a text command in FLUENT[**9**]. The use of NIST is essential since the fluid properties are near the region of the pseudocritical point of water. The fluid properties change considerably in a very narrow range within this region which causes the solver to become unstable.

Results

The results show that for the given fluxes in Table 2, initial iterations oscillated outside the range of the NIST properties database resulting in a crash of the solver. An adjustment to the input fluxes was made to eliminate this challenge.

Axial variation of coolant properties

The coolant density and temperature are uniform at the inlet but become varied with the continuous addition of heat along the subchannel. The coolant temperature and velocity increase, while the density from the inlet to the outlet decreases in accordance with the heat flux applied to the fuel elements.

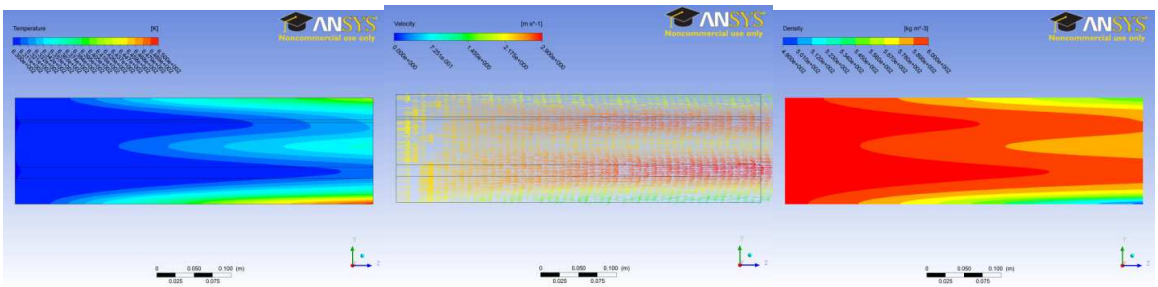

(a) Temperature contour **(b) Velocity contour** **(c) Density contour**

Figure 3: Axial Flow Variation from Inlet to Outlet; (a) Temperature contour, (b) Velocity contour and (c) Density contour

Temperature variation of coolant

A three-dimensional variation can be simulated by plotting cross-sectional temperature variations at intervals along the subchannel. This captures the details omitted by a one-dimensional model. The one-dimensional model assumes a single coolant temperature at different nodes across the fuel bundle [**80**].

Figure 4 shows a temperature gradient at intervals along the bundle. As expected, an increase of the temperature of the coolant is seen along the bundle. The temperature of the coolant at the narrow regions in the subchannel shows a significant increase in temperature along the subchannel than the coolant region far from the wall.

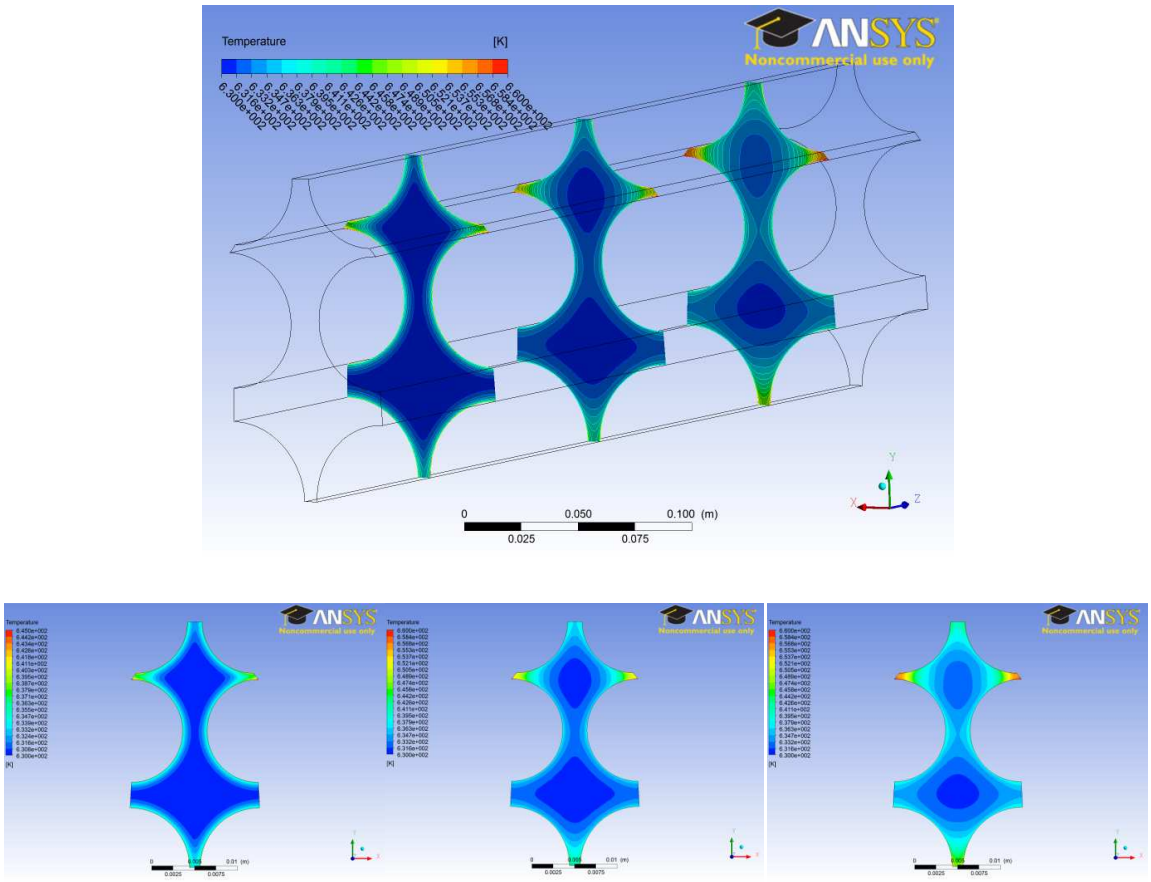

(a) z = 0.1 m **(b) z = 0.25 m** **(c) z = 0.4 m**

Figure 4: Axial cross-sectional temperature variation at a distance (z) from subchannel inlet; (a) z = 0.1 m, (b) z = 0.25 m and (c) z = 0.4 m

The fluid is essentially unheated at z = 0.1 m but the narrow region of the coolant shows a 25 ^{o}C difference in temperature with the coolant region farthest from the wall. At z = 0.25 m, a temperature gradient is observed across the fluid moving from the wall to the centre of the subchannel. The coolant between the narrow spacing between elements 25 and 10, and 24 and 9 (refer to Figure 1) maintains the highest fluid temperature in the subchannel. The top and bottom spaces between elements 24 and 15, and 2 and 3 respectively begin to significantly heat up at this point. At z = 0.4 m, the temperature gradient shows a more even variation with a 30 ^{o}C temperature difference between the narrow spacing and

the centre of the subchannel. The coolant in the upper subchannel shows a more varied temperature profile than the coolant in the lower subchannel.

The reason for the high temperature regions across the cross-sectional can be explained by low coolant velocity. Low coolant velocity means low heat transport properties which in turn causes heat to build up close to the wall of the element in the narrow region. The narrow spacing between the elements contains the fluid with the highest temperature which subsequently means pseudocritical phenomena will first occur at this region.

Velocity variation of coolant

The velocity profile at is plotted at the same intervals as the temperature profiles. The low velocity regions are located close to the wall as expected from the no-slip boundary condition. The coolant region farthest from the wall at the inlet has a maximum velocity of 2.9 m/s. The velocity distribution becomes more uniform along the channel with a decrease of the average velocity. This decrease of the velocity becomes less significant from z = 0.25 m to z = 0.4 m when compared to the change from z = 0.1 m to z = 0.25 m. This suggest that the flow is developing from z = 0.1 m to z = 0.25 m and is almost fully developed between z = 0.25 m to z = 0.4 m.

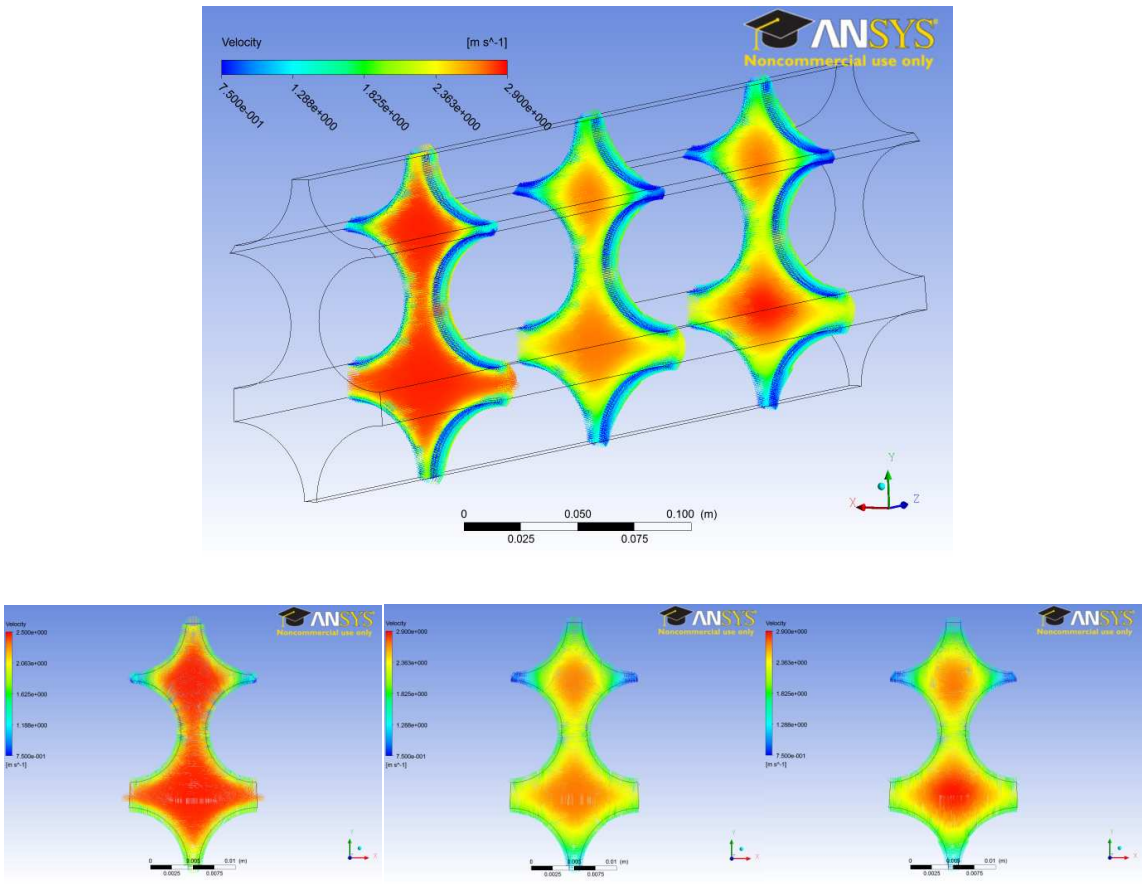

(a) z = 0.1 m **(b) z = 0.25 m** **(c) z = 0.4 m**

Figure 5: Axial cross-sectional velocity variation at a distance (z) from subchannel inlet; (a) z = 0.1m, (b) z = 0.25 m and (c) z = 0.4 m

The coolant region with low velocity is located at the narrow regions of the subchannel. The upper subchannel has a more pronounced effect of low velocity than the lower subchannel. The profile at z = 0.4 m, shows a larger area with coolant velocity close to maximum flow velocity. This is expected as the lower subchannel has a higher flow area than the upper subchannel. The effect of the no-slip boundary on the wall is less evident at the centre of the lower subchannel.

Density variation of coolant

The coolant density across the subchannel decreases from the inlet to the outlet. At a distance of z = 0.1 m downstream from the inlet, the coolant density is uniform at 620 kg.m^{-3} across the subchannel. The bulk density is close to 590 kg.m^{-3} at a distance of z = 0.4 m downstream from the inlet and in the subchannel region with narrow spacing, the value is close to 480 kg.m^{-3}.

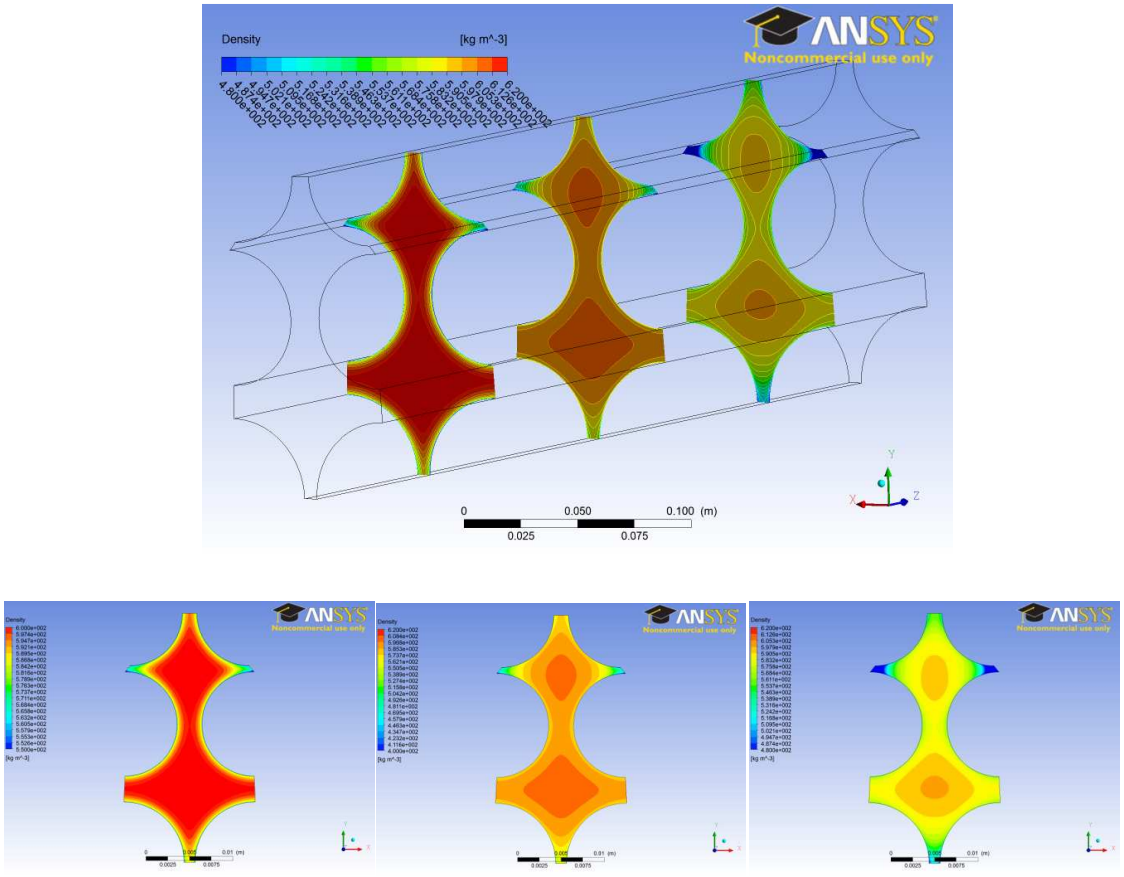

(a) z = 0.1m **(b) z = 0.25m** **(c) z = 0.4m**

Figure 6: Axial cross-sectional density variation at a distance (z) from subchannel inlet; (a) z = 0.1m, (b) z = 0.25m and (c) z = 0.4m

As the coolant heats up along the subchannel, the density decreases with minimum values located at the narrow spacing located in the upper subchannel. A low density region is located in the lower region of the lower subchannel. The coolant in the upper region of the upper subchannel has higher density compared to the lower region of the lower subchannel due to the better heat transport properties. The low density regions result from high heat transfer coupled with low fluid velocity in the region. The results show the expected change in properties across the subchannel.

Conclusion

A CFD analysis was performed for a selected subchannel in a CANFLEX-type bundle. A constant heat flux was applied to the elements surrounding the subchannel and temperature, velocity and density gradients were obtained at different positions along the bundle. The variations show that the pseudocritical point will first occur at the narrow regions close to the wall.

While work has been done on a reference subchannel, it would be useful to compare the variation of properties independently for the subchannels contained in the reference subchannel. Varying the base heat flux boundary condition will be useful for simulating a more representative model for the fuel bundle. An improvement to the model will include redefining the mesh to reduce extreme variations seen at the narrow regions in the subchannel, as well as to allow fluid flow to completely develop before the heated length of the bundle. Mesh refinement can be performed to obtain a higher order of convergence. The RANS approach gives a convergence of 10^{-5}. An unsteady solution may yield better convergence for the model and will be investigated in future work.

APPENDIX B: PRESSURE DROP AND HEAD LOSS SAMPLE CALCULATIONS

Test Section

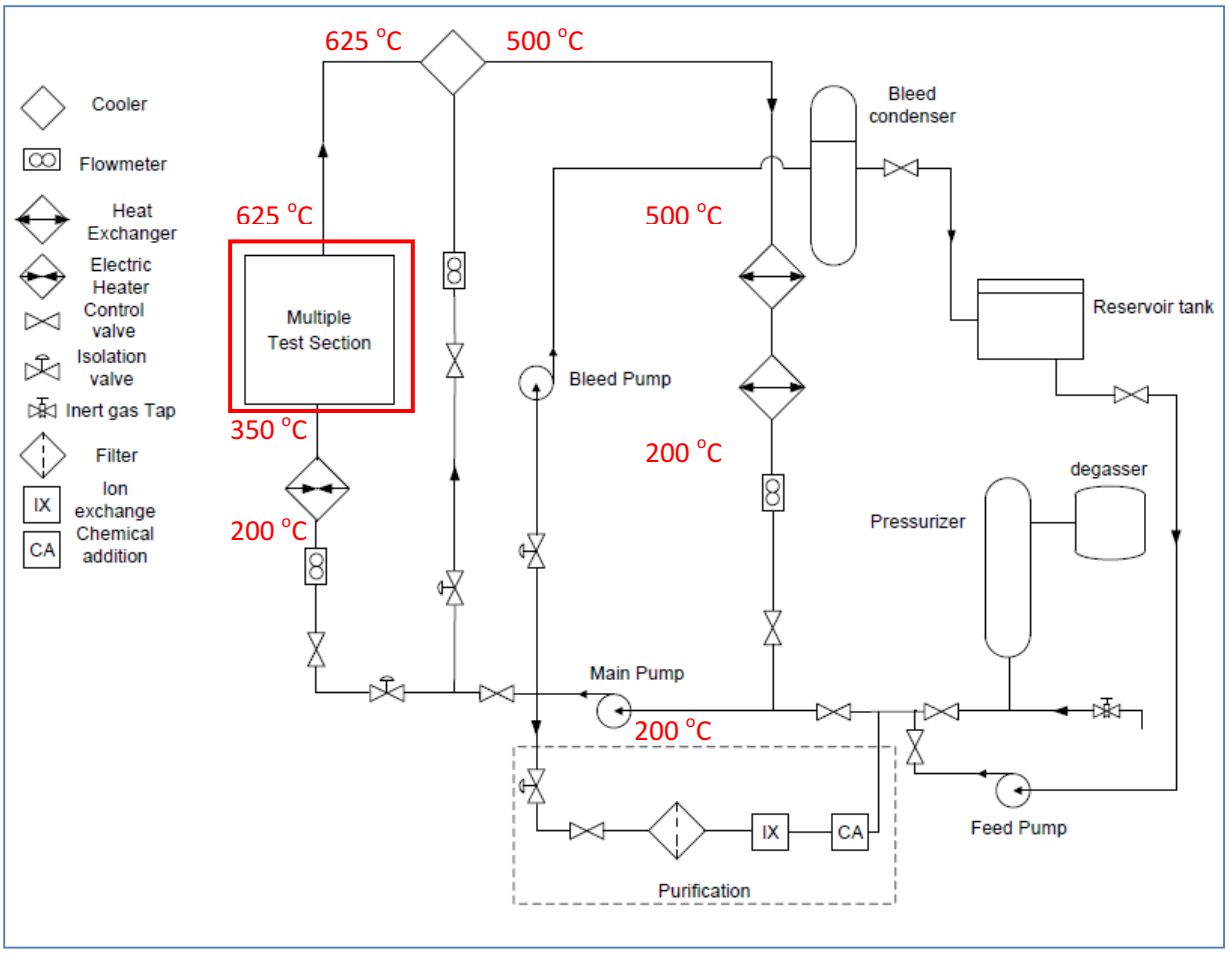

Value	Inlet (Control Volume)	Outlet (Control Volume)	Pseudo Critical Point
Temperature (T)	**350 °C**	**625 °C**	**384 °C**
Pressure (P)	**25.092 MPa**	**25 MPa**	**25.0 MPa**
Density (ρ)	**628.73 Kg/m^3**	**67.584 Kg/m^3**	**356 Kg/m^3**

Estimated test section length	4 m
Estimated pseudocritical point	1.2 m
Steel Roughness (ε)	0.045 mm
Reynolds number	124500
Diameter of pipe	0.00752 m
Friction Factor (f)	0.032

Pressure drop after pseudocritical point

$$\frac{p_1^2-p_2^2}{2\times P_1} = f \times \frac{L}{D} \times \frac{\rho_1}{2} \times V_{ave}{}^2 \times \frac{T_{ave}}{T_1}$$

T_1 = (384+273) K = 657 K

T_{ave} = (504.5+273) K = 777.5 K

ρ_1 = 353.3 Kg/m^3

f = 0.032

L = 2.8 m

D = 0.00752 m

P_2 = 25 MPa

$V_{ave} = G/\rho_{ave}$ = 1206/210.4 = 5.73 m/s

$$P_1^2 - P_2^2 = 2 \times P_1 \times f \times \frac{L}{D} \times \frac{\rho_1}{2} \times V_{ave}{}^2 \times \frac{T_{ave}}{T_1}$$

$$P_1^2 - (25 \times 10^6)^2 = 163560 P_1$$

P_1= 25.082 MPa

Pressure drop before pseudocritical point

$$\frac{p_1^2-p_2^2}{2\times P_1} = f \times \frac{L}{D} \times \frac{\rho_1}{2} \times V_{ave}{}^2 \times \frac{T_{ave}}{T_1}$$

T_1 = (350+273) K = 623 K

T_{ave} = (367+273) K = 640 K

ρ_1 = 628.7 Kg/m^3

f = 0.032

L = 1.2 m

D = 0.00752 m

P_2 = 25.02 MPa

$V_{ave} = G/\rho_{ave}$ = 1206/492.4 = 2.45

$$P_1^2 - P_2^2 = 2 \times P_1 \times f \times \frac{L}{D} \times \frac{\rho_1}{2} \times V_{ave}{}^2 \times \frac{T_{ave}}{T_1}$$

$$P_1^2 - (25.082 \times 10^6)^2 = 19796 P_1$$

P_{inlet} = 25.092 MPa

Pressure Drop in Test Section = 0.092 MPa

Losses – Major Loss (Friction)

Head loss after pseudocritical point

$$h_{L\,major} = f\frac{\ell}{D}\frac{V_{ave}{}^2}{2g}$$

ℓ=2.8 m
D = 0.00752 m
V_{ave} = 5.73m/s

Therefore $h_{L\,major}$ = 19.94 m

Head loss after pseudocritical point

ℓ=1.2 m
D = 0.00752 m
V_{ave} = 2.45 m/s

Therefore $h_{L\,major}$ = 1.56 m

Therefore total head loss in test section $h_{L\,major}$ = 21.5 m

Test Section to Cooler (Length - 1 m)

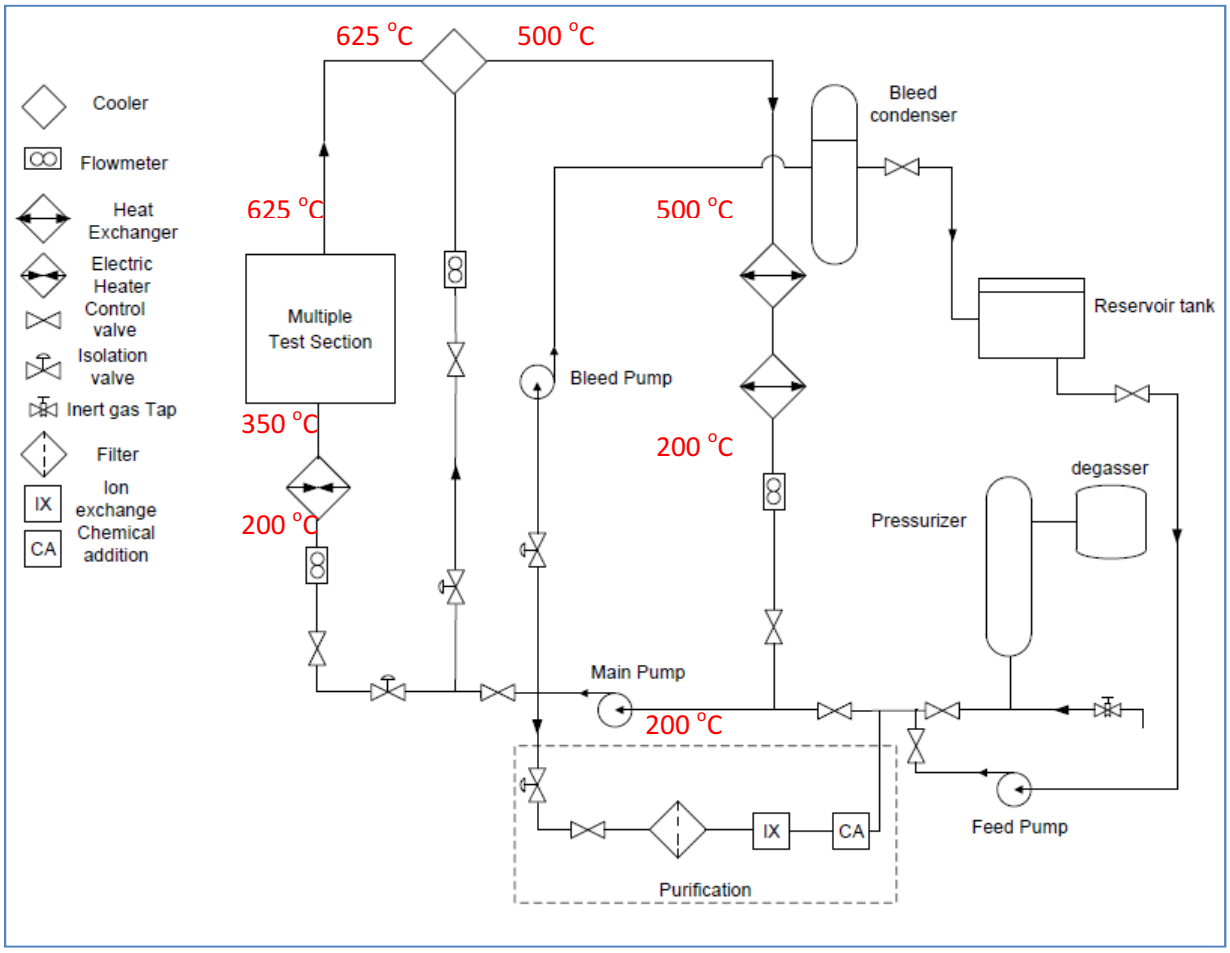

Value	Inlet (Control Volume)	Outlet (Control Volume)
Temperature (T)	**625 °C**	**625 °C**
Pressure (P)	**25 MPa**	**?**
Density (ρ)	**64.810 Kg/m^3**	**64.810 Kg/m^3**

Estimated test section to cooler length	1 m
Steel Roughness (ε)	0.045 mm
Reynolds number	124500
Diameter of pipe	0.00752 m
Friction Factor (f)	0.032

Pressure drop in section

$$\frac{p_1^2 - p_2^2}{2 \times P_1} = f \times \frac{L}{D} \times \frac{\rho_1}{2} \times V_{ave}{}^2 \times \frac{T_{ave}}{T_1}$$

T_1 = (625+273) K = 923 K

T_{ave} = (625+273) K = 923 K

ρ_1 = 64.810 Kg/m^3

f = 0.032

L = 1 m

D = 0.00752 m

P_1 = 25 MPa

$V_{ave} = G/\rho_{ave}$ = 1206/64.810 = 18.61 m/s

$$P_1^2 - P_2^2 = 2 \times P_1 \times f \times \frac{L}{D} \times \frac{\rho_1}{2} \times V_{ave}{}^2 \times \frac{T_{ave}}{T_1}$$

$$P_2^2 = P_1^2 - 2 \times P_1 \times f \times \frac{L}{D} \times \frac{\rho_1}{2} \times V_{ave}{}^2 \times \frac{T_{ave}}{T_1}$$

P_2 = 24.952 MPa

Pressure Drop in Section = 0.048 MPa

Losses – Major Loss (Friction), Minor Loss (Elbow)

Major head loss in section

$$h_{L\,major} = f \frac{\ell}{D} \frac{V_{ave}{}^2}{2g}$$

ℓ=1 m

D = 0.00752 m

V_{ave} = 18.61 m/s

Therefore $h_{L\,major}$ = 75.03 m

Minor head loss in section

$$h_{L\,minor} = K_L \frac{V^2}{2g}$$

Minor head loss	Value
Number of regular 90^o threaded elbows	3
$K_{L\,elbow}$	1.5
$h_{L\,elbow}$ (m)	79.43

Therefore total head loss in section from test section to cooler = 154.46 m

Cooler Section (length of pipe in cooler = 8 m)

Lab Enclosure Dimensions:

Height – 9 m
Width – 2 m
Length - 4.8 m

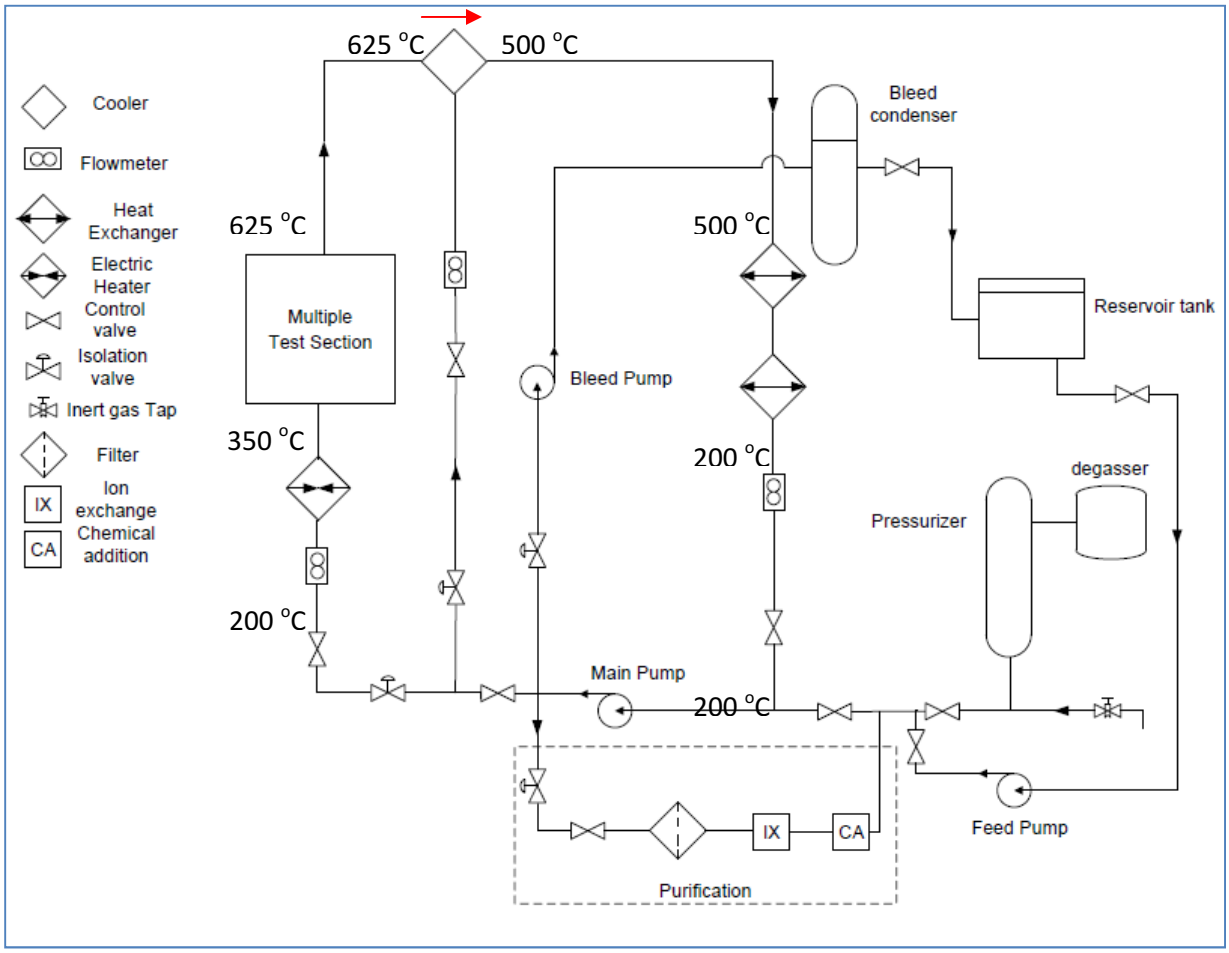

Value	Inlet (Control Volume)	Outlet (Control Volume)
Temperature (T)	**650 °C**	**500 °C**
Pressure (P)	**24.952 MPa**	**?**
Density (ρ)	**64.672 Kg/m^3**	**64.672 Kg/m^3**

Estimated length of pipe in cooler	8 m
Steel Roughness (ε)	0.045 mm
Reynolds number	124500
Diameter of pipe	0.00752 m
Friction Factor (f)	0.032

Pressure drop in section

$$\frac{p_1^2-p_2^2}{2\times P_1} = f \times \frac{L}{D} \times \frac{\rho_1}{2} \times V_{ave}{}^2 \times \frac{T_{ave}}{T_1}$$

T_1 = (650+273) K = 923 K

T_{ave} = (575+273) K = 848 K

ρ_1 = 64.672 Kg/m^3

f = 0.032

L = 8 m

D = 0.00752 m

P_1 = 24.952 MPa

$V_{ave} = G/\rho_{ave}$ = 1206/77.095 = 19.53 m/s

$$P_1^2 - P_2^2 = 2 \times P_1 \times f \times \frac{L}{D} \times \frac{\rho_1}{2} \times V_{ave}{}^2 \times \frac{T_{ave}}{T_1}$$

$$P_2^2 = P_1^2 - 2 \times P_1 \times f \times \frac{L}{D} \times \frac{\rho_1}{2} \times V_{ave}{}^2 \times \frac{T_{ave}}{T_1}$$

P_2 = 24.563 MPa

Pressure Drop in cooler = 0.389 MPa

Losses – Major Loss (Friction), Minor Loss (Elbow)

Major head loss in section

$$h_{L\,major} = f\frac{\ell}{D}\frac{V_{ave}{}^2}{2g}$$

ℓ=8 m

D = 0.00752 m

V_{ave} = 19.53 m/s

Therefore $h_{L\,major}$ = 661.8 m

Minor head loss in section

$$h_{L\,minor} = K_L\frac{V^2}{2g}$$

Minor head loss	Value
Number of regular 90° flanged elbows	10
$K_{L\,elbow}$	0.3
$h_{L\,elbow}$ (m)	58.32

Therefore total head loss in cooler = 720.12 m

Cooler to Heat Exchanger Section (2 m)

Lab Enclosure Dimensions:

Height – 9 m
Width – 2 m
Length - 4.8 m

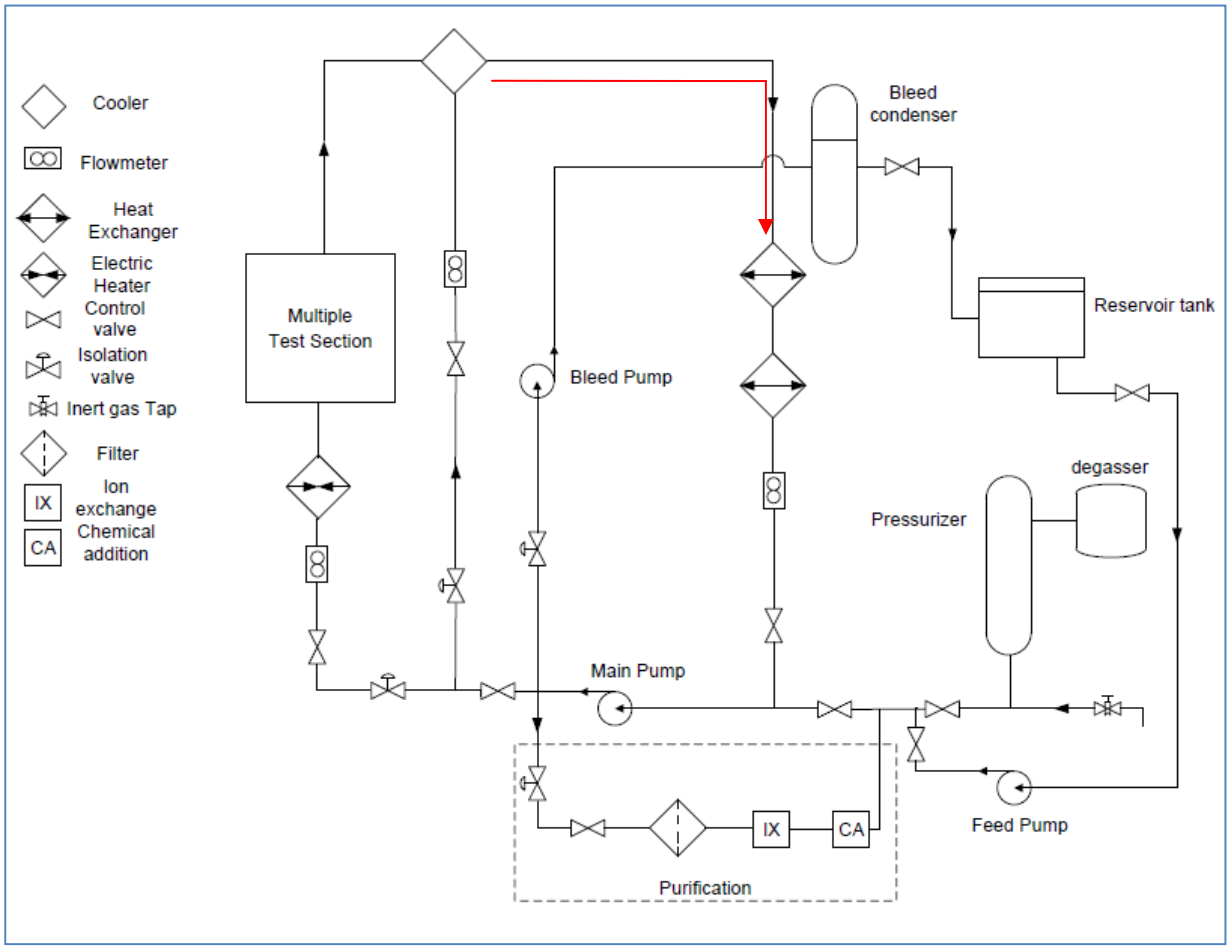

Value	Inlet (Control Volume)	Outlet (Control Volume)
Temperature (T)	**500 °C**	**500 °C**
Pressure (P)	**24.563 MPa**	**?**
Density (ρ)	**87.691 Kg/m^3**	**87.691 Kg/m^3**

Estimated length of pipe	2 m
Steel Roughness (ε)	0.045 mm
Reynolds number	124500
Diameter of pipe	0.00752 m
Friction Factor (f)	0.032

Pressure drop in section

$$\frac{p_1^2 - p_2^2}{2 \times P_1} = f \times \frac{L}{D} \times \frac{\rho_1}{2} \times V_{ave}{}^2 \times \frac{T_{ave}}{T_1}$$

T_1 = (500+273) K = 773 K

T_{ave} = (500+273) K = 773 K

ρ_1 = 87.691 kg/m^3

f = 0.032

L = 2 m

D = 0.00752 m

P_1 = 24.563 MPa

$V_{ave} = G/\rho_{ave}$ = 1206/87.691 = 13.75 m/s

$$P_1^2 - P_2^2 = 2 \times P_1 \times f \times \frac{L}{D} \times \frac{\rho_1}{2} \times V_{ave}{}^2 \times \frac{T_{ave}}{T_1}$$

$$P_2^2 = P_1^2 - 2 \times P_1 \times f \times \frac{L}{D} \times \frac{\rho_1}{2} \times V_{ave}{}^2 \times \frac{T_{ave}}{T_1}$$

P_2 = 24.492 MPa

Pressure Drop in section = 0.071 MPa

Losses – Major Loss (Friction)

Major head loss in section

$$h_{L\,major} = f \frac{\ell}{D} \frac{V_{ave}{}^2}{2g}$$

ℓ=2 m

D = 0.00752 m

V_{ave} = 13.75 m/s

Therefore $h_{L\,major}$ = 82.01 m

Minor head loss in section

$$h_{L\,minor} = K_L \frac{V^2}{2g}$$

Minor head loss	Value
Number of regular 90° flanged elbows	2
$K_{L\,elbow}$	1.5
$h_{L\,elbow}$ (m)	28.90

Therefore total head loss in section = 100.91 m

Heat Exchanger Section (12 m)

Lab Enclosure Dimensions:

Height – 9 m
Width – 2 m
Length - 4.8 m

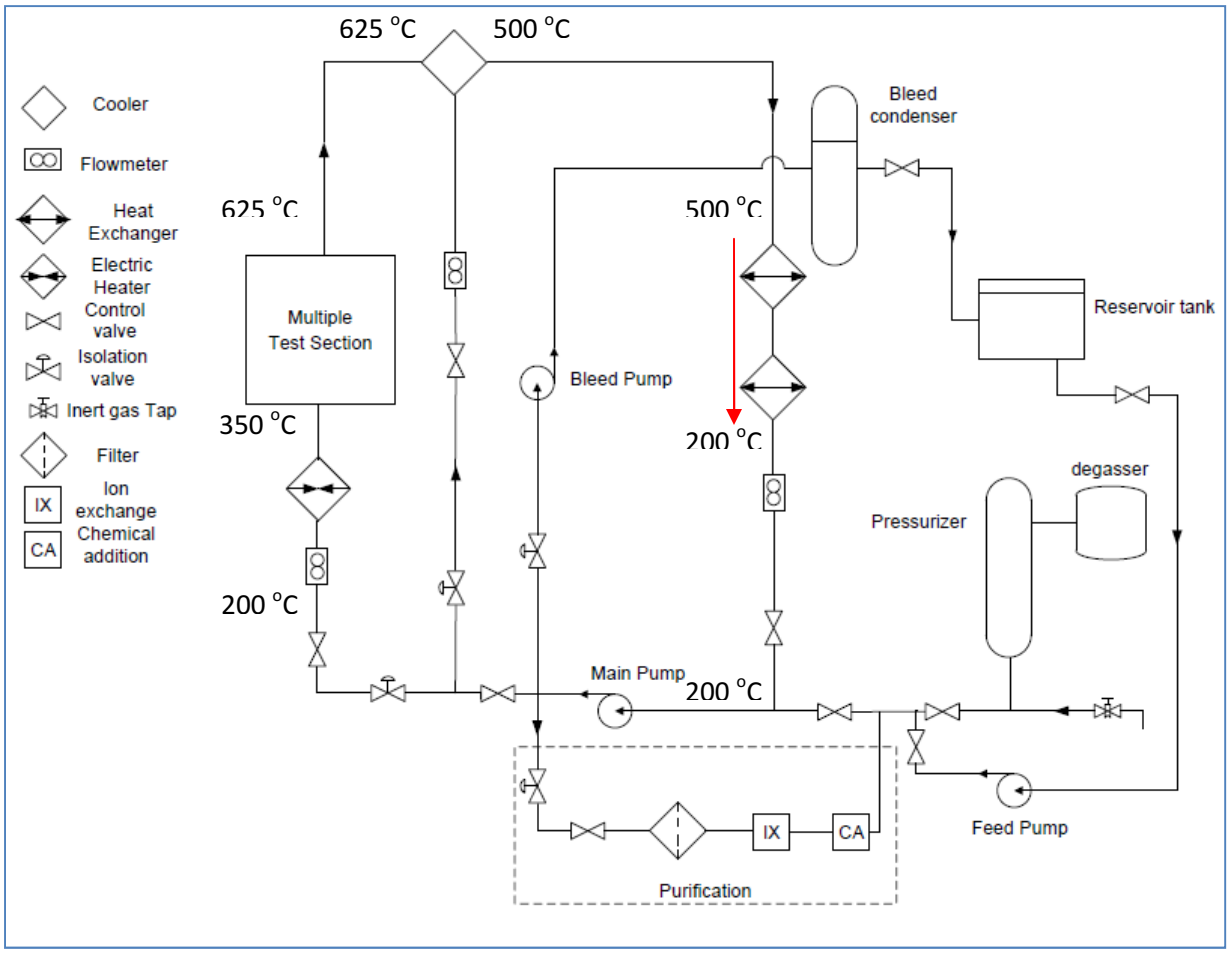

Value	Inlet (Control Volume)	Outlet (Control Volume)
Temperature (T)	**500 °C**	**200 °C**
Pressure (P)	**24.492 MPa**	**?**
Density (ρ)	**87.691 Kg/m^3**	**881.04 Kg/m^3**

Estimated length of pipe in heat exchanger	12 m
Steel Roughness (ε)	0.045 mm
Reynolds number	124500
Diameter of pipe	0.00752 m
Friction Factor (f)	0.032

Pressure drop in section

$$\frac{p_1^2 - p_2^2}{2 \times P_1} = f \times \frac{L}{D} \times \frac{\rho_1}{2} \times V_{ave}{}^2 \times \frac{T_{ave}}{T_1}$$

T_1 = (500+273) K = 773 K

T_{ave} = (350+273) K = 623 K

ρ_1 = 87.691 kg/m^3

f = 0.032

L = 12 m

D = 0.00752 m

P_1 = 24.492 MPa

$V_{ave} = G/\rho_{ave}$ = 1206/484.37 = 2.49 m/s

$$P_1^2 - P_2^2 = 2 \times P_1 \times f \times \frac{L}{D} \times \frac{\rho_1}{2} \times V_{ave}{}^2 \times \frac{T_{ave}}{T_1}$$

$$P_2^2 = P_1^2 - 2 \times P_1 \times f \times \frac{L}{D} \times \frac{\rho_1}{2} \times V_{ave}{}^2 \times \frac{T_{ave}}{T_1}$$

P_2 = 24.489 MPa

Pressure Drop in Section = 0.003 MPa

Losses – Major Loss (Friction)

Major head loss in section

$$h_{L\,major} = f \frac{\ell}{D} \frac{V_{ave}{}^2}{2g}$$

ℓ=12 m

D = 0.00752 m

V_{ave} = 2.49 m/s

Therefore $h_{L\,major}$ = 16.14 m

Minor head loss in section

$$h_{L\,minor} = K_L \frac{V^2}{2g}$$

Minor head loss	Value
Number of regular 90° flanged elbows	16
$K_{L\,elbow}$	0.3
$h_{L\,elbow}$ (m)	1.52

Therefore total head loss in heat exchanger = 17.66 m

Heat Exchanger to pump (4 m)

Lab Enclosure Dimensions:

Height – 9 m
Width – 2 m
Length - 4.8 m

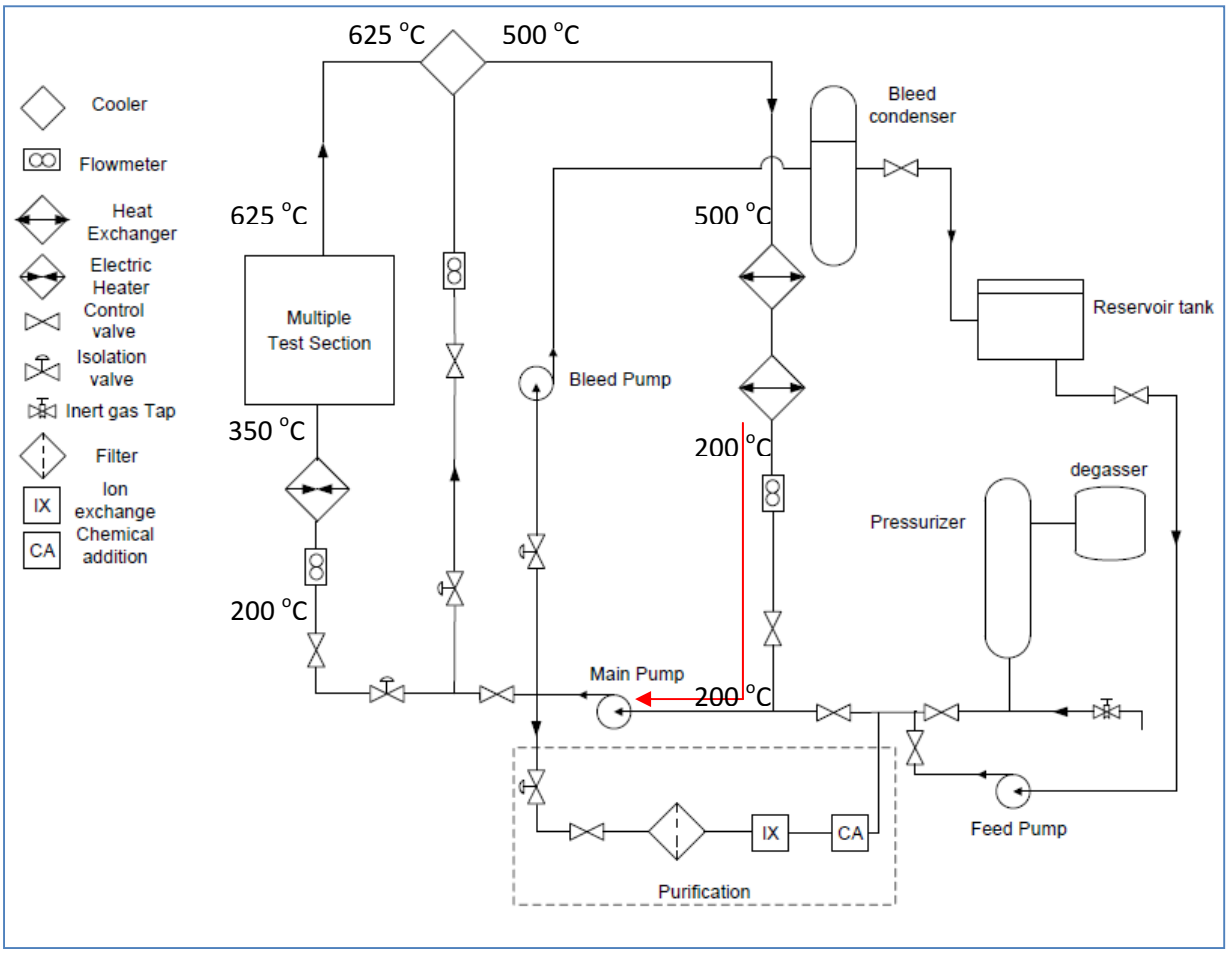

Value	Inlet (Control Volume)	Outlet (Control Volume)
Temperature (T)	**200 °C**	**200 °C**
Pressure (P)	**24.489 MPa**	**?**
Density (ρ)	**881.04 Kg/m^3**	**881.04 Kg/m^3**

Estimated length of pipe in heat exchanger	4 m
Steel Roughness (ε)	0.045 mm
Reynolds number	124500
Diameter of pipe	0.00752 m
Friction Factor (f)	0.032

Pressure drop in section

$$\frac{p_1^2 - p_2^2}{2 \times P_1} = f \times \frac{L}{D} \times \frac{\rho_1}{2} \times V_{ave}{}^2 \times \frac{T_{ave}}{T_1}$$

T_1 = (200+273) K = 473 K

T_{ave} = (200+273) K = 473 K

ρ_1 = 881.04 kg/m^3

f = 0.032

L = 4 m

D = 0.00752 m

P_1 = 24.489 MPa

$V_{ave} = G/\rho_{ave}$ = 1206/881.04 = 1.37 m/s

$$P_1^2 - P_2^2 = 2 \times P_1 \times f \times \frac{L}{D} \times \frac{\rho_1}{2} \times V_{ave}{}^2 \times \frac{T_{ave}}{T_1}$$

$$P_2^2 = P_1^2 - 2 \times P_1 \times f \times \frac{L}{D} \times \frac{\rho_1}{2} \times V_{ave}{}^2 \times \frac{T_{ave}}{T_1}$$

P_2 = 24.475 MPa

Pressure Drop in Section = 0.014 MPa

Losses – Major Loss (Friction), Minor Loss (Valve, Elbow)

Major head loss in section

$$h_{L\,major} = f \frac{\ell}{D} \frac{V_{ave}{}^2}{2g}$$

ℓ=4 m

D = 0.00752 m

V_{ave} = 1.37 m/s

Therefore $h_{L\,major}$ = 1.63 m

Minor head loss in section

$$h_{L\,minor} = K_L \frac{V^2}{2g}$$

Minor head loss	Value
Number of regular 90° flanged elbows	3
$K_{L\,elbow}$	1.5
$h_{L\,elbow}$ (m)	0.43
$K_{L\,valve}$ (fully open)	0.05
$h_{L\,valve}$ (m)	0.00

Therefore total head loss in section = 2.06 m

Pump to Pre-Heater (3 m)

Lab Enclosure Dimensions:

Height – 9 m
Width – 2 m
Length - 4.8 m

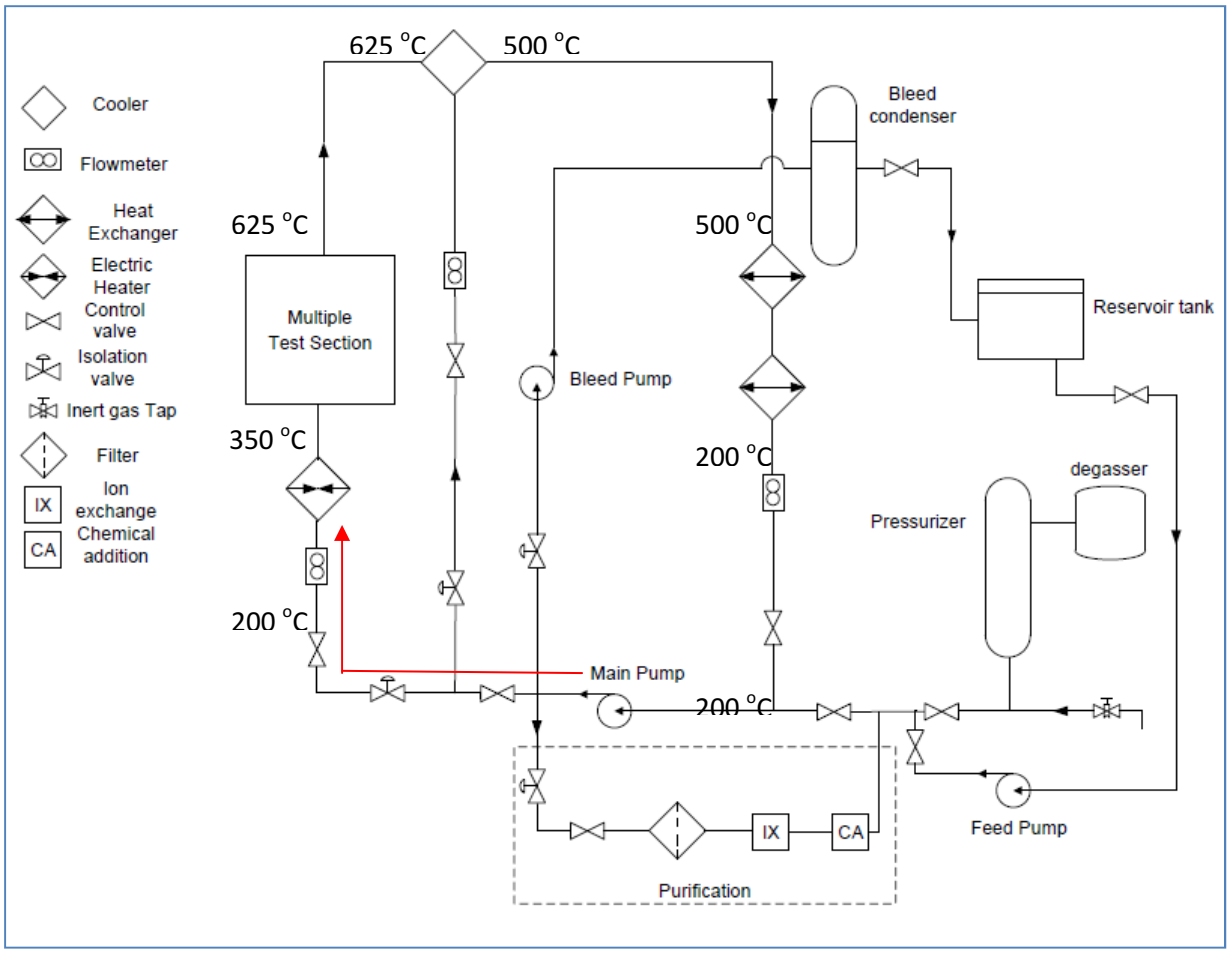

Value	Inlet (Control Volume)	Outlet (Control Volume)
Temperature (T)	**200 °C**	**200 °C**
Pressure (P)	**24.475 MPa**	**?**
Density (ρ)	**881 Kg/m^3**	**881 Kg/m^3**

Estimated length of pipe in heat exchanger	3 m
Steel Roughness (ε)	0.045 mm
Reynolds number	124500
Diameter of pipe	0.00752 m
Friction Factor (f)	0.032

Pressure drop in section

$$\frac{p_1^2-p_2^2}{2\times P_1} = f \times \frac{L}{D} \times \frac{\rho_1}{2} \times V_{ave}{}^2 \times \frac{T_{ave}}{T_1}$$

T_1 = (200+273) K = 473 K

T_{ave} = (200+273) K = 473 K

ρ_1 = **881** kg/m^3

f = 0.032

L = 3 m

D = 0.00752 m

P_1 = 24.475 MPa

$V_{ave} = G/\rho_{ave}$ = 1206/ **881** = 1.37 m/s

$$P_1^2 - P_2^2 = 2 \times P_1 \times f \times \frac{L}{D} \times \frac{\rho_1}{2} \times V_{ave}{}^2 \times \frac{T_{ave}}{T_1}$$

$$P_2^2 = P_1^2 - 2 \times P_1 \times f \times \frac{L}{D} \times \frac{\rho_1}{2} \times V_{ave}{}^2 \times \frac{T_{ave}}{T_1}$$

P_2 = 24.464 MPa

Pressure Drop in Section = 0.011 MPa

Losses – Major Loss (Friction), Minor Loss (Valve, Elbow)

Major head loss in section

$$h_{L\,major} = f\frac{\ell}{D}\frac{V_{ave}{}^2}{2g}$$

ℓ=3 m

D = 0.00752 m

V_{ave} = 1.37 m/s

Therefore $h_{L\,major}$ = 1.22 m

Minor head loss in section

$$h_{L\,minor} = K_L\frac{V^2}{2g}$$

Minor head loss	Value
Number of regular 90° flanged elbows	4
$K_{L\,elbow}$	1.5
$h_{L\,elbow}$ (m)	0.57
$K_{L\,valve}$ (fully open)	0.05
$h_{L\,valve}$ (m)	0.00

Therefore total head loss in section = 1.79m

Pre-Heater (5 m)

Lab Enclosure Dimensions:

Height – 9 m
Width – 2 m
Length - 4.8 m

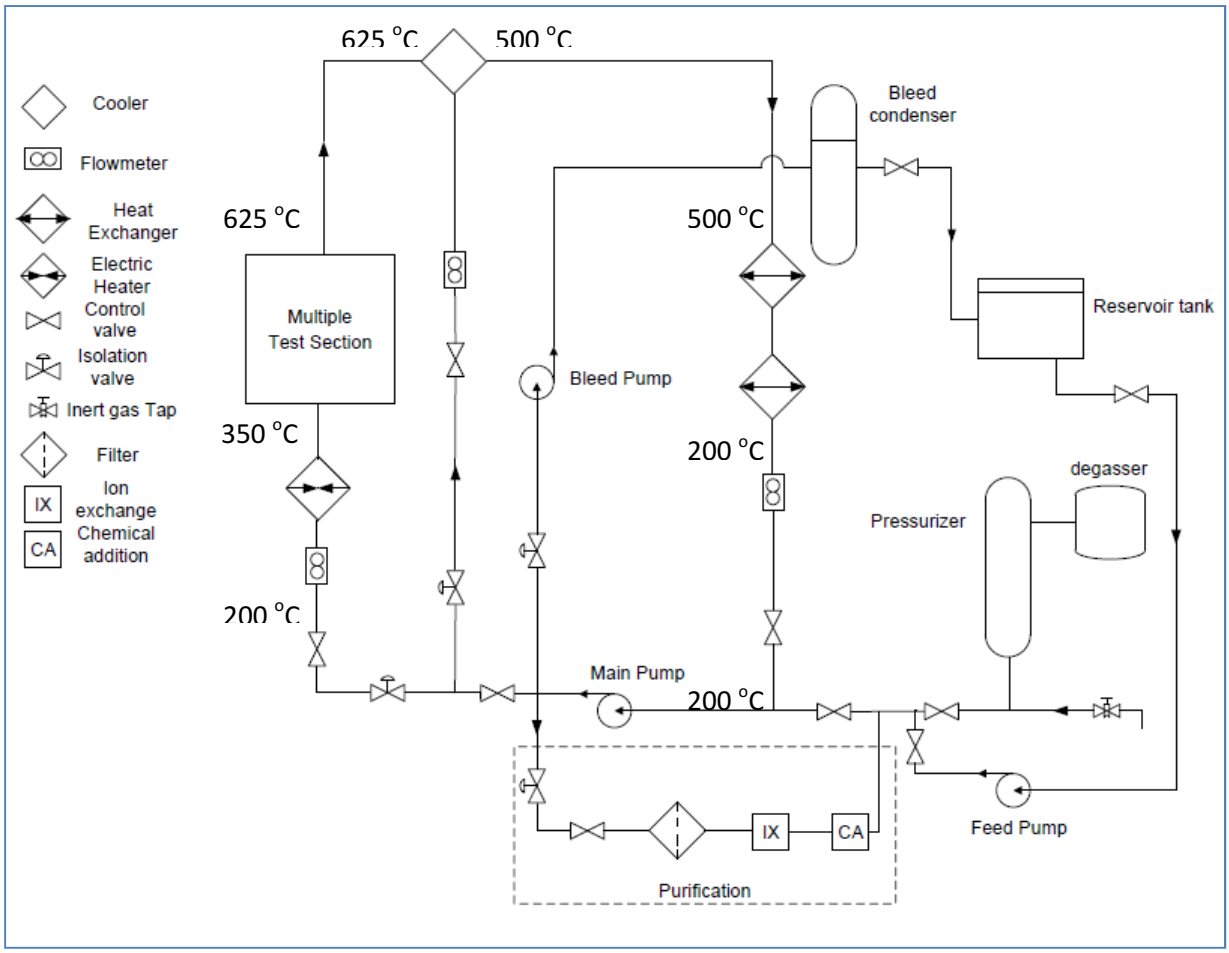

Value	Inlet (Control Volume)	Outlet (Control Volume)
Temperature (T)	**200 °C**	**350 °C**
Pressure (P)	**24.464 MPa**	**?**
Density (ρ)	**881 Kg/m^3**	**628.7 Kg/m^3**

Estimated length of pipe in heat exchanger	5 m
Steel Roughness (ϵ)	0.045 mm
Reynolds number	124500
Diameter of pipe	0.00752 m
Friction Factor (f)	0.032

Pressure drop in section

$$\frac{p_1^2-p_2^2}{2\times P_1} = f \times \frac{L}{D} \times \frac{\rho_1}{2} \times V_{ave}{}^2 \times \frac{T_{ave}}{T_1}$$

T_1 = (200+273) K = 473 K

T_{ave} = (275+273) K = 548 K

ρ_1 = 628.7 kg/m^3

f = 0.032

L = 5 m

D = 0.00752 m

P_1 = 24.464 MPa

$V_{ave} = G/\rho_{ave}$ = 1206/ **754.9** = 1.60 m/s

$$P_1^2 - P_2^2 = 2 \times P_1 \times f \times \frac{L}{D} \times \frac{\rho_1}{2} \times V_{ave}{}^2 \times \frac{T_{ave}}{T_1}$$

$$P_2^2 = P_1^2 - 2 \times P_1 \times f \times \frac{L}{D} \times \frac{\rho_1}{2} \times V_{ave}{}^2 \times \frac{T_{ave}}{T_1}$$

P_2 = 24.445 MPa

Pressure Drop in Section = 0.019 MPa

Losses – Major Loss (Friction), Minor Loss (Valve, Elbow)

Major head loss in section

$$h_{L\,major} = f\frac{\ell}{D}\frac{V_{ave}{}^2}{2g}$$

ℓ=5 m

D = 0.00752 m

V_{ave} = 1.6 m/s

Therefore $h_{L\,major}$ =2.78 m

Minor head loss in section

$$h_{L\,minor} = K_L\frac{V^2}{2g}$$

Minor head loss	Value
Number of regular 90° flanged elbows	6
$K_{L\,elbow}$	1.5
$h_{L\,elbow}$ (m)	1.17

Therefore total head loss in section = 3.95 m

APPENDIX C: MATLAB CODE FOR PRESSURE DROP AND HEAD LOSS CALCULATIONS

Tool Name: System Pressure Loss Analysis Tool (SPLAT)

```
%This program is used to calculate the pressure drop in the loop
clear
y=zeros(8,4);
n=20;

D_test_section_division=linspace(0.001,0.01,n);

Pressure_drop_in_testsection=zeros(1,n);
Overall_pressure_drop_in_loop= zeros(1,n);
Percentage_pressure_drop_in_test_section=zeros(1,n);

for k=1:n



for i=4:4  %Change range to i=1:4 for sensitivity analyses of the
diameter of the loop
%In this section, the mass flux or diameters of the loop or test
section
%can be changed for analyses
D_loop=0.05*(i/4); %Dimensions in m
D_test_section=D_test_section_division(k);
%D_test_section=0.002;

 mass_flow_rate=2.5;
 mass_flux_test_section=3000;
 mass_flux_loop=mass_flow_rate/(pi()/4*D_loop^2);


%Test Section
%Function takes input pressure_drop(T_inlet, T_outlet, P_outlet, L, D,
G)
%and returns Pinlet
%The pressure drop in the test section is split into before & after
%pseudocritical point


P_outlet_test_section=25.000e6;
P_pseudocritical=pressure_drop2(384+273, 625+273,
P_outlet_test_section, 2.8, D_test_section, mass_flux_test_section);
display(P_pseudocritical)

P_inlet_test_section=pressure_drop2(350+273, 384+273, P_pseudocritical,
1.2, D_test_section, mass_flux_test_section);
display(P_inlet_test_section)

P_drop_in_test_section=P_inlet_test_section-P_outlet_test_section;
```

```
display(P_drop_in_test_section);

%This funtion calculates the head loss in the test section
%To every function with the end "..._compressible" is used for
compressible
%fluid calculations
%If the equations for incompressible fluids need to be used, the
funtions
%without the "..._compressible" end is used
%For instance, for incompressible fluid calculations,
%"friction_loss_compressible" function is replaced with "friction_loss"
funtion and the
%appropriate (number of inputs and the values for each) inputs are
changed.
%Another example is replacing the "minor_loss_compressible" funtion
with
%the "minor_loss" funtion
friction_test_section=friction_loss_compressible(350+273, 384+273,
P_pseudocritical, 1.2, D_test_section, mass_flux_test_section);
loss_test_section=friction_test_section;

%Test Section to Cooler
P_outlet_test_section_to_cooler=pressure_drop1(625+273, 625+273,
P_outlet_test_section, 1, D_loop, mass_flux_loop);
display(P_outlet_test_section_to_cooler);
friction_test_section_to_cooler=friction_loss_compressible(625+273,
625+273, P_outlet_test_section, 1, D_loop, mass_flux_loop);
elbow_test_section_to_cooler=minor_loss_compressible(625+273, 625+273,
P_outlet_test_section, 1.5, 3, mass_flux_loop, D_loop);
loss_test_section_to_cooler=friction_test_section_to_cooler+elbow_test_
section_to_cooler;

%Cooler
P_outlet_cooler=pressure_drop1(625+273, 500+273,
P_outlet_test_section_to_cooler, 8, D_loop, mass_flux_loop);
display(P_outlet_cooler);
friction_cooler=friction_loss_compressible(625+273, 500+273,
P_outlet_test_section_to_cooler, 8, D_loop, mass_flux_loop);
elbow_cooler=minor_loss_compressible(625+273, 500+273,
P_outlet_test_section_to_cooler, 1.5, 2, mass_flux_loop, D_loop);
loss_cooler=friction_cooler+elbow_cooler;


%Cooler to heat exchanger
P_outlet_cooler_to_heat_exchanger=pressure_drop1(500+273, 500+273,
P_outlet_cooler, 2, D_loop, mass_flux_loop);
display(P_outlet_cooler_to_heat_exchanger);
friction_cooler_to_heat_exchanger=friction_loss_compressible(500+273,
500+273, P_outlet_cooler, 2, D_loop, mass_flux_loop);
elbow_cooler_to_heat_exchanger=minor_loss_compressible(500+273,
500+273, P_outlet_cooler, 1.5, 2, mass_flux_loop, D_loop);
loss_cooler_to_heat_exchanger=friction_cooler_to_heat_exchanger+elbow_c
ooler_to_heat_exchanger;
```

```
%Heat Exchanger
P_outlet_heat_exchanger=pressure_drop1(500+273, 200+273,
P_outlet_cooler_to_heat_exchanger, 12, D_loop, mass_flux_loop);
display(P_outlet_heat_exchanger);
friction_heat_exchanger=friction_loss_compressible(500+273, 200+273,
P_outlet_cooler_to_heat_exchanger, 12, D_loop, mass_flux_loop);
elbow_heat_exchanger=minor_loss_compressible(500+273, 200+273,
P_outlet_cooler_to_heat_exchanger, 1.5, 3, mass_flux_loop, D_loop);
loss_heat_exchanger=friction_heat_exchanger+elbow_heat_exchanger;


%%%%%%%%%%%%%%%%%%%%%%%%%%%%%%%%%%%%%%%%%%%%%%%%%%%%%%%%%%%%%%%%%%%%%%%
%The compressible fluid head loss fomula stops applying here
%%%%%%%%%%%%%%%%%%%%%%%%%%%%%%%%%%%%%%%%%%%%%%%%%%%%%%%%%%%%%%%%%%%%%%%


%Heat exchanger to feed pump
P_outlet_heat_exchanger_to_pump=pressure_drop1(200+273, 200+273,
P_outlet_heat_exchanger, 4, D_loop, mass_flux_loop);
display(P_outlet_heat_exchanger_to_pump);
friction_heat_exchanger_to_pump=friction_loss(200+273, 200+273,
P_outlet_heat_exchanger, 4, D_loop, mass_flux_loop);
elbow_heat_exchanger_to_pump=minor_loss_compressible(200+273, 200+273,
P_outlet_heat_exchanger, 1.5, 2, mass_flux_loop, D_loop);
valve_heat_exchanger_to_pump=minor_loss_compressible(200+273, 200+273,
P_outlet_heat_exchanger, 0.05, 1, mass_flux_loop, D_loop);
loss_heat_exchanger_to_pump=friction_heat_exchanger_to_pump+elbow_heat_
exchanger_to_pump+...
    valve_heat_exchanger_to_pump;


%Feed pump to pre-heater
P_outlet_pump_to_preheater=pressure_drop1(200+273, 200+273,
P_outlet_heat_exchanger_to_pump, 3, D_loop, mass_flux_loop);
display(P_outlet_pump_to_preheater);
friction_pump_to_preheater=friction_loss(200+273, 200+273,
P_outlet_heat_exchanger_to_pump, 3, D_loop, mass_flux_loop);
elbow_pump_to_preheater=minor_loss_compressible(200+273, 200+273,
P_outlet_heat_exchanger_to_pump, 1.5, 1, mass_flux_loop, D_loop);
valve_pump_to_preheater=minor_loss_compressible(200+273, 200+273,
P_outlet_heat_exchanger_to_pump, 0.05, 1, mass_flux_loop, D_loop);
loss_pump_to_preheater=friction_pump_to_preheater+elbow_pump_to_preheat
er+valve_pump_to_preheater;


%Pre-heater
P_outlet_preheater=pressure_drop1(200+273, 350+273,
P_outlet_pump_to_preheater, 5, D_loop, mass_flux_loop);
display(P_outlet_preheater);
friction_preheater=friction_loss_compressible(200+273, 350+273,
P_outlet_pump_to_preheater, 5, D_loop, mass_flux_loop);
loss_preheater=friction_preheater;


pressure=[P_outlet_test_section,P_outlet_test_section_to_cooler...
```

```
P_outlet_cooler,P_outlet_cooler_to_heat_exchanger,P_outlet_heat_exchang
er,P_outlet_heat_exchanger_to_pump...
    P_outlet_pump_to_preheater,P_outlet_preheater];

length=[0, 2.8, 1.2, 1, 8, 2, 12, 4, 3, 5];
location=[0, 1, 9, 11, 23, 27, 30, 35];
location2=[0, 4, 5, 13, 15, 27, 31, 34, 39];
display(pressure)

system_head_loss=[0,loss_test_section, loss_test_section_to_cooler...

loss_cooler,loss_cooler_to_heat_exchanger,loss_heat_exchanger,loss_heat
_exchanger_to_pump...
    loss_pump_to_preheater,loss_preheater];

system_head=cumsum(system_head_loss);

%specifying degree of polynomial
coeff=polyfit(location,pressure,3);
y(:,i)=1e-6*polyval(coeff,location);
%Value of the y_calculated are sourced from the Appendix C
y_calculated=[25, 24.952, 24.563, 24.492, 24.489, 24.475, 24.464,
24.445];

end

for j=1:4
Hold on
plot(location, y(:,j), 'b*-')
%axis([0 40 24.55 25.05]);
grid
xlabel('location (m)')
ylabel('pressure (MPa)')
title('Pressure drop in loop')
end
Hold off

%Percentage of pressure drop in test section as a percentage of loop.
Pressure_drop_in_testsection(k)= (P_inlet_test_section-
P_outlet_test_section);
Overall_pressure_drop_in_loop(k)=(P_inlet_test_section-
P_outlet_preheater);
Percentage_pressure_drop_in_test_section(k)=Pressure_drop_in_testsectio
n(k)/Overall_pressure_drop_in_loop(k)*100;

end

%This is finds the total head in the loop
total_head= system_head(1,9);
%This plot is to find out how the head varies along the loop
plot(location2, system_head)

%To calculate NPSH (Net positive suction head)
%NPSH=(Po-Pv/pho*g)-total_head_loss)
```

```
%Po=vapor pressure at a particular temperature
%This calculates the NPSH available which is specified by the system
%The NPSH required is specified by the pump manufacturer should be less
%than the NPSH available
NPSH=(25E6-1.621E6)/(9.81*881)-total_head;
%NPSH is adequate enough to prevent cavitation since the
%NPSH availabe is much greater than the NPSH required
```

```
%%%%%%%%%%%%%%%%%%%%%%%%%%%%%%%%%%%%%%%%%%%%%%%%%%%%%%%%%%%%%%%%%%%%%%%%%%%%
%%%%%%%%%%%%%%%%%%%%%%%%%%%%%%%%%%%%%%%%%%%%%%%%%%%%%%%%%%%%%%%%%%%%%%%%%%%%
%Minor loss compressible function
function [minor] = minor_loss_compressible(T1, T2, P2, K, N, G, D)

g=9.81; %m/s^2
rho1=refpropm('D','T',T1,'P',P2*0.001,'water');
rho2=refpropm('D','T',T2,'P',P2*0.001,'water');

rho_ave=(rho1+rho2)/2;

% V_ave=G/rho_ave;


minor=K*N*(1.253*10^-6*(G*pi()/4*D^2)^2/(D^4))/9.81;

end
%%%%%%%%%%%%%%%%%%%%%%%%%%%%%%%%%%%%%%%%%%%%%%%%%%%%%%%%%%%%%%%%%%%%%%%%%%%%
%%%%%%%%%%%%%%%%%%%%%%%%%%%%%%%%%%%%%%%%%%%%%%%%%%%%%%%%%%%%%%%%%%%%%%%%%%%%
```

```
%%%%%%%%%%%%%%%%%%%%%%%%%%%%%%%%%%%%%%%%%%%%%%%%%%%%%%%%%%%%%%%%%%%%%%%%%%%%
%%%%%%%%%%%%%%%%%%%%%%%%%%%%%%%%%%%%%%%%%%%%%%%%%%%%%%%%%%%%%%%%%%%%%%%%%%%%
%Friction loss compressible function
function [h_friction] = friction_loss_compressible(T1, T2, P2, L, D, G)

g=9.81; %m/s^2
rho1=refpropm('D','T',T1,'P',P2*0.001,'water');
rho2=refpropm('D','T',T2,'P',P2*0.001,'water');

f=0.032;
rho_ave=(rho1+rho2)/2;

% V_ave=G/rho_ave;
h_friction=f*(L/D)*(1.253*10^-6*(G*pi()/4*D^2)^2/(D^4))/9.81;

end
%%%%%%%%%%%%%%%%%%%%%%%%%%%%%%%%%%%%%%%%%%%%%%%%%%%%%%%%%%%%%%%%%%%%%%%%%%%%
%%%%%%%%%%%%%%%%%%%%%%%%%%%%%%%%%%%%%%%%%%%%%%%%%%%%%%%%%%%%%%%%%%%%%%%%%%%%
```

```
%%%%%%%%%%%%%%%%%%%%%%%%%%%%%%%%%%%%%%%%%%%%%%%%%%%%%%%%%%%%%%%%%%%%%%%%%%%%
%%%%%%%%%%%%%%%%%%%%%%%%%%%%%%%%%%%%%%%%%%%%%%%%%%%%%%%%%%%%%%%%%%%%%%%%%%%%
%Minor loss function
function [minor] = minor_loss(T1, T2, P2, K, N, G)

g=9.81; %m/s^2
rho1=refpropm('D','T',T1,'P',P2*0.001,'water');
rho2=refpropm('D','T',T2,'P',P2*0.001,'water');

rho_ave=(rho1+rho2)/2;

V_ave=G/rho_ave;
minor=K*N*(V_ave^2/(2*g));

end
%%%%%%%%%%%%%%%%%%%%%%%%%%%%%%%%%%%%%%%%%%%%%%%%%%%%%%%%%%%%%%%%%%%%%%%%%%%%
%%%%%%%%%%%%%%%%%%%%%%%%%%%%%%%%%%%%%%%%%%%%%%%%%%%%%%%%%%%%%%%%%%%%%%%%%%%%



%%%%%%%%%%%%%%%%%%%%%%%%%%%%%%%%%%%%%%%%%%%%%%%%%%%%%%%%%%%%%%%%%%%%%%%%%%%%
%%%%%%%%%%%%%%%%%%%%%%%%%%%%%%%%%%%%%%%%%%%%%%%%%%%%%%%%%%%%%%%%%%%%%%%%%%%%
%Friction loss function
function [h_friction] = friction_loss(T1, T2, P2, L, D, G)

g=9.81; %m/s^2
rho1=refpropm('D','T',T1,'P',P2*0.001,'water');
rho2=refpropm('D','T',T2,'P',P2*0.001,'water');

f=0.032;
rho_ave=(rho1+rho2)/2;

V_ave=G/rho_ave;
h_friction=f*(L/D)*(V_ave^2/(2*g));

end
%%%%%%%%%%%%%%%%%%%%%%%%%%%%%%%%%%%%%%%%%%%%%%%%%%%%%%%%%%%%%%%%%%%%%%%%%%%%
%%%%%%%%%%%%%%%%%%%%%%%%%%%%%%%%%%%%%%%%%%%%%%%%%%%%%%%%%%%%%%%%%%%%%%%%%%%%
```

APPENDIX D: MATLAB CODE FOR HEAT EXCHANGER

Tool Name: Heat Exchanger Analysis Tool (HEAT)

```
%Last changed February 28, 2012
%This is a program to determine the size of the heat exchanger required
for
%cooling the superheated fluid for a shell and tube type.

clear all;

%constants are listed here

tube_fluid='water';
shell_fluid='water';
massflow_shell=5; %kg/s
massflow_tube=0.35;  %kg/s (0.35 is the mass flow rate required for the
loop

D_inner=0.05; % diameter in m
D_outer=0.06;  % diameter in m
massflux_tube=massflow_tube/(pi()*(D_inner^2)/4);

no_of_tubes=24;
k=16; %Thermal conductivity of stainless steel tube in W/mK
%vel_tube=1.926;  %m/s

%Uncomment the part below to calculate the lenght for each tube in the
heat
%exchanger
%%%%%%%%%%%%%%%%%%%%%%%%%%%%%%%%%%%%%%%%%%%%%%%%%%%%%%%%%%%%%%%%%%%%%%%
%%%%
massflow_tube=massflow_tube/no_of_tubes;%For each tube in the heat
exchanger
D_inner=0.0085; %For each tube in the heat exchanger
D_outer=0.01; %For each tube in the heat exchanger
%%%%%%%%%%%%%%%%%%%%%%%%%%%%%%%%%%%%%%%%%%%%%%%%%%%%%%%%%%%%%%%%%%%%%%%



%The value of the energy lost to the shell side of the HX is determined
%first
%The boundary conditions of the heat exchanger are listed below

%Tube contains hot fluid
temp_hot_in=625+273.15; %temp in kelvin
temp_hot_out=530.5+273.15; %temp in kelvin
p_hot_in=24.592*10^3; %pressure in kPa
p_hot_out=24.563*10^3; %pressure in kPa

%Shell contains cold fluid
temp_cold_in=25+273.15; %temp in kelvin
temp_cold_out=50+273.15;%temp in kelvin
p_cold_in=1*10^3; %pressure in kPa
p_cold_out=1*10^3; %pressure in kPa
```

```
n=1000; %division along the tube of the HX
temp_hot=linspace(temp_hot_in,temp_hot_out,n);
p_hot=linspace(p_hot_in,p_hot_out,n);
enthalpy_hot=zeros(size(n)); %initialization
enthalpy_hot(1)=refpropm('H','T',temp_hot(1),'P',p_hot(1),tube_fluid);
q=zeros(size(n-1));

for i=2:n

enthalpy_hot(i)=refpropm('H','T',temp_hot(i),'P',p_hot(i),tube_fluid);
%units of specific heat in J/(kg K)
   q(i)=enthalpy_hot(i)-enthalpy_hot(i-1);
end

q_total=massflow_tube*sum(q)*no_of_tubes  % this is the total energy
that needs to extracted by heat exchanger

%The next step is to calculate the total heat tranfer coefficients

%This is the heat transfer coefficient of the hot side
m=1000;
temp_hot=linspace(temp_hot_in,temp_hot_out,m);
temp_wall_hot=temp_hot-50;  %Assumption here is wall temp is always 50
celsuis lower than bulk temp for
%simplicity
p_hot=linspace(p_hot_in,p_hot_out,m);

Cp_hot_2=zeros(size(m));
Cp_wall_hot_2=zeros(size(m));
k_hot=zeros(size(m));
k_wall_hot=zeros(size(m));
rho_bulk_hot=zeros(size(m));
rho_wall_hot=zeros(size(m));
dyn_vis_bulk_hot=zeros(size(m));
dyn_vis_wall_hot=zeros(size(m));
Pr_bulk_hot=zeros(size(m));
Pr_wall_hot=zeros(size(m));
Pr_film_hot=zeros(size(m));
Re_bulk_hot=zeros(size(m));
Nu_hot=zeros(size(m));
h_hot=zeros(size(m));

for j=1:m

Cp_hot_2(j)=refpropm('C','T',temp_hot(j),'P',p_hot(j),tube_fluid);

k_hot(j)=refpropm('L','T',temp_hot(j),'P',p_hot(j),tube_fluid);
k_wall_hot(j)=refpropm('L','T',temp_wall_hot(j),'P',p_hot(j),tube_fluid
);
rho_bulk_hot(j)=refpropm('D','T',temp_hot(j),'P',p_hot(j),tube_fluid);
rho_wall_hot(j)=refpropm('D','T',temp_wall_hot(j),'P',p_hot(j),tube_flu
id);
dyn_vis_bulk_hot(j)=refpropm('V','T',temp_hot(j),'P',p_hot(j),tube_flui
d);
```

```
dyn_vis_wall_hot(j)=refpropm('V','T',temp_wall_hot(j),'P',p_hot(j),tube
_fluid);

Pr_bulk_hot(j)=dyn_vis_bulk_hot(j).*Cp_hot_2(j)./k_hot(j);  %dynamic
viscosity of bulk
Pr_wall_hot(j)=dyn_vis_wall_hot(j).*Cp_hot_2(j)./k_wall_hot(j);
%dynamic viscosity at wall conditions
Pr_film_hot(j)=mean([Pr_bulk_hot(j),Pr_wall_hot(j)]);

Re_bulk_hot(j)=massflux_tube*D_inner/dyn_vis_bulk_hot(j);

Nu_hot(j)=0.0061*Re_bulk_hot(j)^0.904*Pr_film_hot(j)^0.684*(rho_wall_ho
t(j)/rho_bulk_hot(j))^0.564; %Nusselt number of fluid in tube using
Mokry's correlation
h_hot(j)= Nu_hot(j)*k_hot(j)/D_inner;    %heat transfer coefficient

end



%display(mean(Nu_hot));
% display(mean(h_hot));

%This is the heat transfer coefficent of the cold side
temp_cold=linspace(temp_cold_in,temp_cold_out,m);
temp_wall_cold=temp_hot;  %Assumption here is wall temp is equal to
temp wall hot
p_cold=linspace(p_cold_in,p_cold_out,m);

Cp_cold_2=zeros(size(m));
Cp_wall_cold_2=zeros(size(m));
k_cold=zeros(size(m));
k_wall_cold=zeros(size(m));
rho_bulk_cold=zeros(size(m));
rho_wall_cold=zeros(size(m));
dyn_vis_bulk_cold=zeros(size(m));
dyn_vis_wall_cold=zeros(size(m));
Pr_bulk_cold=zeros(size(m));
Pr_wall_cold=zeros(size(m));
Pr_film_cold=zeros(size(m));
Re_bulk_cold=zeros(size(m));
Nu_cold=zeros(size(m));
h_cold=zeros(size(m));

for k=1:m

Cp_cold_2(k)=refpropm('C','T',temp_cold(k),'P',p_cold(k),shell_fluid);

k_cold(k)=refpropm('L','T',temp_cold(k),'P',p_cold(k),shell_fluid);
k_wall_cold(k)=refpropm('L','T',temp_wall_cold(k),'P',p_cold(k),shell_f
luid);
rho_bulk_cold(k)=refpropm('D','T',temp_cold(k),'P',p_cold(k),shell_flui
d);
```

```
rho_wall_cold(k)=refpropm('D','T',temp_wall_cold(k),'P',p_cold(k),shell
_fluid);
dyn_vis_bulk_cold(k)=refpropm('V','T',temp_cold(k),'P',p_cold(k),shell_
fluid);
dyn_vis_wall_cold(k)=refpropm('V','T',temp_wall_cold(k),'P',p_cold(k),s
hell_fluid);

Pr_bulk_cold(k)=dyn_vis_bulk_cold(k).*Cp_cold_2(k)./k_cold(k);
%dynamic viscosity of bulk
Pr_wall_cold(k)=dyn_vis_wall_cold(k).*Cp_cold_2(k)./k_wall_cold(k);
%dynamic viscosity at wall conditions
Pr_film_cold(k)=mean([Pr_bulk_cold(k),Pr_wall_cold(k)]);

Re_bulk_cold(k)=4*massflow_shell/(pi()*D_outer*dyn_vis_bulk_cold(k));

Nu_cold(k)=0.0061*Re_bulk_cold(k)^0.904*Pr_film_cold(k)^0.684*(rho_wall
_cold(k)/rho_bulk_cold(k))^0.564; %Nusselt number of fluid in tube
using Mokry's correlation
h_cold(k)= Nu_cold(k)*k_cold(k)/D_inner;    %heat transfer coefficient

end


%display(mean(Nu_cold));
% display(mean(h_cold));

U=1/(1/mean(h_hot)+
D_outer/2*log(D_outer/D_inner)/k+(D_outer/D_inner)*(1/mean(h_cold))); %
Total heat transfer coefficient

deltaT1=temp_hot_in-temp_cold_out; %for counter flow heat exchangers
deltaT2=temp_hot_out-temp_cold_in;
deltaT_lm=(deltaT2-deltaT1)/log(deltaT2/deltaT1);

Cmax=massflow_shell*mean(Cp_cold_2)  %Cmin for NTU method where Cmax=0
units in W/K
Cmin=massflow_tube*mean(Cp_hot_2)
q_max=Cmin*(temp_cold_in-temp_hot_in);  % in watts

espilon=q_total/q_max; %epsilon represents the effectiveness in the NTU
method

NTU=0.1;   %This value was obtained from page 691 3rd Edition of
incorpera knowing what epsilon is

L=abs(NTU*Cmin/(U*2*pi()*D_outer)); %Lenght of heat exchanger in meters
using NTU =UA/Cmin
L2=abs((q_total/no_of_tubes)/(deltaT_lm*U*(2*pi()*D_outer)));


display('Using the NTU method, the length of the tube in the heat
exchanger is');
display(L)
```

```
display('Using the LMTD method, the length of the tube in the heat
exchanger is');
display(L2)
```

APPENDIX E: NUSSELT NUMBER CORRELATIONS FOR SUPERCRITICAL FLUIDS

Authors	**Correlations**
Gupta et al. 2010 [**90**]	$\mathrm{Nu_w} = 0.004\,\mathrm{Re_w^{0.923}}\,\overline{\mathrm{Pr}}_\mathrm{b}^{0.773}\left(\frac{\mu_w}{\mu_b}\right)^{0.366}\left(\frac{\rho_w}{\rho_i}\right)^{0.186}$
Mokry et al. 2009 [**91**]	$\mathrm{Nu_x} = 0.0061\,\mathrm{Re_x^{0.904}}\,\overline{\mathrm{Pr}}_\mathrm{x}^{0.684}\left(\frac{\rho_w}{\rho_b}\right)^{0.564}$
Jackson et al. 2002 [**120**]	$\mathrm{Nu_w} = 0.0183\,\mathrm{Re_b^{0.82}}\,\mathrm{Pr_b^{0.5}}\left(\frac{\rho_w}{\rho_b}\right)^{0.3}\left(\frac{\overline{\mathrm{Cp}}_\mathrm{b}}{\mathrm{Cp_b}}\right)^{n}$
Gorban et L. 1990 [**76**]	$\mathrm{Nu_b} = 0.0094\,\mathrm{Re_b^{0.86}}\,\mathrm{Pr_b^{-0.15}}$
Dyadyakin et al. 1977 [**85**]	$\mathrm{Nu_w} = 0.0021\,\mathrm{Re_b^{0.8}}\,\overline{\mathrm{Pr}}_\mathrm{b}^{0.7}\left(\frac{\rho_w}{\rho_b}\right)^{0.45}\left(\frac{\mu_b}{\mu_i}\right)^{0.2}\left(\frac{\rho_b}{\rho_i}\right)^{0.1}$
Swenson et al. 1965 [**18**]	$\mathrm{Nu_w} = 0.00459\,\mathrm{Re_w^{0.923}}\,\mathrm{Pr_w^{0.613}}\left(\frac{\rho_w}{\rho_b}\right)^{0.231}$
Bishop et al. 1964 [**121**]	$\mathrm{Nu_x} = 0.0069\,\mathrm{Re_x^{0.9}}\,\overline{\mathrm{Pr}}_\mathrm{x}^{0.66}\left(\frac{\rho_w}{\rho_b}\right)^{0.43}$
Value of n is calculated as:	$n = 4$; when $1.2 \times T_{pc} < T_b < T_w$ and $T_b < T_w < T_{pc}$ $n = 0.4 + 0.2\left(\frac{T_w}{T_{pc}} - 1\right)$; when $T_b < T_{pc} < T_w$ $n = 0.4 + 0.2\left(\frac{T_w}{T_{pc}} - 1\right)\left[1 - 5\left(\frac{T_b}{T_{pc}} - 1\right)\right]$; when $T_{pc} < T_b < 1.2 \times T_{pc}$ and $T_b < T_w$

APPENDIX F: CORROSION CHARACTERISTICS OF VARIOUS METALS WITH DIFFERENT FLUIDS

This table shows different metals and their compatibility with different fluids [**122**]. The table is intended to give only a general indication of how various metals will react when in contact with certain fluids. This is not absolute since corrosion rates depend on the concentration of fluid, temperature, and pressure. This table can only be used as a guide. A = normally suitable; B = minor to moderate effect, proceed with caution; C = unsatisfactory.

Fluid	SS304	SS316	Hastelloy C276	Hastelloy B2	Monel 400
Acetic Acid, Air Free	C	A	A	A	A
Alcohols	A	A	A	A	A
Ammonium Chloride	C	B	A	A	B
Carbon Dioxide, Dry	A	A	A	A	A
Carbon Dioxide, Wet	A	A	A	A	A
Freon, Dry	A	A	A	A	A
Freon, Wet	B	A	A	A	A
Hydrochloric Acid (Aerated)	C	C	B	A	C
Hydrochloric Acid (Air Free)	C	C	B	A	C
Sodium Hydroxide	B	A	A	A	A
Water (Sea)	C	B	A	A	A
Water (Distilled)	A	A	A	A	A

APPENDIX G: CANDU PRESSURE CONTROL

CANDU pressurizer

In CANDU reactors, it is required that pressure be controlled at all power levels. Pressure control can be done by using a pressurizer. A pressurizer is a large vessel which is controlled at saturated conditions by heaters to provide a pressure source for the circuit.

During warm-up of the reactor, inventory change of heavy water will occur as the unit is manoeuvred between 0-100%. Typically, a heat transfer system (HTS) will swell as much as 60 m^3 on warmup with an additional swell of 10-20 m^3 as power is raised from 0 to 100% full power. The majority of the inventory change occurs during warm-up of the unit to about 250 ^oC (approximately three times the change which occurs between 0-100% full-power).

These conditions consequently force two methods of pressure control to be used on most CANDU reactors, depending on the power level. These two pressure control modes are known as wide range (solid mode) and narrow range (normal mode).

Wide range (solid mode) control

The solid mode control system is used for warm up and cool down operations. The term ‘solid’ implies that no compressible vapour exists within the system to cushion pressure transients which means the system is non-boiling and the pressurizer is isolated (in stations using pressurizers). In this mode, pressure control is done by feed and bleed action by inventory addition and removal.

When the heat transfer system pressure is at its setpoint, the feed and bleed action is not required. At pressures higher than the setpoint, the bleed action

removes inventory from the HTS and lowers the pressure. The feed action increases pressure if the pressure falls below the setpoint.

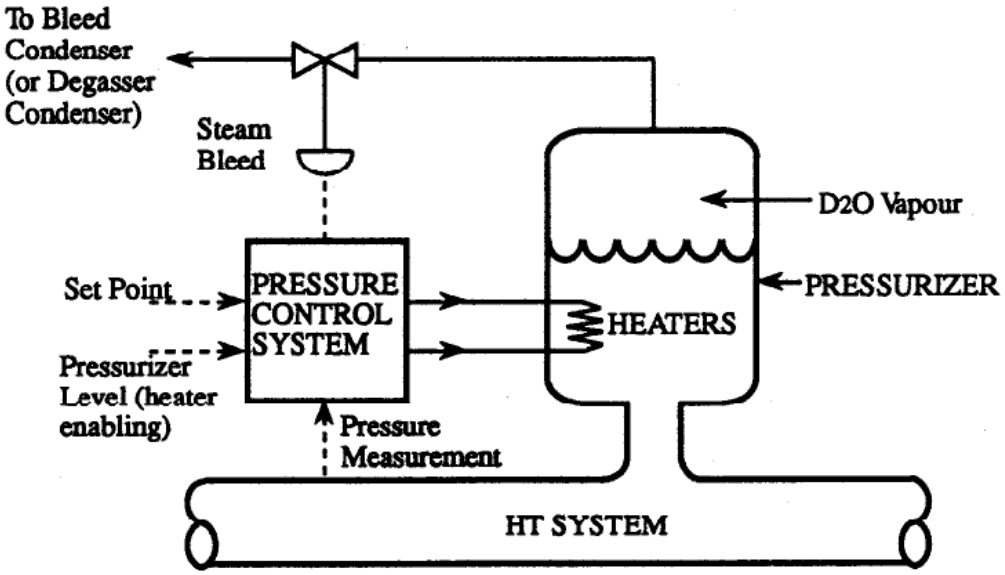

Schematic of feed and bleed system control

Figure 5.14 shows the feed and bleed action in a CANDU. The bleed valve is at near-fully-open conditions during warm-up to remove the swelling heavy water from the HTS. When cooling the system, the feed valve is open fully to feed the system to make up for the D_2O contraction.

During solid mode operation, the pressurizer is isolated from the HTS by an isolation valve. After the solid mode has been reached in the system, saturation conditions are established in the pressurizer (9 MPa, 304 ^{o}C for CANDU). The electric heaters and steam bleed valves are used to achieve this state. When pressure is too high, the steam bleed valves open and the heating elements are

switched off. The steam valves close and heaters are switched on when the pressure is too low.

Narrow range (normal mode) control

In this mode, the pressurizer is no longer isolated from the HTS. Pressure control under this condition is performed solely by the pressurizer with the help of the heaters and the steam bleed valves. The feed and bleed system is used only for purification and inventory control purposes.

The working fluid expands and excess flows into the pressurizer during power increase. In case of large swelling, the feed and bleed system is used to ensure that the pressurizer never becomes full of liquid (a condition referred to as “solid”) in order not to lose control of the pressure in the HTS.

In normal mode, the pressurizer is used to control the HTS pressure. This is achieved by the heater and steam bleed valve. The pressure in the pressurizer is controlled by the heater and the steam bleed valve. The fluid in the pressurizer is kept at saturation condition and as the heater is turned on, the saturation temperature increases, hence increasing the saturation pressure. If the pressure exceeds the setpoint, the heater is switched off and steam is discharged from the pressurizer’s vapour space via the steam bleed valves to a degasser condenser (bleed condenser) to reduce the pressure. Similarly, a decrease in the HTS pressure will require the heaters to be switched on to increase the system pressure.

APPENDIX H: FLOWMETER TYPES

This section discusses flowmeter types that were considered for the SPETA design. Mass flowmeters are the most suitable for supercritical conditions because they measure mass flow rate which does not change with density at supercritical condition.

Five flowmeter types that can be used to measure flow include differential pressure, positive displacement, velocity, mass, and open channel flowmeters. Differential pressure types include orifice plate, venturi tube, flow nozzle, flow tube, pitot tube, elbow tap, target, and rotameter (variable area). Positive displacement flowmeters include reciprocating piston, oval gear, rotary vane. The various velocity flowmeters are the turbine, electromagnetic, ultrasonic Doppler, ultrasonic transit-time, and momentum exchange flowmeters. Coriolis and thermal flowmeters are the two types of mass flowmeters. Open channel flowmeters include weir and flume meters.

Positive displacement flowmeters operate by separating liquids accurately into batches and measuring flow in increments. They are more suitable for flow measurements of viscous fluids or where a simple mechanical meter is needed.

Differential pressure flowmeters are by far the most common types currently being used with over 50 percent of all liquid flow measurement applications using this type of unit. The flow is measured with the correlation that the pressure drop across the meter is proportional to the square of the flow rate. Orifice plate meters are the most used liquid flowmeters to date. An orifice meter is basically a device that constricts liquid to produce a pressure difference. The pressure difference is measured by taps on either side of the plate. The advantage of the orifice meters is that there are no moving parts and their cost does not increase significantly with pipe size since they can be adapted to the application after installation. They are usually installed in the pipe between two flanges. Rotameters or variable-area meters are also differential pressure devices where a float rest freely at the bottom of a tube and the level of the float is proportional

to the liquid flow rate. Another flowmeter used to measure liquid flow rate are velocity meters.

Velocity meters operate linearly with respect to the volume flow rate. They are generally used to measure liquid flow. Turbine meters, when properly installed, have good accuracy, particularly for low viscous liquids. However, due to the gas-like nature of the supercritical fluid in the loop, mass flowmeters are preferred for measuring mass flow rate at supercritical conditions although turbine meters are more accurate for liquid flow rate measurements.

Mass flowmeters are more accurate for mass related processes like heat transfer. There are various designs of mass flowmeters, but the most used one for fluid flow applications is the Coriolis meter. Coriolis meter measures the mass flow directly using the Coriolis force, avoiding volumetric to mass flow rate conversions like most flowmeters. Since mass is always conserved the meter is particularly suitable when the fluid viscosity varies with velocity at a given temperature and pressure as in the case of supercritical fluids.

APPENDIX I: BASCO TYPE-500 HEAT EXCHANGER

This is the reference heat exchanger design that was used design the heat exchanger for the SPETA. The Basco type-500 heat exchanger design is a shell and tube heat exchanger manufactured by API Heat Transfer [**107**]. They are available in straight or U-tube configurations and are typically made of SS-304. This heat exchanger type contains a number of tubes in the shell which depends on the size and the power rating of the heat exchanger. Baffles are heat transfer enhancers which are located in the shell around the tubes. The heat exchangers have brackets for mounting based on application. Typical Basco-500 heat exchangers have external diameters within dimensions ranging from 7.6-30.5 cm (3-12") and are 35.6-304.8 cm (14-120") long.

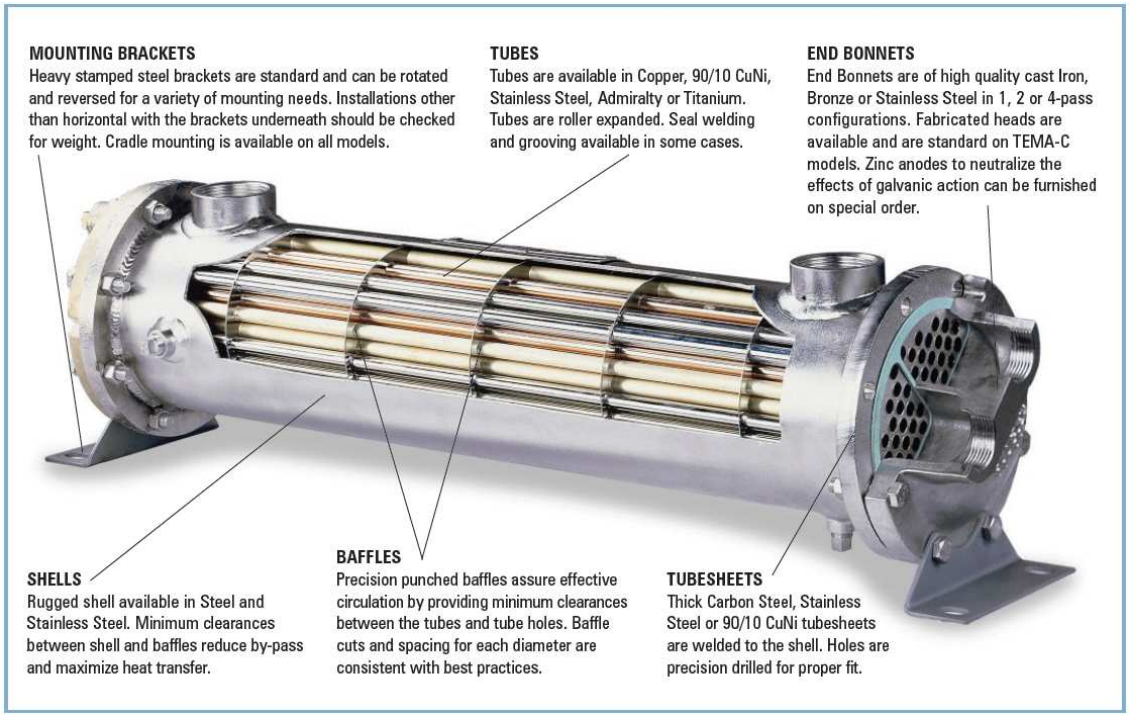

Basco Type-500 Shell and Tube Heat Exchanger [**107**]

APPENDIX J: HEAT EXCHANGER DESIGNED BY BRAMPTON PLATE

This section shows the design of a suitable heat exchanger for SPETA designed by Brampton Plate and Structural Steel Rolling Inc [**123**], a local heat transfer vendor. This section shows a heat exchanger that was independently designed by Brampton Plate using the SPETA boundary conditions.

Heat Exchanger Specification Sheet

1	Company: Research UOIT											
2	Location: OSHAWA											
3	Service of Unit: Water / Water				Our Reference:							
4	Item No.: HX-1				Your Reference:							
5	Date: March 18 - 2012			Rev No.: 0	Job No.:							
6	Size 6--48		in	Type BEM	Hor	Connected in	1 parallel	1 series				
7	Surf/unit(eff.)	24.5	ft²	Shells/unit 1			Surf/shell (eff.)	24.5	ft²			
8	**PERFORMANCE OF ONE UNIT**											
9	Fluid allocation			Shell Side			Tube Side					
10	Fluid name			Water			Water					
11	Fluid quantity, Total		lb/h	45478			2689					
12	Vapor (In/Out)		lb/h	0	0		0	0				
13	Liquid		lb/h	45478	45478		2689	2689				
14	Noncondensable		lb/h	0	0		0	0				
15												
16	Temperature (In/Out)		°F	77	122		1157	572				
17	Dew / Bubble point		°F									
18	Density Vapor/Liquid		lb/ft³	62.32	61.84		33.084	44.692				
19	Viscosity		cp	0.8974	0.5512		0.0389	0.0952				
20	Molecular wt, Vap											
21	Molecular wt, NC											
22	Specific heat		BTU/(lb F)	1.0012	0.9998		1.3164	1.1682				
23	Thermal conductivity		BTU/(ft h F)	0.347	0.365		0.245	0.3				
24	Latent heat		BTU/lb									
25	Pressure (abs)		psi	145	144.55		3626	3625.72				
26	Velocity		ft/s	3.29			0.56					
27	Pressure drop, allow./calc.		psi	7.25	0.45		37.71	0.28				
28	Fouling resist. (min)		ft² h F/BTU	0.0005			0.001	0.0014 Ao based				
29	Heat exchanged 2047285		BTU/h			MTD corrected		735.55	°F			
30	Transfer rate, Service 113.52			Dirty 126.02		Clean 164.37						BTU/(h ft² F)
31	**CONSTRUCTION OF ONE SHELL**							**Sketch**				
32				Shell Side		Tube Side						
33	Design/vac/test pressure:g		psi	160/ /		3628/ /						
34	Design temperature		°F	190		1220						
35	Number passes per shell			1		1						
36	Corrosion allowance		in	0		0						
37	Connections In		in	1 3/ -		1 1.25/ -						
38	Size/rating Out			1 3/ -		1 1/ -						
39	Nominal Intermediate			/ -		/ -						
40	Tube No. 54	OD 0.5		Tks-Avg 0.065	in	Length 4	ft	Pitch 0.625	in			
41	Tube type Plain			#/in Material SS 304			Tube pattern 30					
42	Shell SS 304	ID 6.407	OD 6.625	in	Shell cover	-						
43	Channel or bonnet SS 304				Channel cover	-						
44	Tubesheet-stationary SS 304		-		Tubesheet-floating	-						
45	Floating head cover -				Impingement protection None							
46	Baffle-crossing SS 304	Type Single segmental		Cut(%d) 41.55	H	Spacing: c/c 12.75	in					
47	Baffle-long -		Seal type			Inlet 14.4375	in					
48	Supports-tube	U-bend		Type								
49	Bypass seal		Tube-tubesheet joint	Exp.								
50	Expansion joint -		Type None									
51	RhoV2-Inlet nozzle 972		Bundle entrance 77		Bundle exit 77		lb/(ft s²)					
52	Gaskets - Shell side -		Tube Side		Flat Metal Jacket Fibe							
53	Floating head -											
54	Code requirements	ASME Code Sec VIII Div 1			TEMA class R - refinery service							
55	Weight/Shell 2191.5		Filled with water 2138.6		Bundle 905.8		lb					
56	Remarks											
57												
58												

Heat Exchanger Thermal Design **Shell&Tube V7.3** **Page 3**

File: UOIT Research.EDR Date: 24/03/2012 Time: 3:15:10 AM
Company: Research UOIT
Location: OSHAWA
Service of Unit: Water / Water Our Reference:
Item No.: HX-1 Your Reference:
Date: March 18 - 2012 Rev No.: 0 Job No.:

Basic Geometry

Unit Configuration

Exchanger Type		BEM	Tube number (calcs.)		54
Position		Hor	Tube length actual	ft	4
Arrangement		1 par 1 ser	Tube passes		1
Baffle type		Single segmental	Tube type		Plain
Baffle number			Tube O.D.	in	0.5
Spacing (center-center)	in	12.75	Tube pitch	in	0.625
Spacing at inlet	in	14.4375	Tube pattern		30

		Shell	Kettle	Front head	Rear head
Outside diameter	in	6.625		15.657	15.657
Inside Diameter	in	6.407		6.407	6.407

		Shell Side		Tube Side	
		Inlet	Outlet	Inlet	Outlet
Nozzle type					
Number of nozzles		1	1	1	1
Actual outside diameter	in	3.5	3.5	1.66	1.315
Inside diameter	in	3.068	3.068	0.896	0.599
Height under nozzle	in	1.3297	1.3297		
Dome inside diameter	in				
Vapor belt inside diameter	in				
Vapor belt inside width	in				
Vapor belt slot area	in²				
Impingement protection		No impingement	No impingement	No impingement	
Distance to tubesheet	in	40.25	7.5		

File: UOIT Research.EDR Date: 24/03/2012 Time: 3:15:11 AM
Company: Research UOIT
Location: OSHAWA
Service of Unit: Water / Water Our Reference:
Item No.: HX-1 Your Reference:
Date: March 18 - 2012 Rev No.: 0 Job No.:

Tubes

Tubes					
Type		Plain	Total number		54
Outside diameter	in	0.5	Number of tubes plugged		0
Inside diameter	in	0.37	Tube length actual	ft	4
Wall thickness	in	0.065	Tube length effective	ft	3.4688
Area ratio Ao/Ai		1.35	Tubesheet thickness	in	3.0625
Pitch	in	0.625	Material		SS 304
Pattern		30	Thermal conductivity	BTU/(ft h F)	12.522
External enhancement			Internal enhancement		
Low circumferential fins			**Low longitudinal fins**		
Fin density	#/in		Fin number		0
Fin height	in		Fin thickness	in	
Fin thickness	in		Fin height	in	
Tube root diameter	in		Fin spacing	in	
Tube wall thickness under fin	in		Cut and twist length	in	
Tube inside diameter under fins	in				

File: UOIT Research.EDR Date: 24/03/2012 Time: 3:15:11 AM
Company: Research UOIT
Location: OSHAWA
Service of Unit: Water / Water Our Reference:
Item No.: HX-1 Your Reference:
Date: March 18 - 2012 Rev No.: 0 Job No.:

Baffles

Baffles					
Type		Single segmental	Baffle cut: inner / outer / interm		
Tubes in window		Yes	Actual (% diameter)	/ 41.55 /	
Number		2	Nominal (% diameter)	/ 40 /	
Spacing (center-center)	in	12.75	Actual (% area)	/ 39.3 /	
Spacing at inlet	in	14.4375	Cut orientation		H
Spacing at outlet	in	14.4375	Thickness	in	0.1875
Spacing at central in/out for G,H,I,J shells	in		Tube rows in baffle overlap		2
Spacing at center of H shell	in		Tube rows in baffle window		2.5
End length at front head	in	17.625	Baffle hole - tube od diam clearance	in	0.0313
End length at rear head	in	17.625	Shell id - baffle od diam clearance	in	0.125

VariableBaffles

Baffle spacing	in
Baffle cut percent, outer	
Baffle cut percent, inner	
Number of baffle spaces	
Baffle region length	in
Baffle cut area percent, outer	
Baffle cut area percent, inner	

File: UOIT Research.EDR Date: 24/03/2012 Time: 3:15:11 AM
Company: Research UOIT
Location: OSHAWA
Service of Unit: Water / Water Our Reference:
Item No.: HX-1 Your Reference:
Date: March 18 - 2012 Rev No.: 0 Job No.:

Supports Misc. Baffles

Supports-tube		Longitudinal Baffle	
Supports in endspace at front head	0	Thickness	in
Supports in endspace at rear head	0	Window length at front head	in
Supports between baffles	0	Window length at center	in
Support blanking baffle	No	Window length at rear head	in
Supports at U-bend	0		
Supports at each G,H,J shell inlet and I shell outlet	0		
Supports at center of H shell	0		
Supports for K, X shells	0		
Special support at inlet nozzle	No		

Bundle

Bundle					
Shell ID to center 1st tube row	in		Tube passes		1
From top		1.3297	Tube pass layout		Ribbon (single band)
From bottom		1.3297	Tube pass orientation		Standard (horizontal)
From right		0.4535	U-bend orientation		undefined
From Left		0.4535	Horizontal pass lane width	in	
Impingement protection		None	Vertical pass lane width	in	
Impingement distance	in		Interpass tube alignment		No
Impingement plate diameter	in		Deviation in tubes/pass		0
Impingement plate width	in		Outer tube limit	in	5.907
Impingement plate length	in		Shell id - bundle otl diam clearance	in	0.5
Impingement plate thickness	in		Tie rod number		4
Gross surface area per shell	ft²	28.3	Tie rod diameter	in	0.376
Effective surface area per shell	ft²	24.5	Sealing strips (pairs)		1
Bare tube area per shell	ft²	24.5	Tube to tubesheet joint		Exp.
Finned area per shell	ft²	0	Tube projection from front tsht	in	0.125
U-bend area per shell	ft²	0	Tube projection from rear tsht	in	0.125

File: UOIT Research.EDR Date: 24/03/2012 Time: 3:15:11 AM
Company: Research UOIT
Location: OSHAWA
Service of Unit: Water / Water Our Reference:
Item No.: HX-1 Your Reference:
Date: March 18 - 2012 Rev No.: 0 Job No.:

Mechanical Details

Internal enhancements		
Tube insert type		None
Twisted tape 360 deg twist pitch	in	
Twisted tape thickness	in	
hiTRAN part number		

Cost/Weight

Weights	lb	Cost data	Dollar(US)
Shell	188.7	Labor cost	43549
Front head	576.6	Tube material cost	290
Rear head	520.4	Material cost (except tubes)	9784
Shell cover			
Bundle	905.8		
Total weight - empty	2191.5	Total cost (1 shell)	53623
Total weight - filled with water	2138.6	Total cost (all shells)	53623

File: UOIT Research.EDR Date: 24/03/2012 Time: 3:15:11 AM
Company: Research UOIT
Location: OSHAWA
Service of Unit: Water / Water Our Reference:
Item No.: HX-1 Your Reference:
Date: March 18 - 2012 Rev No.: 0 Job No.:

Setting Plan

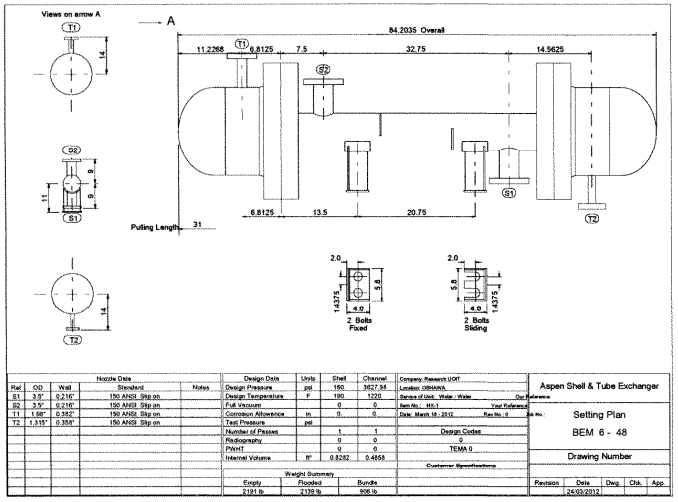

File: UOIT Research.EDR Date: 24/03/2012 Time: 3:15:11 AM
Company: Research UOIT
Location: OSHAWA
Service of Unit: Water / Water Our Reference:
Item No.: HX-1 Your Reference:
Date: March 18 - 2012 Rev No.: 0 Job No.:

Tube Layout

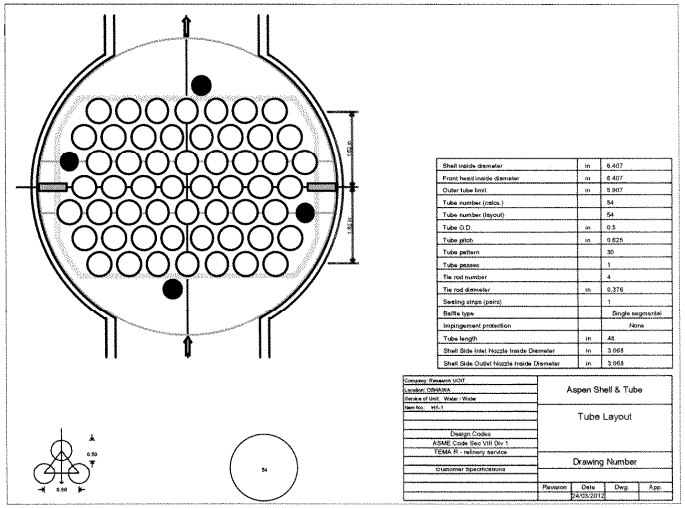

APPENDIX K: CONTRIBUTIONS TO KNOWLEDGE

A. Adenariwo, G.D. Harvel, M. Veslin, F. McCluskey, and J.S. Chang, “Transient Two-Phase Interfacial Parameter Measurements using Ultrasonic Pulse-Echo Methods in a Natural Circulation Loop”, Proceedings of the 19th International Conference on Nuclear Engineering (ICONE-19), Chiba, Japan, 2011, May 16-19.

M. Kinakin, A. Adenariwo, G.D. Harvel, and I. Pioro, “Modelling of Heat Transfer between Two Fuel Subchannels in Supercritical Water Conditions using Computational Fluid Dynamics”, Proceedings of the 5th International Symposium on Supercritical Water Reactors (ISSCWR-5), Vancouver, Canada, 2011, March 13-16.